CALCULATION OF SATELLITE ORBITS UNDER PERTURBATIONS EFFECT

A Thesis
Submitted to the Department of Astronomy and Space
College of Science
University of Baghdad

In Partial fulfillment for the requirements of the Degree of
Doctor of Philosophy in Astronomy and Space Science

BY
WESAM TALEB WAES
(M. Sc. 2000)

Supervisor
Assist Prof. Dr. Abdul-Rahman H. S. Al-Mohammadi

Thw al-Hijjah 1432

November 2011

بسم الله الرحمن الرحيم

((وآية لهم الليل نسلخ منه النهار فإذا هم مظلمون (٣٧) والشمس تجري لمستقر لها ذلك تقدير العزيز العليم (٣٨) والقمر قدرنه منازل حتى عاد كالعرجون القديم (٣٩) لا الشمس ينبغي لها أن تدرك القمر ولا الليل سابق النهار وكل في فلك يسبحون (٤٠))) .

(صدق الله العظيم)

يس الآيات (٣٧-٤٠)

قال الرسول محمد (صلى الله عليه واله وسلم)

((أفضل الأعمال على ظهر الأرض ثلاثة:- طلب العلم ،والجهاد ،والكسب من الحلال : فطالب العلم حبيب الله، والمجاهد ولي الله، والكاسب من الحلال كريم على الله))

(صدق رسول الله)

قال الأمام علي بن أبي طالب (عليه السلام)

((لا تجعلوا علمكم جهلا ويقينكم شكا ، إذا علمتم فأعملوا ، وإذا تيقنتم فأقدموا))

إهداء

إلى مهجة القلب وشفائها وخير الأنام

وسيد الخلق أجمعين

محمد ابن عبد الله (صلى الله عليه وسلم)

إلى العين التي لا تنام ، والنهر الجاري ، وواحة الحنان

والقلب الواسع ، ومصدر نجاحي

والدتي وزوجتي

إلى من هيئوا إلي طريق النجاح

إخوتي

إلى من جادوا علي من علمهم وخبرتهم

أساتذتي

إلى من شاركوني بمساعداتهم وخبرتهم

زملاء الدراسة

Supervisor Certification

I certify that this thesis was prepared by "***WESAM TALEB WAES*** " under my supervision at the Department of Astronomy and Space, College of Science, University of Baghdad as a partial fulfillment of the requirements needed to award the degree of Ph. D. of Science in Astronomy and Space.

Signature :

Name : **Dr. Abdul-Rahman H. Saleh Al-Mohammadi**

Title : Assist Professor

Address : Department of Astronomy and Space , College of Science, University of Baghdad

Date: / / 2011

Certification of the Head of the Department

In view of the available recommendation, I forward this thesis for debate by the examination committee.

Signature :

Name : **Dr. Kamal M. A.**

Title : Assist Professor

Address : Head of Astronomy and Space Department, College of Science, University of Baghdad

Date: / / 2011

Examination Committee

We members of the Examining Committee, certify that after reading this thesis and examining the student "***WESAM TALEB WAES*** " in its contents and, in our opinion that it is adequate for the award of the degree of Ph. D. of Science in Astronomy and Space.

Signature:
Name: Pr. Dr. Rashed H. Al-Neaemi
(Chairman)
Date: / / 2011

Signature:
Name: Pr. Dr. Majed M. Jarad
(Member)
Date: / / 2011

Signature:
Name: As. Pr. Dr. Mohamed J. Al-Bermani
(Member)
Date: / / 2011

Signature:
Name: As. Pr. Dr. Loay Kadhem
(Member)
Date: / / 2011

Signature:
Name: As. Pr. Dr. Nihad Ali Karem
(Member)
Date : / / 2011

Signature:
Name: As.Pr. Dr. Abdul-Rahman H. S. Al-Mohammadi
(Supervisor)
Date: / / 2011

Approved by the Dean of the College of Science, ***Baghdad University***

Signature:
Name: Pro. Dr. Saleh Mahdi Ali
(Dean)
Date: / / 2011

Acknowledgements

I wholeheartedly appreciate the unwavering support of my advisor **Dr. Abdul-Rahman H. S. Al-Mohammadi**. It is an honor to have worked with a man of such brilliance, dedication, and vision. I am also indebted to head of Astronomy and Space department for his understanding when I needed him the most.

My family, mother, brothers and my wife were always willing them to provide input on design decisions and refused to ever allow me to become discouraged. I thank them for all their assistance.

Wesam

Abstract

There are many perturbations that affect on artificial satellites which may deviate its current path tends to change its orbital elements. Such perturbations are gravitational and non-gravitational and the equation of motion can be solved for all perturbations by using numerical integration methods.

In this research, the actual position and velocity components of satellites were calculated at any instant of time. Hence calculating the actual orbital elements which are affected by five types of perturbations (Oblatness of Earth, Atmospheric drag, Solar radiation pressure, and Solar and Lunar attraction). This leads to know which the perturbations are dominated with altitudes for LEO and MEO.

Computer code program was designed by using QB-language to solve the Runge- Kutta and Adams Bashforth methods with integration by Cowll's method, the program called "Re-Correct of Satellite Orbital Elements"; also many subprograms are designed to calculate all functions needed.

The summation of all the perturbations formulae were solved to find the actual position and velocity at any instant of time, which leads to the calculation of the orbital elements that are perturbed, and which of these have more effect with that perturbation for all the following cases:

$h_p = 95,600,1200,3000 Km$ and $i = 8^\circ, 63.4^\circ, 85^\circ$

The variation for all orbital elements through 33 period are calculated, also the solar flux index $(F_{10.7})$, scale high (H) and the radial distance for Sun (r_s) and Moon (r_l) with center of Earth are calculated, which depend on the lunching date of the satellite as well as the change them with time of the satellite rotation beginning from passage in perigee point. Also the lifetime of satellite are calculated.

Contents

Acknowledgements

Abstract ……..……. *I*

Contents ……..……. *II*

Terminology ……..… *VI*

Chapter 1. General Introduction and Review *1*

1.1 Introduction …….….… *1*

1.2 Conic section orbits ……. *3*

1.3 Orbital classifications …….……... *4*

1.3.1 Centric orbit classifications …….…….. *5*

1.3.2 Altitude classifications …….……... *7*

1.3.3 Inclination classifications …..…….……... *8*

1.3.4 Eccentricity classifications ..…….……... *9*

1.4 Review of previous works …….……... *11*

1.5 The aim of thesis …..…….……... *17*

Chapter 2. Dynamic of elliptical orbit *18*

2.1 Introduction ……..…….…… *18*

2.1.1 The N-Body problem …….… *19*

2.1.2 Two-Body problem ……..... 20

2.2 Elliptical orbit geometry ……....….. 21

2.3 Solving Kepler's equation …….. 28

2.4 Definition of classical orbital elements and matrix transformation ……..……. 29

2.5 Calculation of orbital elements from position and velocity coordinates … 33

Chapter 3. Perturbations of Satellite orbit 36

3.1 Introduction …. …….. 36

3.2 Orbital perturbations ……. 37

3.3 Perturbation due to Oblateness of Earth ……..... 39

3.4 Perturbation due to atmospheric drag ……..... 43

3.4.1 Drag forces …….. 45

3.4.2 Drag coefficient C_D *……. 47*

3.4.3 Calculation of the relative velocity of satellite …….…. 48

3.4.4 Calculation of atmospheric density (r *) …….. 50*

3.5 Solar gravity perturbation …….. 52

3.6 Lunar gravity perturbation ……. 55

3.7 Solar radiation pressure perturbation (SRP) …….…. 58

3.8 Satellite lifetime prediction ……..... 61

Chapter 4. Solution of perturbation equation 63

4.1 Introduction …….. 63

4.2 Solution methods of perturbation equation ……..….. 64

4.2.1 Cowell's method ……. 65

4.2.2 Encke's method ……. 67

4.2.3 Variation of parameters method …….….. 69

4.3 Numerical integration methods …….… 70

4.3.1 Single-Step method …….. 71

4.3.2 Multi-Step method ……. 73

Chapter 5. Results and Discussion ……...…..……. 76

5.1 Introduction ……...……. 76

5.2 Discussion of the figures ……. 78

a- Comparison between five order Runge-Kutta method and four order Adams Bashforth method ……..... 78

b- Atmospheric drag perturbation …….…….…… 80

c- Oblatness of Earth perturbation …….… *87*

d- Solar radiation pressure perturbation ……...…… *95*

e- Lunar attraction perturbation ……..…… *102*

f- Solar attraction perturbation …….…… *102*

g- Lunar attraction perturbation at hp=3000 Km ……..…… *115*

h- Solar attraction perturbation at hp=3000 Km ....….…… *115*

i- All perturbations result ……..….... *120*

5.3 Discussion of the tables ……..…….. 130

Chapter 6. Conclusions and future works …….. 139

6.1 Conclusions ……... 139

6.2 Future works ……... 141

References …… 142

Appendix A …..……..…. 153

Appendix B ……..…… 155

Appendix C ……..…… 158

Appendix F ……...…. 164

1.1 Introduction

The first man-made spacecraft was launched in 1957, the satellite orbits have already been studied two centuries before. Starting from Newton's formulation of the law of gravity, scientists sought continuously to develop and refine analytical theories describing the motion of the Earth's only natural satellite the Moon. Today, several thousand man-made satellite's orbit around the Earth, together with countless pieces of space debris. Much as celestial mechanics studies the laws of motion of solar system bodies, the branch of astrodynamics is concerned with the mathematical and physical description of artificial satellite orbits, as well as their control. Here, the term orbit refers to a trajectory that is essentially periodic in nature, and does not consider the special case of objects leaving the realm of the Earth towards interplanetary space.

There are a number of compelling reasons to lunch a satellite into orbits. Satellites are the only means of obtaining in sit measurements of the upper atmosphere or the Earth's magnetosphere. Astronomical telescopes in orbits provide an uncorrupted, diffraction-limited view of the sky at all regions of the electromagnetic spectrum. By the very nature of things, one has to leave the Earth to collect large-scale images of its continents, oceans, and atmosphere. The satellites are able to communicate with a large number of places on Earth simultaneously, thus forming the basis for worldwide telephone and data networks as well as TV transmissions. Finally, constellations of navigation satellites nowadays provide the means for precision localization and aircraft navigation around the world.

Even though elaborate models have been developed to compute the motion of artificial Earth satellites to the high level of accuracy required for many applications today, the main features of their orbits may still be

described by a reasonably simple approximation. This is due the fact that the force resulting from the Earth's central mass rules out all other forces acting on the satellite by several orders of magnitude, in much the same way as the attraction of the Sun governs the motion of the planets.

The laws of planetary motion, which were found empirically by Kepler about 401 years ago, may, therefore, equally well be applied to a satellite's orbit around the Earth. The basic laws of orbital motion are derived from first principles. For this purpose, a satellite is considered whose mass is negligible compared to the Earth's mass. Assuming the Earth to be spherically symmetric, without atmosphere and no other body affect on the satellite orbit, the acceleration of the satellite is given by Newton's law of gravity. The magnitude of the acceleration is proportional to the inverse square of the satellite's distance (r) from the Earth's center.

There are many forces that affect the satellite orbits which are known as perturbations. These cause departure in the orbital elements about the original values, and lead to deviation in current path of satellite orbit. These perturbation are classified into two types:

1. Gravitational perturbation, such as Oblatness of Earth, Ocean Tide and 3rd-body attraction.
2. Non-Gravitational perturbation, such as atmospheric drag force, solar radiation pressure, Earth radiation pressure.

The types of orbits and satellite orbital classifications are applied here, also made review for the past research works.

1.2 Conic section orbits

A conic section, is a curve formed by passing a plane through a right circular cone. As shown in the figure (1.1), the angular orientation of the plane relative to the cone determines whether the conic section is circle, ellipse, parabola, or hyperbola [1].

A circle and an ellipse arise when the intersection of cone and plane is a bounded curve. The circle is a special case of the ellipse (0<eccentricity<1) in which the plane is perpendicular to the axis of the cone when eccentricity =0. If the plane is parallel to a generator line of the cone, the conic is called a parabola and eccentricity=1. Finally, if the intersection is an unbounded curve and the plane is not parallel to a generator line of the cone, the shape of orbit is a hyperbola and eccentricity>1. In the latter case the plane will intersect both halve of the cone, producing two separate curves.

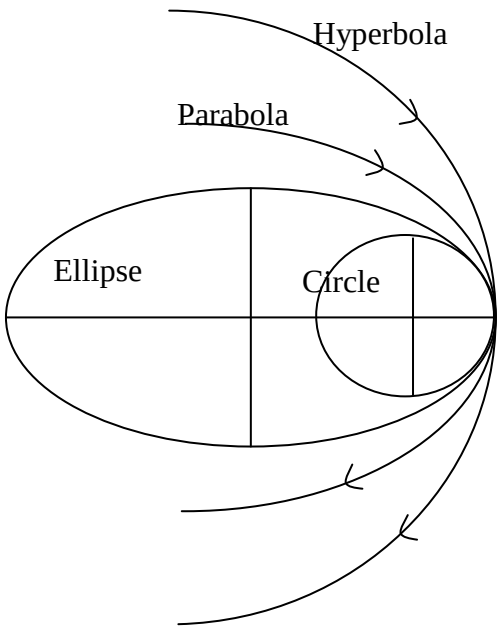

Figure (1.1): Conic sections [1].

1.3 Orbital classifications

The first satellite, Sputnik 1, was put into orbit around Earth and was therefore in geodetic orbit. By far this was the most common type of orbit with approximately 2456 artificial satellites orbiting the Earth [2]. Geodetic orbits may be further classified by their altitude, inclination and eccentricity.

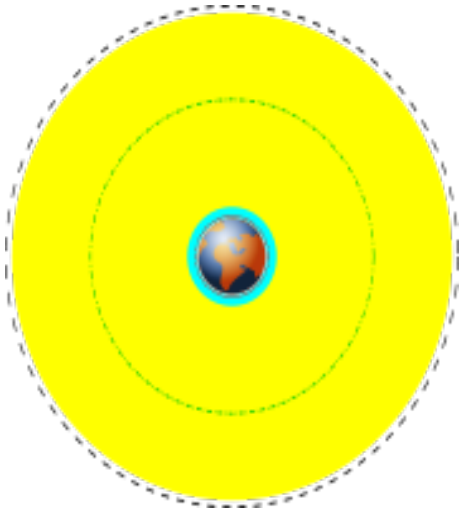

Figure (1.2): Types of satellite Earth orbits [2].

Various Earth orbits to scale, see figure (1.2); cyan represents Low Earth Orbit (LEO), yellow represents Medium Earth Orbit (MEO), the black dashed line represents geosynchronous orbit, the green dash-dot line the orbit of Global Positioning System (GPS) satellites, and the red dotted line the orbit of the International Space Station (ISS).

The commonly used altitude classifications are Low Earth Orbit (LEO), Medium Earth Orbit (MEO) and High Earth Orbit (HEO). Low Earth orbit is any orbit below 2000 km, and Medium Earth Orbit is any orbit higher than that but still below the altitude for geosynchronous orbit at 35786 km. High Earth Orbit is any orbit higher than the altitude for geosynchronous orbit [2].

1.3.1 Centric orbit classifications

1. **Galactocentric orbit**: An orbit about the center of a galaxy. Earth's sun follows this type of orbit about the galactic center of the Milky Way.
2. **Heliocentric orbit**: An orbit around the Sun. In our Solar System, all planets, comets, and asteroids are in this orbit, also many artificial satellites and pieces of space debris.
3. **Planet centric orbit**: An orbit around planets, such as its moons or artificial satellites.
4. **Geocentric orbit**: An orbit around the planet Earth, such as the Moon or artificial satellites. This type can be classified as :

4-a- Polar orbit

An orbit that passes above or nearly above both poles of the planet on each revolution, see figure (1.3). Therefore it has an inclination of 90° (or very close to 90°). Which allows the satellite to see virtually every part of the Earth as the Earth rotates underneath it. It takes approximately 60-90 minutes for the satellite to complete one orbit. These satellites have many uses such as measuring ozone concentrations in the stratosphere or measuring temperatures in the atmosphere.

4-b- Sun synchronous orbit

This orbit allows a satellite to pass over a section of the Earth at the same time of day. Since there are 365 days in a year and 360° degrees in a circle, it means that the satellite has to shift its orbit by approximately one degree per day, see figure (1.4). These satellites orbit at an altitude between 600 to 1000 Km, example LandSat at altitude 905 Km. They make use of the fact that since the Earth is not perfectly round (the Earth bulges in the center, the bulge near the equator will cause additional gravitational force to act on the

satellite), which causes the satellite's orbit to either proceed or recede. These orbits are used for satellites that need a constant amount of sunlight. Satellites that take pictures of the Earth would work best with bright sunlight, while satellites that measure long wave radiation would work best in complete darkness.

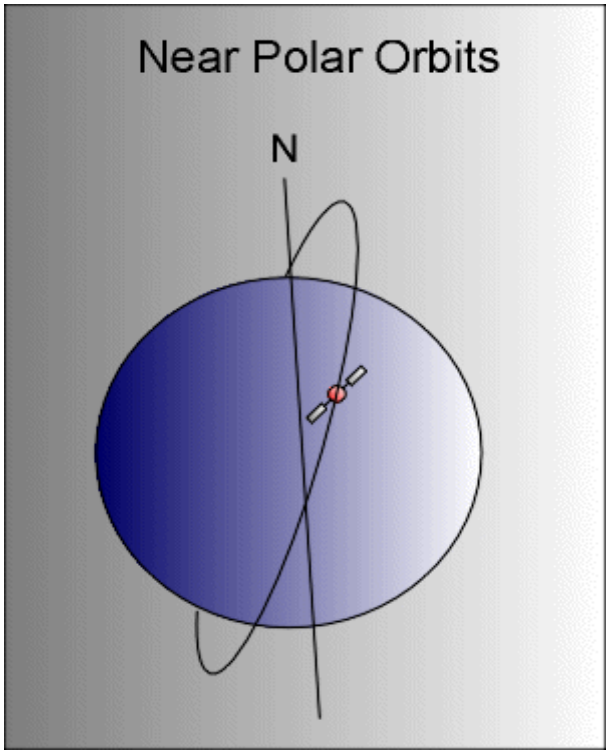

Figure (1.3): Polar Orbit [2].

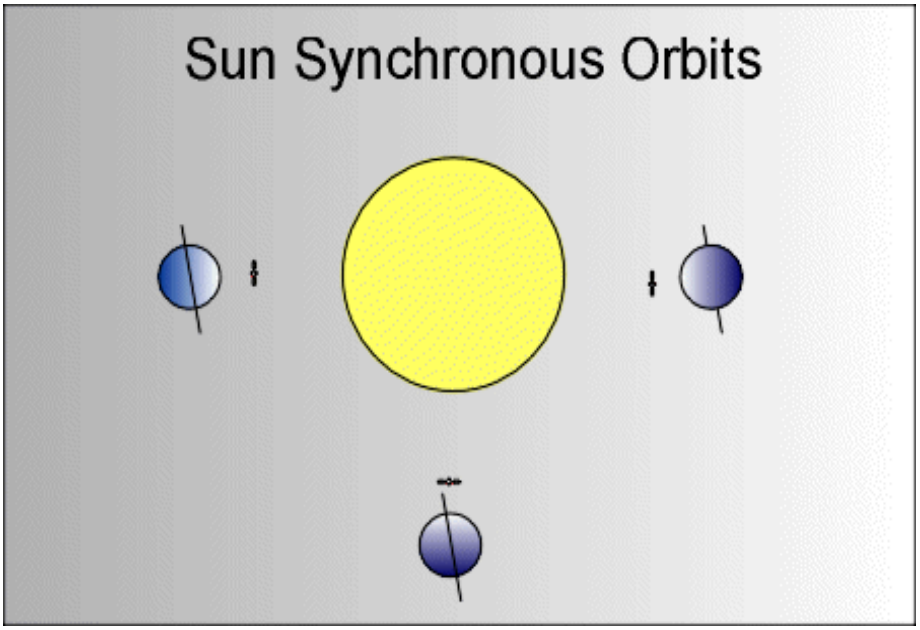

Figure (1.4): Sun Synchronous Orbit [2].

4-c- Geosynchronous orbit

Satellites in these orbits rotate around the Earth at the same rate as the Earth's spin and inclination $\left(0^{o} < i < 180^{o}\right)$. The Earth actually takes 23 hours, 56 minutes, and 4.09 seconds to make one full revolution, so based on Kepler's laws of planetary motion, this would put the satellite at approximately 35,790Km above the Earth, see figure (1.5). The satellites are located near the equator since at this altitude, there is a constant force of gravity from all directions. At other altitude, the bulge at the center of the Earth would pull on the satellite. Geosynchronous orbits allow the satellite to observe almost a full hemisphere of the Earth. These satellites are used to study large scale phenomenon such as hurricanes, or cyclones. These orbits are also used for communication satellites.

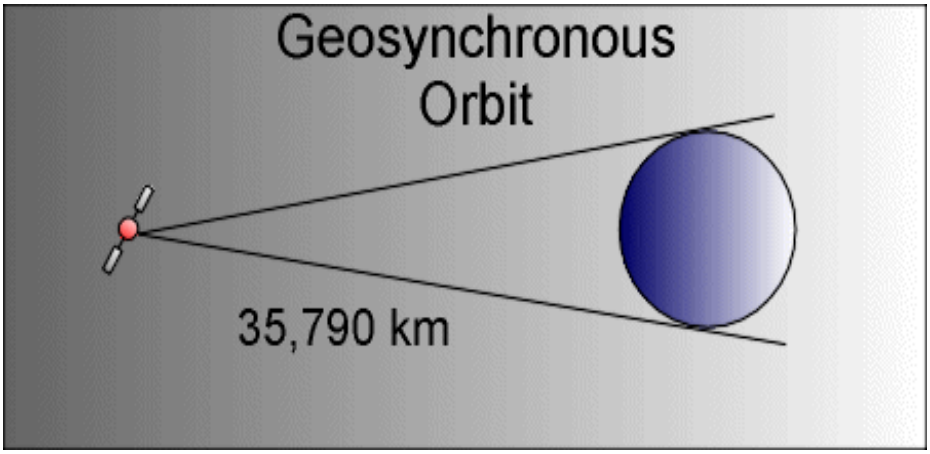

Figure (1.5): Geosynchronous Orbit [2].

1.3.2 Altitude classifications

- **Low Earth Orbits (LEO)**: These are Geocentric orbits ranging in altitude from 0-2000 km.
- **Medium Earth Orbits (MEO)**: These are Geocentric orbits ranging in altitude from 2000km, to just below geosynchronous orbit at 35786 km, also known as an intermediate circular orbits.

- **High Earth Orbits (HEO)**: Geocentric orbits above the altitude of geosynchronous orbit 35786 km, see figure (1.6).

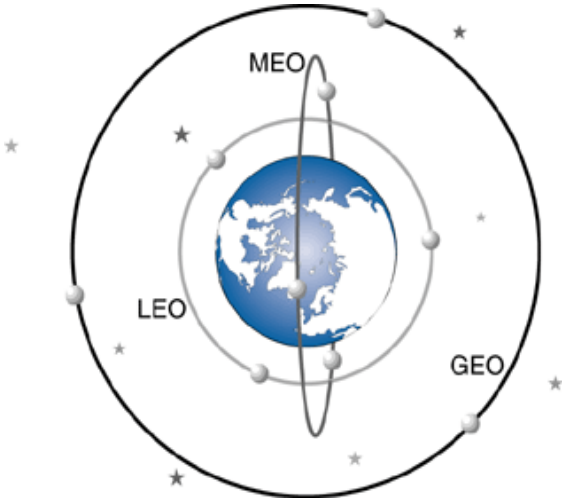

Figure (1.6): Kinds of Altitude Earth Orbits [2].

1.3.3 Inclination classifications

- **Equatorial orbit**: An orbit whose inclination in reference to the equatorial plane is small inclination.
- **Geostationary orbit (GSO)**: It is a geosynchronous orbit with an inclination near from equatorial $(i\ @zero)$. To an observer on the ground this satellite would appear as a fixed point in the sky, and the altitude is usually about 36000 Km [2].
- **Polar orbit**
- **Retrograde orbit**: An orbit with an inclination of more than 90°. Rather, orbits counter to the direction of rotation of the planet. Apart from those in sun-synchronous orbit, few satellites are launched into retrograde orbit because the quantity of fuel required to launch them is much greater than for a retrograde orbit. This is because when the rocket starts out on the ground, it already has an eastward component of velocity equal to the rotational velocity of the planet at its launch site latitude.

1.3.4 Eccentricity classifications

1- Circular orbit: An orbit that has an eccentricity =0 and whose path traces a circle.

Hohmann transfer orbit: An orbital maneuver that moves a spacecraft from one circular orbit to another using two engine impulses. This maneuver was named after Walter Hohmann.

2- Elliptic orbit: An orbit with an eccentricity as ($0< e<1$) and whose orbit traces the path of an ellipse.

a- Geosynchronous transfer orbit: An elliptic orbit where the perigee is at the altitude of a Low Earth Orbit (LEO) and the apogee is at the altitude of a geosynchronous orbit.

b- Geostationary transfer orbit: An elliptic orbit where the perigee is at the altitude of a Low Earth Orbit (LEO) and the apogee is at the altitude of a geostationary orbit.

c- Molniya orbit: A highly elliptic orbit with inclination of 63.4^{o} and orbital period of half a sidereal day (roughly 12 hours), see figure (1.7). Such a satellite spends most of its time over a designated area of the planet.

d- Tundra orbit: A highly elliptic orbit with inclination of 63.4^{o} and orbital period of one sidereal day (roughly 24 hours), see figure (1.8). Such a satellite spends most of its time over a designated area of the planet.

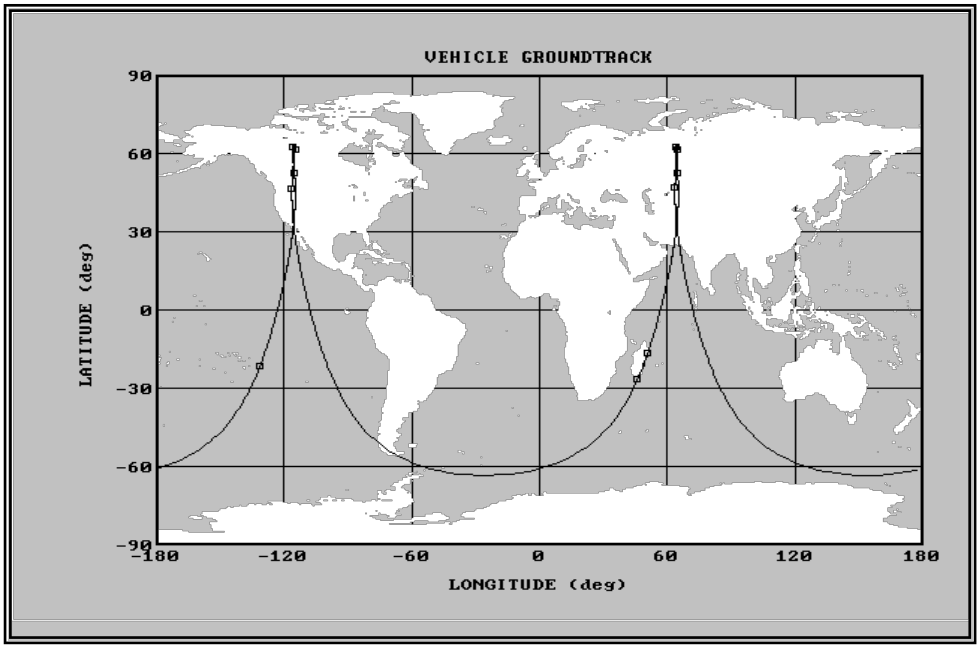

Figure (1.7): Molniya orbit [1].

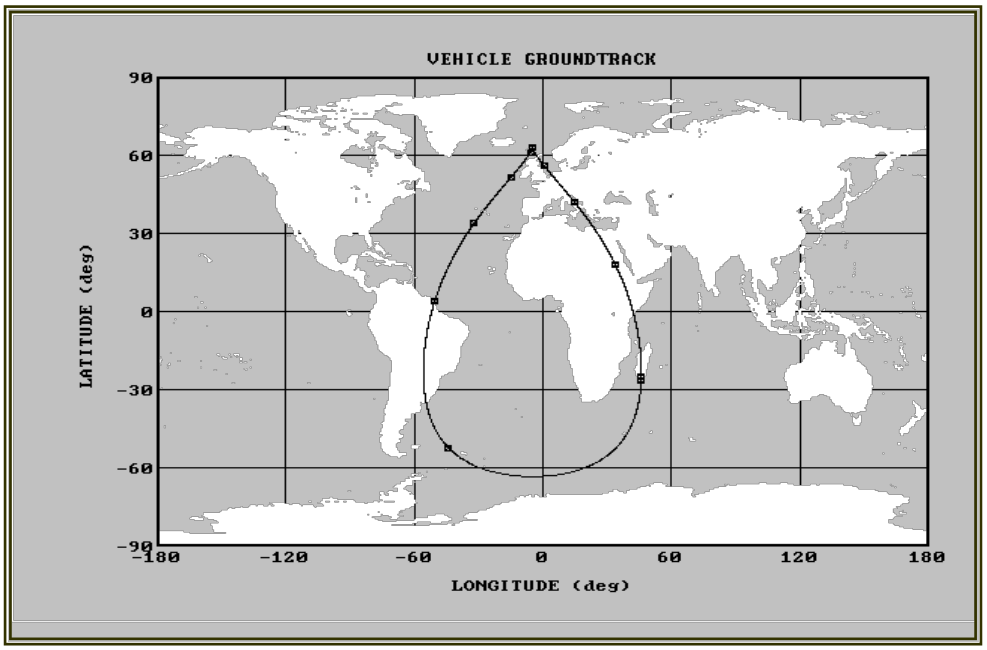

Figure (1.8): Tundra orbit [1].

3- Hyperbolic orbit: An orbit with the eccentricity > 1. Such an orbit has a velocity in excess of the escape velocity and as such, it will escape the gravitational pull of the planet and continue to travel infinitely.

4- Parabolic orbit: An orbit with the eccentricity = 1. Such an orbit has a velocity equal to the escape velocity and therefore it will escape the

gravitational pull of the planet and travels until its velocity relative to the planet becomes 0. If the speed of such an orbit is increased it will become a hyperbolic orbit.

a- Escape orbit (EO): A high-speed parabolic orbit where the object has an escape velocity and is moving away from the planet.

b- Capture orbit: A high-speed parabolic orbit where the object has an escape velocity and is moving toward the planet [2].

1.4 Review of previous works

King-Hele (1956) used perturbations of a satellite orbit near the Earth which was caused by the Earth's oblateness and the atmosphere [3]. Blitzer (1959) obtained estimates of the lunisolar disturbances, using methods of classical mechanics, but only for the secular terms [4]. Kozai (1959) developed the main secular and long-period terms of the disturbing function due to the lunisolar perturbations in terms of the orbital elements of the satellite, the Sun and the Moon [5]. Musen (1960) derived first order expressions for the rates of change in the osculating elements caused by the direct solar radiation pressure [6]. He used the method of variation of vector elements. This research would be later expanded by Musen, Bailie and Upton (1961) to include the Para lactic term in the disturbing function [7].

Kozai (1961) developed the main secular and long period terms of the disturbing function due to the lunisolar perturbations in terms of the orbital elements of the satellite, the Sun and the Moon [8]. After that, Kozai (1962) studied the problem of secular perturbations of asteroids with high inclination and eccentricity, assuming that they are perturbed by Jupiter, which is supposed to be in a circular orbit around the Sun [9]. In the same year, Kaula (1962) developed the Lunar and Solar disturbing function for a close satellite

and developed a quasi potential for the radiation pressure effects to be used in the equation of motion. He did not obtain the solution [10].

Frick and Garber (1962) used a linear analysis to show that the result of the lunisolar attraction was changing the orbital plane with small oscillations [11]. In this sequence, Cook (1962) used the Lagrange's planetary equations to obtain expressions for the variation of the orbital elements during one revolution of the satellite and for the rate of variation of the same elements [12]. Frick & Garber (1962, Part III) had discussed the in-plane perturbations of a Geosynchronous satellite under the gravitational effects of the sun, the moon and the oblate Earth. They assumed that the Sun, the Moon, and the Earth all lie in the plane of the ecliptic and the satellite's orbital plane and that the reference plane coincide with the Earth's equatorial plane. Kozai (1963) introduced the Lagrange's planetary equations and the disturbing function due to the Sun and to the Moon, including both secular and long periodic terms [13]. Again Kozai (1965) approached that problem and included indirect terms of the disturbance due to the alteration of the terrestrial flattening due to these forces [14].

During the seventies, the subject was studied again. Giacaglia (1973) obtained the disturbing function for the disturbance of the Moon using ecliptic elements for the Moon and equatorial elements for the satellite. Secular, long and short period terms were calculated and expressed in a closed form [15]. Kozai (1973) developed an alternative method for the calculation of the lunisolar disturbances. The disturbing function was expressed in terms of the orbital elements of the satellite and the polar geocentric coordinates of the Sun and the Moon. The secular and long period terms were derived by numerical integration and the short period terms were obtained analytically [16]. Sehnal (1975) discussed the direct solar radiation pressure, as one of the non-gravitational forces, from all its different aspects [17].

The theory of atmospheric drag and its influence on Earth orbiting satellites has been well analyzed and studied by King-Hele (1964, as well as earlier works in 1969 and 1987) for an in-depth treatment of the effects of atmospheric drag on Earth satellites [18, 19, 20]. Many works on astrodynamics - for examples Danby (1962), Escobal (1965), Bate et al. (1971), Battin (1987), Roy (1988) and Chobotov (1996) [21, 22, 23, 24, 25, 26]. Other relevant works include Kaplan (1976), wertz (1978) and Larson et al (1992) [27, 28, 29]. Some articles on the subject can be found I El'yasberg et al. (1967) and Morando (1970) [30, 31]. Langton(1969) give a treatment of the physical structure of the Earth's atmosphere [32].

In the following decade, Hough (1981) studied the effects of the lunisolar disturbance in orbits close to the inclinations 63.4° and 116.6° (critical inclinations with respect to the geopotential of the Earth) and concluded that the effects are significant in high altitudes [33]. Anselmo *et al.* (1983) had analyzed the perturbations due to solar radiation pressure, only, on the orbit of a high artificial satellite [34]. Schatten and Sofia (1987) developed a monthly estimate of $F_{10.7}$. Notice solar flux index $(F_{10.7})$ changes during the course of a single solar cycle (11 years) [35].

Bhatnagar and Manjeet (1990) studied the gravitational effects of the Sun, the Moon and the oblatness of the Earth and they determined the radial deviation (Δr) and the tangential deviation $(r_c \Delta q)$ Here r_c represents the synchronous altitude [36]. Broucke (1992) developed the general form of the disturbing function of the third body which was truncated after the term of second order in the expansion of Legendre polynomials [37]. After that, Costa and Prado (1998) expanded the order of this model to the order eight [38, 39]. Delhaise and Morbidelli (1993) investigated the lunisolar effects of a geosynchronous artificial satellite orbiting near the critical inclination,

analyzing each harmonic formed by a combination of the satellite and the Moon's longitude of the node. He demonstrated that the dynamics induced by these harmonics did not show resonance phenomena [40].

Toshihiro Kubo-oka and Sengoku (1999) developed a radiation pressure model of the relay satellite of SELENE. The shape of the satellite was assumed to be a combination of a regular octagonal pillar and a column. Radiation forces acting on each part of the spacecraft were calculated independently and summed vectorially to obtain the mean acceleration of the satellite center of mass [41]. In particular, Prado (2002) studied the perturbation in a lunar satellite for direct orbits and the lifetimes of orbits around the natural satellites of the Solar System [42].

Perturbing forces are driving satellites out of the Keplerian orbit. Such forces are classified into two major groups; gravitational and nongravitational perturbing force. Eanes et al. (1995) worked on geodynamics satellites, also Seeber (2003), Hofmann et al (2001), Eshagh et al (2003), Eshagh (2003a), and Leick (1995) [43, 44, 45, 46, 47, 48]. Wolf (2000) worked on some low Earth orbiting satellites of about 1000 km altitude [49]. Su (2000) studied the GEO, MEO satellites and like GPS, GLONAS [50], Santos (1994) investigated the real time kinematics orbit improvements of GPS satellites for short and long base line computations [51]. Buffet (1985) studied the perturbations of orbital elements of the GPS satellites [52]. All these researchers have worked on the satellites of altitude larger than 800km. Eshagh and Najafi (2007) evaluated the perturbations in orbital elements of a low Earth orbiting satellite at 545 Km. The outcome of a numerical orbit integration process are the position and velocity vectors of a satellite in an inertial coordinate system [53].

Solórzano and Prado (2004) studied the effect of the third body perturbation in spacecrafts. They developed a semi-analytical study of the perturbation caused in a spacecraft by a single averaged model. One of the most important applications is to calculate the effect of Lunar and Solar perturbations on high-altitude Earth satellites [54]. Bar-Sever and Kuang (2005) introduced a set of solar pressure models for Global Positioning System (GPS) satellites based on in-orbit tracking data, and analyzed the performance of the models for satellites outside eclipse seasons [55]. Prado (2005) developed a semi-analytical study of the perturbation effected on a spacecraft by a third body involved in the dynamics and calculated the effect of lunar and solar perturbations on high altitude Earth satellites [56].

Frank, Bruce and Robert (2006) used empirical models to estimate satellite atmospheric drag for low altitude. Model accuracies have shown little improvement before 35 years. They developed a new Jacchia-Bowman 2006 (JB2006) empirical model to command a high accuracy satellite drag Model (HASDM) program. This model was built on analytical height profiles of the temperature, which depend on latitude, local time, day of year, solar activity index $F_{10.7}$ and geomagnetic activity index (Kp) [57].

Narumi and Hanada (2007) presented new expressions for the rate of change in orbital elements to account for gravitational forces of the Sun and Moon. They analyzed the long-term effects of orbital perturbations based on the analytic models of third body forces and conventional analytical models of atmospheric drag, solar radiation pressure, and zonal harmonics [58].

Domingos, Vilhena and Prado (2008) presented a semi-analytical and numerical study of the perturbation effected on a spacecraft by a third-body using a double averaged analytical model with the disturbing function expanded in Legendre polynomials up to the second order [59].

Vallado and Finkleman (2008) examined derives approaches to represent gas dynamic drag effects on Low Earth Orbit (LEO) satellites. Although the total drag force on a satellite can be measured, the physics of gasdynamic resistance, dynamics of the orbiting body, and characteristics of the atmosphere are inextricably combined. Investigators must hypothesized physical relationships among the drag force, body shape, size, and orientation, the distribution of density, and the predictive assessment of density. Drag coefficients determined under one set of hypotheses are often employed improperly in orbital assessments that use a different set of hypotheses [60].

El-Salam, Abdel-Aziz, El-Saftawy and Radwan (2008) dealt with constructing a conditionally periodic solution for the motion of an Earth artificial satellite taking into account the oblateness of the Earth (which truncated beyond the second zonal harmonic (J_2) and the Luni-Solar attractions [61]. Wright (2008) examined the secular effects of the oblateness (J_2) perturbation on close proximity satellites, analyzed the deputy's position and velocity with respect to the chief and adjusts the initial conditions of the deputy in an attempt to minimize the secular effects of (J_2) perturbations [62].

Nadia A. Saad, Kh. I. Khalil and Magdy Y. Amin (2010) obtained a new analytical solution for the motion of high-altitude Earth satellites. The basic idea is to study the joint effects of direct solar radiation pressure and the gravitation of the Earth, Moon and the Sun on the orbits of the satellites. The mathematical model includes the zonal harmonics of the geopotential effects up to J_4. The solution is intended to be used for ephemeris predictions for orbits whose orbital semimajor axes are in the range of 15000 to 70000 kms [63].

Daniel, du Plessis and Steyn (2010) studied two or more satellites that operate in a certain configuration relative to each other in certain low Earth orbit (LEO) satellite missions. They introduced a simple concept of utilizing atmospheric drag, a natural phenomenon which is normally considered as an unwanted disturbance, to achieve this type of constellation control including the effects of a number of significant orbital perturbations [64]. Costa and Prado (2010) developed a semi-analytical study of the perturbation effected on a spacecraft by a third body involved in the dynamics [65].

1.5 The aim of thesis

All of the preceding works represent fundamental contributions to the subject. In the present work a more calculations are used with the idea of complementing the existent literature. Some recent studies have provided numeric comparisons. **In this research**, studying more perturbations that important effects on the artificial satellites orbit and with more altitudes and inclinations, that perturbations are oblatness of Earth, atmospheric drag, solar radiation pressure (SRP) and third-body (Moon and Sun) identically and summation of all effected of perturbations in one equation to find the perturbations on the satellite orbit.

QB-basic language used to solve the equation of motion by 5th order Runge-Kutta numerical method and other numerical method such 4th order Adams-Bashforth, aiming to find the actual orbital elements from calculations the variation of orbital elements through satellite rotation. The solar flux index $(F_{10.7})$, scale high (H), density of the atmosphere (r) and the radial distance for Sun (r_s) and Moon (r_l) with center of Earth are calculated with the satellite rotation.

3.1 Introduction

Satellite orbit perturbations arise from the non-spherical Earth with its non-homogeneous distribution of mass, atmospheric drag force and the existence of other celestial bodies. With the effect of perturbations, a satellite orbit will not simply be the two-body motion but it changes perpetually. Generally, two main aspects should be taken into consideration: one effects is the disturbance time; the other is the magnitude of the disturbance force with respect to the Earth gravity. The variation in one of the orbital elements vs time can be illustrated in figure (3.1)

Secular variation represents a linear change with extremely long time effect relative to the period. Long-period variation lasts longer than one orbit period, while short-period variation is shorter than the variation through any orbit. Different variations are included in analysis depending on the demands of the mission [75].

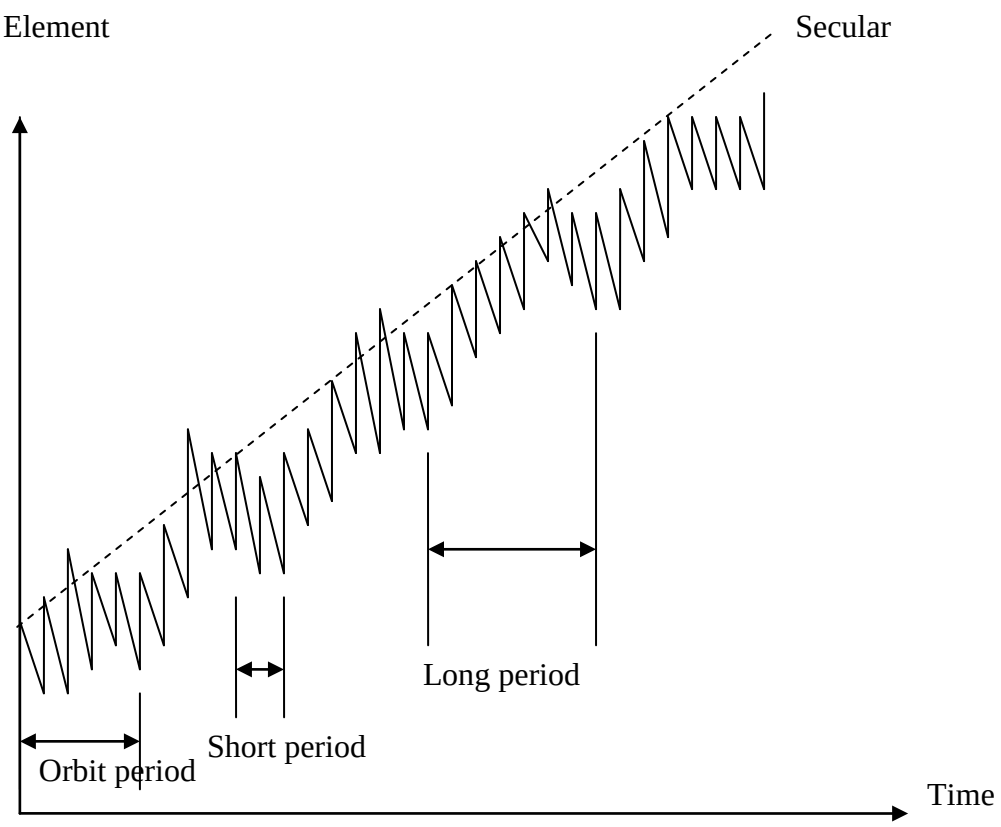

Fig (3.1) : Variations of an orbital element with time [75].

The magnitude of disturbance varies with the altitude of the satellite. In LEO orbit, J_2 and atmospheric drag are dominant, but in HEO orbit atmospheric drag can be ignored because of the dramatic drop of the atmospheric density in outer space figure (3.2). Third body perturbations from the Sun and Moon increase when the distance between the satellite and the Earth increases [76].

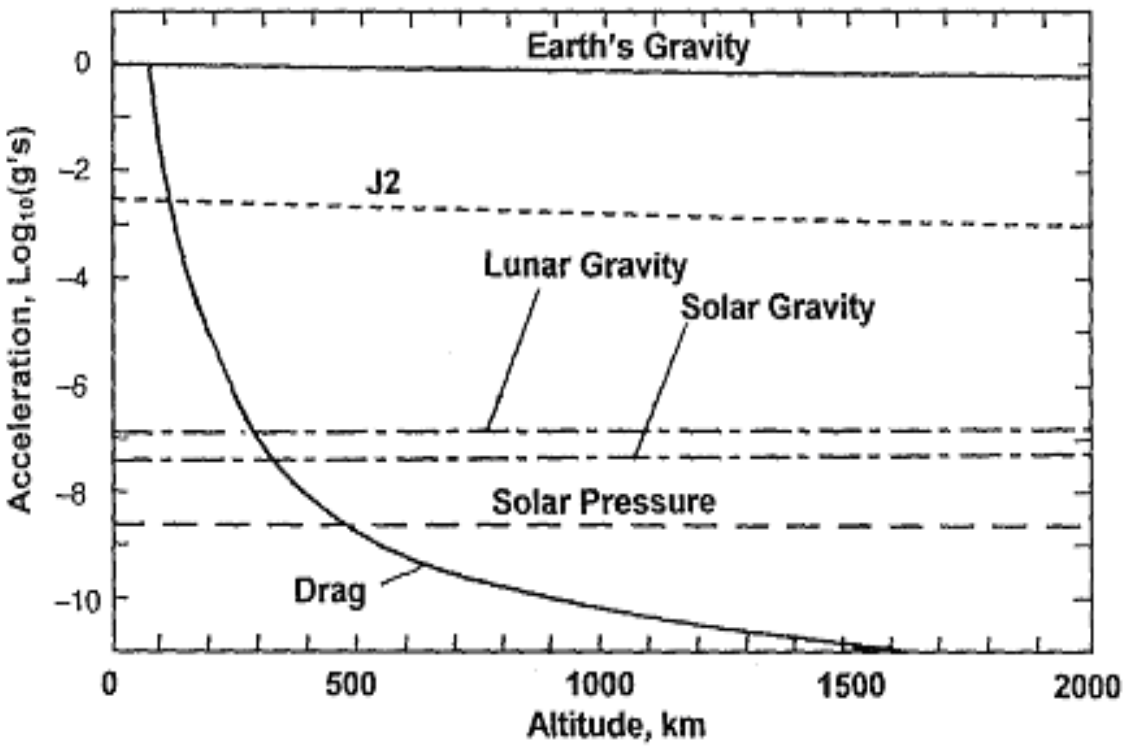

Fig (3.2): Relative importance of orbit perturbations [76].

3.2 Orbital perturbations

Propagation allows us to move a satellite's state vector through time. It is usually found in analytical (fast but moderately inaccurate), numerical (slower, but very accurate), and semi-analytical (a combination of analytical and numerical) techniques. Special perturbations (used interchangeably with numerical methods and Cowell's formulation) are the simplest and most straightforward of all the propagation methods. An advantage is the fact that

the solution contains all secular and periodic variations introduced by the perturbing forces. The solution rests with solving the perturbed equation of motion for multiple perturbing forces, adding each of the accelerations, and numerically integrating [77].

$$\ddot{\vec{r}} = -\frac{m}{r^3}\vec{r} + \vec{a}_{perturbed} \qquad \text{.....(3.1)}$$

Where

$$\vec{a}_{perturbed} = \vec{a}_{non_spherical} + \vec{a}_{drag} + \vec{a}_{N-body} + \vec{a}_{SRP} + \vec{a}_{others} \qquad \text{.....(3.2)}$$

The acceleration labeled non-spherical refers only to the perturbing acceleration caused by the non-spherical portion of the mass distribution of the central body (Earth). To account for all the major perturbations (central body, drag, third body, solar radiation, ocean and solid Earth tides, and others) expressions for each of these accelerations must be formed.

The perturbations that effects the satellite can be classified into two types:

1. Gravitational perturbation: such as; obletness of Earth, N-body attraction and others.
2. Non-gravitational perturbation: such as; Atmospheric Drag, Solar Radiation Pressure and others.

These four type of the perturbations mentioned here, will be used in this research and are described in this chapter.

3.3 Perturbation due to Oblateness of Earth

The Earth is not the point gravitational source assumed in Newton's gravitational law; in fact both its shape and mass distribution lead to non-inverse square law effects on an orbiting satellite. An accurate model of the Earth can be obtained through the use of as series of spherical harmonics which effectively represent a gravitational body as a series of mass centers, some more dominant than others, the most dominant term being that of a perfectly uniform sphere, see Appendix C.

The gravitational potential of the Earth can be written as [25,26]:

$$U_E(r,\lambda,\phi) = -\frac{m}{r}\left[\sum_{n=0}^{\infty}\left(\frac{r_E}{r}\right)^n \sum_{m=0}^{n}\left(C_{nm}\cos(m\lambda) + S_{nm}\sin(m\lambda)\right)\times P_{nm}(\sin(\phi))\right]$$

$$= -\frac{m}{r}\left[\sum_{n=0}^{\infty}\left(\frac{r_E}{r}\right)^n \sum_{m=0}^{n} J_{nm}\cos(m(\lambda - \lambda_{nm}))P_{nm}(\sin(\phi))\right] \quad \text{.....(3.3)}$$

r_E represents the mean radius of the Earth which is equal to 6378.165 Km

And

$P_{nm}(\sin\phi)$ is the associated Legendre polynomials given below:

$$P_n(x) = \frac{1}{2^n n!}\frac{d^n}{dx^n}\left[\left(x^2 - 1\right)^n\right] \qquad -1 \le x \le 1 \quad \text{.....(3.4)}$$

$$P_{nm}(x) = (1 - x^2)^{\frac{m}{2}} \frac{d^m}{dx^m}[P_n(x)] \qquad -1 \le x \le 1 \quad ; m \le n \qquad \text{.....(3.5)}$$

J_{nm} and l_{nm} instead of C_{nm} and S_{nm}, see Appendix C

The various types of harmonics resulting from equation (3.3) are illustrated in figure (3.3), and are described in Appendix C.

Zonal P_{n0} Sectorial $P_{nm}(n \neq 0)$ Tesseral $P_{nm}(n \neq m \neq 0)$

Figure (3.3): Various types of harmonic coefficients. White-Elevation above; Black-Elevation below mean spherical surface [26].

Let n=0, the term is the inverse square law component and if the origin of the coordinate system is at the center of gravity of the Earth then J_{10} and J_{11} will be equal zero. Using this information, equation (3.3) can be rewritten as:

$$U_E(r, l, f) = -\frac{m}{r}\left[1 + \sum_{n=2}^{\infty} \left(\frac{r_E}{r}\right)^n J_{n0} P_n(\sin(f))\right]$$

$$+\sum_{n=2}^{\infty}\sum_{m=1}^{n}\left(\frac{r_E}{r}\right)^n P_{nm}(\sin(f))J_{nm}\cos(m(l-l_{nm}))] \quad \text{.....(3.6)}$$

And also it can be rewritten as:

$$U = U_0 + U_{pertu.} \quad \text{.....(3.7)}$$

Which consist of two parts:

The first part: represents non-perturbation function, which is:

$$U_0 = -\frac{m}{r} \quad \text{.....(3.8)}$$

The second part: represent the perturbation function due to Oblatness of Earth, given as:

$$U_{pertu.} = -\frac{m}{r}[\sum_{n=2}^{\infty}\left(\frac{r_E}{r}\right)^n J_{n0}P_n(\sin(f)) + \sum_{n=2}^{\infty}\sum_{m=1}^{n}\left(\frac{r_E}{r}\right)^n P_{nm}(\sin(f))J_{nm}\cos(m(l-l_{nm})) \quad \text{.....(3.9)}$$

When considering only the terms that contain the value of J_2, since the other value of J_n are much smaller than value of J_2, The perturbation function can then be approximated to as (see Appendix C):

$$U_{pertu.} = -\frac{m}{r}\sum_{n=2}^{\infty}\left(\frac{r_E}{r}\right)^n J_2 P_n(\sin(f)) \quad \text{.....(3.10)}$$

The perturbation acceleration along the radial distance can now be found from the perturbing potential as:

$$\vec{a} = \vec{\nabla} U \qquad \ldots\ldots\ldots\

3.4 Perturbation due to atmospheric drag

Drag is the resistance offered by atmosphere. Drag force acts in a direction opposite to the direction of the satellite motion. It is the greatest during launching satellite and at final orbit [57, 75].

When the orbit perigee height is below 1000 Km, the atmospheric drag effect becomes increasingly important. Drag, unlike other perturbation forces, is a non-conservative force and will continuously take energy away from the orbit. Thus, the orbit semi-major axis and the period are gradually decreasing because of the effect of drag tend to increasing in the orbit velocity, the reason is Kepler's law ($m = n^2 a^3 = cons\tan t$). The effect of atmospheric friction is to speed up the motion of the satellite as it spirals inward. The effect of atmospheric drag on a satellite orbit is illustrated in figure (3.4).

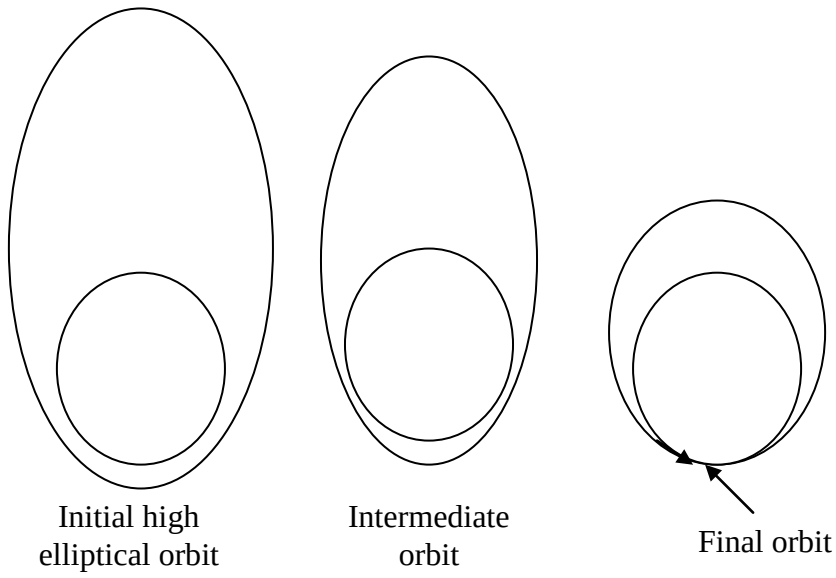

Figure (3.4): The shape of satellite orbit decay due to Atmospheric drag [25].

Since the drag is greatest at perigee, where the velocity and atmospheric density are greatest, the energy drain is also greatest at this point. Under this dominant negative impulse at perigee, the orbit will become more circular in each revolution. The elliptic orbit first becomes circular as the apogee altitude decreases to the same value of perigee and then rapidly spirals into the dense atmosphere. The atmospheric drag is expressed by the drag force per unit of mass in the following form:

$$F_D = -\frac{1}{2} C_D \rho \times v^2 A \quad \text{.....(3.16)}$$

Divide both sides of equation by mass of satellite to obtain the acceleration of the atmospheric drag

$$\vec{a}_{drag} = -\frac{1}{2} \rho \frac{C_D A}{m} v_{rel.}^2 \frac{\vec{v}_{rel.}}{|\vec{v}_{rel.}|} \quad \text{.....(3.17)}$$

C_D drag coefficient [79].

ρ atmosphere density at specific altitude.

A effective cross-section area.

$v_{rel.}$ the satellite relative velocity with respect to the atmosphere.

It can be seen from this equation that a high ratio of cross-sectional area to mass produces the greatest drag.

Therefore, aerodynamic design of satellite structure should be taken into account A/m for low earth orbits such that the ratio should be minimized. The shape of satellite studying the outer atmosphere should be spherical with high A/m ratio.

An accurate prediction of the satellite motion under the influence of drag requires a good density model of the upper atmosphere. Over the past three decades, various density models have been developed, with varying degrees of complexity and fidelity [26].

For near-circular orbits, the orbit semi-major axis decay rate can be computed by the following simple equation:

$$\frac{da}{dt} = -na^2 \left(\frac{rg}{BC}\right) \qquad \text{.....(3.18)}$$

$n =$ mean motion

$g =$ gravitational acceleration at sea level, and equal $9.8 m/\sec^2$

$BC =$ ballistic coefficient = $\frac{m}{(C_D A)}$

BC represents another measure of the satellite's susceptibility to drag effects. With this definition, a low BC means that drag will affect the satellite significantly and vice versa. These quantities have many definitions, so it is very important to understand which one is being used [58].

3.4.1 Drag forces

Although, the Keplerian relations are useful approximations for the orbit determination, the precision orbit computation requires the consideration of the disturbing force, which causes the motion to deviate from a pure conic form. The atmospheric drag force is dominated in low earth orbit [80, 81].

This force can be resolved into rectangular components, T is the tangential component (in the plane of the orbit perpendicular to the radius vector, in the direction of motion), S the radial component (in the radial direction) and W

the normal component (perpendicular to the plane of the orbit), see figure (3.5).

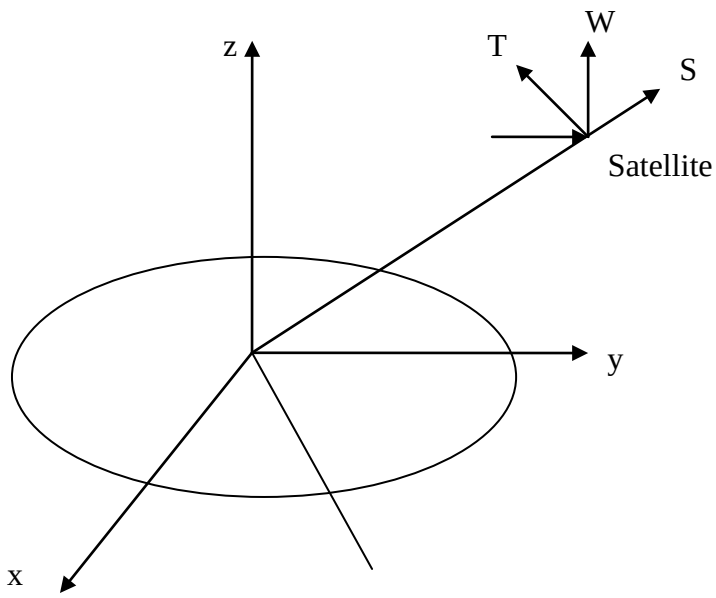

Figure (3.5): Force components to the Atmospheric drag [25].

The force S and T which lie in the orbit plane cannot change the orientation of the orbit plane in space, and therefore cause no change in the inclination (i) and the longitude of the ascending node (W). Changes in the argument of perigee (w) and true anomaly (f) will cause changes in the semi-major axis a and eccentricity (e), and therefore, cause changes in the true anomaly not caused by the satellite motions. The drag force is in opposite direction to the satellite motion, so that $F = -T$ and normal component tends to zero (such $S = W = 0$), and it is given by equation (3.16) [25, 27].

In order to study the atmospheric drag that affects the orbital elements of satellite, modification to Gaussian equations must be made.

3.4.2 Drag coefficient C_D

The drag coefficient depends on the reflectivity of the satellite as well as on the velocity of the satellite. For a velocity of satellite v greater than thermal velocity v_T of the gas particles, the drag coefficient can be expressed as [82]:

$$C_D = \delta \times \left[2 + \frac{4}{3}\left(\frac{v_T}{v}\right)^2 - \frac{2}{15}\left(\frac{v_T}{v}\right)^4 \right] \quad \text{.....(3.19)}$$

δ is the accommodation coefficient representing the reflective properties of the satellite's surface. For a perfect absorber $\delta = 1$, and for $\delta = 2$ all incoming particles are reemitted in the opposite direction. For a spherical aluminum satellite, Alfonso [82] gives values of C_D and δ assuming a diffuse remission process and a hyper thermal free flow (satellite velocity greater than thermal velocity), see tables (3.1) and (3.2).

Table (3.1): Accommodation coefficient δ for different molecular species [82].

Accommodation coefficient δ	
Hydrogen	1.4
Helium	1.3
Oxygen	1.1

Table (3.2): Drag coefficient C_D and relative thermal velocity $\frac{v_T}{v}$ as a function of atmospheric temperature and molecular species [82].

	Hydrogen (HEO)	Helium (MEO)	Oxygen (LEO)

$T(K^0)$	$\frac{v_T}{v}$	C_D	$\frac{v_T}{v}$	C_D	$\frac{v_T}{v}$	C_D
800	0.72	3.71	0.36	2.82	0.18	2.25
1200	0.88	4.14	0.44	2.93	0.22	2.27
2000	1.14	4.90	0.57	3.15	0.29	2.32

For a low circular satellite, $\frac{v_T}{v} \gg 0.15$, the heavier species dominate (δ ~1.1). For this case the typical drag coefficient of 2.25 is used for drag computations. However, for higher altitude orbits the C_D value increases. For a circular orbit at 3500 km $\frac{v_T}{v} \gg 0.72$.

At this height hydrogen dominates during periods of low solar activity (T~ 600 K°), while helium dominates during periods of high solar activity (T~1500 K°). Thus, the C_D value can change from less than 3 to over 4 depending upon the exospheric temperature.

The drag analysis for this research employs orbit-averaged perturbation equations derived by King- Hele (1964) and Bowman (2000) [18, 83]. For the height range of 2000 km to 4000 km the main density constituent varies between H and He depending upon the exospheric temperature.

3.4.3 Calculation of the relative velocity of satellite

For some satellites, the mass is assumed to be constant. Noticing that the v_{rel} is not the velocity vector typically found in the state vector. This velocity vector is relative to the atmosphere.

Actually, the Earth's atmosphere has a mean motion due to the rotation, and the local winds are superimposed on this mean motion. Notice also that

the force of drag is opposite to the velocity vector at all times. This is the primary use for the STW coordinate system. For a non-spherical satellite, companion aerodynamic forces, such as lift and drag forces, must also be considered.

The velocity vector relative to the rotating atmosphere is given by [73]

$$v_{rel} = \frac{dr}{dt} - w_{Earth} \times r \quad \ldots\ldots\ldots\

$$v_{rz} = v_z \qquad \text{.....(3.23)}$$

The magnitude of the relative velocity becomes

$$v_{rel}(mag) = \sqrt{v_{rx}^{\ 2} + v_{ry}^{\ 2} + v_{rz}^{\ 2}} \qquad \text{.....(3.24)}$$

3.4.4 Calculation of atmospheric density (r)

There are a number of empirical atmospheric density models used for predicted the atmospheric density. These include the Jacchia 71 [84], Jacchia 77 [85], the Drag Thermal Model (DTM) [86], DTM-2000 [87], MSIS-90 [88] and NRLMSISE-00 [89]. The density r is an empirically determined function of r, although in a number of studies it is approximated by a simple exponential law

$$r = r_0 \quad \exp\left[-\frac{(h_h - h_0)}{H}\right] \qquad \text{.....(3.25)}$$

Where h_h is the altitude, h_0 represents the standard altitude (usually taken to be the altitude of perigee), r_0 is the density at the standard altitude h_0 (see table (3.3)).

Table (3.3): Change density (r_0) with standard altitude (h_0) [73, 78].

altitude (h_0) (Km)	Density (r_0) (Kg/m^3)
90	5.71E-7
100	9.8 E-9
200	2.7 E-10
300	2.225 E-11
400	4.77 E-12

500	1.0478 E-12
600	3.1225 E-13
700	9.3025 E-14
800	3.3425 E-14
900	1.3575 E-14
1000	6.715 E-15
>1000	6.715 E-15

Table (3.3) shows that the density of atmosphere decreases with increase of the height, and the density is equal to zero at $h_h >$ 1000Km, so that the magnitude of the drag is neglected (or equal zero) at $h_h >$ 1000Km.

H is the scale height (assumed constant). The scale height is that vertical distance in which the density changes by an exponential factor and depends upon the altitude. H is about 6 Km at sea level and 8 Km at Everest mountain high, reaching 40 Km at a height of about 200 Km.

Scale height can be calculated by a set of equations depending on temperature and height, equations given by [19, 90]

$$T_T = 900 + 2.5 \times (F_{10.7} - 70) + 1.5 \times Ap \quad \text{(Kelvin)} \quad \ldots\ldots\ldots\ldots\ldots\ldots\ldots(3.26)$$

$$M_h = 27 - 0.012 \times (h - h_p) \quad \ldots\ldots\ldots\ldots\ldots\ldots\ldots\ldots\ldots\ldots\ldots(3.27)$$

$$H = \frac{T_T}{M_h} \quad \text{(Km)} \quad \ldots\ldots\ldots\ldots\ldots\ldots\ldots\ldots\ldots\ldots\ldots(3.28)$$

Ap planetary index, is computed every 24 hours, hovers just above zero in quiet times, but may rise to above 400 at times of major geomagnetic storms.

$F_{10.7}$ represent the solar flux index, which is a convenient indicator of solar radiation energy at a wavelength of 10.7 cm. there are many indicators of solar activity, such as, the sun-spots which represent the dark regions of different sizes that appear on the sun surface. Sun-spots phenomenon is usually associated with solar flares, prominence and filaments as additional sources of activity [91]. A relation exists between the number of days and $F_{10.7}$ can be expressed as follow [92]:

$$F_{10.7} = 145 + 75\cos(0.001696 \times t_d + 0.35 \times \sin(0.00001695)) \quad \text{.....(3.29)}$$

t_d is the number of days from 1 January, 1981 until now.

3.5 Solar gravity perturbation

The solar gravity perturbation can be modeled as a third body effect in inertial geocentric axes, it explained as [93]:

$$\vec{a}_s = \frac{\mu_s \vec{r}}{r_s^3}\left[3(i_r \times i_s)i_s - i_r\right] \quad \text{.....} \quad (3.30)$$

Where

$$\mu_s = GM_s = 1.327124 * 10^{11}\left(N \times Km^2 / Kg\right)$$

r_s radial distance between center of Sun and Earth, which vary between $147 \times 10^6 Km$ *and* $152 \times 10^6 Km$ along a year.

i_s unit vector of the distance between centre of Sun and Earth, and measured in Km.

i_r unit vector of the distance between Satellite and centre of Earth, and measured in Km.

The corresponding vector directions are illustrated in figure (3.6).

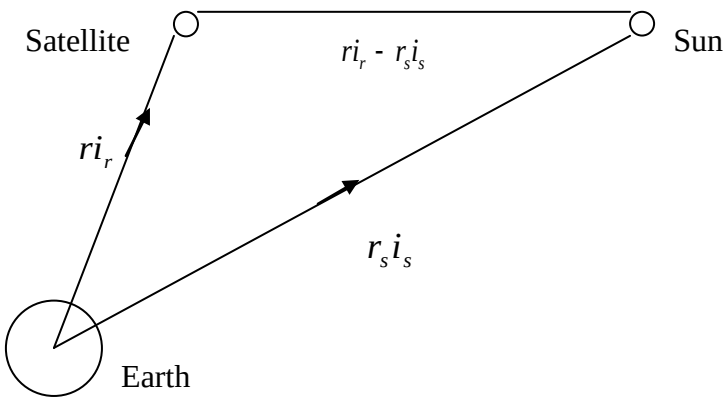

Figure (3.6): Solar gravity geometry [94].

Before using equation (3.30) the position vectors of the Earth and Sun are required. A series of empirical approximations quoted below [94].

The geometric mean longitude and mean anomaly of the Sun at any epoch can be approximately found as follow:

$$l_s = 280^0.46645 + 36000^0.76983Tu + 0^0.0003032Tu^2 \quad \text{.....(3.31)}$$

Tu represent the number of Julian centuries

$$M_s = 357^0.52910 + 35999^0.05030Tu - 0^0.0001559Tu^2 - 0^0.00000048Tu^3 \quad \text{..... (3.32)}$$

The equation of centre for Sun is then

$$C = \left(1^0.9146 - 0^0.004817Tu - 0^0.000014Tu^2\right)\sin\left(M_s\right)$$

$$+\left(0^0.019993 - 0^0.000101Tu\right)\sin\left(2M_s\right) + 0^0.00029\sin\left(3M_s\right) \quad \text{.....(3.33)}$$

The eccentricity of the Earth orbit and the obliquity of the ecliptic (the angle between equator and ecliptic) are:

$$e_s = 0^0.016708617 - 0^0.000042037Tu - 0^0.0000001236Tu^2 \quad \text{.....(3.34)}$$

$$e_o = 23^0.439291 - 0^0.013004Tu - 1^0.639' \; 10^{-7}Tu^2 + 5^0.03' \; 10^{-7}Tu^3 \quad \text{..... (3.35)}$$

In the above five equations the variable 'Tu' is the number of Julian centuries from the year 2000.0 epoch. It is calculated from the Julian date (JD) as follows [74, 95]:

$$Tu = \frac{JD - 2451545}{36525} \qquad \ldots\ldots\ldots\

$$\vec{r} = r_s \begin{bmatrix} \cos(f_s)\cos(a_s) \\ \cos(f_s)\sin(a_s) \\ \sin(f_s) \end{bmatrix} \quad \ldots\ldots\ldots\ldots\ldots\ldots\ldots\ldots\ldots\ldots\ldots\ldots (3.41)$$

3.6 Lunar gravity perturbation

As in the case of solar gravity the effects of the Moon will be treated as a third body acting on the satellite. Although the mass of the Moon is much lower than that of the Sun the reduced distance between perturbing body and satellite makes the Lunar perturbation about equal to the Solar. Re-writing equation (3.30), replacing the Solar variables by the equivalent Lunar ones.

$$a_l = \frac{\mu_l r}{r_l^3}\left[3(i_r \times i_l)i_l - i_r\right] \quad \ldots\ldots\ldots\ldots\ldots\ldots\ldots\ldots\ldots\ldots\ldots\ldots (3.42)$$

Where

$$\mu_l = GM_l = 4.902794 * 10^3 \left(N \times Km^2 / Kg\right)$$

r_l radial distance between center of Moon and Earth which must be calculated later

i_l unit vector of the distance between centre of Moon and Earth

i_r unit vector of the distance between Satellite and centre of Earth

The relationships between the vectors used in this equation are illustrated in figure (3.7).

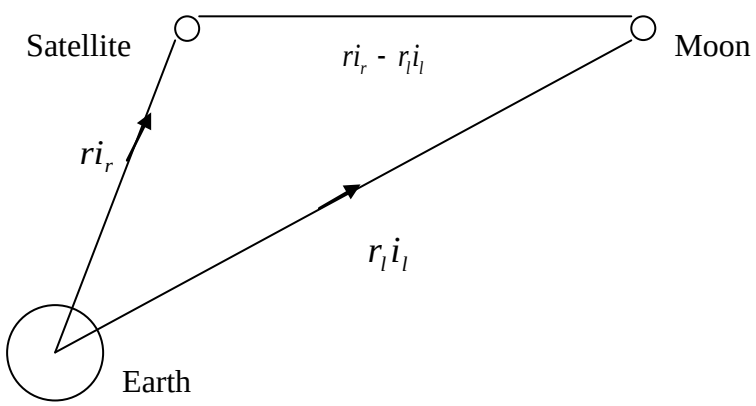

Figure (3.7): Lunar gravity geometry [94].

Again the biggest problem is calculating the Moon's position at a given point in time.

Series expansions similar to those for the Sun exist for the lunar coordinates as well. Due to the strong solar and terrestrial perturbations, a larger number of terms are, however, needed to describe the lunar motion in terms of the mean arguments of the lunar and solar orbit. The following relations allow the computation of lunar longitude and latitude with a typical accuracy of several arc minutes and about 500 Km in the lunar distance. The calculation of the perturbations is based on five fundamental arguments [74]:

The mean longitude L_0 of the Moon

The Moon's mean anomaly l

The Sun's mean anomaly l¢

The mean angular distance of the Moon from the ascending node F, and

The difference D between the mean longitudes of the Sun and the Moon.

The longitude of the ascending node W is not explicitly employed.

It is obtained from the difference W= $L_0 - F$.

$$L_0 = 218^0.31617 + 481267^0.88088.Tu - 1^0.3972.Tu \quad \ldots\ldots\ldots\ldots\ldots\ldots\ldots\ldots (3.43)$$

$$l = 134^0.96292 + 477198^0.86753.Tu \quad \ldots\ldots\ldots\ldots\ldots\ldots\ldots\ldots (3.44)$$

$$l¢ = 357^0.52543 + 35999^0.04944.Tu \quad \ldots\ldots\ldots\ldots\ldots\ldots\ldots\ldots (3.45)$$

$$F = 93^0.27283 + 483202^0.01873.Tu \quad \ldots\ldots\ldots\ldots\ldots\ldots\ldots\ldots (3.46)$$

$$D = 297^0.85027 + 445267^0.11135.Tu \quad \ldots\ldots\ldots\ldots\ldots\ldots\ldots\ldots (3.47)$$

Using these values the Moon’s longitude with respect to the equinox and ecliptic of the year 2000 may be expressed as:

$$
\begin{aligned}
\lambda_l = L_0 &+ 22640\sin(l) + 769\sin(2l) \\
&- 4586\sin(l - 2D) + 2370\sin(2D) \\
&- 668\sin(l') - 412\sin(2F) \\
&- 212\sin(2l - 2D) - 206\sin(l + l' - 2D) \\
&+ 192\sin(l + 2D) - 165\sin(l' - 2D) \\
&+ 148\sin(l - l') - 125\sin(D) \\
&- 110\sin(l + l') - 55\sin(2F - 2D)
\end{aligned}
\qquad \ldots\ldots\ldots\ldots\ldots\ldots\ldots\ldots\ldots\ldots \quad (3.48)
$$

Here, the first two terms describe the motion in an ellipse of eccentricity $e = 0.055$, whereas the remaining terms denote the various perturbations. The lunar latitude is given as [74]:

$$
\begin{aligned}
\beta_l = 18520.\sin(F + \lambda - L_0 &+ 412\sin(2F) + 541\sin(l')) \\
&- 526\sin(F - 2D) + 44\sin(l + F - 2D) \\
&- 31\sin(-l + F - 2D) - 25\sin(-2l + F) \\
&- 23\sin(l' + F - 2D) + 21\sin(-l + F) \\
&+ 11\sin(-l' + F - 2D)
\end{aligned}
\qquad \ldots\ldots\ldots\ldots\ldots\ldots\ldots\ldots\ldots\ldots \quad (3.49)
$$

Where the leading term is due to the inclination of Moon's orbit relative to the ecliptic, which amounts to approximately 5.1°. Finally the Moon's distance from the center of the Earth is:

$$
\begin{aligned}
r_l = [385000 &- 20905.\cos(l) - 3699.\cos(2D - l) \\
&- 2956.\cos(2D) - 570.\cos(2l) + 246.\cos(2l - 2D) \\
&- 205.\cos(l' - 2D) - 171.\cos(l + 2D) \\
&- 152.\cos(l + l' - 2D)] \quad Km
\end{aligned}
\qquad \ldots\ldots\ldots\ldots\ldots\ldots\ldots\ldots\ldots\ldots \quad (3.50)
$$

Where terms smaller than 150 Km have been neglected.

The spherical ecliptic coordinate may again be converted to equatorial Cartesian coordinates using the transformation

$$
r_l = R_x(-\varepsilon_o)\begin{pmatrix} r_l.\cos(\lambda_l)\cos(\beta_l) \\ r_l.\sin(\lambda_l)\cos(\beta_l) \\ r_l.\sin(\beta_l) \end{pmatrix} \qquad \ldots\ldots\ldots\ldots\ldots\ldots\ldots\ldots\ldots\ldots \quad (3.51)
$$

3.7 Solar radiation pressure perturbation (SRP)

A satellite that is exposed to solar radiation experiences a small force that arises from the absorption or reflection of photons. In contrast to the gravitational perturbations discussed, the acceleration due to the solar radiation depends on the satellite's mass, surface area and the optical properties of the satellite faces.

Solar radiation pressure is determined by the solar flux

$$\Phi = \frac{\Delta E}{A\Delta t} \qquad \text{.....} \quad (3.52)$$

i.e. by the energy ΔE that passes through an area A in a time interval Δt. A single photon of energy E_y carries an impulse

$$p_n = \frac{E_n}{c} \qquad \text{.....} \quad (3.53)$$

Where c is the velocity of light. Accordingly, the total impulse of an absorbing body that is illuminated by the sun changes by

$$\Delta p = \frac{\Delta E}{c} = \frac{\Phi}{c} A\Delta t \qquad \text{.....} \quad (3.54)$$

During the time Δt. This means that the satellite experiences a force

$$F = \frac{\Delta p}{\Delta t} = \frac{\Phi}{c} A \qquad \text{.....} \quad (3.55)$$

that is proportional to the cross-section A or, equivalently, to pressure where

$$P = \frac{\Phi}{c} \qquad \text{.....} \quad (3.56)$$

In a distance of 1AU from the Sun –i.e. in the vicinity of the Earth-the solar flux amounts to $\Phi \approx 1367 Wm^{-2}$ [97], and the solar radiation pressure is, therefore, given by $P_0 \approx 4.56 \times 10^{-6} Nm^{-2}$ if one assumes that the satellite's surface A absorbs all photons and is perpendicular to the incoming radiation.

The more general case of a satellite surface with an arbitrary orientation is illustrated in figure (3.8), for the cases of complete absorption (reflectivity $e=0$) and complete specula reflection (reflectivity $e=1$). In contrast to specula reflection, the diffuse reflection of light is neglected in the sequel.

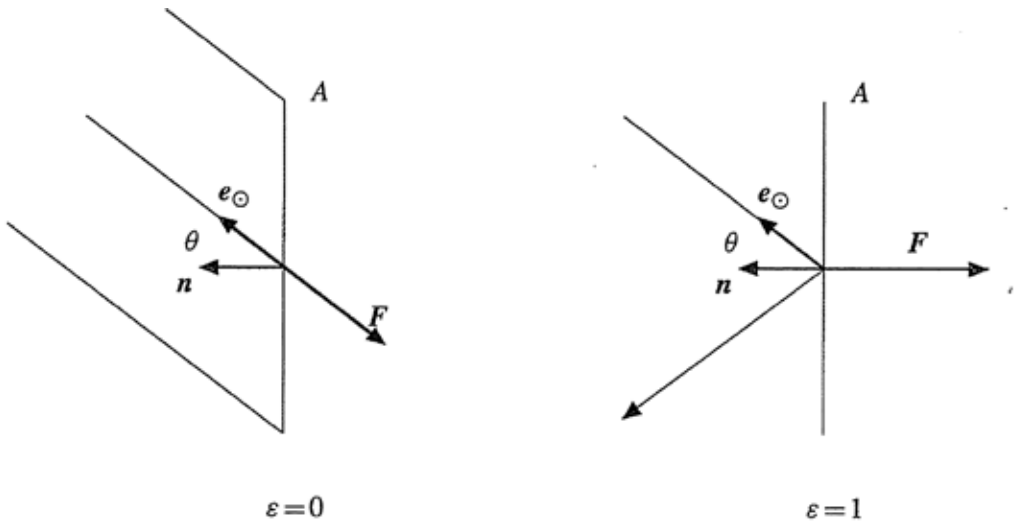

Figure (3.8): The force due to solar radiation pressure for absorbing ($e=0$) and reflecting ($e=1$) surface elements [74].

The normal vector n gives the orientation of the surface A. It is inclined at an angle q to the vector e_0 which points into the direction of the Sun. For an absorbing surface, it follows from the consideration given above that the force

$$F_{abs} = -P_0 \cos(q) A e_0 \qquad \text{(3.57)}$$

where $\cos(q)A$ is the cross-section of the bundle of light that illuminates A. For a reflecting surface, the force is not, in general, directed away from the Sun, since no impulse is transferred in the direction parallel to the surface. Due to the reflected light rays, the impulse transferred in the direction of $\hat{n}$ is twice as large, as in the case of pure absorption, and the resulting force is given by [74]:

$$F_{refl} = -2P_0 \cos(q) A \cos(q) \hat{n} \qquad \text{(3.58)}$$

Both formulas may be combined for a body that reflects a function e of the incoming radiation ΔE, while it absorbs the remaining energy $(1-e)\Delta E$:

$$F = -P_0 \cos(q) A[(1-e)e_0 + 2e\cos(q)\hat{n}] \quad \text{.....} (3.59)$$

For typical materials used in the construction of satellites, the reflectivity e lies in the range from 0.2 to 0.9, see table (3.4).

Table (3.4): Reflectivity, absorption and radiation pressure coefficient of selected satellite components [98].

Material	e	$1-e$	$CR \approx 1+e$
Solar panel	0.21	0.79	1.21
High-gain antenna	0.30	0.70	1.30
Aluminum coated mylar solar sail	0.88	0.12	1.88

Due to the eccentricity of the Earth's orbit, the distance between an Earth-orbiting satellite and the Sun varies between 1.47×10^6 Km and 1.52×10^6 Km during the course of a year. This results in an annual variation of the solar radiation pressure by about $\pm 3.3\%$, since the solar flux decreases with the square of the distance from the Sun.

Accounting for this dependence, one finally obtains the following expression for the acceleration of a satellite due to the solar radiation pressure:

$$\ddot{r} = -P_0 \frac{1AU^2}{r_s^2} \frac{A}{m} \cos(q)[(1-e)e_0 + 2e\cos(q)\hat{n}] \quad \text{.....} (3.60)$$

Here (m) means the satellite's mass and $\cos(q)$ may be calculated from

$$\cos(q) = \hat{n}^T e_0 \quad \text{.....} (3.61)$$

both $\hat{n}$ and e_0 are unit vectors.

For many applications (e.g. satellites with large solar arrays) it suffices to assume that the surface normal n points in the direction of the Sun. In this case equation (3.60) may further be simplified, yielding

$$\ddot{r} = -P_0 C_R \frac{A}{m} \frac{\vec{r}_s}{r_s^3} AU^2 = \vec{a}_{SRP} \quad \ldots\ldots\ldots\ldots\ldots\ldots\ldots\ldots\ldots\ldots\ldots\ldots \quad (3.62)$$

$AU = 149.7 \times 10^6 Km$ (Astronomical Unit), which defined the semi major axis of Earth. And the radiation pressure coefficient C_R stands for

$$C_R = 1 + e \quad \ldots\ldots\ldots\ldots\ldots\ldots\ldots\ldots\ldots\ldots\ldots\ldots\ldots\ldots\ldots\ldots \quad (3.63)$$

Equation (3.62) is commonly used in orbit determination programs with the option of estimating C_R as free parameter. Orbital perturbation due the solar radiation pressure may thus be accounted for with high precision, even if no details of the satellites structure, orientation and reflectivity are known [99, 100, 101, 102].

3.8 Satellite lifetime prediction

The lifetime is the time from the beginning to the destruction or escape to other type of orbit. The basic principle to know satellite lifetime, for elliptical orbit only, depends upon two orbital elements, the semi-major axis (a) and the eccentricity (e), because it indicates the size and shape of orbit.

Thus, when

$e \to 0$ near to circular orbit

Also

$\frac{da}{dt} \to \infty$ the satellite orbit destroyed

The condition when $a @ r_e = 6378.165 Km$ for LEO, it's due to drag force, but $a_{pert.} >> a$ for MEO and HEO, this is due to SRP and 3rd-body attraction, and eccentricity becomes larger than one ($e > 1$).

For circular orbit, the following relation between period P and semi-major axis (a) can be given as

$$P^2 m = 4 p^2 a^3 \qquad \text{……..(3.64)}$$

The reduction in the period due to atmospheric drag is given by [90]

$$\frac{dP}{dt} = -3 \rho a r \left(\frac{A C_d}{m} \right) \qquad \text{……..(3.65)}$$

P Period of satellite (period time)

The value of $\frac{dP}{dt} = 0$ reduced and approaches zero.

Therefore, it's very easy to calculate lifetime of satellite at LEO by using equations (3.64) and (3.65), because of the large effects of drag perturbation.

The lifetime of satellites is very large for MEO and HEO, because the satellites becomes out of the largest force, which is atmospheric drag, and accelerated toward Moon and Sun, also effect by SRP.

.

2.1 Introduction

Kepler, originally working with his teacher Brahe (1601), developed the theories which are known as **Kepler's three laws** (1601-1618):

First Law: The orbits of the planets are an ellipse, and the Sun at a focus.
Second Law**:** The line joining the planet to the sun sweeps out equal areas in equal times.
Third Law: The square of the period of a planet is proportional to the cube of its mean distance to the sun [66].

Some years later, **Newton** published a book called Principia, which contained the now famous **Newton's Laws of Motion** [66, 67]:

First Law: Every body continues in its state of rest or of uniform motion in a straight line unless it is compelled to change that state by forces impressed upon it.

Second Law: Change of motion is proportional to the applied force and takes place in the same direction of the force.

Third Law: To every action there is always a reaction opposite in direction and equal in magnitude and place in the same action line.

Newton's second law can be written mathematically as:

$$å F = m\ddot{r} = \frac{dp}{dt} = m\frac{d^2r}{dt^2} \qquad \text{.....(2.1)}$$

Where F is the external force, m is the mass of the object, and $\ddot{r}$ is the acceleration of the object, p is the linear momentum for orbiting bodies;

Newton's second law is the sum of the gravitational forces resulting in **Newton's Law of gravitation**, which can be written as:

$$F_g = -\frac{GM_c m}{r^3}\vec{r} \quad \ldots\ldots\ldots\ldots\ldots\ldots\ldots\ldots\ldots\ldots\ldots\ldots\ldots\ldots\ldots\ldots\ldots\ldots\ldots\ldots(2.2)$$

Where F_g is the gravitational force on the object, G is the universal gravitational constant ($G = 6.67259 \times 10^{-11}\ N.m^2/Kg^2$), M_c is the mass of the central body, and $(\vec{r})$ is the vector from the central body to the object (m). The gravitational coefficient (m) is a constant for each body. The value of (m) for various celestial bodies is defined as:

$$m = GM_c \quad \ldots\ldots\ldots\ldots\ldots\ldots\ldots\ldots\ldots\ldots\ldots\ldots\ldots\ldots\ldots\ldots\ldots\ldots(2.3)$$

For the Earth as

$$m_E = 3.986021 \times 10^5 \left(N \times Km^2 / Kg\right)$$

2.1.1 The N-Body problem

The total force of gravity on any body is the sum of each of the gravitational force vectors from all the other bodies in the system, therefore

$$F_g = -GM_c \sum_{i=1}^{n} \frac{m_i}{r_i^3}\vec{r}_i \qquad (n = 1,2,3.....) \quad \ldots\ldots\ldots\ldots\ldots\ldots\ldots\ldots\ldots\ldots(2.4)$$

Considering any other external forces factor (F_{other}) into the total force (F_{total}) equation gives

$$F_{total} = F_g + F_{other} \quad \ldots\ldots\ldots\ldots\ldots\ldots\ldots\ldots\ldots\ldots\ldots\ldots\ldots\ldots(2.5)$$

The most general form of the equation of motion for an N-body system can be written as:

$$\ddot{r}_i = \frac{F_{total}}{m_i} - \frac{F_g}{m_i} \quad \ldots\ldots\ldots\ldots\ldots\ldots\ldots\ldots\ldots\ldots\ldots\ldots\ldots\ldots(2.6)$$

Examples of external forces represented by F_{other} include Sun, Moon attraction and other plants. These effects, known as perturbing forces, are further

described in Chapter 3. When the forces from all sources are analyzed, the gravitational force from the central body typically dominates, and is essentially equal to the net force, under most circumstances. As a result, the other forces can be assumed to be negligible, leading to the simpler two-body analysis of the problem.

2.1.2 Two-Body problem

The general equation of motion can be written, by using Newton's laws of motion with the general gravitational law (see appendix A), as

$$\ddot{r} + \frac{m}{r^3} r = 0 \qquad \text{.....(2.7)}$$

The orbits described by this equation are conic sections, having a constant energy E_C that can be expressed as:

$$E_c = m\left(\frac{v^2}{2} - \frac{m}{r}\right) \qquad \text{.....(2.8)}$$

Where $(\frac{1}{2}mv^2)$ represent the kinetic energy

And $(-mm/r)$ represent the potential energy

Whereas Ec its orbital energy constant. It is used to specify orbital shape, as below [22, 25, 26].

When Ec <0 the shape of orbit is ellipse

Ec =0 the shape of orbit is parabola

Ec >0 the shape of orbit is hyperbola

Whereas the equation of angular momentum (h) is described by taking the cross product to the equation of motion (2.7)

$$r \times \frac{d^2 r}{dt^2} = 0 \qquad \text{.....(2.9)}$$

Integrating this equation, it become as:

$$\vec{r} \times \frac{d\vec{r}}{dt} = h \qquad \text{……..…….(2.10)}$$

Which represents the equation of conservation of orbital angular momentum (h), which is known an orbital constant [26, 67].

The angular momentum vector normal to the orbital plane, which involve position and velocity vectors, equation (2.10) can be rewritten as:

$$\vec{h} = \vec{r} \times \vec{v} \qquad \text{……..…….(2.11)}$$

Where v is the velocity of the body. And the magnitude of h is:

$$h = rv\sin f \qquad \text{… …….(2.12)}$$

Where f : the angle between lines drawn perpendicular to the position and the velocity vectors

2.2 Elliptical orbit geometry

In a two-body problem, all orbits are conic sections, and can thus be described by the same set of variables. Figure (2.1) shows a sample of elliptical orbit and the terminology used in describing it. The size and the shape of an orbit can be described by the lengths of the semi major axis (a) and the semi minor axis (b). The eccentricity (e) of an orbit is a parameter describing the shape in terms of the relationship between the semi major and the semi minor axes. The semi-Latus rectum (p) is the perpendicular distance between the semi major axis (in focus) and the orbit. The true anomaly angle (f) is the angle between the semi major axis and the position vector of the orbiting satellite as measured from the focus of the orbit.

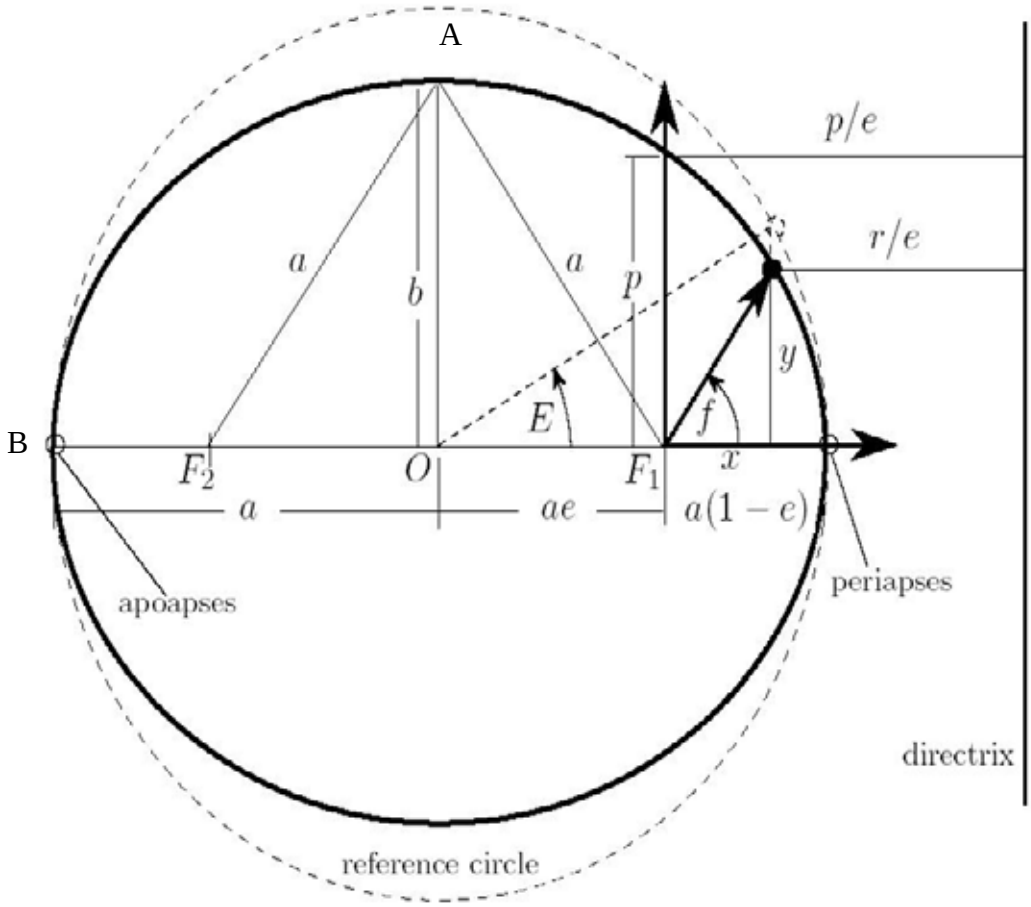

Figure (2.1): Geometry of an elliptical orbit [68].

Some equations describing the position of the satellite relative to the massive body are true for all orbits. Orbits fall under three main shapes: elliptical, parabolic, and hyperbolic, whereas the circle is a special case from the elliptical orbit which is utilized in this research and described here. The semi minor axis (b) and the semi-Latus rectum (p) written as:

$$p = a(1 - e^2) \quad \text{.....(2.13)}$$

$$b = a\sqrt{(1 - e^2)} \quad \text{.....(2.14)}$$

From figure (2.1), the eccentricity (e) is:

$$e = \frac{OF_1}{OB} \quad \text{tends to}$$

$$e = \sqrt{1 - \frac{p}{a}} \qquad \text{……(2.15)}$$

Whereas

$$p = \frac{h^2}{m} \qquad \text{……(2.16)}$$

Since

$$e = \sqrt{1 - \frac{\left(\frac{h^2}{m}\right)}{a}} \qquad \text{……(2.17)}$$

The radial distance from the central body to the satellite can be related to the true anomaly, and is derived from the equation of motion (see Appendix B):

$$r = \frac{p}{1 + e\cos f} \qquad \text{……(2.18)}$$

As the area of elliptical shape is (πab), and the time of period (T) is given from Kepler's second law h as:

$$h = \frac{2\pi ab}{T} \qquad \text{……(2.19)}$$

By substituting relations (2.16), (2.13) and (2.14) in above relation, T can be written as:

$$T = 2\pi\sqrt{\frac{a^3}{m}} \qquad \text{……(2.20)}$$

Which represent Kepler's third Law

Since the vector of angular distance rotate by 2π during orbital revolution T, the mean motion n is given as

$$n = \frac{2\pi}{T} \qquad \text{……(2.21)}$$

Therefore

$$n = \sqrt{\frac{m}{a^3}} \qquad \text{……..……...….(2.22)}$$

Although the true anomaly f has a convenient direct geometric interpretation, it is not always mathematically convenient to express the satellite location through this angle. Instead, the mean anomaly M is typically used in describing the location of a satellite in an orbit.

Although the mean anomaly has no convenient geometric definition, it does vary linearly with time according to the equation:

$$M = M_0 + n(t - t_0) \qquad \text{…….…...….…(2.23)}$$

Where M_0 is the mean anomaly at time t_0, and n is the mean motion of the satellite, which is related to the gravitational coefficient and the semi-major axis of the orbit (see equation (2.22)).

A sample elliptic orbit is illustrated in figure (2.1), with a central body located at focus F1, the eccentricity of an ellipse can vary from $0 \pounds e < 1$ and this is represented in relation (2.17)

From figure (2.2), the radial distance r_w to the point can be related to the Cartesian orbital coordinates x_w, y_w and z_w as:

$$x_w = r\cos f \qquad \text{…….…….…….…(2.24)}$$

$$y_w = r\sin f \qquad \text{…….…….…….…(2.25)}$$

$$z_w = 0 \qquad \text{…….…….…….…(2.26)}$$

$$r_w = \sqrt{x_w^2 + y_w^2} \qquad \text{…..…….…….…….…(2.27)}$$

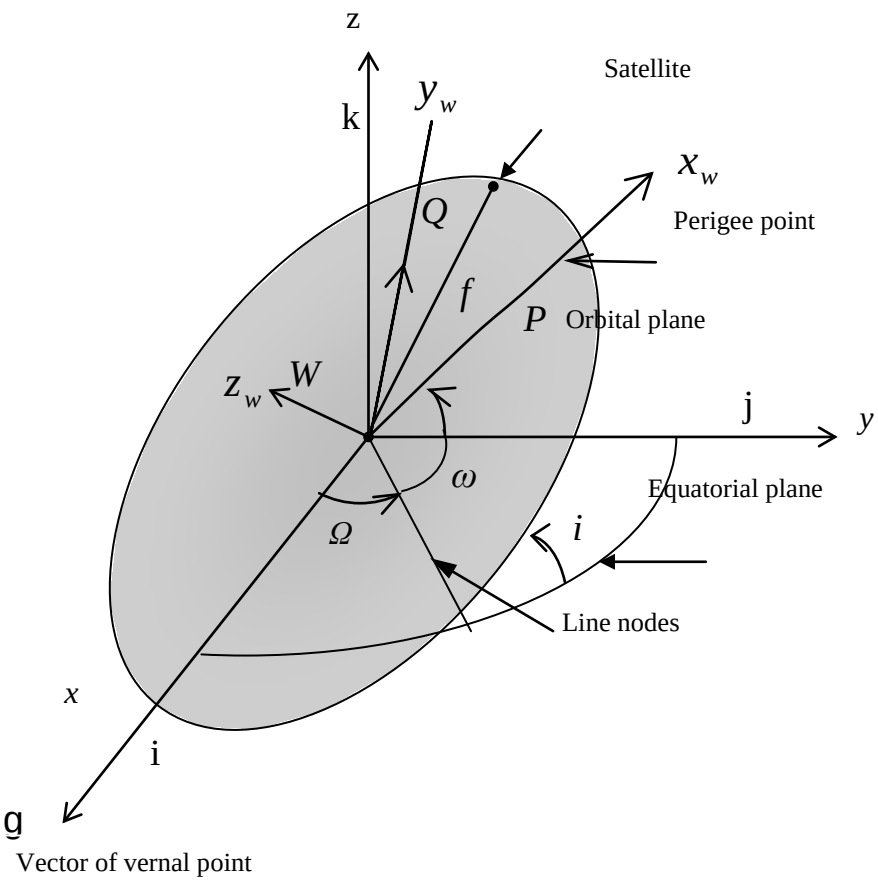

Fig.(2.2): Equatorial and Orbital Plane with Euler's angels [25].

The distance of the perigee (the point of closest approach to the primary focus) and the apogee (the farthest point on the orbit from the focus) can be expressed as:

$$r_p = \frac{p}{1+e} = a(1-e) \qquad \text{.....(2.28)}$$

$$r_a = \frac{p}{1-e} = a(1+e) \qquad \text{.....(2.29)}$$

In addition to the true anomaly (f), the eccentric anomaly (E) is often used to define the location of the satellite in orbit. Imagine the ellipse being“stretched” along the semi minor axis into the shape of a perfect reference circle. The angular distance of the new orbit location relative to the

ellipse center is the eccentric anomaly shown in figure (2.1). The position of satellite related to the eccentric anomaly is given as [68]:

$$r = a(1 - e\cos E) \qquad \text{…….(2.30)}$$

And the relation between true anomaly (f) and eccentric anomaly (E) written as:

$$\tan\frac{f}{2} = \sqrt{\frac{1+e}{1-e}}\tan\frac{E}{2} \qquad \text{…….(2.31)}$$

The mean anomaly of an elliptic orbit is related to the eccentric anomaly as:

$$M = E - e\sin E \qquad \text{…….(2.32)}$$

For the special case of an elliptical orbit when $e = 0$, a circular orbit is formed and it remains constant with $r = a$ so the required velocity for the orbit is

$$v_c = \sqrt{\frac{m}{r}} = 7.905389 Km/Sec \qquad \text{…….(2.33)}$$

Equations (2.24) and (2.25) can be rewritten depending on equations (2.30) and (2.31) as follow:

$$x_w = a(\cos E - e) \qquad \text{…….(2.34)}$$

$$y_w = a\sin E\left(\sqrt{(1 - e^2)}\right) \qquad \text{…….(2.35)}$$

The orbital velocity of the satellite which can be resolved into radial and tangential components as:

$$v^2 = \dot{r}^2 + r^2\dot{f}^2 \qquad \text{…….(2.36)}$$

Where the first and second term can be obtained by taking the derivative of equation (2.18) with respect to time, using equation (2.13):

$$\dot{r} = \frac{p}{(1+e\cos f)^2} e \sin f \, \dot{f}^2 \qquad \text{.....(2.37)}$$

After series of mathematical steps [25], equation (2.36) becomes

$$v^2 = \mu\left(\frac{2}{r} - \frac{1}{a}\right) \qquad \text{.....(2.38)}$$

Which represents the orbital velocity of the satellite at any instant of time, it depends on the semi major axis of orbit (a) and on r.

The equation of velocity can be obtained at perigee v_p and apogee v_a by substituting r_a and r_p from equations (2.28), (2.29) instead of r in equation (2.38) to get:

$$v_p = \left(\frac{\mu}{a}\left(\frac{1+e}{1-e}\right)\right)^{\frac{1}{2}} \qquad \text{.....(2.39)}$$

$$v_a = \left(\frac{\mu}{a}\left(\frac{1-e}{1+e}\right)\right)^{\frac{1}{2}} \qquad \text{.....(2.40)}$$

The angle between orbital velocity vector and the component of velocity $r\dot{f}$ is called flight path angle, and is given as follow:

$$h = \tan^{-1}\left(\frac{e \sin f}{1+e\cos f}\right) \qquad \text{.....(2.41)}$$

This angle is very important to launching the satellite and its continuation in orbit. It equals (0^0) to circular orbit and $< 90^0$ for elliptical orbits [22, 26, 69].

2.3 Solving Kepler's equation

Kepler's relates the time t to the coordinates x_w and y_w in the orbital plane via the eccentric anomaly. In order to obtain the position of the satellite at time t, one needs to know the time of perigee passage t_p and semi major axis a to calculate the mean anomaly M. The value of E may be calculated from equation (2.32), which can be rewritten as:

$$E(t) - e\sin E(t) = n \times (t - t_p) = M(t) \qquad \text{.....(2.42)}$$

And finally obtain x_w and y_w from equations (2.34) and (2.35).

Kepler's equation can be solved by iterative methods only. A common way is to start with an approximation of

$$E_0 = M \qquad \text{.....(2.43)}$$

And employ **Newton's Raphson method** to calculate successive refinements E_i until the result changes by less than a specified amount from one iteration to the next. Defining an auxiliary function

$$f(E) = E - e\sin E - M \qquad \text{.....(2.44)}$$

The solution of Kepler's equation is equivalent to finding the root of $f(E)$ for a given value of M. Applying Newton's Raphson method for this purpose, an approximate root E_i of f may be improved by computing

$$E_{i+1} = E_i - \frac{f(E_i)}{f'(E_i)} = E_i - \frac{E_i - e\sin(E_i) - M}{1 - e\cos(E_i)} \qquad \text{.....(2.45)}$$

And in equation (2.45) for $i =$ next value when $\Delta E_i < e \ (e \gg 0)$, where ΔE_i is given as follows:

$$\Delta E_i = \frac{f(E_i)}{f'(E_i)} \qquad \text{.....(2.46)}$$

Note that this expression has to be evaluated with E in radians $\left(1rad = \rho / 180^0\right)$ and not in degree, to avoid erroneous results.

The starting value $E_0 = M$ recommended above is well suited for small eccentricities, since E only differs from M by a term of order e. For highly eccentric orbits (e.g. $e > 0.8$) the iteration should be started from $E_0 = \rho$ to avoid any convergence problems during the iteration [70, 71, 72].

In the end step, the position coordinates of the satellite can calculated at any instant of time so that to terminate from calculated the value of eccentric anomaly E, using equations (2.34), (2.35) and (2.27) to calculate position coordinates x_w, y_w, r_w.

The velocity coordinates can obtained from derivation of the position coordinates with respect to time as:

$$\dot{x}_w = -\frac{\sqrt{\mu a}}{r}\sin E \qquad \text{.....(2.47)}$$

$$\dot{y}_w = \frac{\sqrt{\left(1 - e^2\right)\mu a}}{r}\cos E \qquad \text{.....(2.48)}$$

$$\dot{z}_w = \frac{\sqrt{\mu a}}{r} e \sin E \qquad \text{.....(2.49)}$$

2.4 Definition of classical orbital elements and matrix transformation

Classical orbital elements are parameters frequently used to identify a specific orbit. It consists of five constants and one quantity varying with time. With these 6 parameters, the position and velocity of satellite in the orbit is uniquely determined. Note that all these parameters are defined in the Earth Centered Inertial (ECI) coordinate.

Semi-major axis (a): it is the distance between the geometric center of the orbital ellipse and the point of perigee.

Eccentricity (e): this parameter describes how flattened the ellipse is compared with a circle and show the shape of the ellipse.

Inclination (i): the angle between the orbital and equatorial plane measured in a plane perpendicular to a line defining their respective intersection. An inclination more than 90^0 means the satellite's motion is retrograde and its direction of revolution around the Earth being opposite to that Earth's rotation.

Right Ascension of Ascending Node (RAAN or Ω): the angle measured in the equatorial plane between the principle axis (vernal equinox) and the line defining the intersection of the equatorial and orbital plane, as a point in the orbit plane passes through the equator in the sense negative to positive with respect to the z-axis.

Argument of perigee (ω): the angle measured in the orbital plane from the line defined by the longitude of the ascending node to another line in the orbital plane.

True anomaly (f): the angle from the eccentricity vector to the satellite position vector. Both mean anomaly M and eccentric anomaly E are used in the calculations of orbit parameters.

The angles i, Ω and ω are the classical orientation angles (Euler's angles), used to define the position of the orbital plane in space (see fig. (2.2)), their range is defined in table (2.1).

Table (2.1): limiting value of Euler's angles [73].

variable	The Range
i	$0 \pounds i \pounds p$
Ω	$0 \pounds \Omega \pounds 2p$
ω	$0 \pounds \omega \pounds 2p$

The satellite's position in space may be expressed as a function of Euler's angles by a sequence of three elementary transformations. It is defined by the unit vectors P, Q and W $= \frac{h}{h}$.

In order to express the position of satellite in equatorial coordinates, this need to using the Gauss's vectors (Matrix Transformation) R , this contains the Euler's angles (i, Ω, ω) [22, 26, 73].

The elements of Matrix Transformation, see references [22, 74], are given as:

$$\begin{aligned} P_x &= \cos\omega \cos\Omega - \sin\omega \sin\Omega \cos i \\ P_y &= \cos\omega \sin\Omega + \sin\omega \cos\Omega \cos i \\ P_z &= \sin\omega \sin i \end{aligned} \qquad \ldots\ldots\ldots\ldots\ldots\ldots\ldots\ldots\ldots\ldots(2.50)$$

$$\begin{aligned} Q_x &= -\sin\omega \cos\Omega - \cos\omega \sin\Omega \cos i \\ Q_y &= -\sin\omega \sin\Omega + \cos\omega \cos\Omega \cos i \\ Q_z &= \cos\omega \sin i \end{aligned} \qquad \ldots\ldots\ldots\ldots\ldots\ldots\ldots\ldots\ldots\ldots(2.51)$$

$$\begin{aligned} W_x &= \sin\Omega \sin i \\ W_y &= -\cos\Omega \sin i \\ W_z &= \cos i \end{aligned} \qquad \ldots\ldots\ldots\ldots\ldots\ldots\ldots\ldots\ldots\ldots(2.52)$$

Since

$$R = \begin{bmatrix} P_x & P_y & P_z \\ Q_x & Q_y & Q_z \\ W_x & W_y & W_z \end{bmatrix} \qquad \ldots\ldots\ldots\ldots\ldots\ldots\ldots\ldots\ldots\ldots(2.53)$$

The position and the velocity coordinates must be converted from orbital plane (x_w, y_w, z_w) to equatorial plane (x, y, z) by using Gauss's matrix R^{-1} as the following:

$$R^{-1} = \begin{bmatrix} P_x & Q_x & W_x \\ P_y & Q_y & W_y \\ P_z & Q_z & W_z \end{bmatrix} \qquad \ldots\ldots\ldots\ldots\ldots\ldots\ldots\ldots\ldots\ldots\ldots\ldots(2.54)$$

Therefore, the relation between equatorial and orbital plane axes given as:

$$\begin{bmatrix} x \\ y \\ z \end{bmatrix} = R^{-1} \begin{bmatrix} x_w \\ y_w \\ z_w \end{bmatrix} \qquad \ldots\ldots\ldots\ldots\ldots\ldots\ldots\ldots\ldots\ldots\ldots\ldots(2.55)$$

Since

$$\begin{aligned} x &= P_x x_w + Q_x y_w + W_x z_w \\ y &= P_y x_w + Q_y y_w + W_y z_w \\ z &= P_z x_w + Q_z y_w + W_z z_w \end{aligned} \qquad \ldots\ldots\ldots\ldots\ldots\ldots\ldots\ldots\ldots\ldots(2.56)$$

Then, the radial distance of satellite from the center of Earth (r) may be written as:

$$r = \sqrt{\left(x^2 + y^2 + z^2\right)} \qquad \ldots\ldots\ldots\ldots\ldots\ldots\ldots\ldots\ldots\ldots\ldots(2.57)$$

Also, by the same way for the velocity vectors, which is written as:

$$\begin{bmatrix} \dot{x} \\ \dot{y} \\ \dot{z} \end{bmatrix} = R^{-1} \begin{bmatrix} \dot{x}_w \\ \dot{y}_w \\ \dot{z}_w \end{bmatrix} \qquad \ldots\ldots\ldots\ldots\ldots\ldots\ldots\ldots\ldots\ldots\ldots\ldots(2.58)$$

Since

$$\begin{aligned} \dot{x} &= P_x \dot{x}_w + Q_x \dot{y}_w + W_x \dot{z}_w \\ \dot{y} &= P_y \dot{x}_w + Q_y \dot{y}_w + W_y \dot{z}_w \\ \dot{z} &= P_z \dot{x}_w + Q_z \dot{y}_w + W_z \dot{z}_w \end{aligned} \qquad \ldots\ldots\ldots\ldots\ldots\ldots\ldots\ldots\ldots\ldots\ldots(2.59)$$

Such as, the magnitude of velocity is:

$$v = \sqrt{\left(\dot{x}^2 + \dot{y}^2 + \dot{z}^2\right)} \qquad \ldots\ldots\ldots\ldots\ldots\ldots\ldots\ldots\ldots\ldots\ldots\ldots(2.60)$$

The angular momentum vector $\vec{h}$ can be analyzed into its components as

$$\vec{h} = \hat{i}h_x + \hat{j}h_y + \hat{k}h_z \qquad \text{……..…….(2.61a)}$$

$$\vec{h} = \begin{bmatrix} h_x \\ h_y \\ h_z \end{bmatrix} = \begin{bmatrix} i & j & k \\ x & y & z \\ \dot{x} & \dot{y} & \dot{z} \end{bmatrix} \qquad \text{……..…..…….(2.61b)}$$

Where the components of x, y and z for $\vec{h}$ are given as:

$$h_x = y\dot{z} - z\dot{y}$$

$$h_y = z\dot{x} - x\dot{z}$$

$$h_z = x\dot{y} - y\dot{x} \qquad \text{……...…….(2.62)}$$

Since

$$h = \left|\vec{h}\right| = \sqrt{\vec{h} \times \vec{h}} \qquad \text{…..……(2.63)}$$

2.5 Calculation of orbital elements from position and velocity coordinates

The total of six independent parameter (orbital elements) are required to describe the motion of a satellite around the Earth. Two of these orbital elements (a, e) describe the form of the orbit, one element (M) defines the position along the orbit and the three others $\left(\Omega, i \text{ and } \omega\right)$ define the orientation of the orbit in space. Given these six elements, it is always possible to uniquely calculate the position and velocity vectors.

There is exactly one set of orbital elements that corresponds to given initial values of r and v.

Firstly, calculated semi major axis and eccentricity (a, e) as:

$$a = \left(\frac{2}{r} - \frac{v^2}{m}\right)^{-1} \qquad \text{....……..……(2.64)}$$

$$e = \sqrt{1 - \frac{h^2}{m a}} \qquad \text{……..(2.65)}$$

The eccentricity (e) is calculated by using p and a, see equations (2.16)-(2.17).

Hence the inclination and the right ascension of ascending node are given by [73]:

$$i = \tan^{-1}\left(\frac{\sqrt{W_x^2 + W_y^2}}{W_z}\right) \qquad \text{…….……..(2.66)}$$

$$W = \tan^{-1}\left(-\frac{W_x}{W_y}\right) \qquad \text{...……(2.67)}$$

Where $\left(W = \frac{h}{h}\right)$ ……..(2.68)

And also $\begin{pmatrix} +\frac{h_x}{h} \\ -\frac{h_y}{h} \\ +\frac{h_z}{h} \end{pmatrix} = \begin{pmatrix} +W_x \\ -W_y \\ +W_z \end{pmatrix}$ ……..……..…(2.69)

The Eccentric anomaly (E) is given by

$$E = \tan^{-1}\left(\frac{r \times v / (a^2 n)}{1 - \frac{r}{a}}\right) \qquad \text{……...……(2.70)}$$

Also it can be written as:

$$E = \tan^{-1}\left(\frac{1 - \frac{|r|}{a}}{(x\dot{x} + y\dot{y} + z\dot{z})} \times \sqrt{m \times a}\right) \qquad \text{……..(2.71)}$$

The Eccentric anomaly may be used to obtain the mean anomaly from equation (2.42), with (t) being the epoch of (r) and (v).

The mean anomaly is:

$$M = E - \frac{(x\dot{x} + y\dot{y} + z\dot{z})}{\sqrt{m \times a}} \qquad \text{.....(2.72)}$$

In order to find the Argument of perigee (w), one has to determined the Argument of latitude (f_w) firstly

$$f_w = \tan^{-1}\left(\frac{z}{-x \times W_y + y \times W_x}\right) \qquad \text{.....(2.73)}$$

The true anomaly is given by

$$f = \tan^{-1}\left(\frac{\sin(E) \times \sqrt{(1 - e^2)}}{\cos(E) - e}\right) \qquad \text{.....(2.74)}$$

Taking proper care of the correct quadrant. The result can be used to obtained the Argument of perigee from the equation below

$$w = f_w - f \qquad \text{.....(2.75)}$$

All these angles are calculated by Radian unit, it must be converted to degree unit as follows:

$$angle(^0) = \frac{180^0}{p} \times angle(Rad)$$

Whereas semi major axis (a) and radial distance (r) calculated by Kilo meters (Km).

4.1 Introduction

Perturbation is deviation from some desired or predicted motion. In astronomical terms this can be applied to say that perturbation is something that causes an orbit to deviate from the motion predicted by Keplerian motion.

In dealing with perturbations there are two categories: *special perturbations* and *general perturbations*. All numerical methods fall into the first category which employs direct step by step numerical integration of the equations of satellite motion. In this category the three most commonly used methods will be discussed for use in the orbit perturbations and one of the best will be selected. The second category deals with the analytical integration of series expansions which represent each orbital elements. This category is more complicated, however it can lead to a better understanding of the perturbed orbit.

Although the general perturbation technique has not been used (as already noted) but it has been employed during the validation procedure. In this case, integration of differential equation for the orbital elements is done to represent the approximate perturbed orbit [24, 96].

4.2 Solution methods of perturbation equation

The relative motion of two bodies when acted by perturbing accelerations can be written as:

$$\frac{d^2\vec{r}}{dt^2} + \frac{m_E}{r^3}\vec{r} = \vec{a}_{perturbed} \quad \ldots\ldots\ldots\ldots\ldots\ldots\ldots\ldots\ldots\ldots\ldots\ldots\ldots\ldots(4.1)$$

Providing the perturbation terms on the right hand side of the equation can be calculated, this results in six (three position vectors and three velocity vectors) differential equations which can be found by numerical integration to fully specify the orbit at any particular time.

Alternatively the mentioned unknowns can be written in terms of six other variables (e.g. the classical orbital elements set, see section 2.5). Re-arranging equation (4.1) then leads to a second set of six first order differential equations that when integrated, either analytically or numerically, make it easier to visualize the orbit. A second option is to rewrite the equation into the summation of the ‘best fit’ Newtonian approximations to the starting initial conditions and some much smaller, deviation terms, see section (2.4). Rearranging the equations that leads to six differential equations in the deviation elements can again be integrated and added to the analytical solution to the ‘best fit’ Newtonian orbit to find the actual orbit.

The advantage of the alternative methods is that unlike absolute position and velocity, the new elements can be chosen to vary much less with time, thus increasing the acceptable time step used in numerical integration, decreasing the accumulation of round-off errors and shortening the computation time for a given propagation period. The three methods outlined are known as *Cowell's method*, *Encke's method* and *the variation of parameters*, respectively. These will now be discussed individually in more detail [96].

4.2.1 Cowell's method

For this method the equations of motion of a satellite with perturbation terms are integrated directly. The six variables required from equation (4.1) are composed of three positional components and three velocity components [53, 73, 78, 101]. Usually the method is applied in a rectangular coordinate frame and for geocentric inertial co-ordinates the resulting six first order differential equations to be solved are:

$$\dot{x} = v_x$$

$$\dot{y} = v_y$$

$$\dot{z} = v_z \qquad \ldots\ldots\ldots\ldots\ldots\ldots\ldots\ldots\ldots\ldots\ldots\ldots\ldots\ldots\ldots\ldots\ldots\ldots\ldots\ldots(4.2)$$

$$\dot{v}_x = a_x = (a_p)_x - \left(\frac{\mu_E}{r^3}\right) \times x$$

$$\dot{v}_y = a_y = (a_p)_y - \left(\frac{\mu_E}{r^3}\right) \times y$$

$$\dot{v}_z = a_z = (a_p)_z - \left(\frac{\mu_E}{r^3}\right) \times z \qquad \ldots\ldots\ldots\ldots\ldots\ldots\ldots\ldots\ldots\ldots\ldots\ldots(4.3)$$

Whereas $(a_p)_x = \sum_i (\ddot{x}_p)_i, (a_p)_y = \sum_i (\ddot{y}_p)_i$ *and* $(a_p)_z = \sum_i (\ddot{z}_p)_i$

The integration steps for this method as follows:

1. $t_i = t_0 \quad , \quad r_i = r_0 \quad , \quad v_i = v_0$
2. $t_{i+1} = t_i + \Delta t$

3. $r_{i+1} = r_i + v_i \Delta t$

4. $v_{i+1} = v_i + \left(-\frac{m \times \vec{r}}{r^3} + a_p \right) \times \Delta t$ ……..(4.4)

Automatically, return steps beginning from step 2 to step 4 at $t_i = nT$ (n number of period).

There are two main advantages for this method, its conceptual simplicity (excluding the equations for the perturbing accelerations equations (4.2) and (4.3) are easily implemented), and the fact that it successfully deals with all types of conic section orbits (circular, elliptical, parabolic and hyperbolic).

The main disadvantage of the method is the requirement of small step intervals (or stepsize) during numerical integration which necessitates a longer period to propagate the orbit than the other methods discussed. The results from the position and velocity elements being a function of the total acceleration acting on the satellite, causing them to vary quickly when near a large gravitational body such as the Earth. Some improvement to the method can be made if a polar axis frame is used in place of the Cartesian. In such a frame (r) varies much slower than Cartesian position and velocity, reducing the problem somewhat. In addition by increasing the number of steps the accumulation of round-off errors also increases and the propagated orbit becomes unreliable much more quickly.

4.2.2 Encke's method

It’s a simple method to solve the initial value problem making intelligent use of the solution of the two-body problem equation (2.7). It is attributed to the German astronomer Johann Franz Encke (1791-1865).

For *Encke's method* the position vector of a satellite is written as:

$$\vec{r}_{pertu.} = \vec{r}_0 + \tilde{N}\vec{r} \qquad \text{.....(4.5)}$$

Where $\vec{r}_0$ is the position vector of an unperturbed Newtonian orbit, commonly referred to as the perturbation orbit. Initially at some time $t_{init.}$ (such as $t_0 = 0$) the true orbit and perturbation orbit are identical. As time progresses the difference between $\vec{r}_0$ and $\vec{r}_{pertu.}$ increases due to perturbation accelerations. The geometry is illustrated in figure (4.1) below.

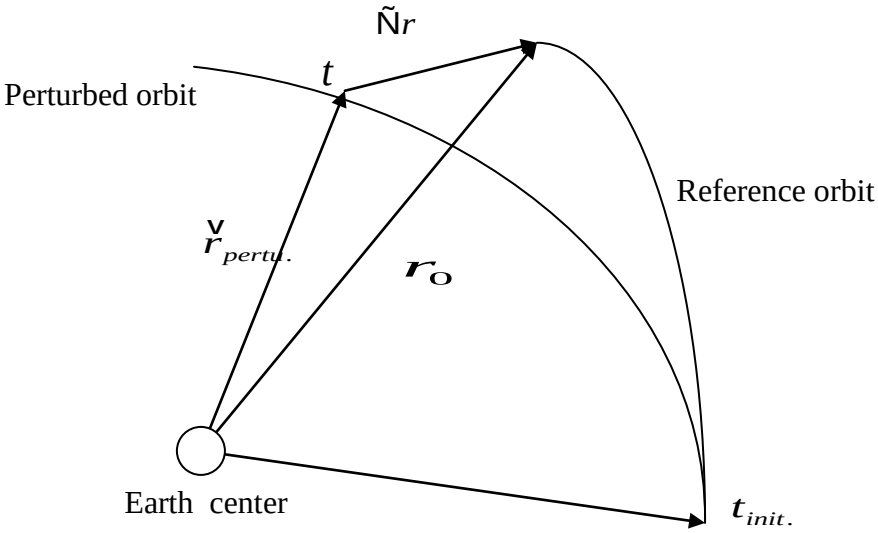

Figure (4.1) : Deviation of perturbed orbit from reference orbit [96].

Substituting equation (4.5) into equation (4.1) and re-arranging gives [96]:

$$\frac{d^2 \tilde{N}\vec{r}}{dt^2} + \frac{m_E}{r^3_0}\tilde{N}\vec{r} = -\frac{m_E}{r^3_0} f(q)\vec{r} + \vec{a}_{perturbed} \quad \text{.....(4.6)}$$

Where

$$f(q) = q \times \frac{3 + 3q + q^2}{1 + (1+q)^{\frac{3}{2}}} \quad \text{.....(4.7)}$$

And

$$q = \frac{\tilde{N}\vec{r} \times (\tilde{N}\vec{r} - 2\vec{r})}{\vec{r} \times \vec{r}} \quad \text{.....(4.8)}$$

Integration of equation (4.6) results in the deviation vector $\tilde{N}\vec{r}$ of the actual orbit from the perturbation orbit.

The advantage of Encke's method lies in the fact that the deviation vector changes much slower than the position vector of the satellite and its derivatives, allowing larger step intervals to be used during integration than in Cowell's method. This in turn reduces the computational load.

The main disadvantage of the method lies in its complexity. As $(t - t_{init.})$ increases the actual and osculating orbits diverge, necessitating the periodic rectification of the osculating orbit so that it again coincides with the actual orbit. In programming terms Encke's method is difficult to implement, requiring the integration procedure to be interrupted periodically while a new oscillating orbit is calculated, adding to the complexity of the program and making it much more likely to contain bugs.

4.2.3 Variation of parameters method

The *Variation of parameters method* may be thought of as a form of Encke's method in which rectification of the osculating orbit is performed continuously rather than at discrete and separate instants of time. The original position and velocity vectors of the satellite motion are transformed into a set of six orbital elements via Lagrange's or Gaussian's matrix [24].

Through careful selection of these elements the resulting equations will have the same advantages as Encke's method without the need for periodically computing a new reference orbit. A popular choice of orbital elements are the *classical elements* (a, e, i, M, w, Ω), however these relate to the orbit geometry is illustrated in figures (2.1) and (2.2). The corresponding six differential equations, correspond to the perturbed orbit, can be found by solving Lagrange's and Gaussian planetary equations [24, 96].

The main advantages of this method are the same as those for Encke's method.

The main disadvantage again is complexity, however once the orbital elements have been defined and the resulting six first order differential equations of motion constructed, the implementation is much simpler than Encke's method. A second, minor problem, is the physical interpretation of the equinoctial elements, however this is overcome by transforming the results into a more 'usable' element set (such as the classical elements) after propagation.

4.3 Numerical integration methods

There are many excellent texts of the subject of numerical integration and it is not the purpose of this section to consider the topic in any detail. However, it is useful to illustrate what methods were considered before programming began to help explain how to chose a method. Since the selected method is required to integrate a series of first order differential equations only this class of equation will be referred to here. It is worth noting that for any set of six orbital elements used in orbit propagation all six must be known simultaneously to enable the calculation of the next set of values.

Numerical integration methods can be divided into two main categories: single step and multi-step. For single step methods only the information relating to the last known mesh point (stepsize) is required to estimate the next set of values where-as for multi-step methods, information about a series of previous mesh points is required, necessitating a boot-up procedure to obtain sufficient information to initially start the multi-step procedure. In the first category, the Runge-Kutta family of methods are commonly used, and in the second category, predictor-corrector techniques (in the case of the variation of parameters, the Adams-Bashforth and Adams-Moulton methods are preferred). In each case the accuracy of the method is determined by its 'order', which refers to the number of successive terms in the original Taylor expansion series (upon which all the methods are based) that were retained when the numerical solution was derived (e.g. a fourth order method will include terms up to and including 'm4' where 'm' is the element being integrated). Increasing the accuracy adversely affects the speed and makes the resulting implementation more complex. Speed, truncation error and stability are all important when considering which technique to use [104].

The results can easily be extrapolated to higher order methods also. The fifth-order Runge Kutta method has been used in this research [67].

4.3.1 Single-Step method

Single-step methods require more computation at each point in the integration than the equivalent multi-step, however they are much simpler to implement in a computer program, leading to less chance of programming error. The most commonly used single-step methods belong to the Runge-Kutta family for which 8th order solutions exist [24]. Under this heading the fourth and fifth order Runge-Kutta-Merson methods will be used in this research. The first, because it is the most commonly used integration scheme of any type on digital computers and the second, because it is included as the boot-up procedure in the propagator. Each equation in equations (4.2) and (4.3) can be approximated to

$$\frac{dy}{dt} = f(t, y) \qquad \text{.....(4.9)}$$

Time 't' is not explicitly used in (4.2) and (4.3), however it is used by the step size. y is the element in question. The fourth order Runge-Kutta solution for the $(i+1)$ mesh point, is given as the ith mesh point value, the integration value for all six equations that represent the vectors of position and velocity (i.e. equations (4.2) and (4.3)) is given as the equation below [73].

$$y_{i+1} = y_i + \frac{1}{6}(k_1 + 2k_2 + 2k_3 + k_4) \qquad \text{.....(4.10)}$$

where (k_1, k_2, k_3, k_4) is calculated as:

$$k_1 = t_{step}{}' \; f(t_i, y_i)$$

$$k_2 = t_{step} \times f\left(t_i + \frac{t_{step}}{2}, y_i + \frac{k_1}{2}\right)$$

$$k_3 = t_{step} \times f\left(t_i + \frac{t_{step}}{2}, y_i + \frac{k_2}{2}\right)$$

$$k_4 = t_{step} \times f\left(t_{i+1}, y_i + k_3\right) \quad \text{.....(4.11)}$$

$$t_{step} = t_{i+1} - t_i \quad \text{.....(4.12)}$$

And the forth-order Runge-Kutta-Fehlberg algorithm is [105]:

$$y_{i+1} = y_i + \left(\frac{25}{216}k_1 + 0k_2 + \frac{1408}{2565}k_3 + \frac{2197}{4104}k_4 - \frac{1}{5}k_5\right) \quad \text{.....(4.13)}$$

Which use five evaluations of k $(k_1, k_2, k_3, k_4, k_5)$ for the fourth-order formula, rather than the usual four, and are given in equation (4.15)

And the fifth-order Runge-Kutta-Fehlberg algorithm is:

$$y_{i+1} = y_i + \left(\frac{16}{135}k_1 + 0k_2 + \frac{6656}{12825}k_3 + \frac{28561}{56430}k_4 - \frac{9}{50}k_5 + \frac{2}{55}k_6\right) \quad \text{..(4.14)}$$

Where $(k_1, k_2, k_3, k_4, k_5, k_6)$ are:

$$k_1 = t_{step} \times f\left(t_i, y_i\right)$$

$$k_2 = t_{step} \times f\left(t_i + \frac{t_{step}}{4}, y_i + \frac{k_1}{4}\right)$$

$$k_3 = t_{step} \times f\left(t_i + \frac{3}{8}t_{step}, y_i + \frac{3}{32}k_1 + \frac{9}{32}k_2\right)$$

$$k_4 = t_{step} \times f\left(t_i + \frac{12}{13} t_{step}, y_i + \frac{1932}{2197} k_1 - \frac{7200}{2197} k_2 + \frac{7296}{2197} k_3\right)$$

$$k_5 = t_{step} \times f\left(t_i + t_{step}, y_i + \frac{439}{216} k_1 - 8k_2 + \frac{3680}{513} k_3 - \frac{845}{4104} k_4\right)$$

$$k_6 = t_{step} \times f\left(t_i + \frac{t_{step}}{2}, y_i - \frac{8}{27} k_1 + 2k_2 - \frac{3544}{2565} k_3 + \frac{1859}{4104} k_4 - \frac{11}{40} k_5\right)$$

……..(4.15)

It is clear that the fifth order equations are much more complex than the fourth. This is one of the problems with numerical integration, as the order of the method increases, in order to reduce long term errors, the complexity increases causing a much slower speed of orbit perturbation.

4.3.2 Multi-Step method

Historically, multi-step numerical integration was used almost exclusively prior to digital computers since it requires less evaluation at each step point, relying more on the accumulated data from the previous mesh points. With digital computers, however, single-step methods began to gain favor due to their conceptual simplicity, ease of implementation (no need for an initialization procedure), and ease with which the step size could be changed.

Conversely, multi-step methods are problematic to implement numerically in a digital computer due to their need for an initialization routine whenever the step size is changed and at the start of the integration. The advantages of multi-step procedures is still speed. A correctly implemented procedure

will be much faster than the equivalent single-step technique.

Multi-step methods can be divided into *explicit* and *implicit* solutions. To apply an implicit method a first estimate is required and this is found from a suitable explicit solution. The use of both multi-step types in this way was called the *Predictor-Corrector* (*PC*) method. Although this requires the evaluation of two functions for each element being integrated (one from the explicit predictor and one from the implicit corrector) at each step in the integration process, this can be used advantageously to monitor the acceptability of the current step size via the difference between predictor and corrector outputs, and if necessary, to calculate a more appropriate value - that will be expanded in the last section.

APC method in the form of a fourth order Adams-Bashforth Predictor, Adams-Moulton corrector will be detailed. In a test using equations (4.1) this technique was found to be around 30% faster than the fifth order Runge-Kutta method when constant step size was used.

The fourth order *Adams-Bashforth* explicit method is [106, 107]:

$$y^{p}{}_{i+1} = y_i + \frac{t_{step}}{24}\left[55 f_i - 59 f_{i-1} + 37 f_{i-2} - 9 f_{i-3}\right]$$

$$f_i = f\left(y_i, t_i\right)$$

$$f_{i-1} = f\left(y_{i-1}, t_{i-1}\right)$$

$$f_{i-2} = f\left(y_{i-2}, t_{i-2}\right)$$

$$f_{i-3} = f\left(y_{i-3}, t_{i-3}\right) \qquad \text{.....(4.16)}$$

where the superscript 'p' stands for predictor. The fourth order *Adams-Moulton* implicit method, which utilizes the predictor value of y_{i+1} is:

$$y^{p}{}_{i+1} = y_i + \frac{t_{step}}{24}\left[9 f_{i+1} + 19 f_i - 5 f_{i-1} + f_{i-2}\right] \qquad \text{.....(4.17)}$$

Where

$$f_{i+1} = f\left(y_{i+1}, t_{i+1}\right) \qquad \text{.....(4.18)}$$

Comparison between equations (4.14), (4.15) and (4.16), (4.17) shows that the 5th order RK routine requires five evaluations of $f(y,t)$ at each step, whereas only one new value is required in the 4th order PC. It is computational reduction which makes multi-step methods less time consuming in operation than single-step methods.

5.1 Introduction

Construction and execution program by using QB Language which called Re-Correct of Satellite Orbital Elements (see Appendix F), the program was calculated the actual orbital elements of artificial satellite with existence of perturbations, which is explained in chapter three. The equation of motion with the existence of individual perturbation and the effect of all perturbation is solved by using fifth-order Runge-Kutta method and forth-order Adams-Bashforth explicit method; these methods were treated by Cowll's technique, as explained in chapter four. The four testing altitudes used here with three satellite orbital elements by just changing inclination (i), and taking eccentricity (e=0.1) are as follows:

Satellite 1: $h_p = 95Km$, $\Omega = 273^0$, $w = 100^0$

Satellite 2: $h_p = 600Km$, $\Omega = 200^0$, $w = 100^0$

Satellite 3: $h_p = 1200Km$, $\Omega = 120^0$, $w = 270^0$

Satellite 4: $h_p = 3000Km$, $\Omega = 120^0$, $w = 270^0$

Firstly, the satellite orbital elements effected by one perturbation change with time (in Hours) is calculated. Three kinds of orbits depending on inclination $(i = 8^o, 63.4^o, 85^o)$ are studied, which are semi-equatorial, critical (as Molinya and Tundra) and polar orbits. The operation return again for all perturbations and also for all effects of perturbations. The magnitudes which are used in the calculations are:

$A = 5.1m^2$

$m = 900Kg$

$J_2 = 1.08264 \times 10^3$

$P_0 = 4.56 \times N / Km^2$

$C_R = 1.3$ (For high-gain in antenna of the satellite material)

$C_D = 2.25$ for Low Earth Orbit (LEO)

$C_D = 2.82$ for Medium Earth Orbit (MEO)

The density of the atmosphere (r) was calculated for different altitudes, which change due to perturbations, it depend on the calculated solar flux $(F_{10.7})$ (see the flowchart F3). So calculation the radial distance about center of Earth for Sun (r_s) and Moon (r_l), and it re-change with Julian Date at any instant time during rotation of satellite when consider launching date of satellite start 1/1/2011 (see the flowchart F4).

Steps of the operation of the program (as explained in appendix F):

1- Calculation of the position and velocity coordinates from Eccentric anomaly (E) by solving Kepler's equation using Newton Raphson's method, considering the first initial condition value at t=0 and $DE_{end} < 10^{-8} = e$, which is used in solving 5-order Runge-Kutta method (see the flowchart F1).
2- Calculation of the satellite orbital element without perturbations from position and velocity coordinates.
3- Calculation of the acceleration perturbations as manifest in flowchart F4.
4- Sum the acceleration un-perturbation vectors and acceleration perturbations vectors to find the actual position and velocity coordinates

by using 5th-order Runge-Kutta method (see the flowchart F5 and the main program as flowchart F7).

5- Finally, calculation of the satellite orbital elements with perturbations (see the flowchart F6).

Also gave results which explain the variation in orbital elements for one period, see tables (5.1)-(5.12), and comparison each results with other researchers such Eshagh and Najafi [53], see tables (5.13).

The perturbations of orbital elements are calculated for all altitudes and inclinations. These are plotted and discussed for different altitudes and for two type of inclinations $\left(i = 8^{o}, 63.4^{o}\right)$.

Thus, the program is designed to calculate the position and velocity coordinates and orbital elements perturbed for any satellite at given initial condition such orbital elements, area, mass, surface material of the satellite and lunching time.

5.2 Discussion of the figures

a- Comparison between five order Runge-Kutta method and four order Adams-Bashforth method

Figures (5.a.1)-(5.a.6) show the comparison between 5th-order Runge-Kutta method and 4th-order Adams-Bashforth explicit method. From these figures it can be seen that the two methods are approximated in results, therefore, 5th-order Runge- Kutta method used here, because it is stable and needs fewer initial conditions.

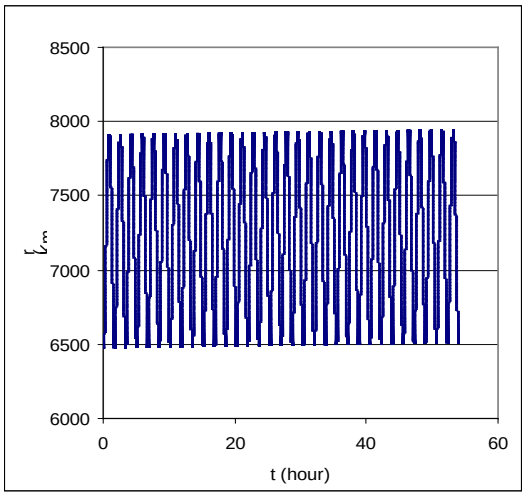

Fig.(5.a.1): Radial distance change with time, without perturbation by using 5-order R-K method at hp=95 Km and $i = 8^{o}$

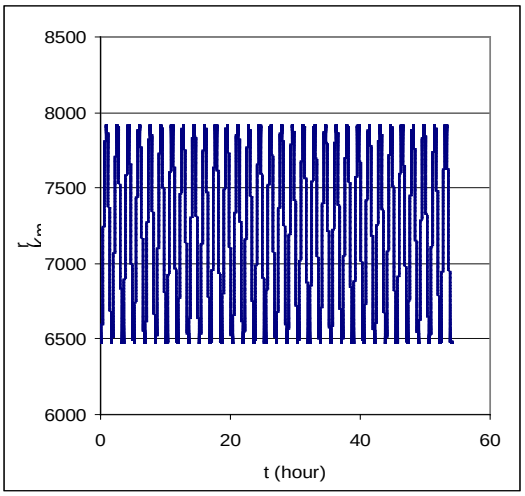

Fig.(5.a.2): Radial distance change with time, without perturbation by using 4-order A-B method at hp=95 Km and $i = 8^{o}$

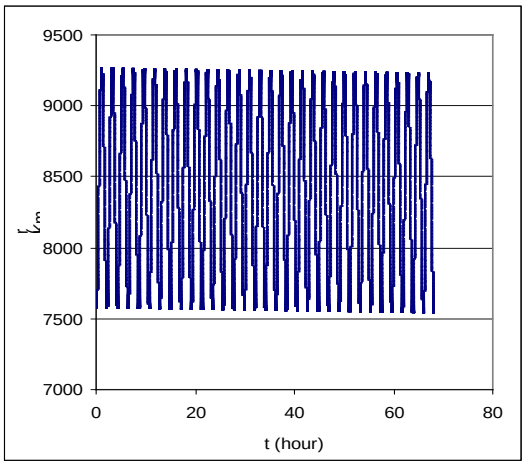

Fig.(5.a.3): Radial distance change with time, without perturbation by using 5-order R-K method at hp=1200 Km and $i = 8^{o}$

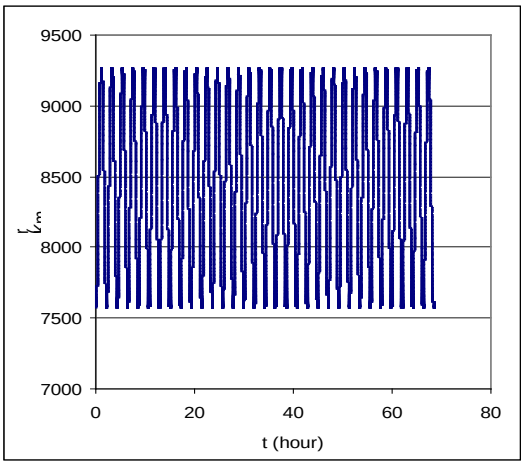

Fig.(5.a.4): Radial distance change with time, without perturbation by using 4-order A-B method at hp=1200 Km and $i = 8^{o}$

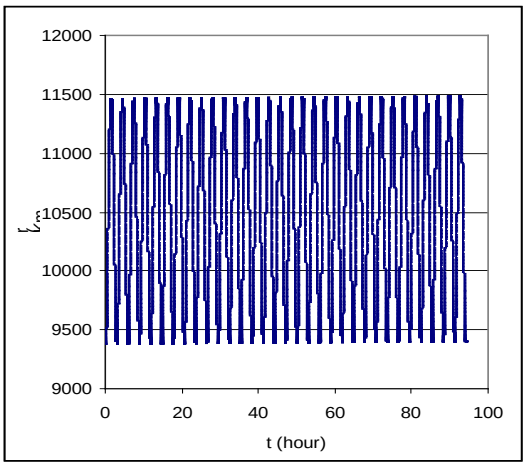

Fig.(5.a.5): Radial distance change with time, without perturbation by using 5-order R-K method at hp=3000 Km and $i = 8^{o}$

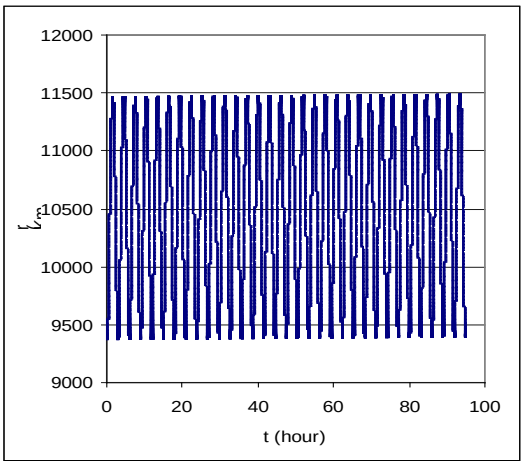

Fig.(5.a.6): Radial distance change with time, without perturbation by using 4-order A-B method at hp=3000 Km and $i = 8^{o}$

b- Atmospheric drag perturbation

Figures (5.b.1) and (5.b.2) shows that the semi-major axis (a) decreases with time, the change is secular and it remains constant through any one rotation but is reduced with time. The magnitude of (a) changes from 7190Km to 7040Km at hp=95 Km and $i = 8^{o}$ about equatorial plane, and it changes from 7190Km to 7025Km at hp=95Km and $i = 63.4^{o}$ (called critical inclination), and it is observed that the magnitude of perturbation at $i = 8^{o}$ is bigger than its value at $i = 63.4^{o}$, therefore atmospheric drag is larger at $i = 8^{0}$.

Figures (5.b.3), (5.b.4), (5.b.5) and (5.b.6) shows that the semi-major axis (a) decreases with time that the decreasing is very small compared with that shown in figures (5.b.1) and (5.b.2), because the density of the atmosphere is reduced at hp=600Km, and is reduced even more at hp=1200Km for all values of inclination $i = 8^{o}, 63.4^{o}$.

Figures (5.b.7) and (5.b.8) shows the eccentricity (e) decreases linearly with time the change is similar at $i = 8^{o}$ and $i = 63.4^{o}$. But there is no change or very small (reach to 1e-4) in the magnitudes of eccentricity at hp=600Km and 1200Km (see figures from (5.b.9) to (5.b.12)). The same behaviors in the inclination (i) (see figures from (5.b.13) to (5.b.18)). But the variation different in discussion of Right ascension of ascending node (RAAN), where RAAN increases with time, this increase is more obvious at low altitude (see figures from (5.b.19) to (5.b.24)).

Also there is no change in value of Argument of perigee (w) and Mean anomaly (see figures from (5.b.25) to (5.b.36)).

Deduce the atmospheric drag perturbation more effected on the semi-major axis (a) and eccentricity (e) than Euler's angles, because the drag force in the direction of the satellite orbit (not normal) and near to zero at hp >1000 Km.

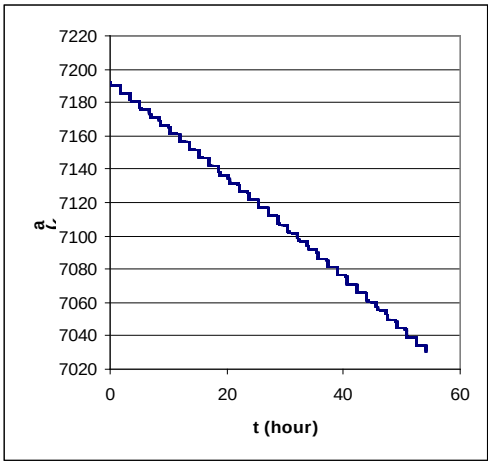

Fig.(5.b.1): Semi-major axis change due to atmospheric drag at hp=95 Km and $i = 8^{o}$

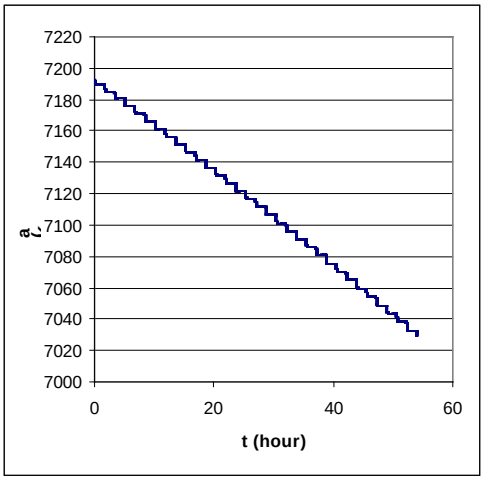

Fig.(5.b.2): Semi-major axis change due to atmospheric drag at hp=95 Km and $i = 63.4^{o}$

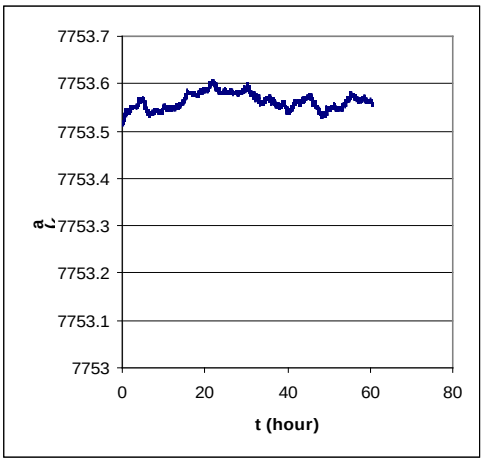

Fig.(5.b.3): Semi-major axis change due to atmospheric drag at hp=600 Km and $i = 8^{o}$

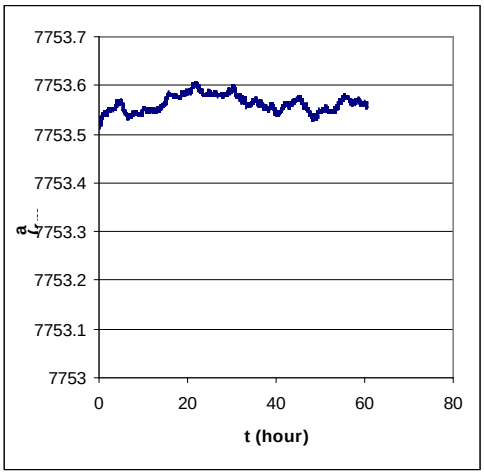

Fig.(5.b.4): Semi-major axis change due to atmospheric drag at hp=600 Km and $i = 63.4^{o}$

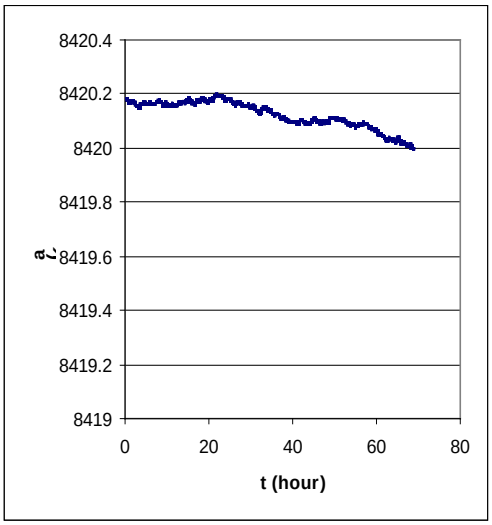

Fig.(5.b.5): Semi-major axis change due to atmospheric drag at hp=1200 Km and $i = 8^{o}$

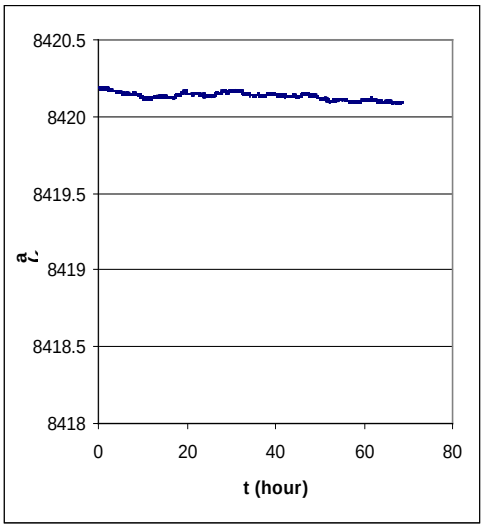

Fig.(5.b.6): Semi-major axis change due to atmospheric drag at hp=1200 Km and $i = 63.4^{o}$

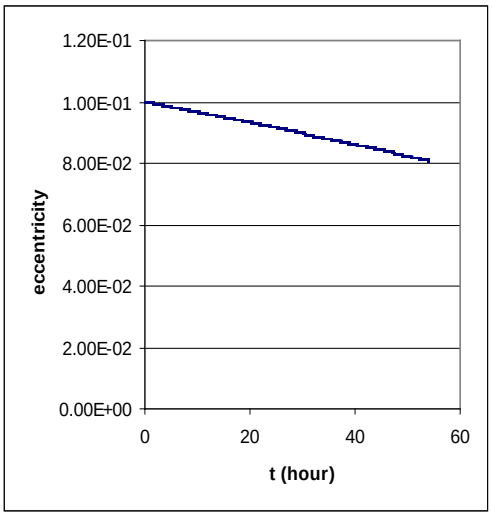

Fig.(5.b.7): Eccentricity change due to atmospheric drag at hp=95 Km and $i = 8^{o}$

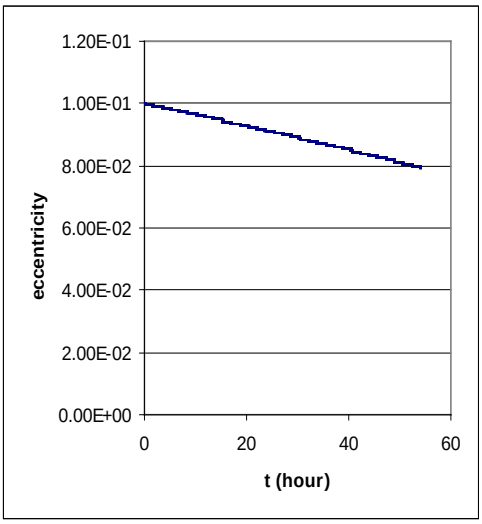

Fig.(5.b.8): Eccentricity change due to atmospheric drag at hp=95 Km and $i = 63.4^{o}$

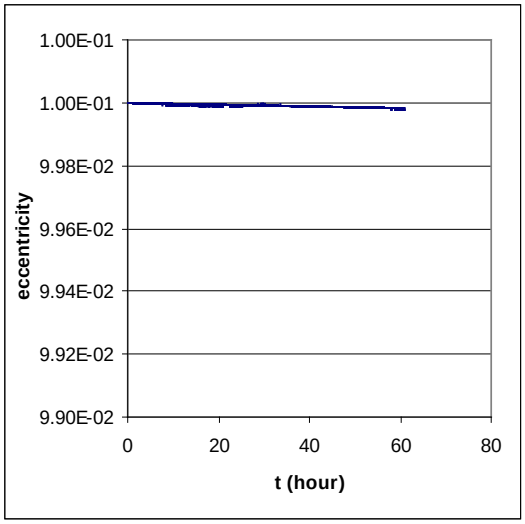

Fig.(5.b.9): Eccentricity change due to atmospheric drag at hp=600 Km and $i = 8^{o}$

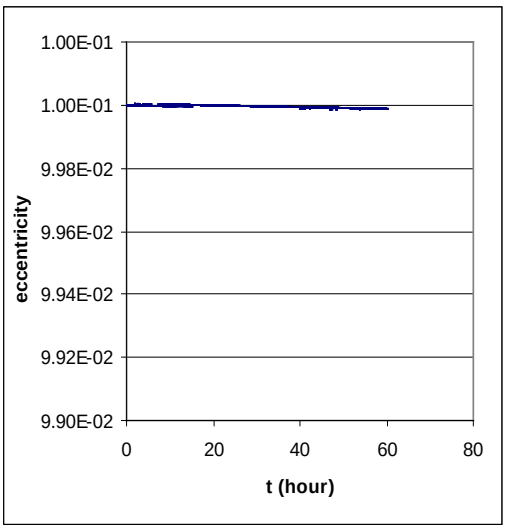

Fig.(5.b.10): Eccentricity change due to atmospheric drag at hp=600 Km and $i = 63.4^{o}$

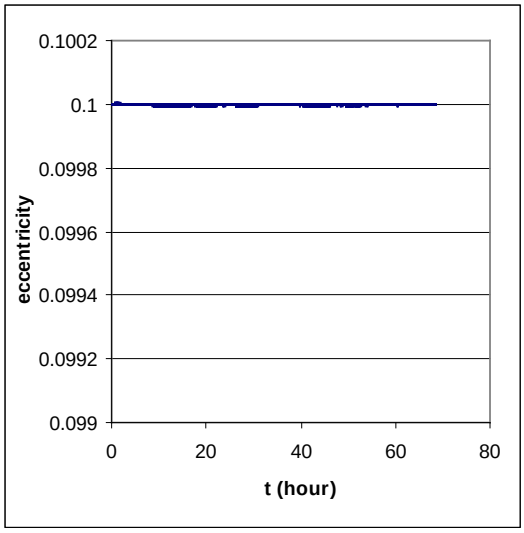

Fig.(5.b.11): Eccentricity change due to atmospheric drag at hp=1200 Km and $i = 8^{o}$

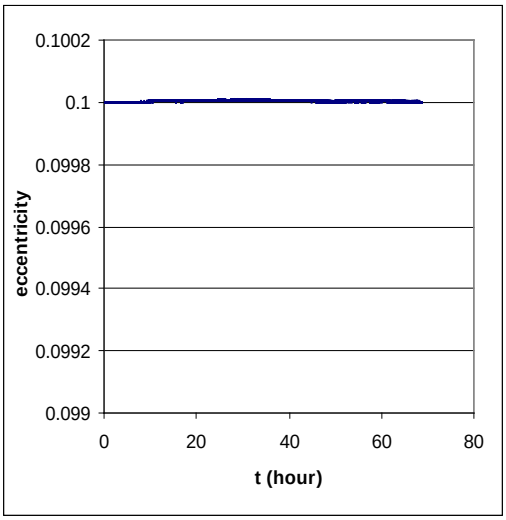

Fig.(5.b.12): Eccentricity change due to atmospheric drag at hp=1200 Km and $i = 63.4^{o}$

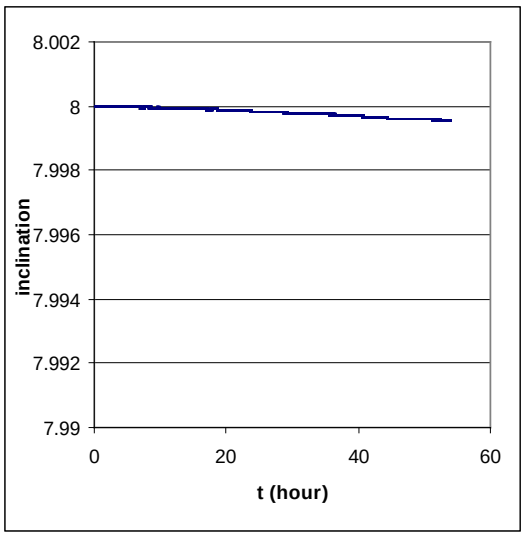

Fig.(5.b.13): Inclination change due to atmospheric drag at hp=95 Km and $i = 8^{o}$

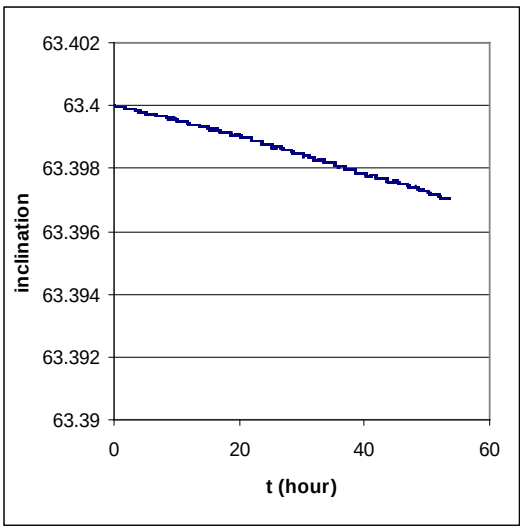

Fig.(5.b.14): Inclination change due to atmospheric drag at hp=95 Km and $i = 63.4^{o}$

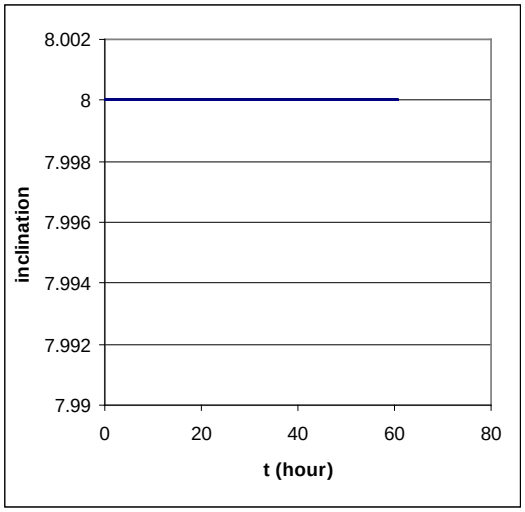

Fig.(5.b.15): Inclination change due to atmospheric drag at hp=600 Km and $i = 8^{o}$

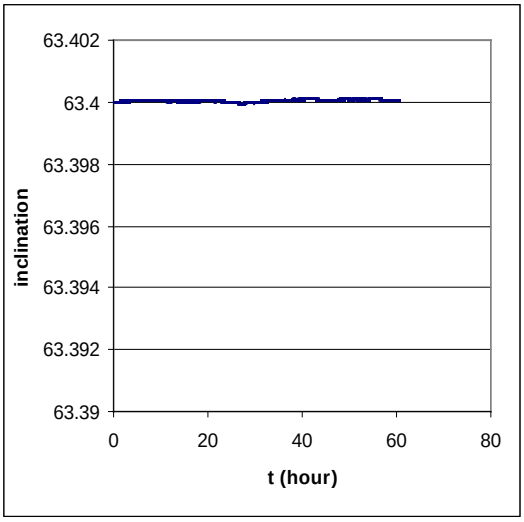

Fig.(5.b.16): Inclination change due to atmospheric drag at hp=600 Km and $i = 63.4^{o}$

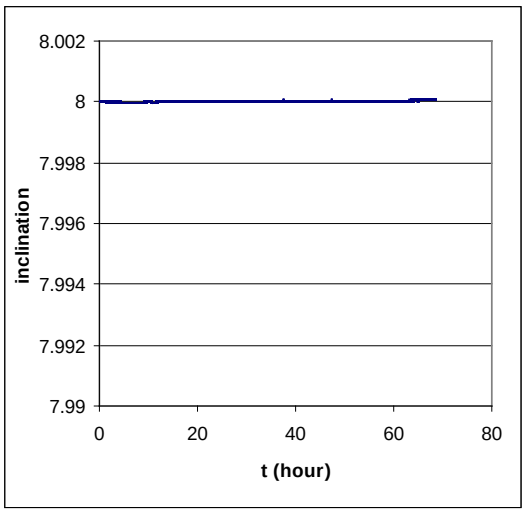

Fig.(5.b.17): Inclination change due to atmospheric drag at hp=1200 Km and $i = 8^{o}$

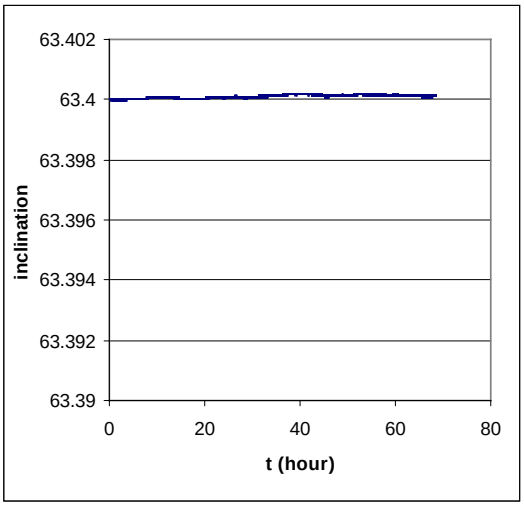

Fig.(5.b.18): Inclination change due to atmospheric drag at hp=1200 Km and $i = 63.4^{o}$

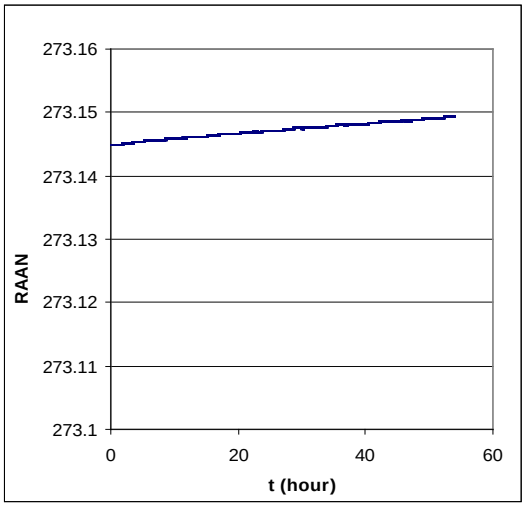

Fig.(5.b.19): Right ascension of ascending node change due to atmospheric drag at hp=95 Km and $i = 8^{o}$

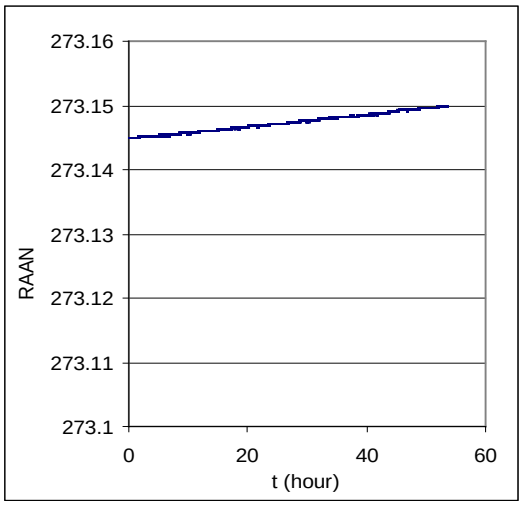

Fig.(5.20): Right ascension of ascending node change due to atmospheric drag at hp=95 Km and $i = 63.4^{o}$

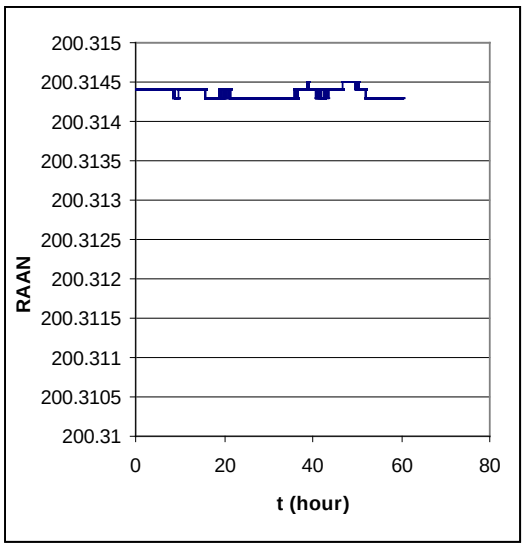

Fig.(5.b.21): Right ascension of ascending node change due to atmospheric drag at hp=600 Km and $i = 8^{o}$

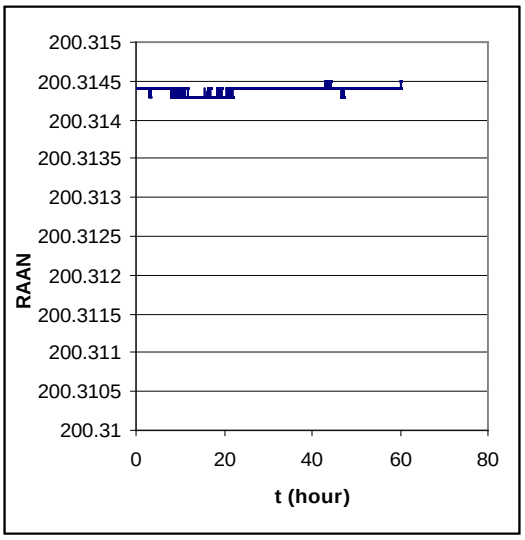

Fig.(5.b.22): Right ascension of ascending node change due to atmospheric drag at hp=600 Km and $i = 63.4^{o}$

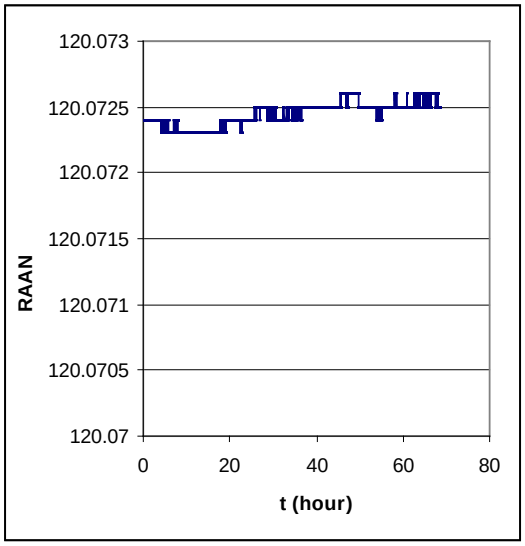

Fig.(5.b.23): Right ascension of ascending node change due to atmospheric drag at hp=1200 Km and $i = 8^{o}$

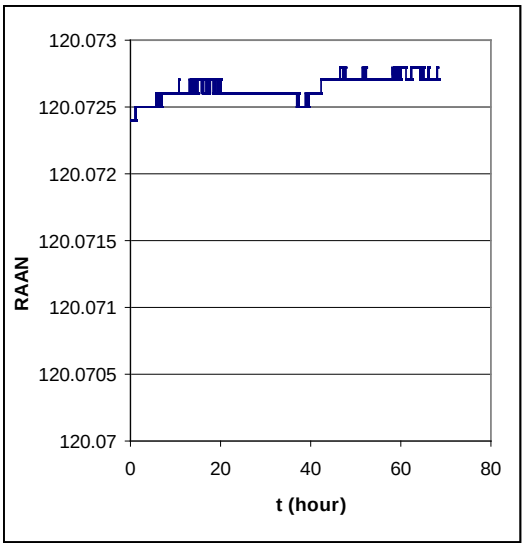

Fig.(5.b.24): Right ascension of ascending node change due to atmospheric drag at hp=1200 Km and $i = 63.4^{o}$

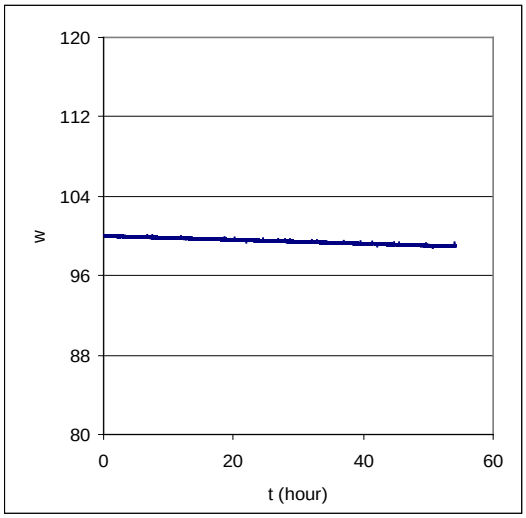

Fig.(5.b.25): Argument of perigee change due to atmospheric drag perturbation at hp=95Km and $i = 8^{o}$

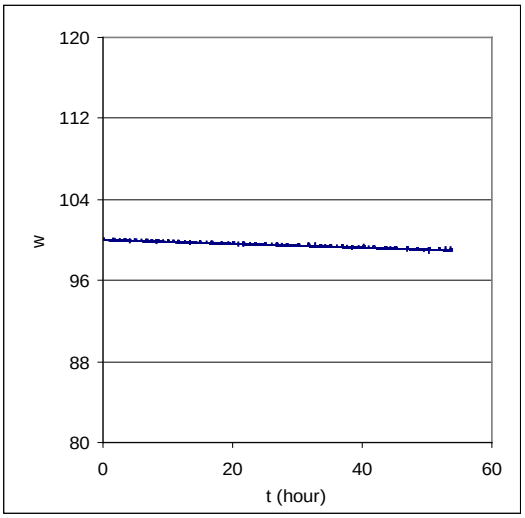

Fig.(5.b.26): Argument of perigee change due to atmospheric drag perturbation at hp=95Km and $i = 63.4^{o}$

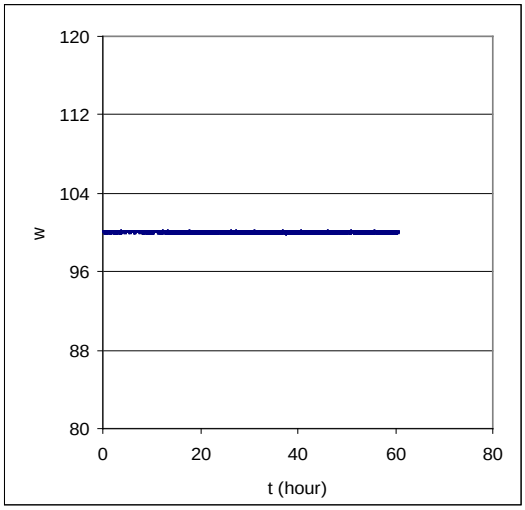

Fig.(5.b.27): Argument of perigee change due to atmospheric drag perturbation at hp=600 Km and $i = 8^{o}$

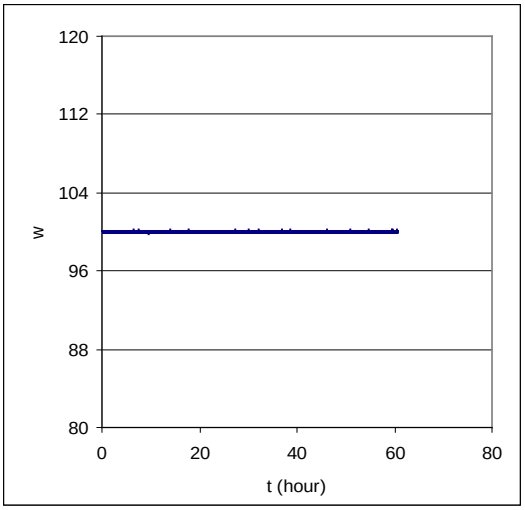

Fig.(5.b.28): Argument of perigee change due to atmospheric drag perturbation at hp=600 Km and $i = 63.4^{o}$

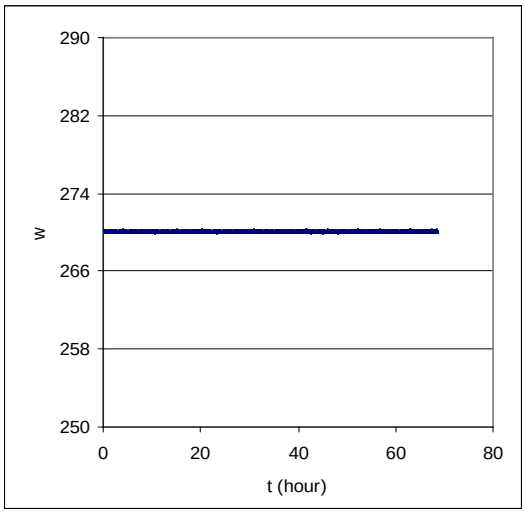

Fig.(5.b.29): Argument of perigee change due to atmospheric drag perturbation at hp=1200 Km and $i = 8^{o}$

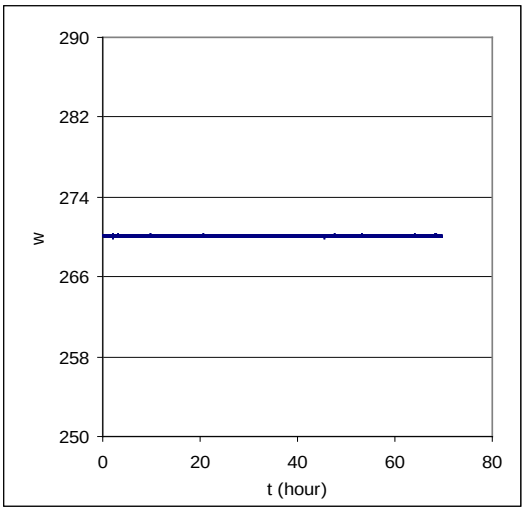

Fig.(5.b.30): Argument of perigee change due to atmospheric drag perturbation at hp=1200 Km and $i = 63.4^{o}$

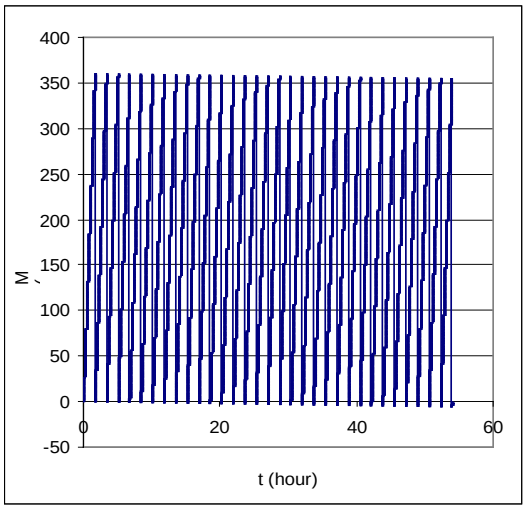

Fig.(5.b.31): Mean anomaly change due to atmospheric drag perturbation at hp=95 Km and $i = 8^{o}$

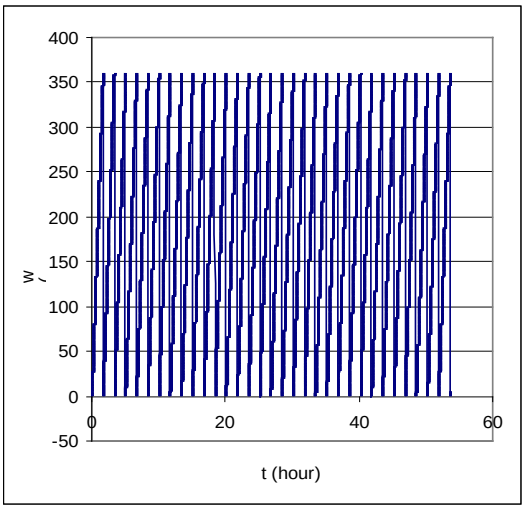

Fig.(5.b.32): Mean anomaly change due to atmospheric drag perturbation at hp=95 Km and $i = 63.4^{o}$

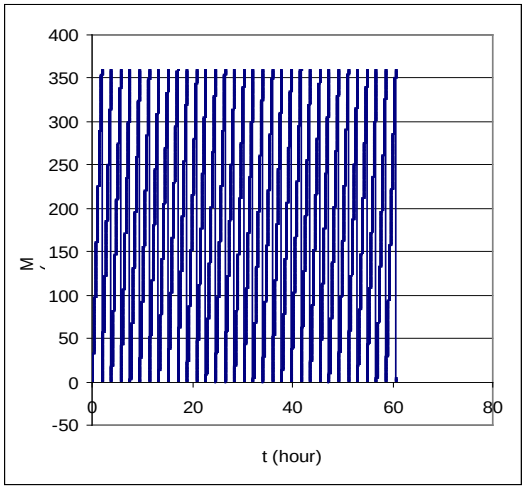

Fig.(5.b.33): Mean anomaly change due to atmospheric drag perturbation at hp=600 Km and $i = 8^{o}$

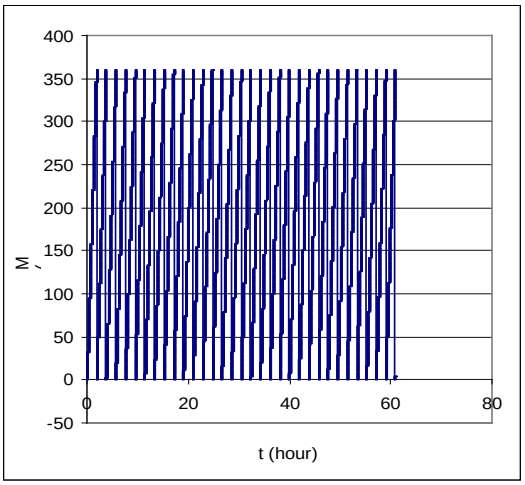

Fig.(5.b.34): Mean anomaly change due to atmospheric drag perturbation at hp=600 Km and $i = 63.4^{o}$

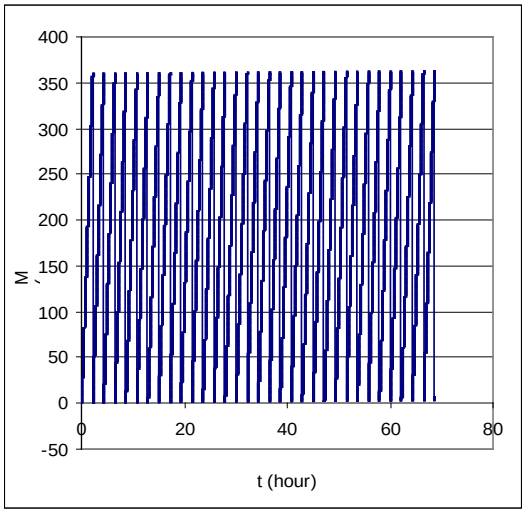

Fig.(5.b.35): Mean anomaly change due to atmospheric drag perturbation at hp=1200 Km and $i = 8^{o}$

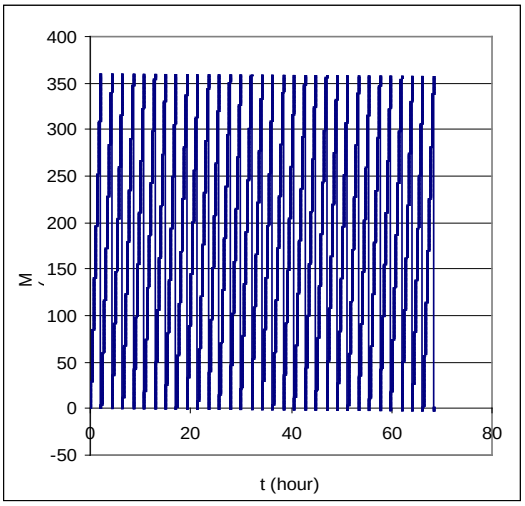

Fig.(5.b.36): Mean anomaly change due to atmospheric drag perturbation at hp=1200 Km and $i = 63.4^{o}$

c- Oblatness of Earth perturbation

Figure (5.c.1) shows that the semi-major axis (a) stable with time just for $i = 8^{o}$, and change as periodic variation between perigee and apogee (7192.5-7189 Km). Figure (5.c.2) shows that the semi-major axis (a) decreases with time and also periodic variation. It changes between (7210.5-7192 Km) during 33 rotation. The periodic change $(\Delta a = 17.5 Km)$ for $i = 63.4^{o}$ is greater than the variation $(\Delta a = 3.5 Km)$ at $i = 8^{o}$. The same behavior is noticed for hp=600 Km (see figures (5.c.3) and (5.c.4)), but the periodic change $(\Delta a = 17 Km)$ for $i = 63.4^{o}$ is greater than the variation $(\Delta a = 3.25 Km)$ at $i = 8^{o}$. The same behavior is observed at hp=1200 Km (see figures (5.c.5) and (5.c.6)), periodic change $(\Delta a = 15 Km)$ for $i = 63.4^{o}$ is greater than the variation $(\Delta a = 3 Km)$ at $i = 8^{o}$. It is observed that the magnitude of perturbation decreases with increasing hp from 95 Km, 600Km to 1200Km for $i = 63.4^{o}$ which is larger than $i = 8^{o}$. Therefore, the oblatness of Earth is less effected for the orbits $i > 60^{o}$.

For altitudes hp=95, 600, 1200 (Km) and $i = 8^{o}$, it observed that the eccentricity (e) changes periodically under the mean value between e=0.1 and e=.098 (see figures (5.c.7), (5.c.9) and (5.c.11)). But the eccentricity (e) changes periodically above the mean value between e=0.1 and e=0.102 for $i = 63.4^{o}$ (see figures (5.c.8), (5.c.10) and (5.c.12)). Also for altitude hp=95, 600, 1200 (Km) and $i = 8^{o}$, it observed that the inclination (i) change periodically between $i = 8^{o}, 8.01^{o}, 8.009^{o}, 8.008^{o}$ sequentially with increasing altitudes (hp) (see figures (5.c.13), (5.c.15) and (5.c.17)). Also the inclination (i) changes periodically between $i = 63.4^{o}, 63.43^{o}, 63.425^{o}, 63.4225^{o}$ sequentially with increasing altitudes (hp) (see figures (5.c.14), (5.c.16) and (5.c.18)).

For altitudes hp=95, 600, 1200 (Km) and $i = 8^{o}, 63.4^{o}$, it show clearly RAAN decreases linearly, and the variation in RAAN at $i = 8^{o}$ decreases with increasing altitude $(DW = 15^{o}, 13^{o}, 11^{o})$ and also $(DW = 7^{o}, 5.5^{o}, 5^{o})$ at $i = 63.4^{o}$ (see figures from (5.c.19) to (5.c.24)). And observed RAAN decreases rapidly compared with other orbital elements, because the oblatness of Earth are most effective on the RAAN, where ascending line more moving for $i = 8^{o}$, the results compared with Eshagh and Najafi [53] whose take $i = 87.3^{o}$ and hp=454 Km, the variation of RAAN equal 1.5 degree.

Argument of perigee (w) increases linearly and periodically with time at inclination $i = 8^{o}$ this because the oblatness of Earth more effected at inclination $i = 8^{o}$ than $i = 63.4^{o}$, and the variation in argument of perigee (w) decreases with increasing altitude from $Dw = 30^{o}$ at hp=95 Km to $Dw = 20^{o}$ at hp=1200 Km (see figures (5.c.25), (5.c.27) and (5.c.29)), but it is remain constant at $i => 63.4^{o}$ (see figures (5.c.26), (5.c.28) and (5.c.30)). There is very small change for Mean anomaly with time at all altitudes (see figures from (5.c.31) to (5.c.36)).

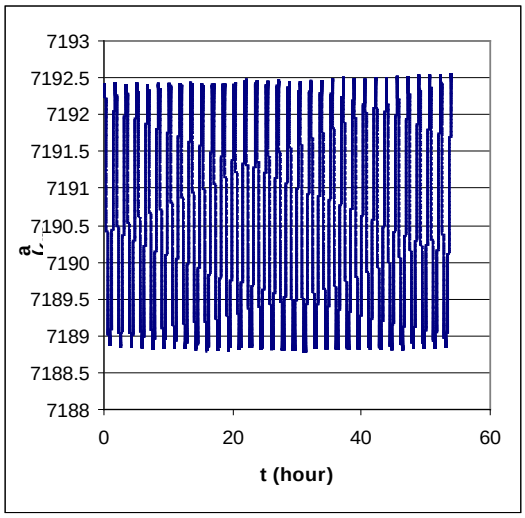

Fig.(5.c.1): Semi-major axis change due to oblatness of Earth at hp=95 Km and $i = 8^0$

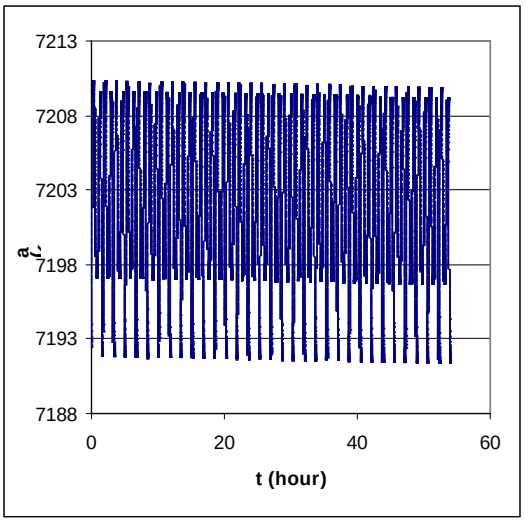

Fig.(5.c.2): Semi-major axis change due to oblatness of Earth at hp=95 Km and $i = 63.4^0$

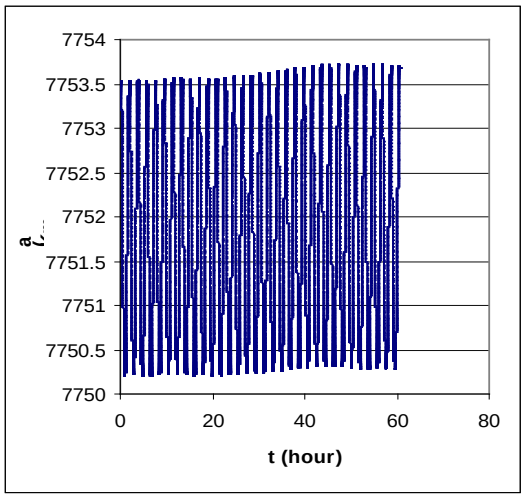

Fig.(5.c.3): Semi-major axis change due to oblatness of Earth at hp=600 Km and $i = 8^0$

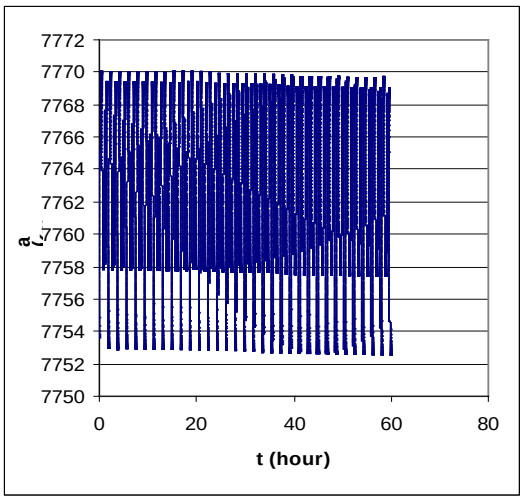

Fig.(5.c.4): Semi-major axis change due to oblatness of Earth at hp=600 Km and $i = 63.4^0$

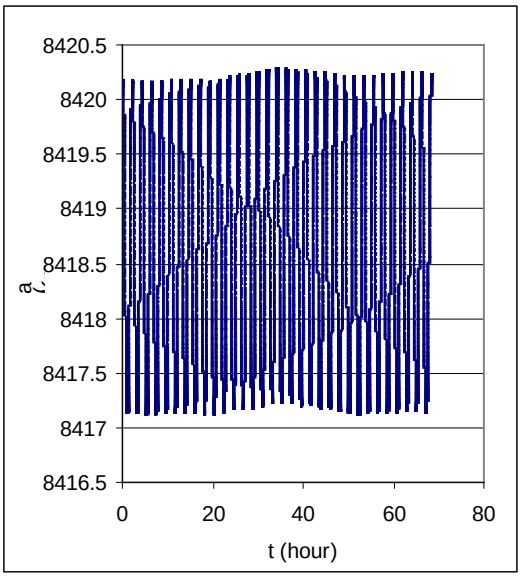

Fig.(5.c.5): Semi-major axis change due to oblatness of Earth at hp=1200 Km and $i = 8^0$

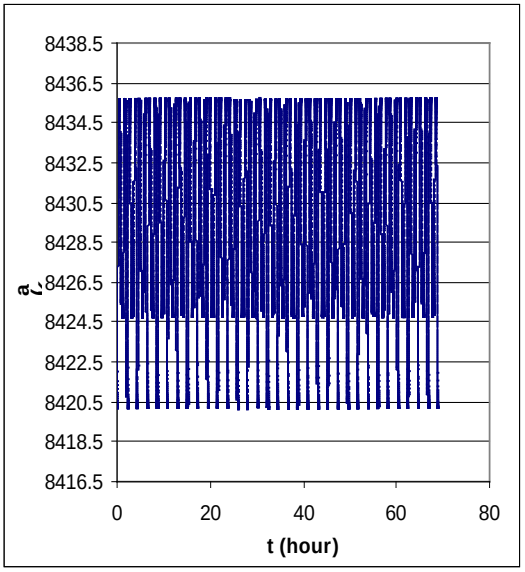

Fig.(5.c.6): Semi-major axis change due to oblatness of Earth at hp=1200 Km and $i = 63.4^0$

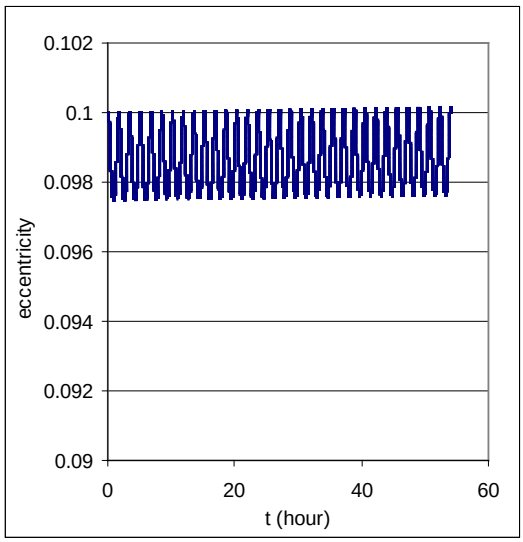

Fig.(5.c.7): Eccentricity change due to oblatness of Earth at hp=95 Km and $i = 8^0$

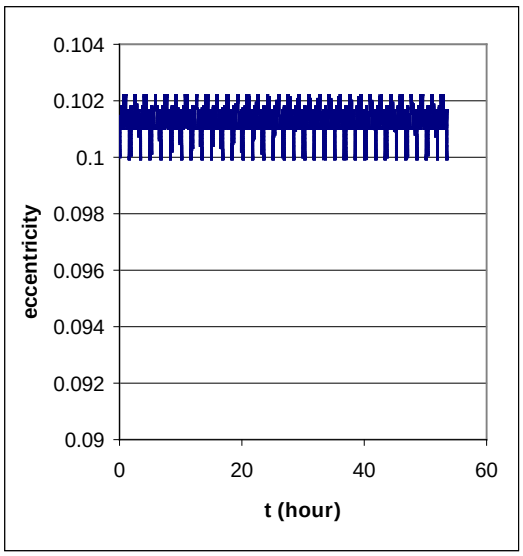

Fig.(5.c.8): Eccentricity change due to oblatness of Earth at hp=95 Km and $i = 63.4^0$

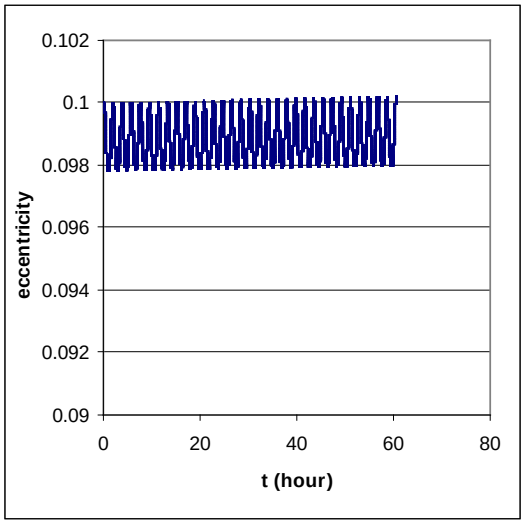

Fig.(5.c.9): Eccentricity change due to oblatness of Earth at hp=600 Km and $i = 8^0$

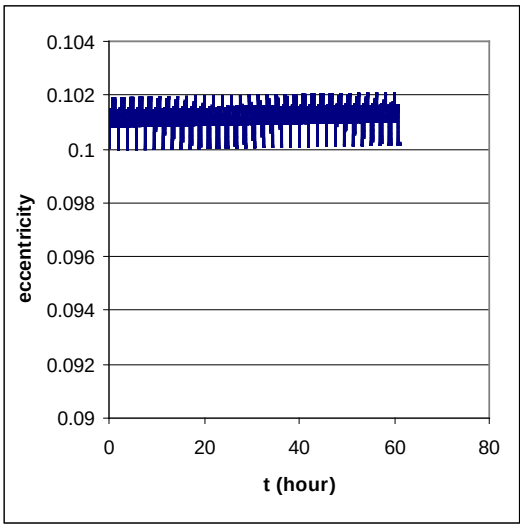

Fig.(5.c.10): Eccentricity change due to oblatness of Earth at hp=600 Km and $i = 63.4^0$

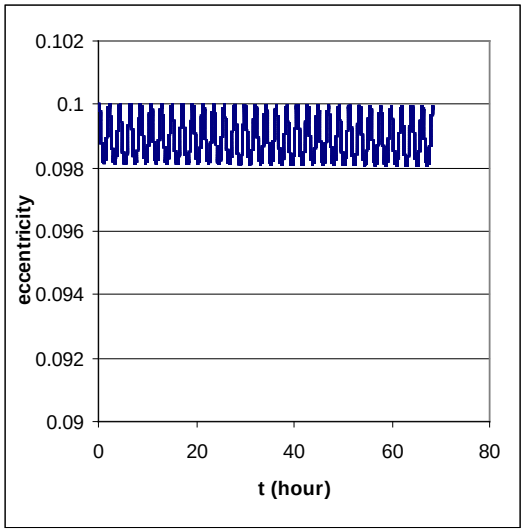

Fig.(5.c.11): Eccentricity change due to oblatness of Earth at hp=1200 Km and $i = 8^0$

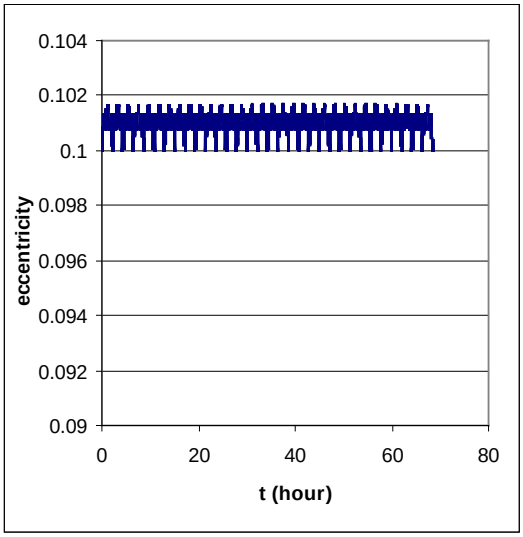

Fig.(5.c.12): Eccentricity change due to oblatness of Earth at hp=1200 Km and $i = 63.4^0$

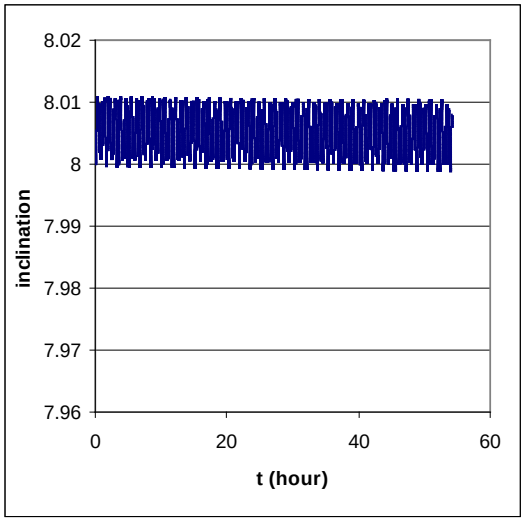

Fig.(5.c.13): Inclination change due to oblatness of Earth at hp=95 Km and $i = 8^0$

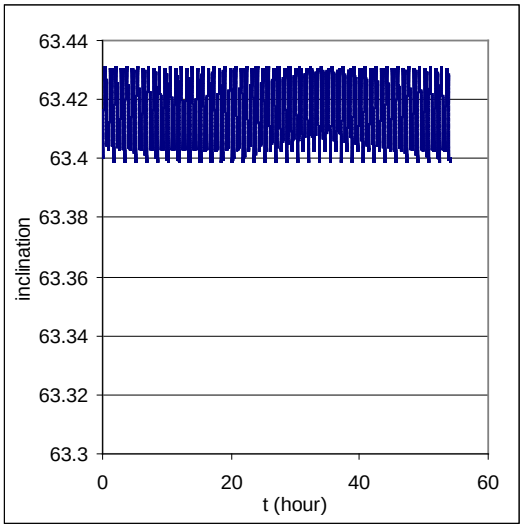

Fig.(5.c.14): Inclination change due to oblatness of Earth at hp=95 Km and $i = 63.4^0$

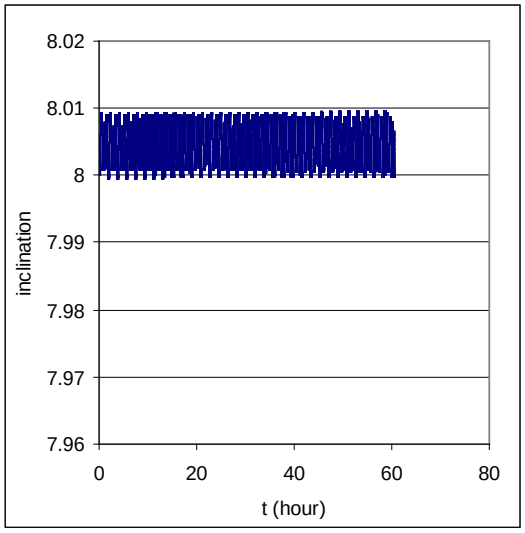

Fig.(5.c.15): Inclination change due to oblatness of Earth at hp=600 Km and $i = 8^0$

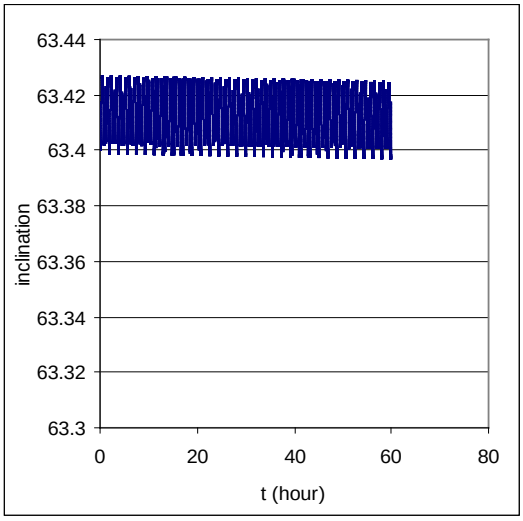

Fig.(5.c.16): Inclination change due to oblatness of Earth at hp=600 Km and $i = 63.4^0$

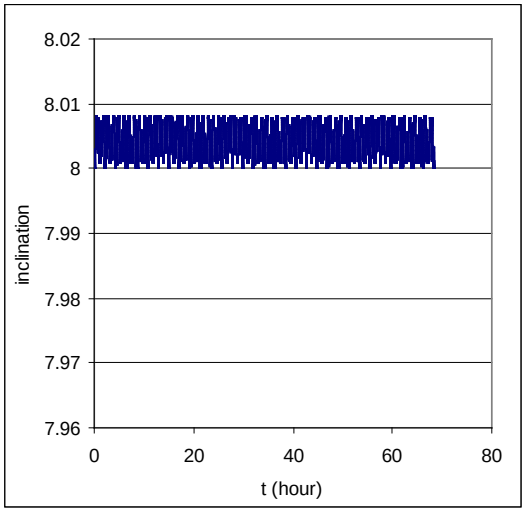

Fig.(5.c.17): Inclination change due to oblatness of Earth at hp=1200 Km and $i = 8^0$

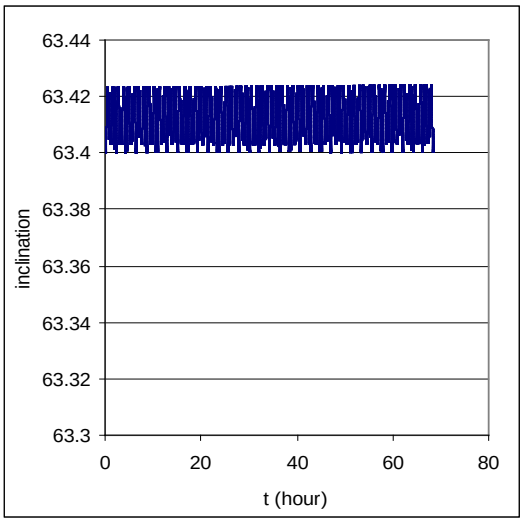

Fig.(5.c.18): Inclination change due to oblatness of Earth at hp=1200 Km and $i = 63.4^0$

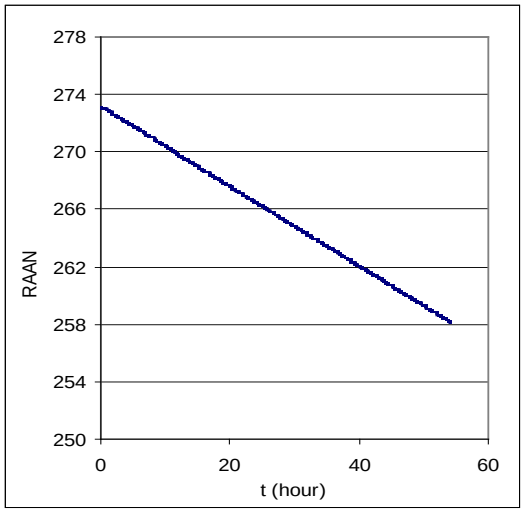

Fig.(5.c.19): Right ascension of ascending node change due to oblatness of Earth at hp=95 Km and $i = 8^0$

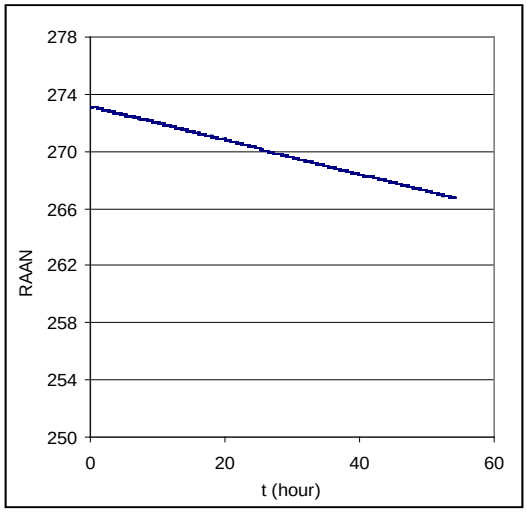

Fig.(5.c.20): Right ascension of ascending node change due to oblatness of Earth at hp=95 Km and $i = 63.4^0$

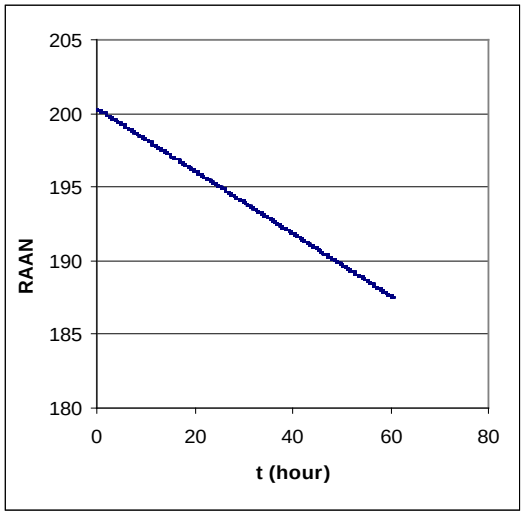

Fig.(5.c.21): Right ascension of ascending node change due to oblatness of Earth at hp=600 Km and $i = 8^0$

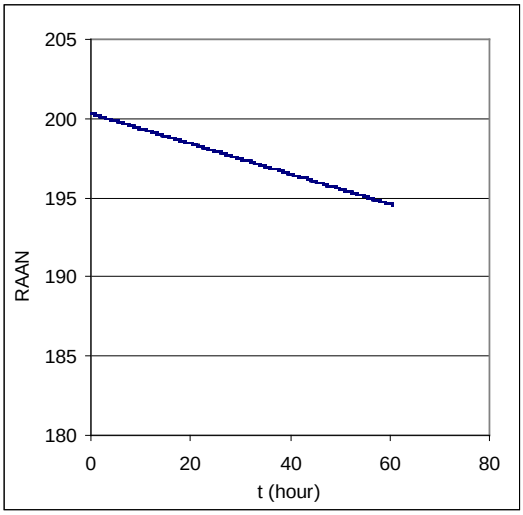

Fig.(5.c.22): Right ascension of ascending node change due to oblatness of Earth at hp=600 Km and $i = 63.4^0$

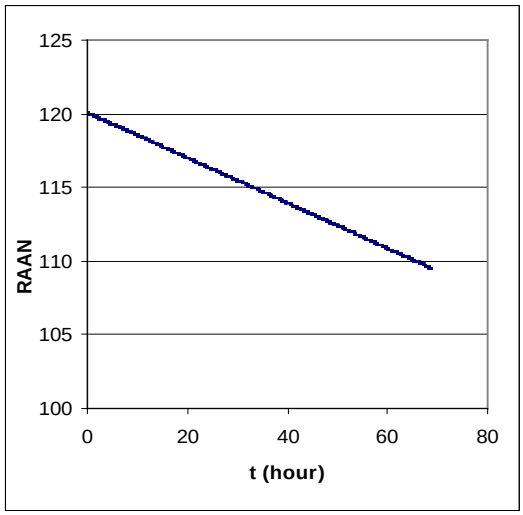

Fig.(5.c.23): Right ascension of ascending node change due to oblatness of Earth at hp=1200 Km and $i = 8^0$

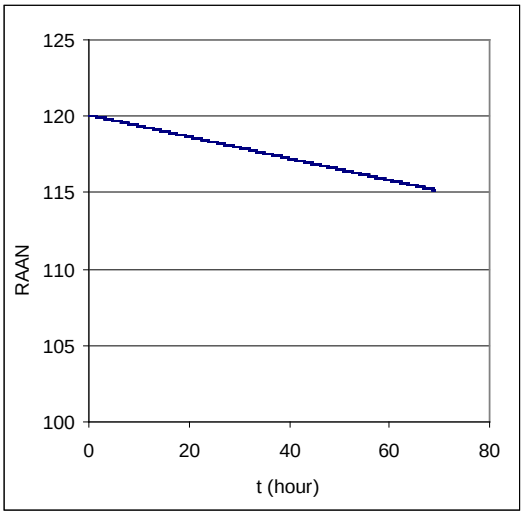

Fig.(5.c.24): Right ascension of ascending node change due to oblatness of Earth at hp=1200 Km and $i = 63.4^0$

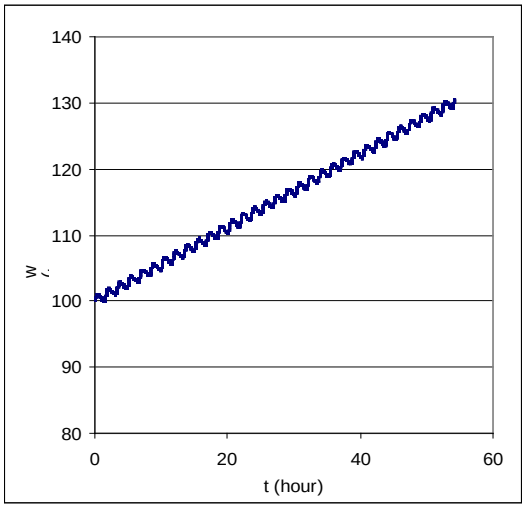

Fig.(5.c.25): Argument of perigee change due to oblatness of Earth perturbation at hp=95Km and $i = 8^0$

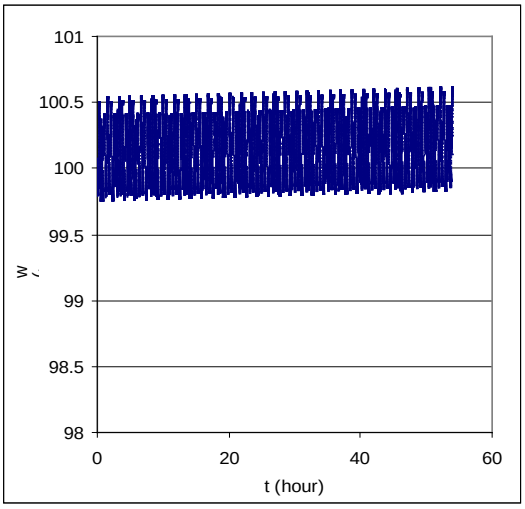

Fig.(5.c.26): Argument of perigee change due to oblatness of Earth perturbation at hp=95Km and $i = 63.4^0$

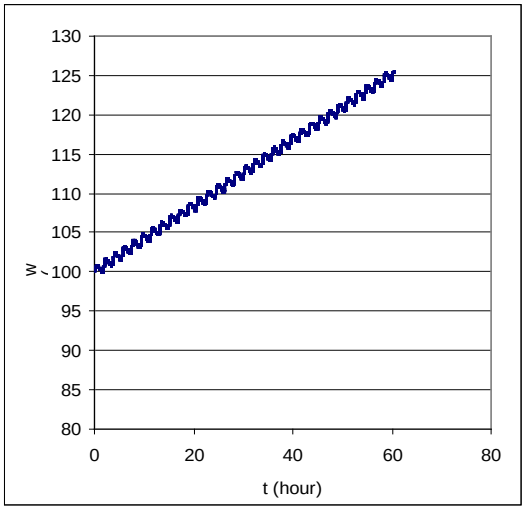

Fig.(5.c.27): Argument of perigee change due to oblatness of Earth perturbation at hp=600Km and $i = 8^0$

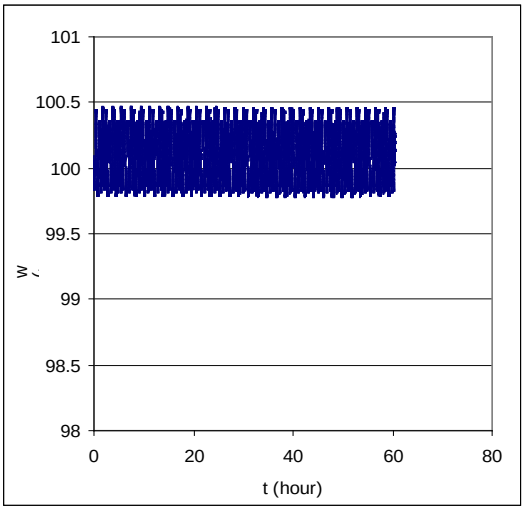

Fig.(5.c.28): Argument of perigee change due to oblatness of Earth perturbation at hp=600Km and $i = 63.4^0$

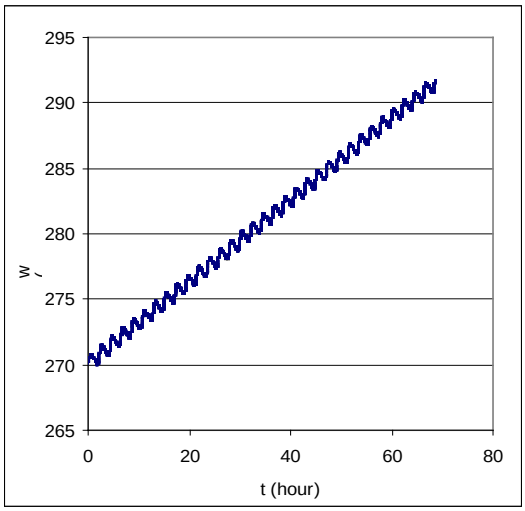

Fig.(5.c.29): Argument of perigee change due to oblatness of Earth perturbation at hp=1200Km and $i = 8^0$

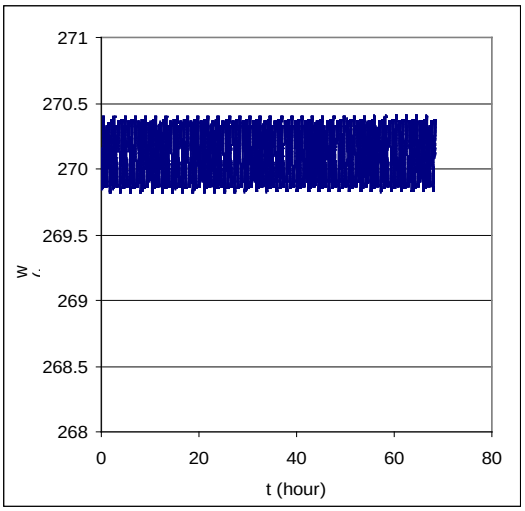

Fig.(5.c.30): Argument of perigee change due to oblatness of Earth perturbation at hp=1200Km and $i = 63.4^0$

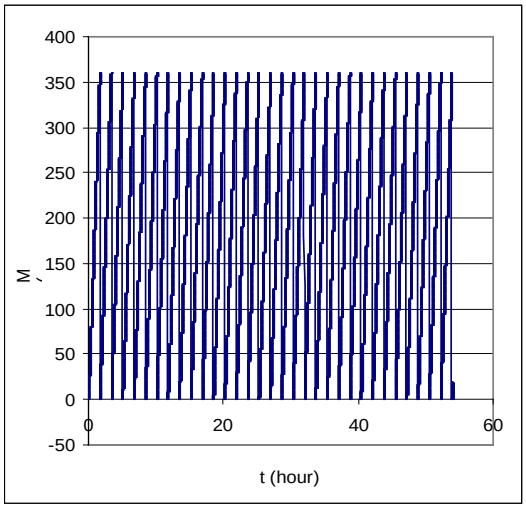

Fig.(5.c.31): Mean anomaly change due to oblatness of Earth perturbation at hp=95 Km and $i = 8^{o}$

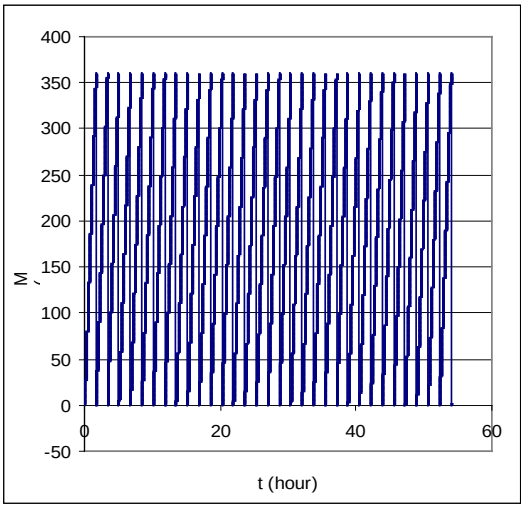

Fig.(5.c.32): Mean anomaly change due to oblatness of Earth perturbation at hp=95 Km and $i = 63.4^{o}$

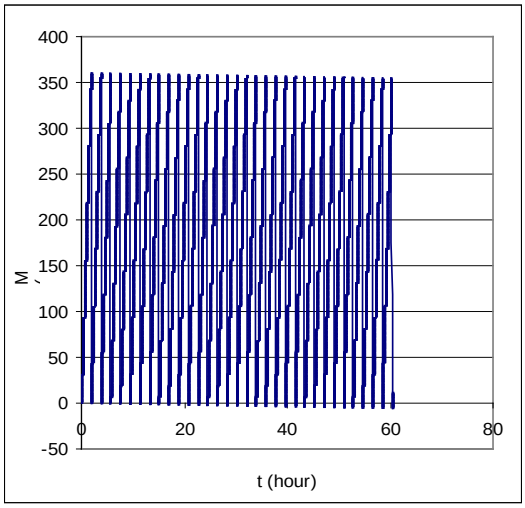

Fig.(5.c.33): Mean anomaly change due to oblatness of Earth perturbation at hp=600 Km and $i = 8^{o}$

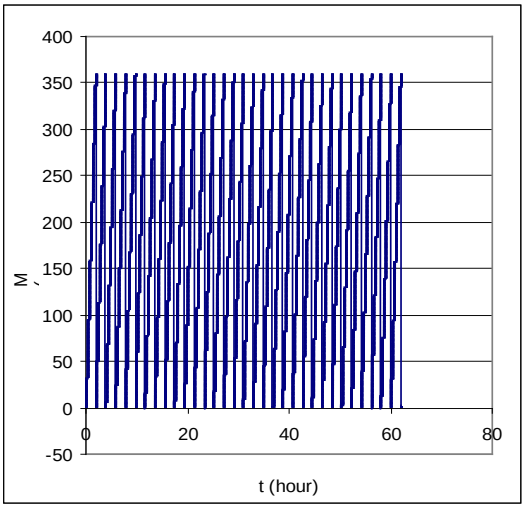

Fig.(5.c.34): Mean anomaly change due to oblatness of Earth perturbation at hp=600 Km and $i = 63.4^{o}$

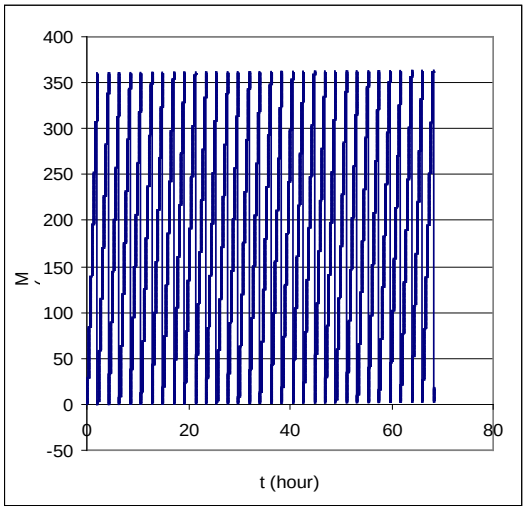

Fig.(5.c.35): Mean anomaly change due to oblatness of Earth perturbation at hp=1200 Km and $i = 8^{o}$

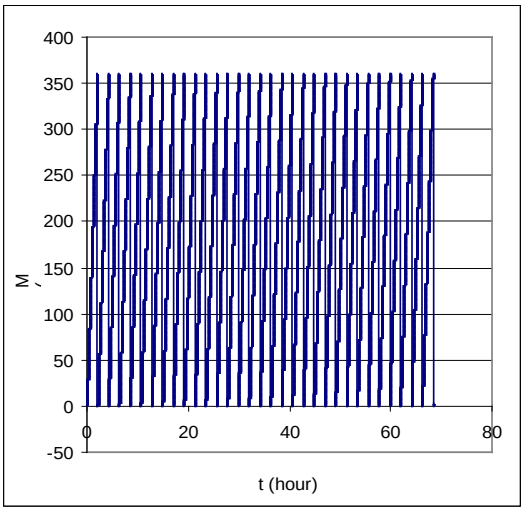

Fig.(5.c.36): Mean anomaly change due to oblatness of Earth perturbation at hp=1200 Km and $i = 63.4^{o}$

d- Solar radiation pressure perturbation

From figures (5.d.1), (5.d.2), (5.d.3), (5.d.4), (5.d.5) and (5.d.6) it can be seen that the short and long periodic variation in semi- major axis (a) with time, and periodic and sinusoidal pattern to 33 periods, for both values of inclinations $i = 8^{o}, 63.4^{o}$, also the same behavior shown in variation of semi-major axis (a) was found in Toshihiro and Sengoku [41].

Figures from (5.d.7) to (5.d.12) shows the secular variation in eccentricity (e) and increases through 33 periods for both values of inclination $i = 8^{o}, 63.4^{o}$, also shown in Eshagh and Najafi [53]. Fewer at $i = 63.4^{o}$ than $i = 8^{o}$ at hp=600, also there are increasing with altitudes hp=95, 600, 1200Km. Figures (5.d.13) to (5.d.18) shows that the inclination (i) increases linearly and periodically with the time for hp=95, 600 Km, except the altitude hp=1200 Km, the change is only periodically.

As for RAAN, it decreases linearly at hp=95, 600 Km for both values of inclination (i) (see figures from (5.d.19) to (5.d.22)), but it increases for hp=1200 Km (see figures (5.d.23), (5.d.24)). The variations are small through one period. Comparing all figures show that perturbation is the largest for $i = 8^{o}$. The secular change in argument of perigee (w) with time for altitude hp=95, 600, 1200 Km with $i = 8^{o}, 63.4^{o}$ was shown in figures from (5.d.25) to (5.d.30), such observation in Eshagh and Najafi [53]. But there is small change in Mean anomaly with time, see figures from (5.d.31) to (5.d.36).

Therefore, one can conclude that solar radiation pressure becomes noticeable above 500Km altitude and becomes more effected than the atmospheric drag at altitude above 900Km. The net effect of that perturbation is to lower the new perigee, raise the new apogee, increase the eccentricity of the orbit and leave the semi-major axis practically unchanged.

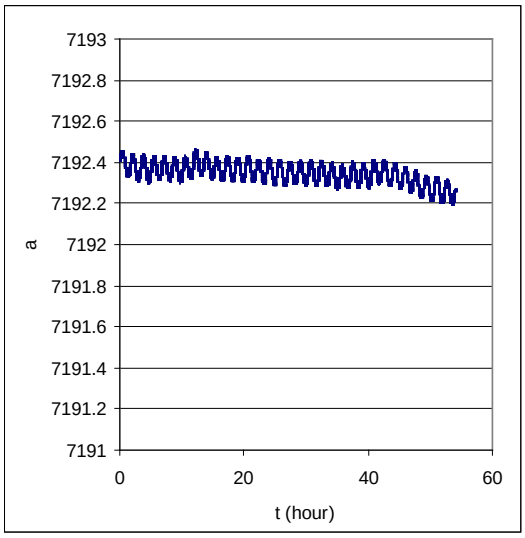

Fig.(5.d.1): Semi-major axis change due to Solar Radiation Pressure at hp=95 Km and $i = 8^{o}$

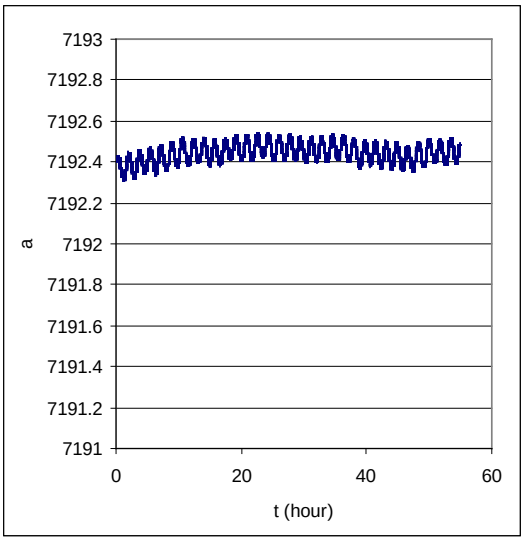

Fig.(5.d.2): Semi-major axis change due to Solar Radiation Pressure at hp=95 Km and $i = 63.4^{o}$

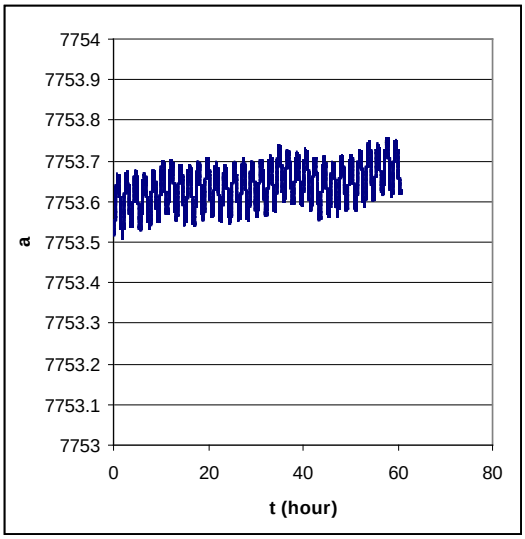

Fig.(5.d.3): Semi-major axis change due to Solar Radiation Pressure at hp=600 Km and $i = 8^{o}$

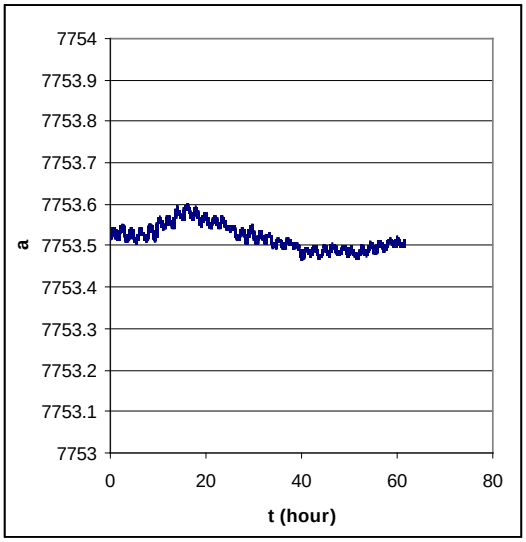

Fig.(5.d.4): Semi-major axis change due to Solar Radiation Pressure at hp=600 Km and $i = 63.4^{o}$

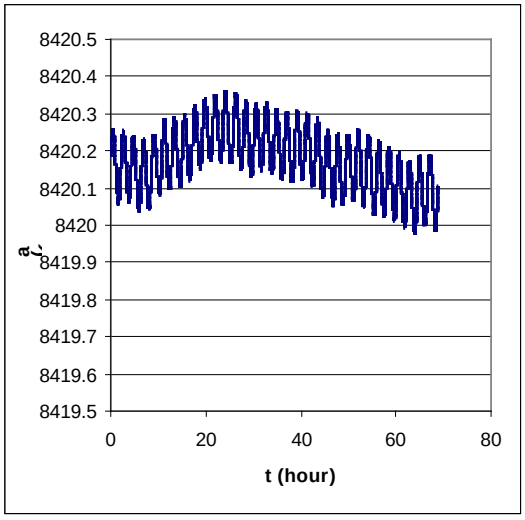

Fig.(5.d.5): Semi-major axis change due to Solar Radiation Pressure at hp=1200 Km and $i = 8^{o}$

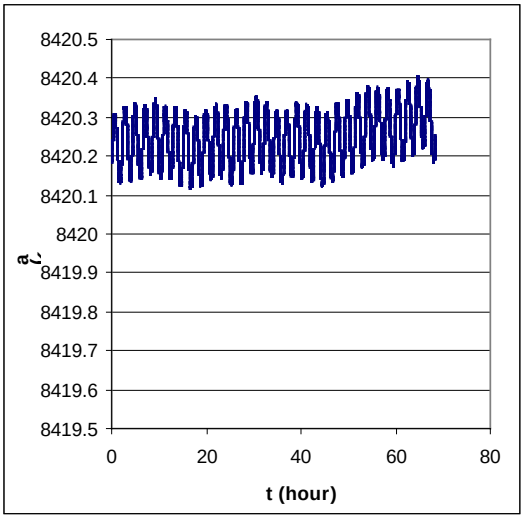

Fig.(5.d.6): Semi-major axis change due to Solar Radiation Pressure at hp=1200 Km and $i = 63.4^{o}$

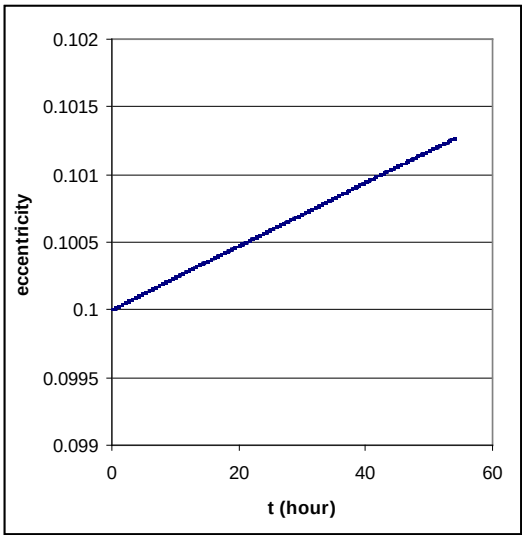

Fig.(5.d.7): Eccentricity change due to Solar Radiation Pressure at hp=95 Km and $i = 8^{o}$

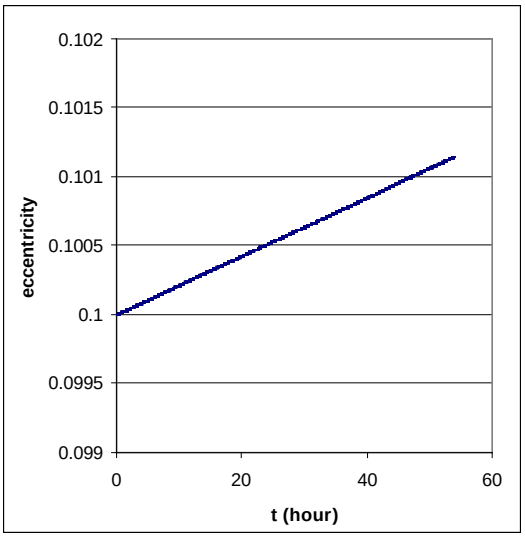

Fig.(5.d.8): Eccentricity change due to Solar Radiation Pressure at hp=95 Km and $i = 63.4^{o}$

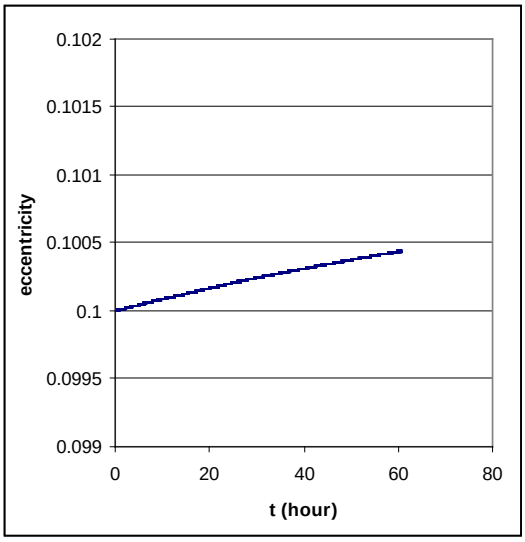

Fig.(5.d.9): Eccentricity change due to Solar Radiation Pressure at hp=600 Km and $i = 8^{o}$

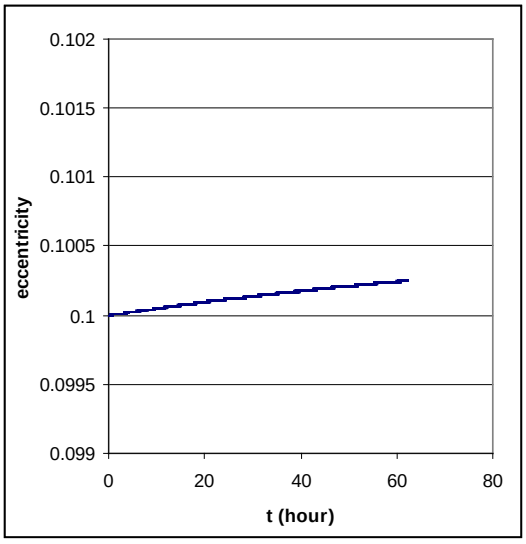

Fig.(5.d.10): Eccentricity change due to Solar Radiation Pressure at hp=600 Km and $i = 63.4^{o}$

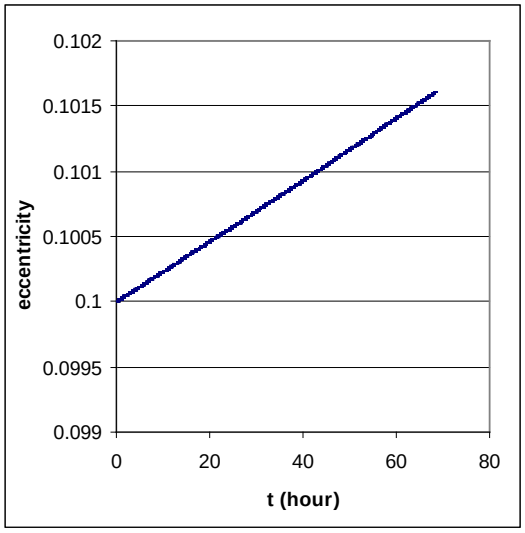

Fig.(5.d.11): Eccentricity change due to Solar Radiation Pressure at hp=1200 Km and $i = 8^{o}$

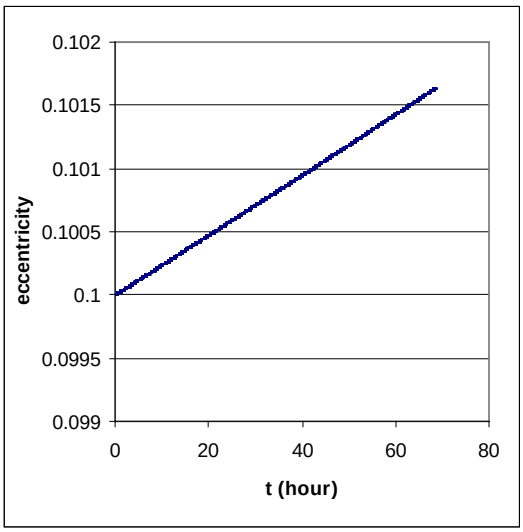

Fig.(5.d.12): Eccentricity change due to Solar Radiation Pressure at hp=1200 Km and $i = 63.4^{o}$

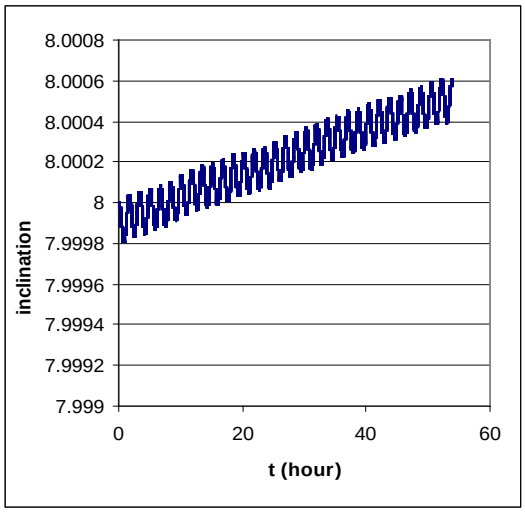

Fig.(5.d.13): Inclination change due to Solar Radiation Pressure at hp=95 Km and $i = 8^{o}$

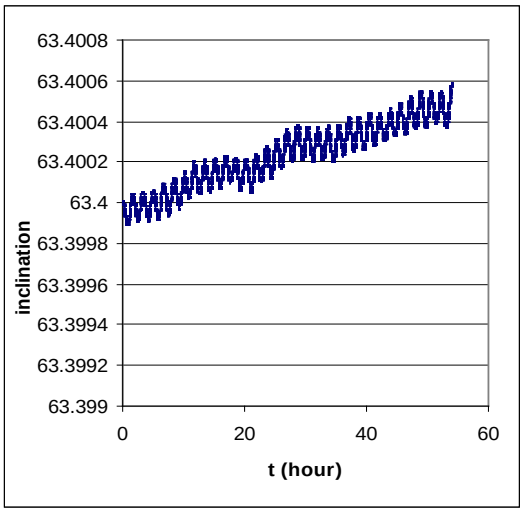

Fig.(5.d.14): Inclination change due to Solar Radiation Pressure at hp=95 Km and $i = 63.4^{o}$

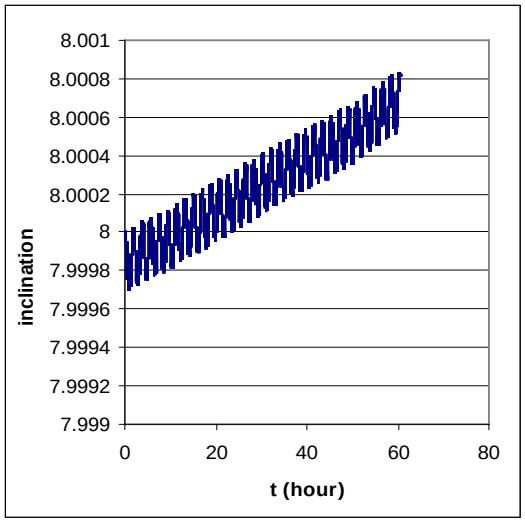

Fig.(5.d.15): Inclination change due to Solar Radiation Pressure at hp=600 Km and $i = 8^{o}$

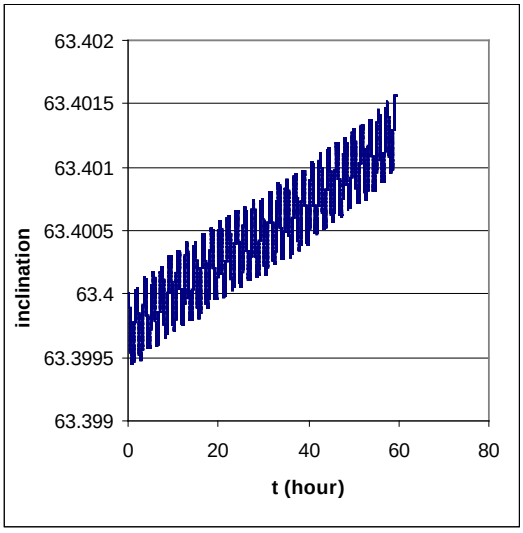

Fig.(5.d.16): Inclination change due to Solar Radiation Pressure at hp=600 Km and $i = 63.4^{o}$

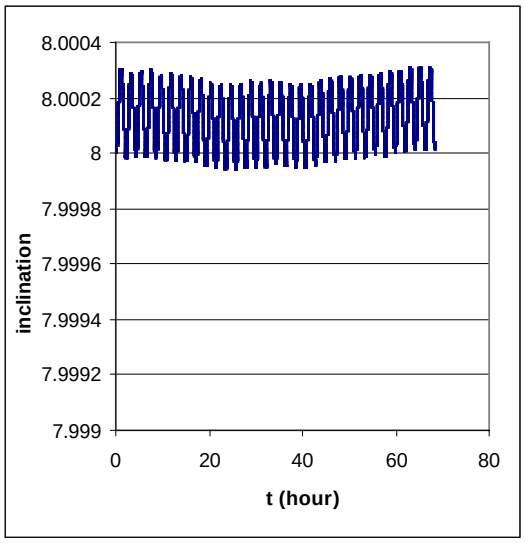

Fig.(5.d.17): Inclination change due to Solar Radiation Pressure at hp=1200 Km and $i = 8^{o}$

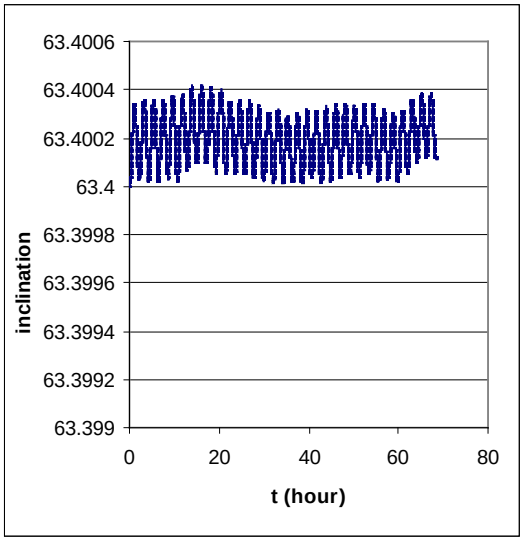

Fig.(5.d.18): Inclination change due to Solar Radiation Pressure at hp=1200 Km and $i = 63.4^{o}$

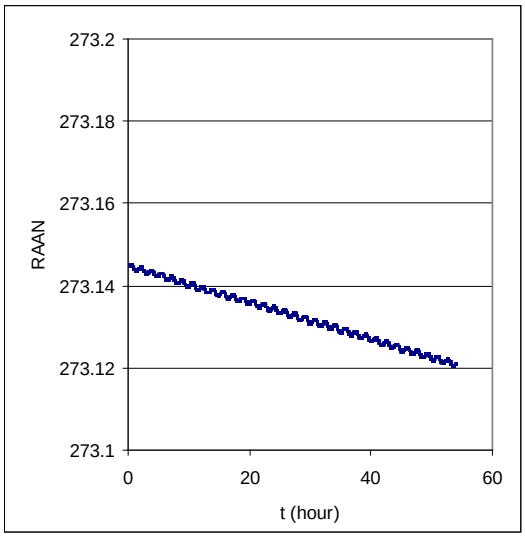

Fig.(5.d.19): Right ascension of ascending node change due to Solar Radiation Pressure at hp=95 Km and $i = 8^{o}$

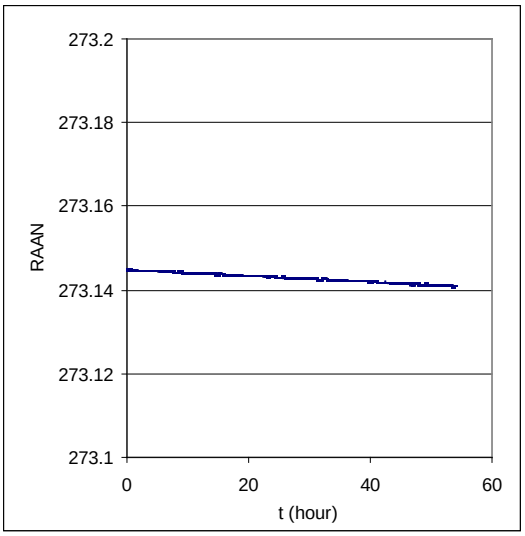

Fig.(5.d.20): Right ascension of ascending node change due to Solar Radiation Pressure at hp=95 Km and $i = 63.4^{o}$

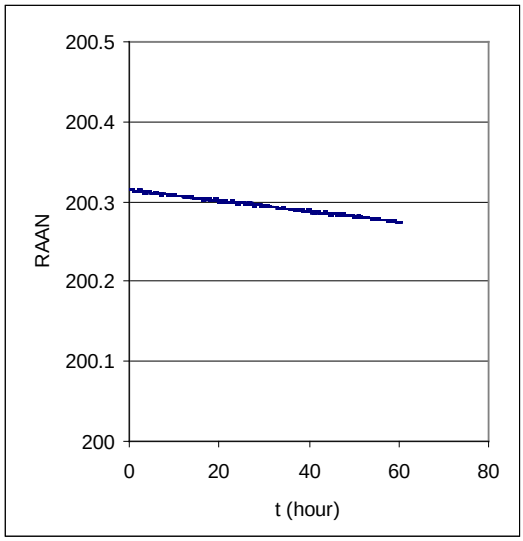

Fig.(5.d.21): Right ascension of ascending node change due to Solar Radiation Pressure at hp=600 Km and $i = 8^{o}$

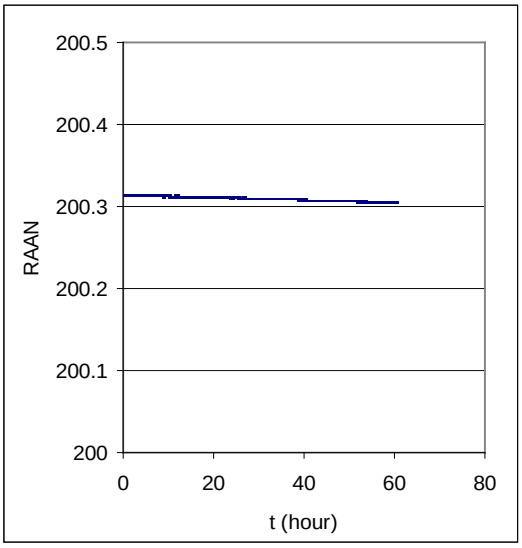

Fig.(5.d.22): Right ascension of ascending node change due to Solar Radiation Pressure at hp=600 Km and $i = 63.4^{o}$

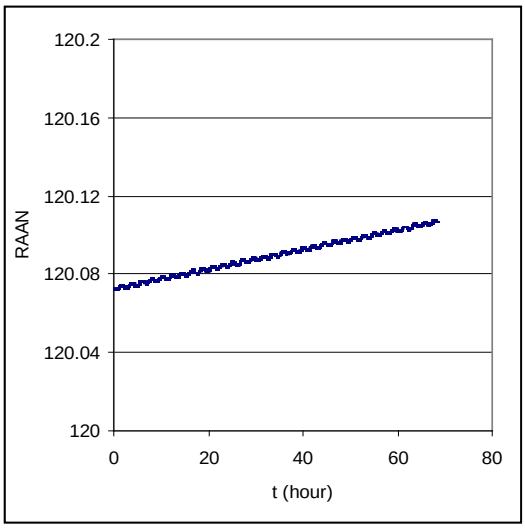

Fig.(5.d.23): Right ascension of ascending node change due to Solar Radiation Pressure at hp=1200 Km and $i = 8^{o}$

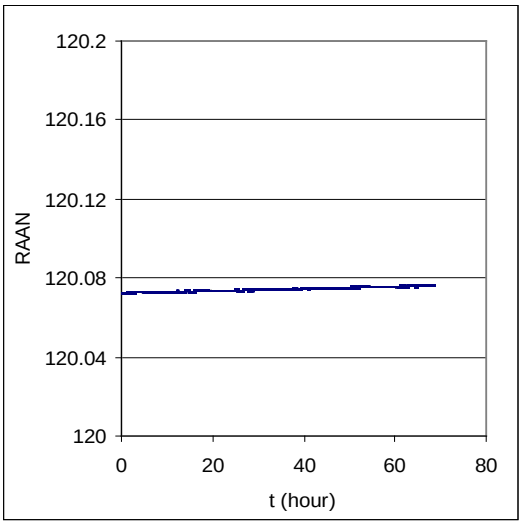

Fig.(5.d.24): Right ascension of ascending node change due to Solar Radiation Pressure at hp=1200 Km and $i = 63.4^{o}$

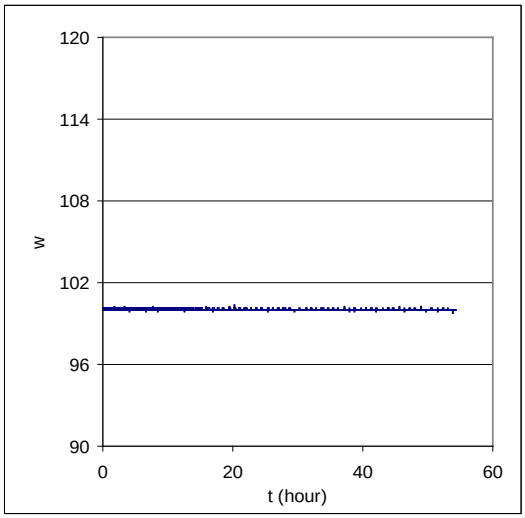

Fig.(5.d.25): Argument of perigee change due to Solar Radiation Pressure at hp=95 Km and $i = 8^{o}$

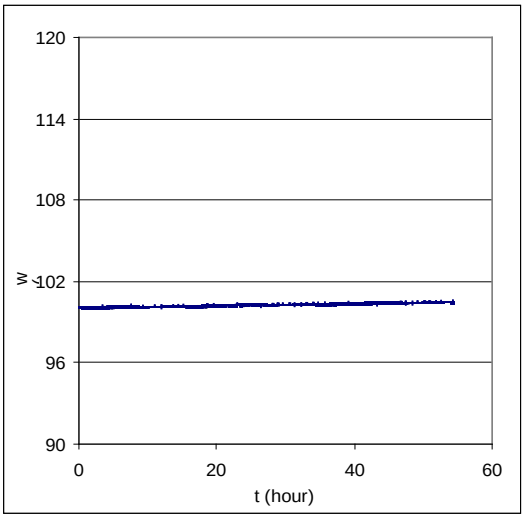

Fig.(5.d.26): Argument of perigee change due to Solar Radiation Pressure at hp=95 Km and $i = 63.4^{o}$

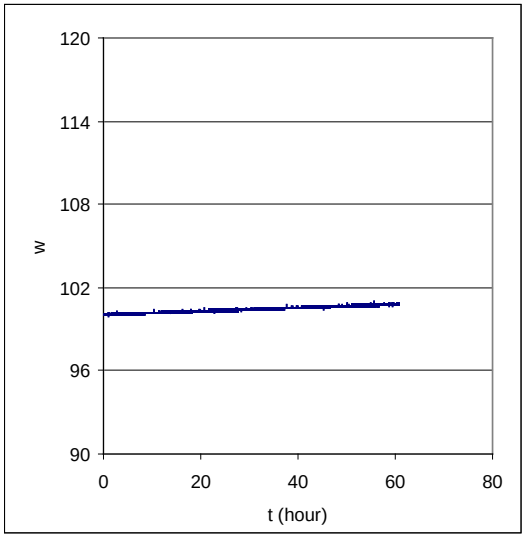

Fig.(5.d.27): Argument of perigee change due to Solar Radiation Pressure at hp=600 Km and $i = 8^{o}$

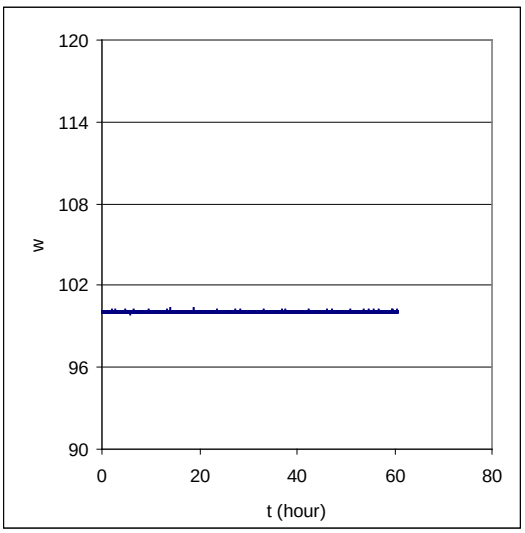

Fig.(5.d.28): Argument of perigee change due to Solar Radiation Pressure at hp=600 Km and $i = 63.4^{o}$

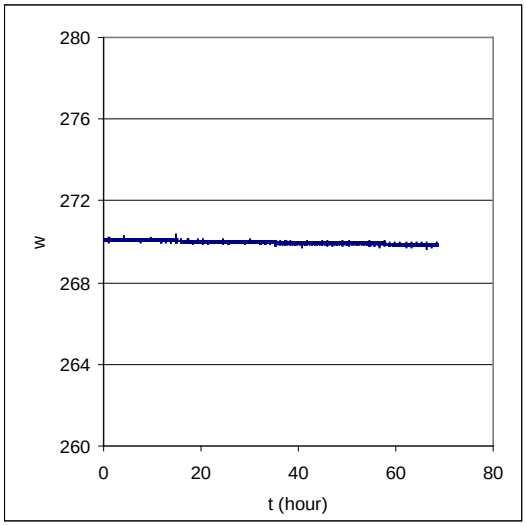

Fig.(5.d.29): Argument of perigee change due to Solar Radiation Pressure at hp=1200 Km and $i = 8^{o}$

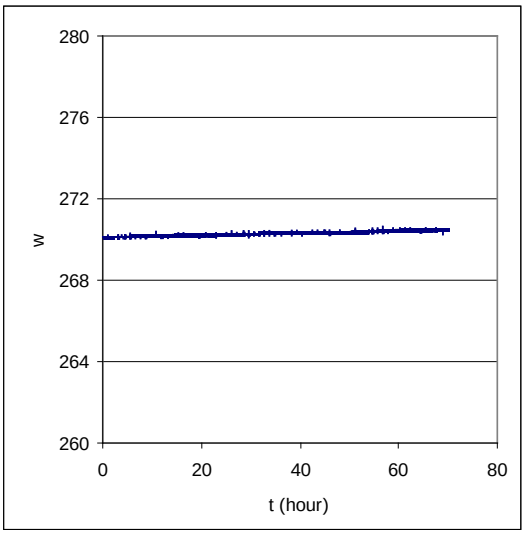

Fig.(5.d.30): Argument of perigee change due to Solar Radiation Pressure at hp=1200 Km and $i = 63.4^{o}$

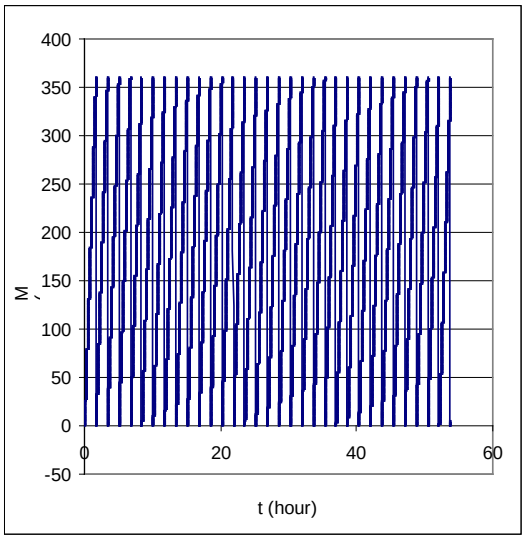

Fig.(5.d.31): Mean anomaly change due to Solar Radiation Pressure at hp=95 Km and $i = 8^{o}$

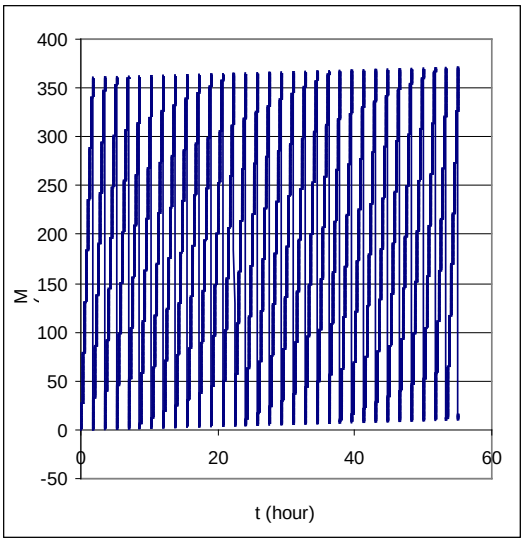

Fig.(5.d.32): Mean anomaly change due to Solar Radiation Pressure at hp=95 Km and $i = 63.4^{o}$

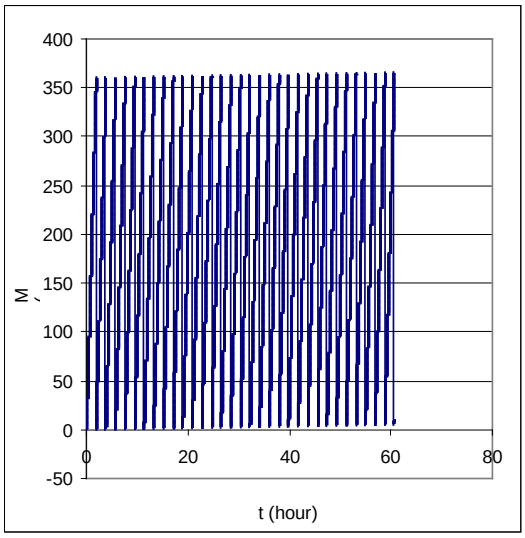

Fig.(5.d.33): Mean anomaly change due to Solar Radiation Pressure at hp=600 Km and $i = 8^{o}$

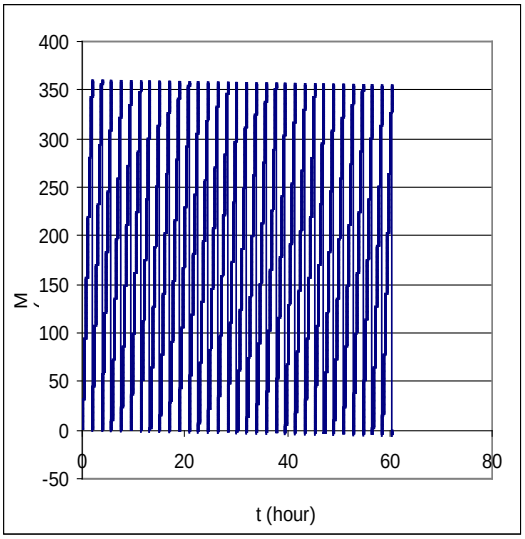

Fig.(5.d.34): Mean anomaly change due to Solar Radiation Pressure at hp=600 Km and $i = 63.4^{o}$

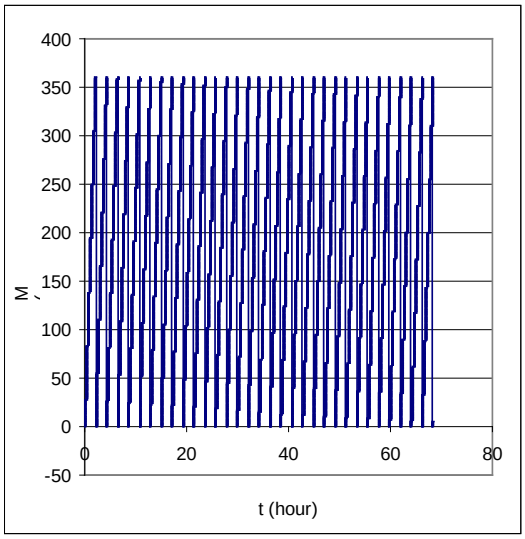

Fig.(5.d.35): Mean anomaly change due to Solar Radiation Pressure at hp=1200 Km and $i = 8^{o}$

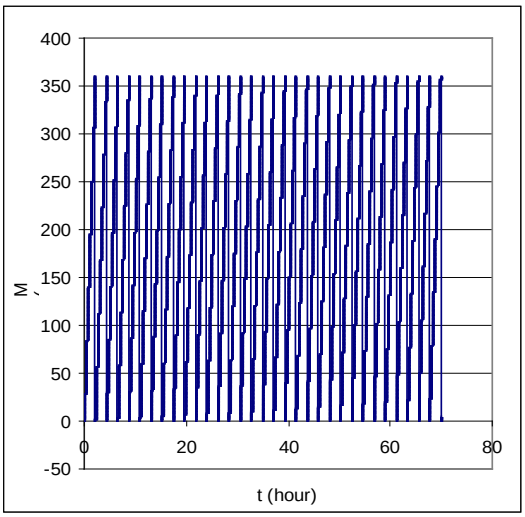

Fig.(5.d.36): Mean anomaly change due to Solar Radiation Pressure at hp=1200 Km and $i = 63.4^{o}$

e- Lunar attraction perturbation

The lunar attraction causes a small change in semi-major axis (a) at hp=95, 600, 1200 Km and $i = 8^{o}, 63.4^{o}$ (see figures from (5.e.1) to (5.e.6)). The same behavior happen in eccentricity (e) and inclination (i) (see figures from (5.e.7) to (5.e.18)), but the curve of figure (5.e.16) shows a little concavity when hp=600 Km and $i = 63.4^{o}$, and the curve of figure (5.e.18) becomes convexity when hp=1200 Km and $i = 63.4^{o}$ through 33 period, this may be due to pull and push the Moon attraction, and it becomes more when the satellite is in the Moon direction. Also RAAN as small decrease with time when $i = 8^{o}, 63.4^{o}$, and DW becomes less with increasing inclination (i), such $i = 63.4^{o}$ (see figures from (5.e.19) to (5.e.24)). Also there is a small change in value of argument of perigee (w) (see figures from (5.e.25) to (5.e.30) and the variation becomes large decreasing for Mean anomaly (M) at altitudes hp=95, 600, 1200 Km.

f- Solar attraction perturbation

The changes of solar attraction due to altitude (hp=95, 600, 1200 Km) and inclination $(i = 8^{o}, 63.4^{o})$ are identical with those for lunar attraction for all orbital elements (see figures (5.f.1) - (5.f.24)). The perturbation effect appear only for inclination (i), it decreases at hp=600Km and increases at hp=1200Km. As the same in Lunar effect. There is small change in values of argument of perigee (w) and Mean anomaly (M) at that altitude hp=95, 600, 1200 Km due to Solar effect, also shown in Eshagh and Najafi [53].

These effects for Lunar and Solar because the radial distance (r_l, r_s) change with date and it depending on the time of satellite rotation.

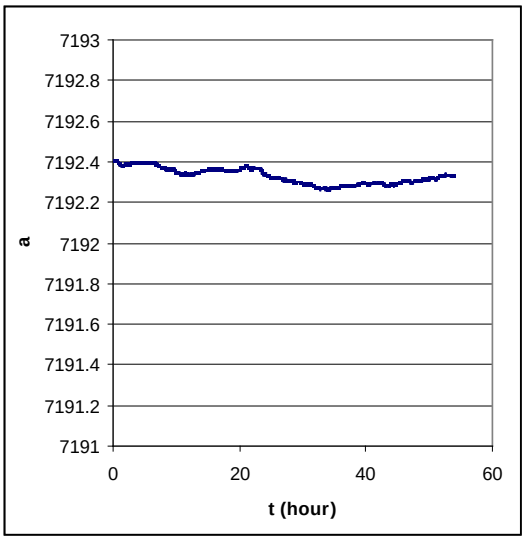

Fig.(5.e.1): Semi-major axis change due to lunar attraction at hp=95 Km and $i = 8^{o}$

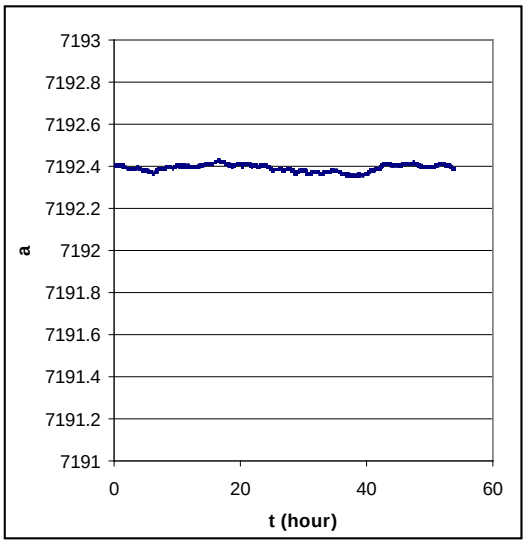

Fig.(5.e.2): Semi-major axis change due to lunar attraction at hp=95 Km and $i = 63.4^{o}$

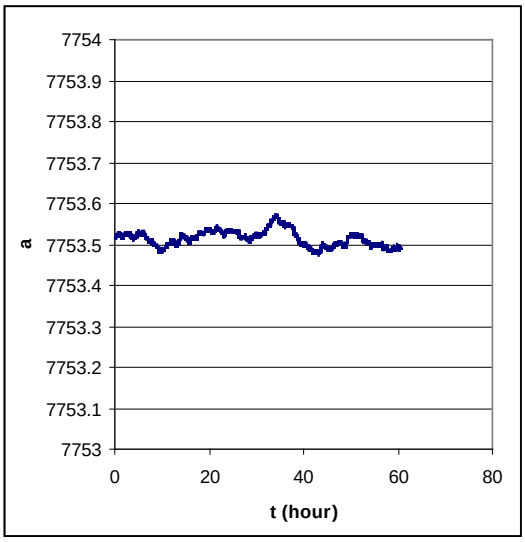

Fig.(5.e.3): Semi-major axis change due to lunar attraction at hp=600 Km and $i = 8^{o}$

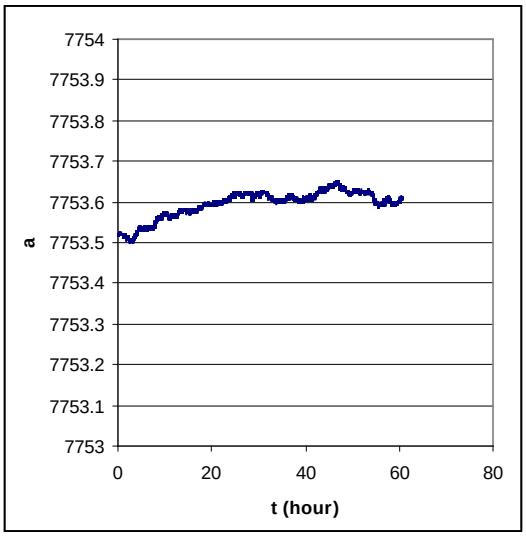

Fig.(5.e.4): Semi-major axis change due to lunar attraction at hp=600 Km and $i = 63.4^{o}$

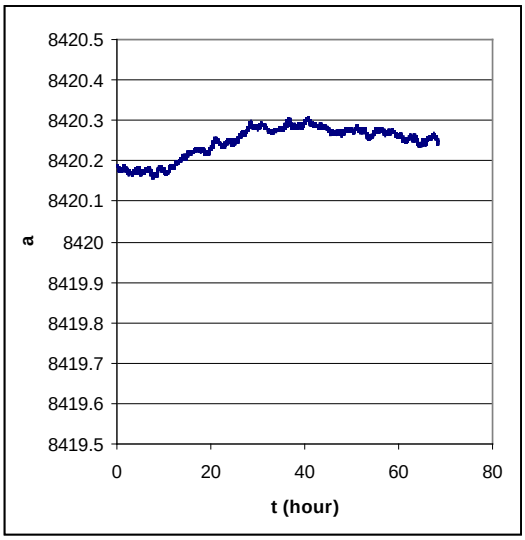

Fig.(5.e.5): Semi-major axis change due to lunar attraction at hp=1200 Km and $i = 8^{o}$

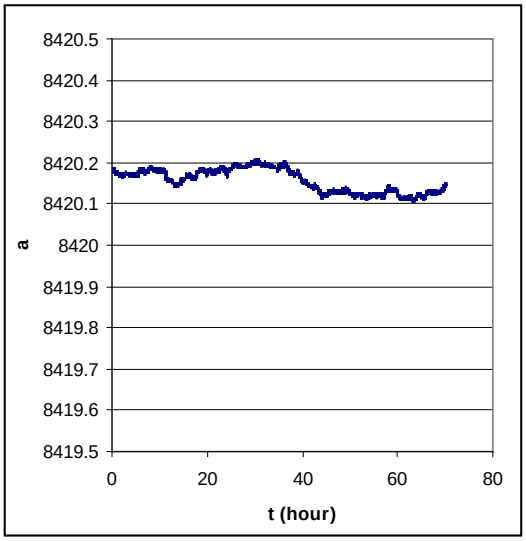

Fig.(5.e.6): Semi-major axis change due to lunar attraction at hp=1200 Km and $i = 63.4^{o}$

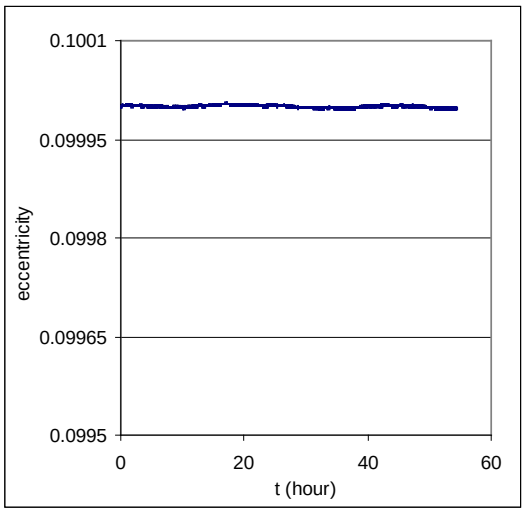

Fig.(5.e.7): Eccentricity change due to lunar attraction at hp=95 Km and $i = 8^{o}$

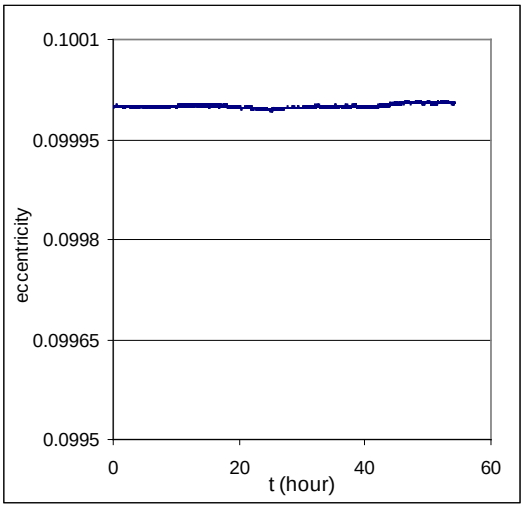

Fig.(5.e.8): Eccentricity change due to lunar attraction at hp=95 Km and $i = 63.4^{o}$

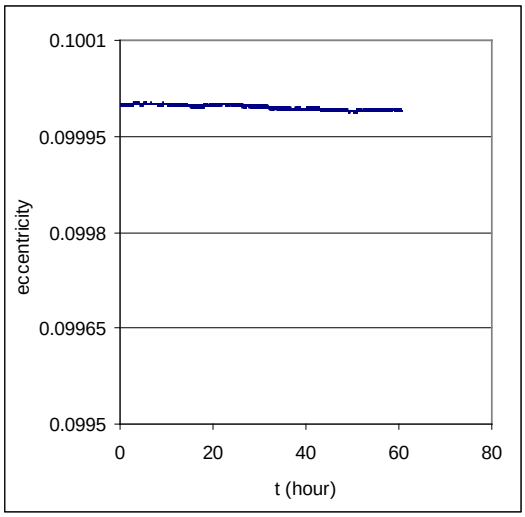

Fig.(5.e.9): Eccentricity change due to lunar attraction at hp=600 Km and $i = 8^{o}$

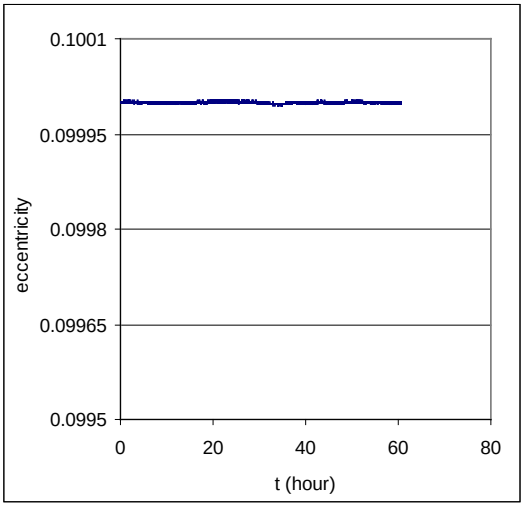

Fig.(5.e.10): Eccentricity change due to lunar attraction at hp=600 Km and $i = 63.4^{o}$

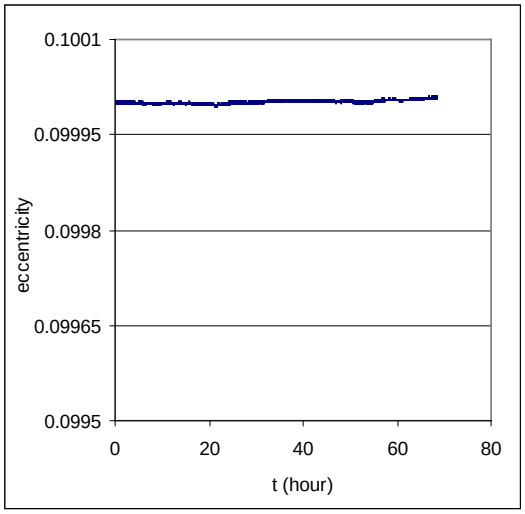

Fig.(5.e.11): Eccentricity change due to lunar attraction at hp=1200 Km and $i = 8^{o}$ **.**

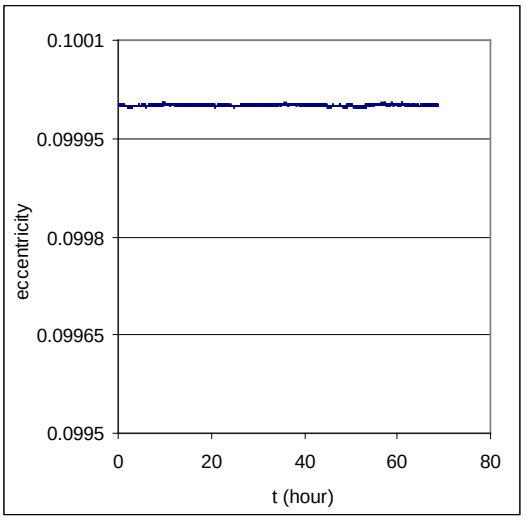

Fig.(5.e.12): Eccentricity change due to lunar attraction at hp=1200 Km and $i = 63.4^{o}$

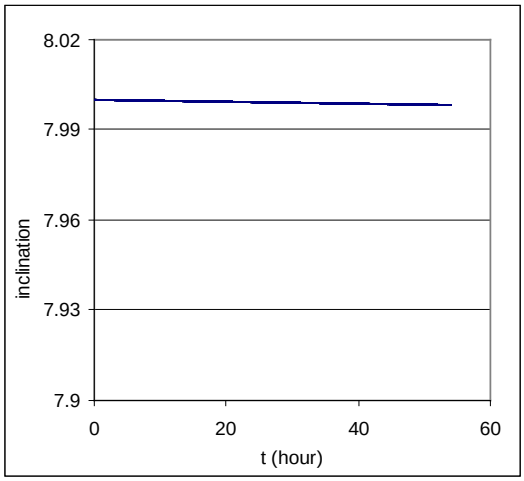

Fig.(5.e.13): Inclination change due to lunar attraction at hp=95 Km and $i = 8^{o}$

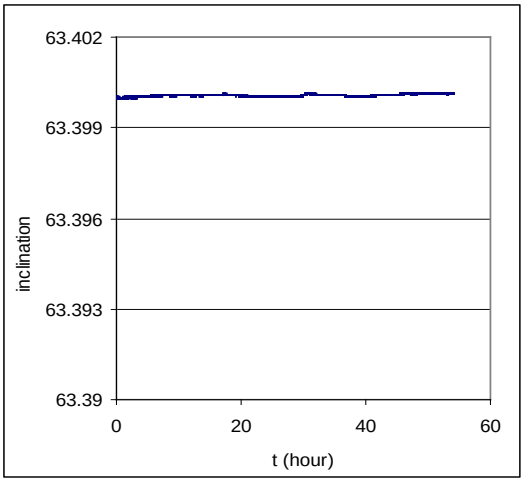

Fig.(5.e.14): Inclination change due to lunar attraction at hp=95 Km and $i = 63.4^{o}$

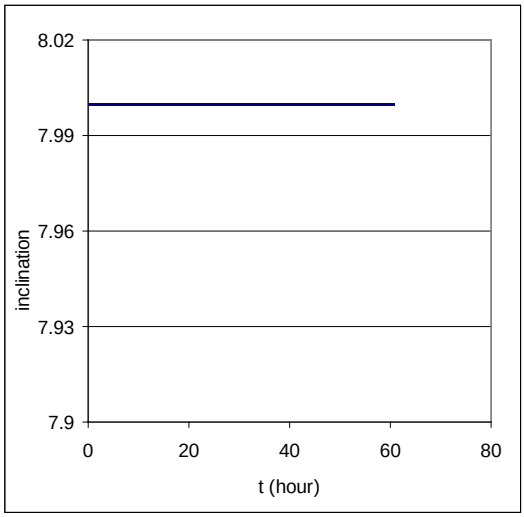

Fig.(5.e.15): Inclination change due to lunar attraction at hp=600 Km and $i = 8^{o}$

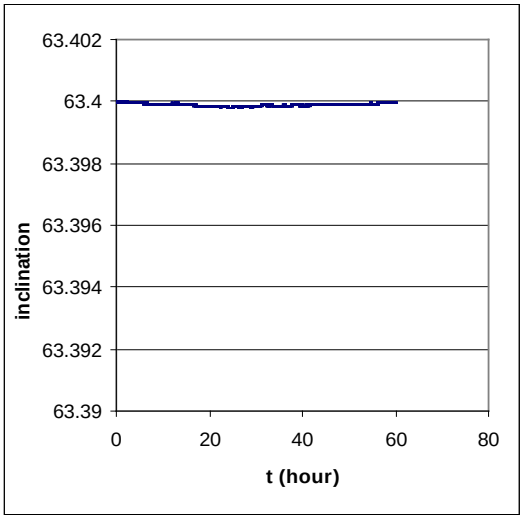

Fig.(5.e.16): Inclination change due to lunar attraction at hp=600 Km and $i = 63.4^{o}$

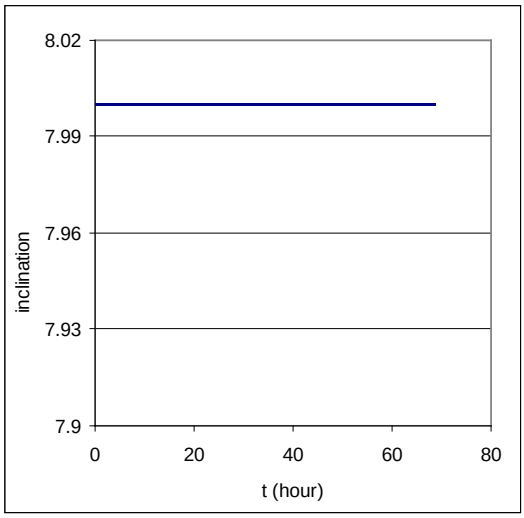

Fig.(5.e.17): Inclination change due to lunar attraction at hp=1200 Km and $i = 8^{o}$

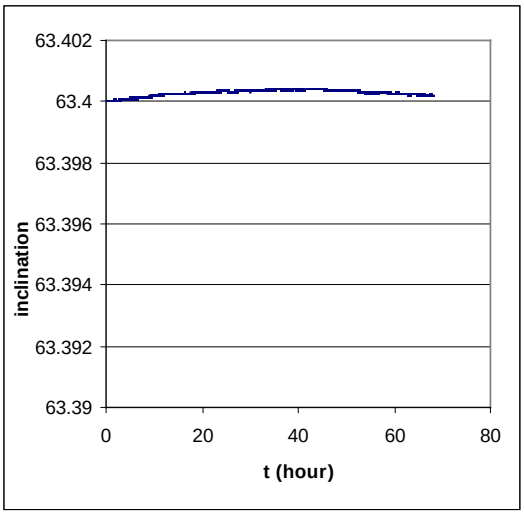

Fig.(5.e.18): Inclination change due to lunar attraction at hp=1200 Km and $i = 63.4^{o}$

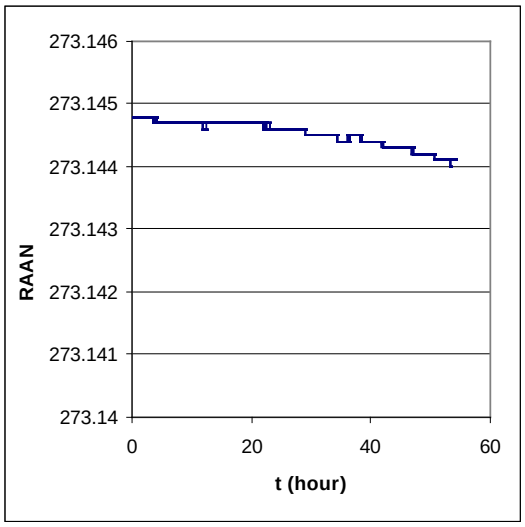

Fig.(5.e.19): Right ascension of ascending node change due to Lunar attraction at hp=95 Km and $i = 8^{o}$

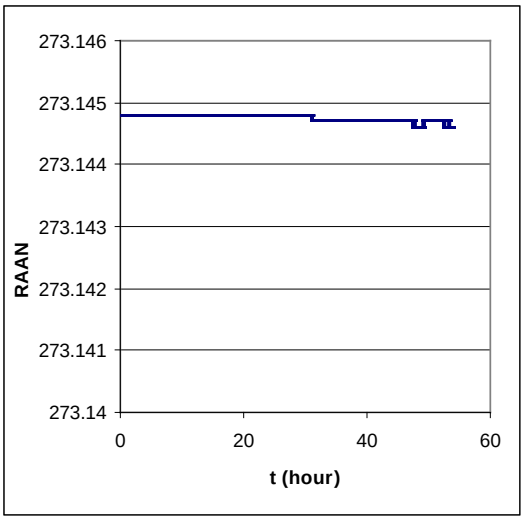

Fig.(5.e.20): Right ascension of ascending node change due to Lunar attraction at hp=95 Km and $i = 63.4^{o}$

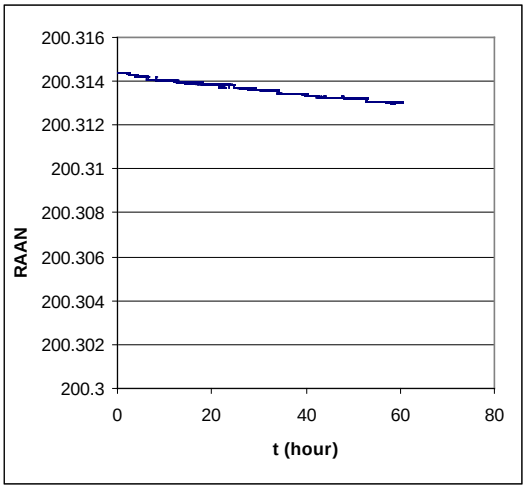

Fig.(5.e.21): Right ascension of ascending node change due to Lunar attraction at hp=600 Km and $i = 8^{o}$

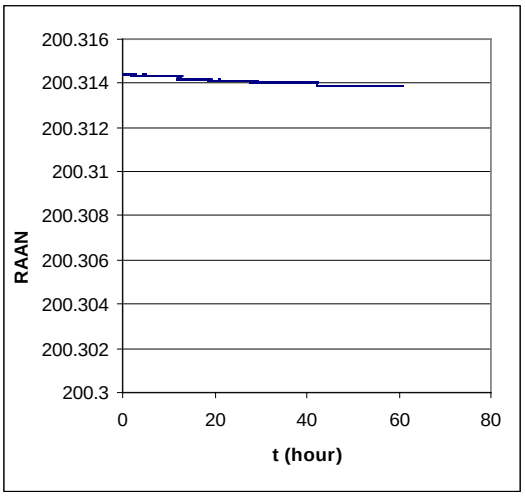

Fig.(5.e.22): Right ascension of ascending node change due to Lunar attraction at hp=600 Km and $i = 63.4^{o}$

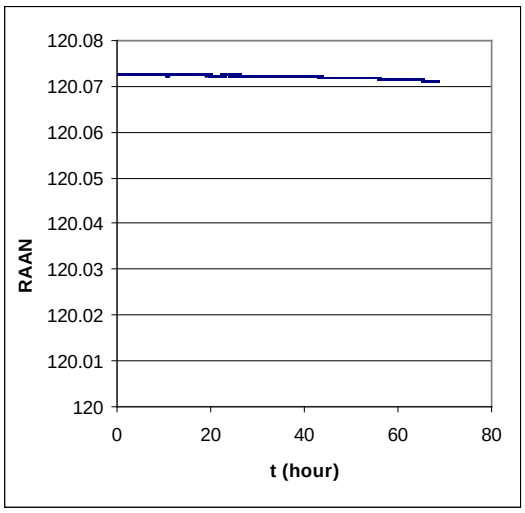

Fig.(5.e.23): Right ascension of ascending node change due to Lunar attraction at hp=1200 Km and $i = 8^{o}$

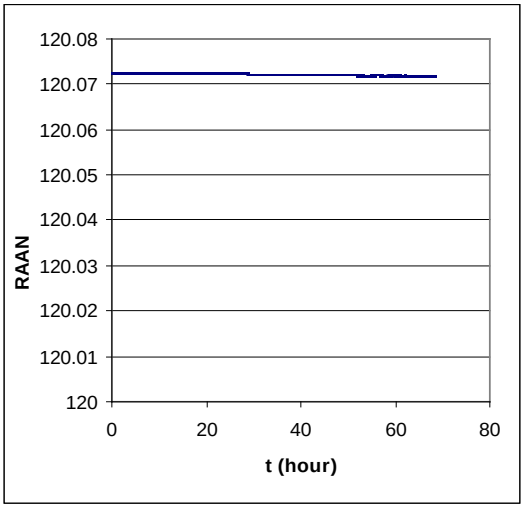

Fig.(5.e.24): Right ascension of ascending node change due to attraction Lunar at hp=1200 Km and $i = 63.4^{o}$

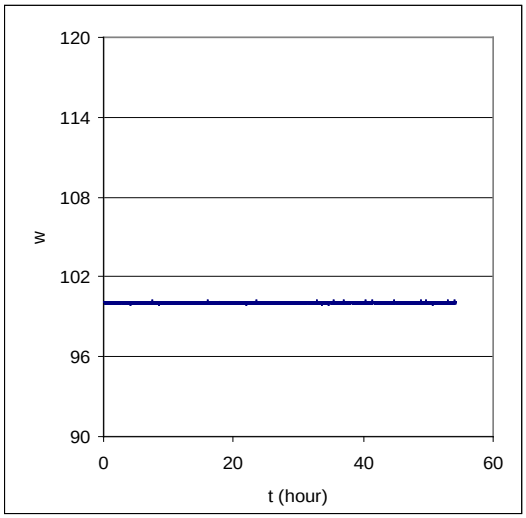

Fig.(5.e.25): Argument of perigee change due to Lunar perturbation at hp=95 Km and $i = 8^{o}$

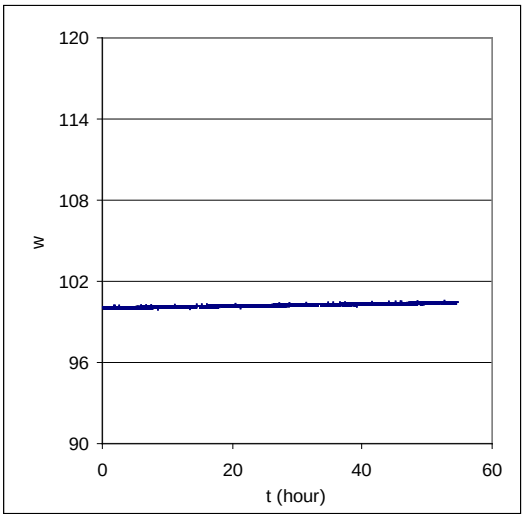

Fig.(5.e.26): Argument of perigee change due to Lunar perturbation at hp=95 Km and $i = 63.4^{o}$

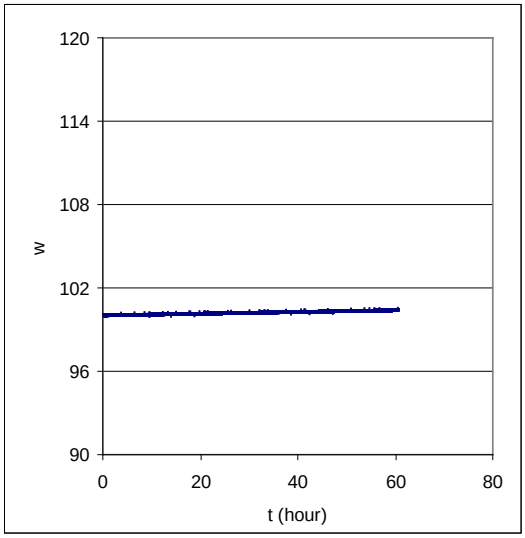

Fig.(5.e.27): Argument of perigee change due to Lunar perturbation at hp=600 Km and $i = 8^{o}$

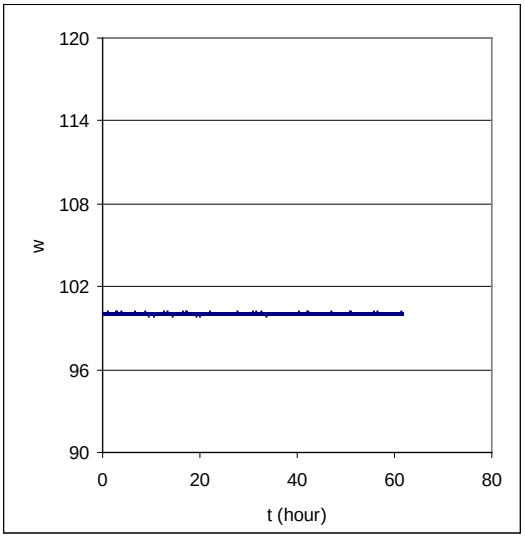

Fig.(5.e.28): Argument of perigee change due to Lunar perturbation at hp=600Km and $i = 63.4^{o}$

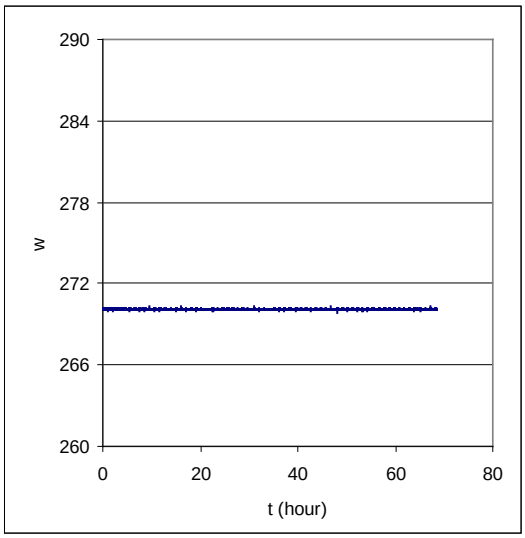

Fig.(5.e.29): Argument of perigee change due to Lunar perturbation at hp=1200 Km and $i = 8^{o}$

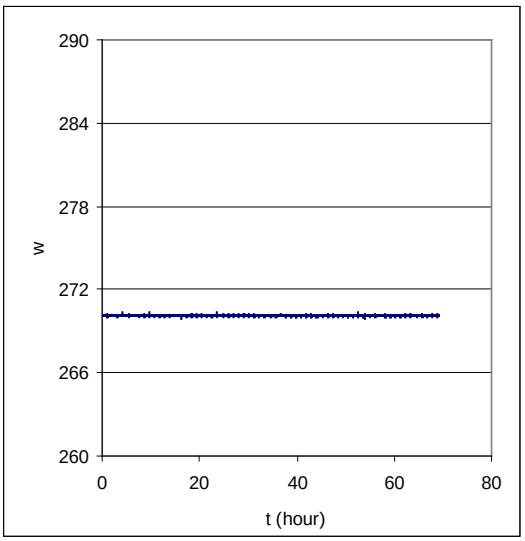

Fig.(5.e.30): Argument of perigee change due to Lunar perturbation at hp=1200 Km and $i = 63.4^{o}$

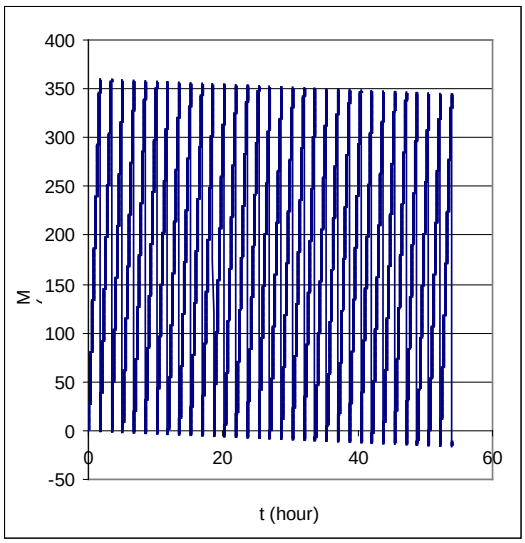

Fig.(5.e.31): Mean anomaly change due to Lunar perturbation at hp=95 Km and $i = 8^{o}$

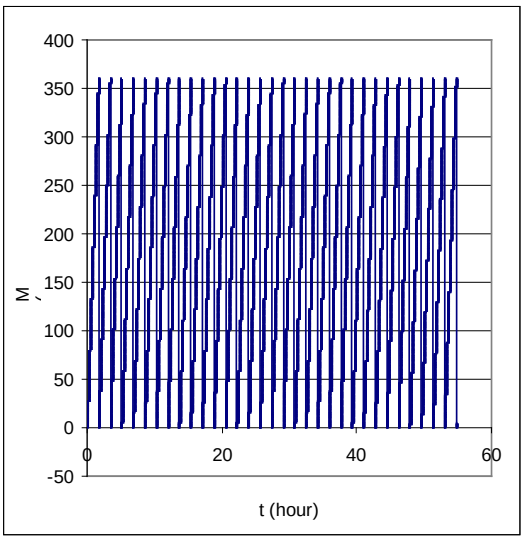

Fig.(5.e.32): Mean anomaly change due to Lunar perturbation at hp=95 Km and $i = 63.4^{o}$

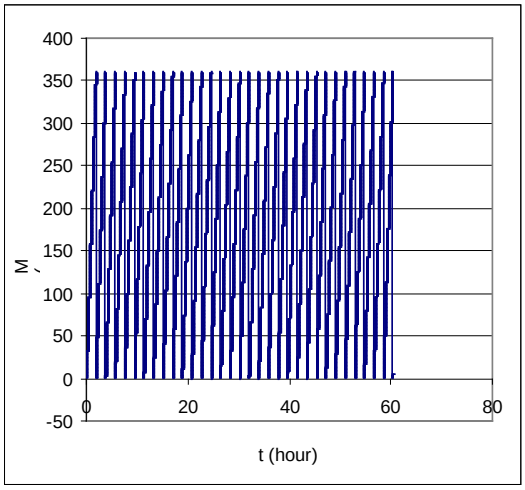

Fig.(5.e.33): Mean anomaly change due to Lunar perturbation at hp=600 Km and $i = 8^{o}$

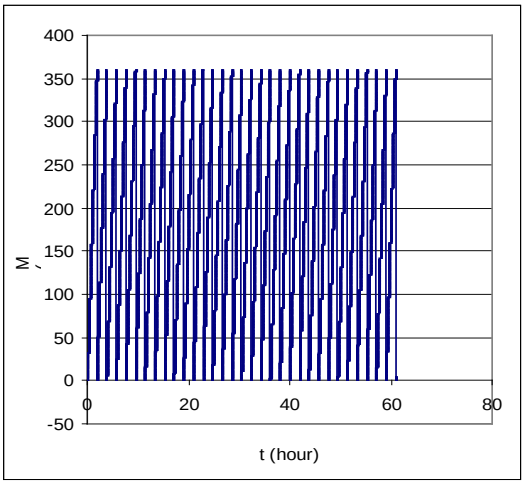

Fig.(5.e.34): Mean anomaly change due to Lunar perturbation at hp=600 Km and $i = 63.4^{o}$

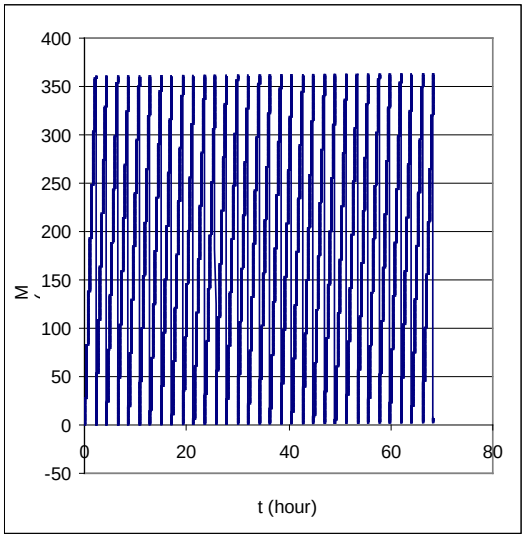

Fig.(5.e.35): Mean anomaly change due to Lunar perturbation at hp=1200 Km and $i = 8^{o}$

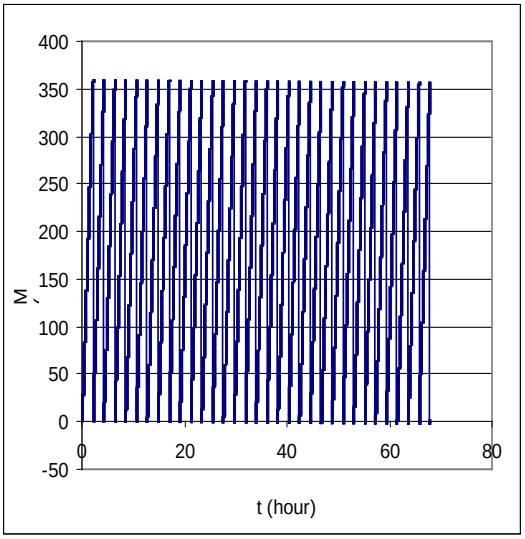

Fig.(5.e.36): Mean anomaly change due to Lunar perturbation at hp=1200 Km and $i = 63.4^{o}$

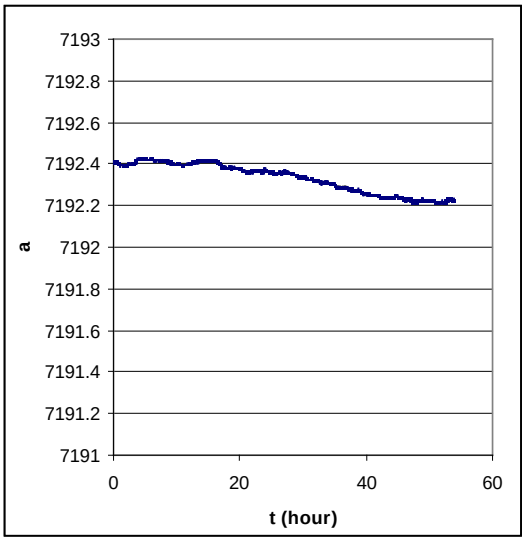

Fig.(5.f.1): Semi-major axis change due to Solar attraction at hp=95 Km and $i = 8^{o}$

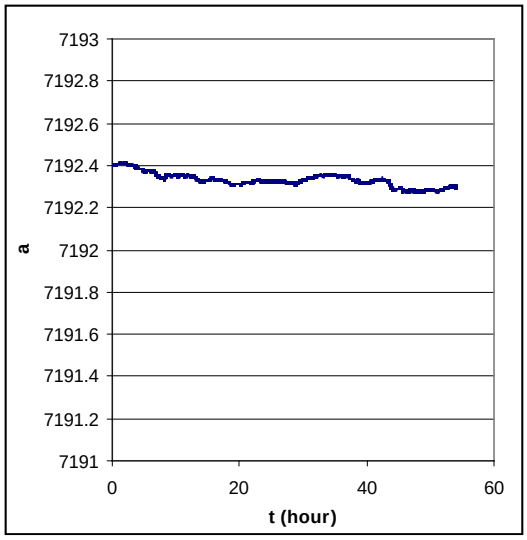

Fig.(5.f.2): Semi-major axis change due to Solar attraction at hp=95 Km and $i = 63.4^{o}$

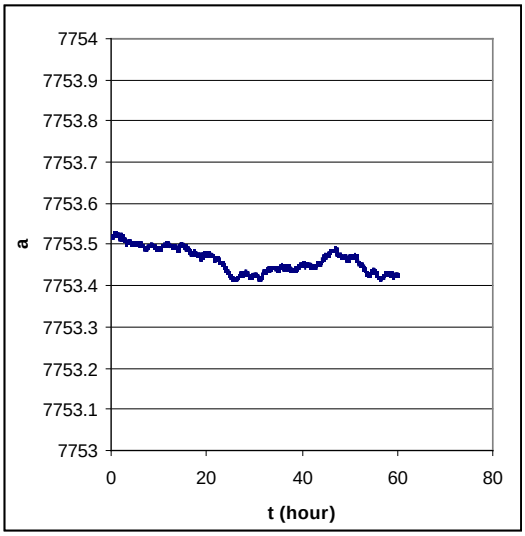

Fig.(5.f.3): Semi-major axis change due to Solar attraction at hp=600 Km and $i = 8^{o}$

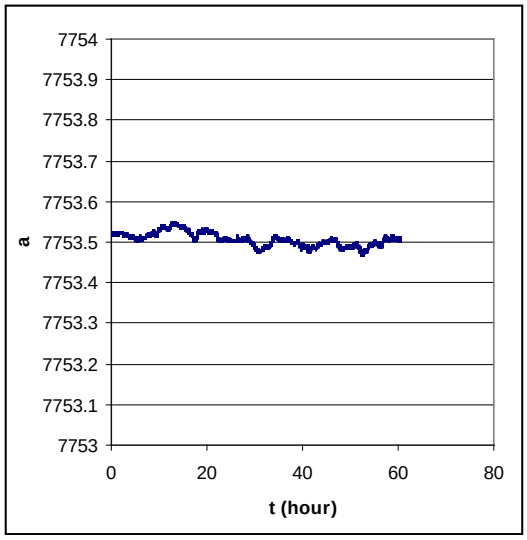

Fig.(5.f.4): Semi-major axis change due to Solar attraction at hp=600 Km and $i = 63.4^{o}$

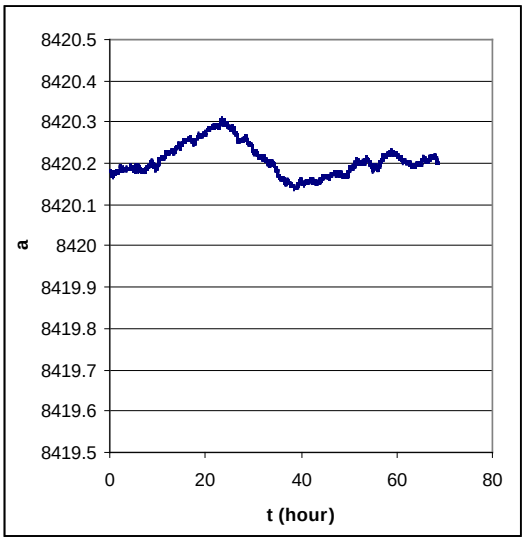

Fig.(5.f.5): Semi-major axis change due to Solar attraction at hp=1200 Km and $i = 8^{o}$

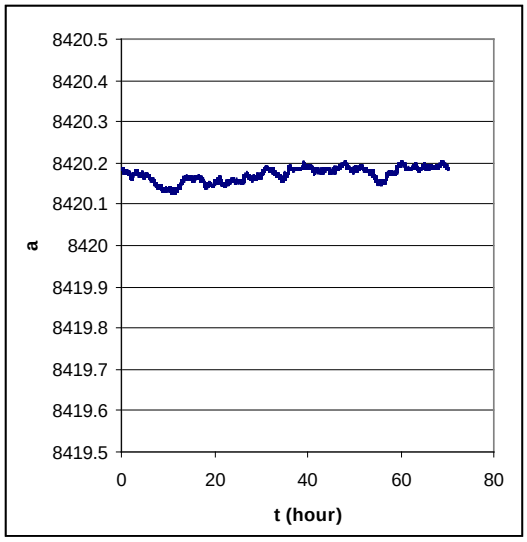

Fig.(5.f.6): Semi-major axis change due to Solar attraction at hp=1200 Km and $i = 63.4^{o}$

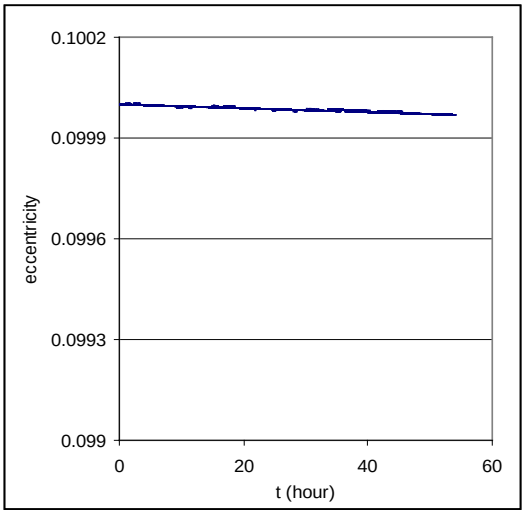

Fig.(5.f.7): Eccentricity change due to Solar attraction at hp=95 Km and $i = 8^{o}$

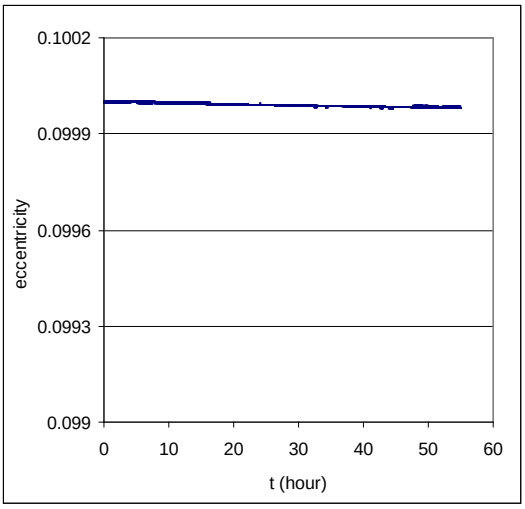

Fig.(5.f.8): Eccentricity change due to Solar attraction at hp=95 Km and $i = 63.4^{o}$

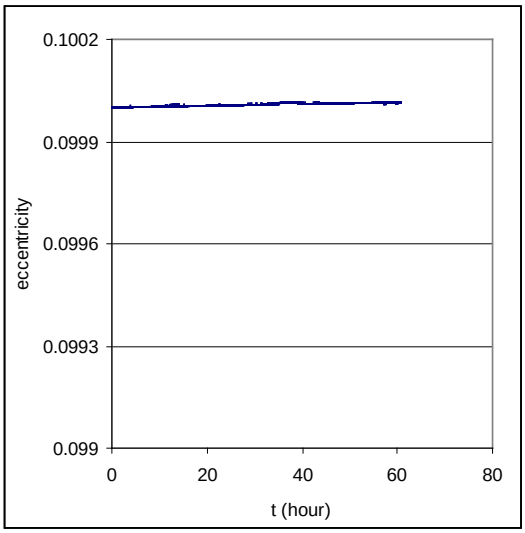

Fig.(5.f.9): Eccentricity change due to Solar attraction at hp=600 Km and $i = 8^{o}$

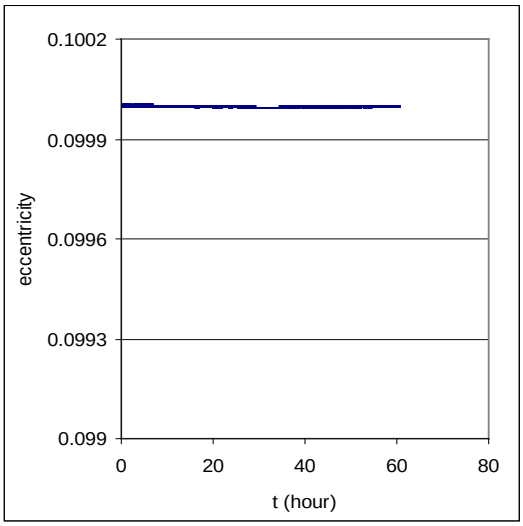

Fig.(5.f.10): Eccentricity change due to Solar attraction at hp=600 Km and $i = 63.4^{o}$

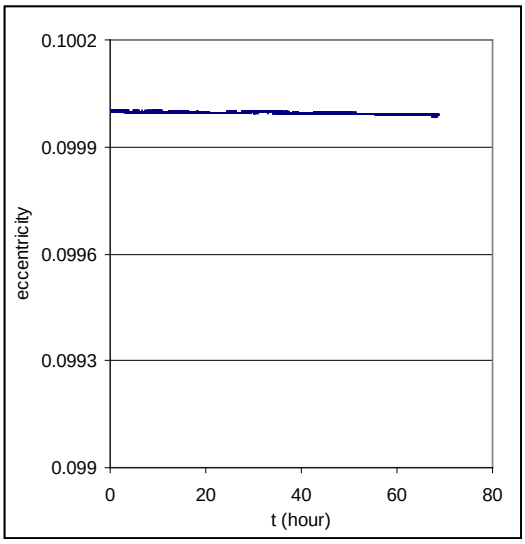

Fig.(5.f.11): Eccentricity change due to Solar attraction at hp=1200 Km and $i = 8^{o}$

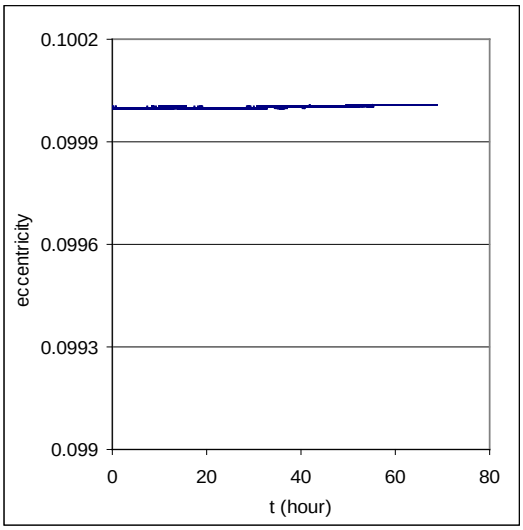

Fig.(5.f.12): Eccentricity change due to Solar attraction at hp=1200 Km and $i = 63.4^{o}$

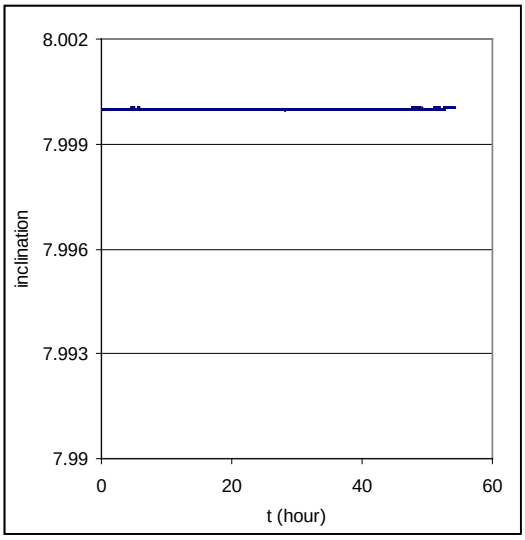

Fig.(5.f.13): inclination change due to Solar attraction at hp=95 Km and $i = 8^{o}$

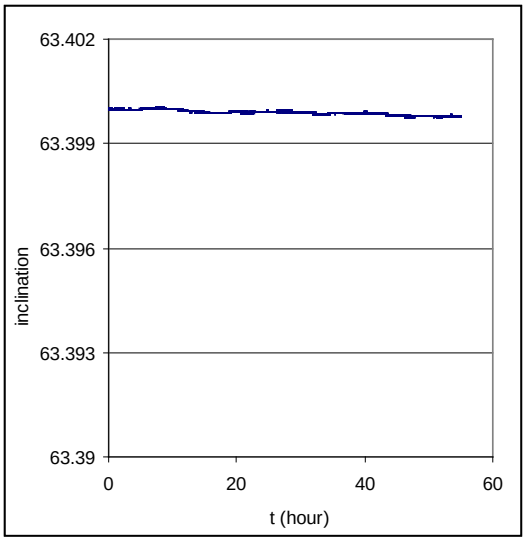

Fig.(5.f.14): inclination change due to Solar attraction at hp=95 Km and $i = 63.4^{o}$

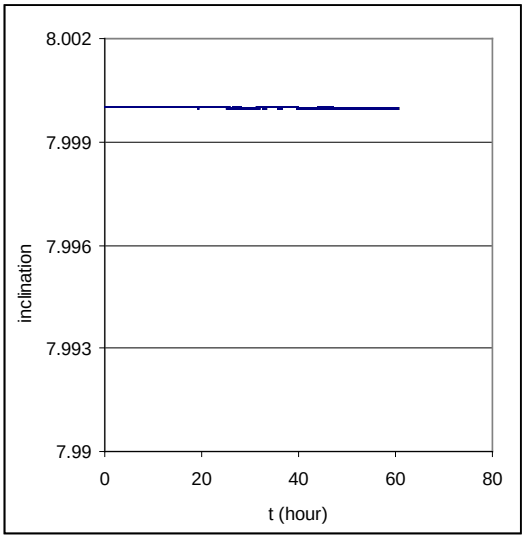

Fig.(5.f.15): inclination change due to Solar attraction at hp=600 Km and $i = 8^{o}$

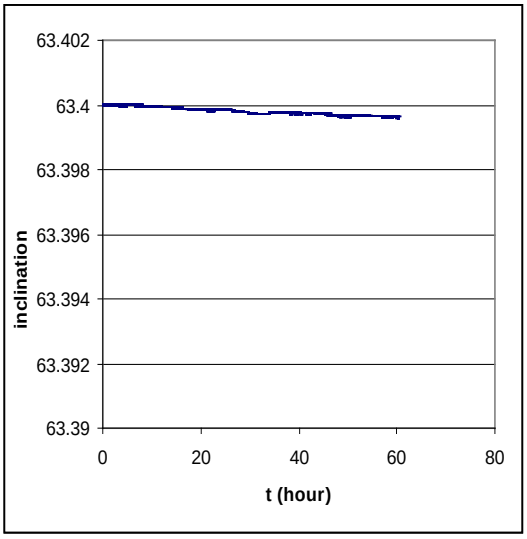

Fig.(5.f.16): inclination change due to Solar attraction at hp=600 Km and $i = 63.4^{o}$

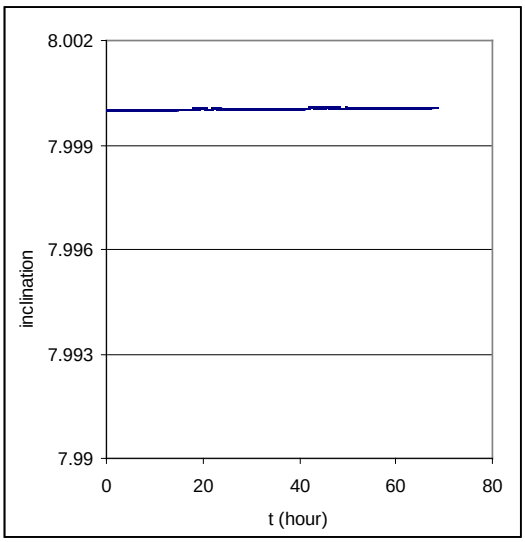

Fig.(5.f.17): inclination change due to Solar attraction at hp=1200 Km and $i = 8^{o}$

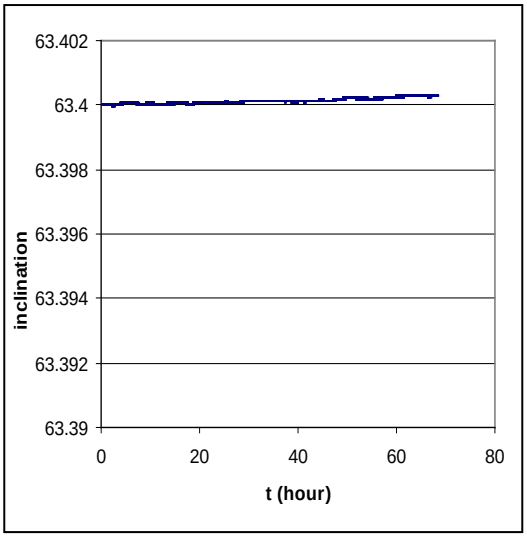

Fig.(5.f.18): inclination change due to Solar attraction at hp=1200 Km and $i = 63.4^{o}$

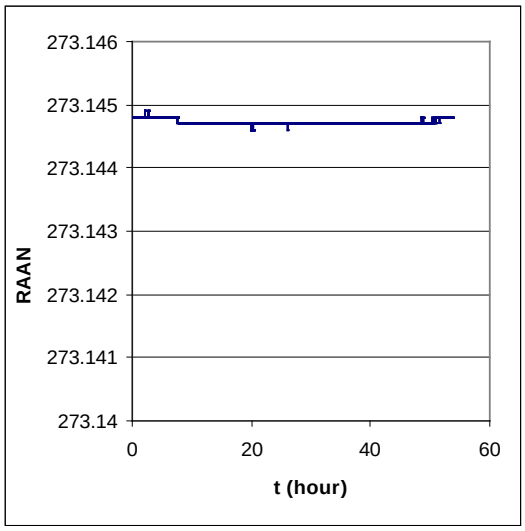

Fig.(5.f.19): Right ascension of ascending node change due to Solar attraction at hp=95 Km and $i = 8^{o}$

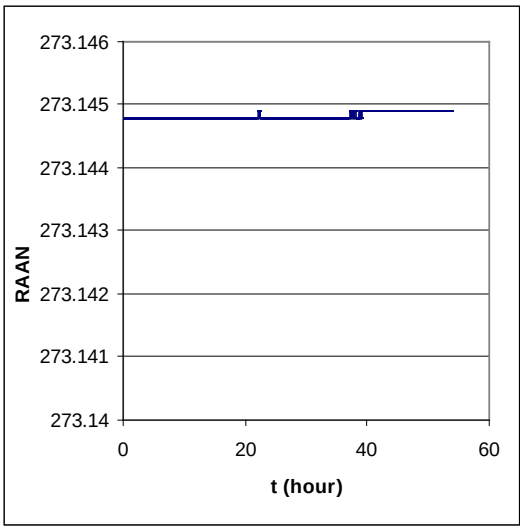

Fig.(5.f.20): Right ascension of ascending node change due to Solar attraction at hp=95 Km and $i = 63.4^{o}$

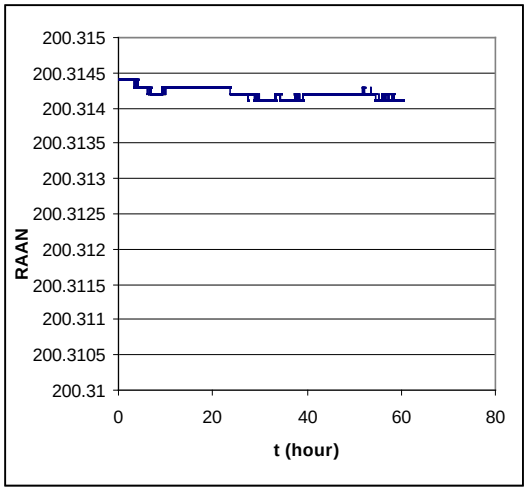

Fig.(5.f.21): Right ascension of ascending node change due to Solar attraction at hp=600 Km and $i = 8^{o}$

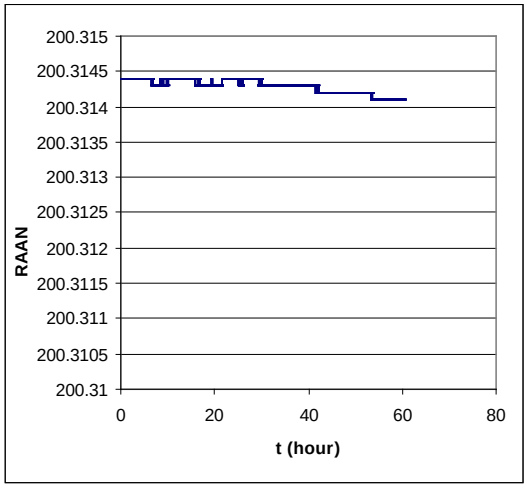

Fig.(5.f.22): Right ascension of ascending node change due to Solar attraction at hp=600 Km and $i = 63.4^{o}$

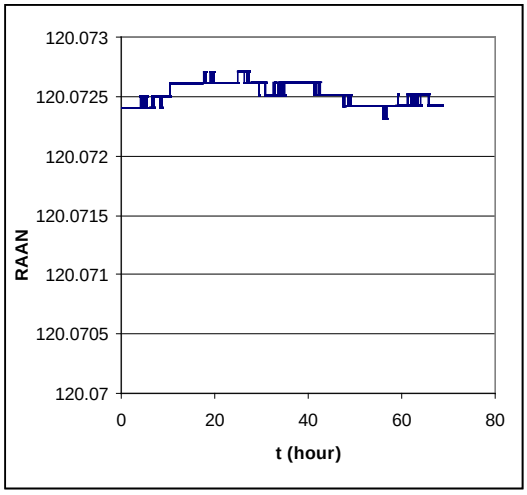

Fig.(5.f.23): Right ascension of ascending node change due to Solar attraction at hp=1200 Km and $i = 8^{o}$

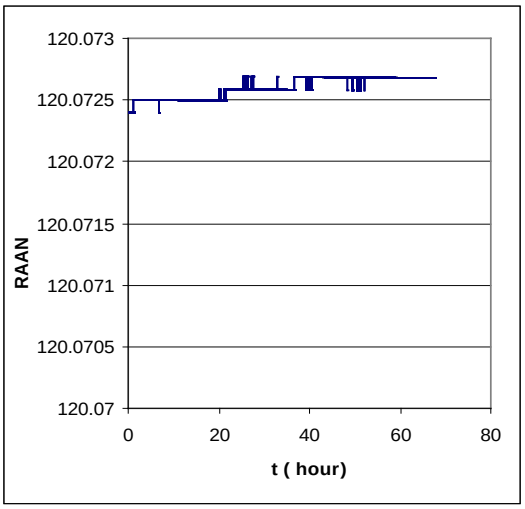

Fig.(5.f.24): Right ascension of ascending node change due to Solar attraction at hp=1200 Km and $i = 63.4^{o}$

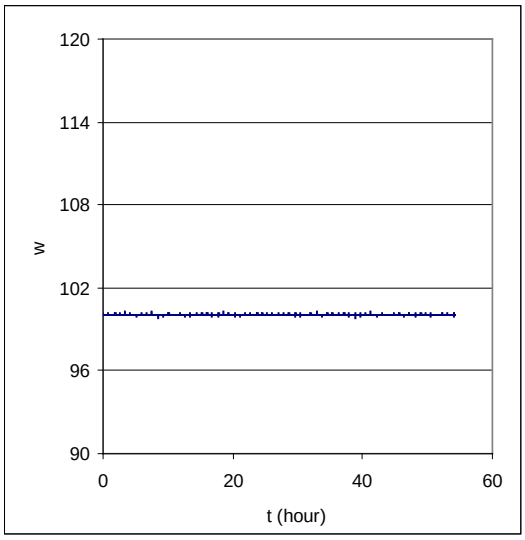

Fig.(5.f.25): Argument of perigee change due to Solar perturbation at hp=95 Km and $i = 8^{o}$

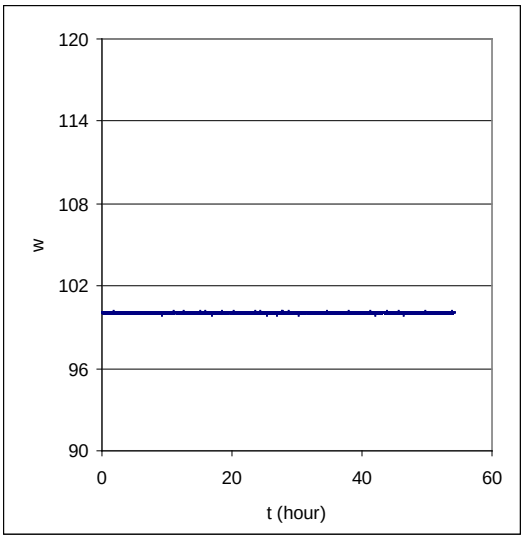

Fig.(5.f.26): Argument of perigee change due to Solar perturbation at hp=95 Km and $i = 63.4^{o}$

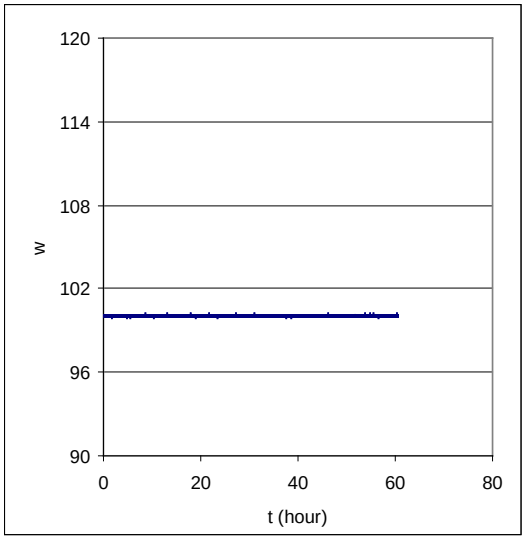

Fig.(5.f.27): Argument of perigee change due to Solar perturbation at hp=600 Km and $i = 8^{o}$

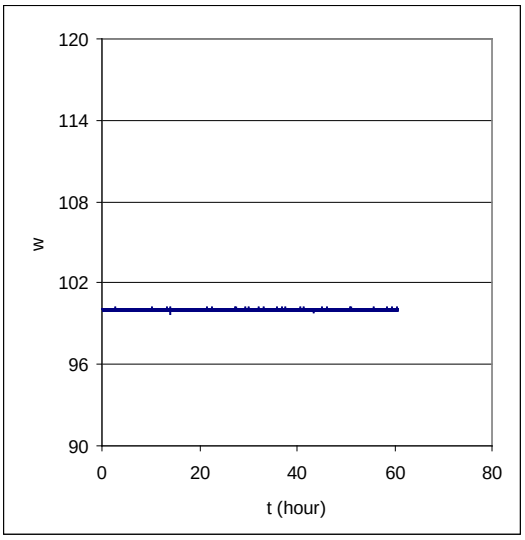

Fig.(5.f.28): Argument of perigee change due to Solar perturbation at hp=600 Km and $i = 63.4^{o}$

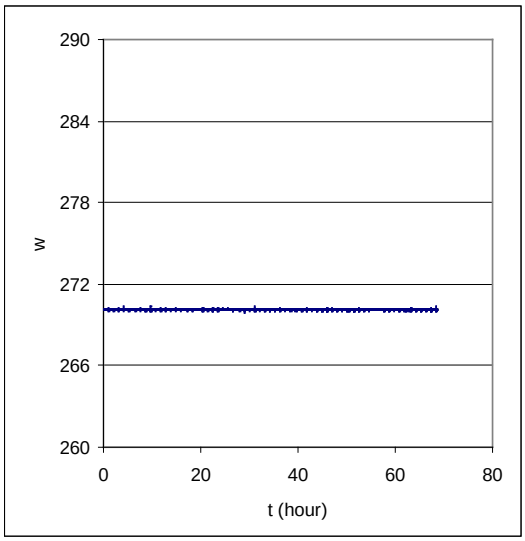

Fig.(5.f.29): Argument of perigee change due to Solar perturbation at hp=1200 Km and $i = 8^{o}$

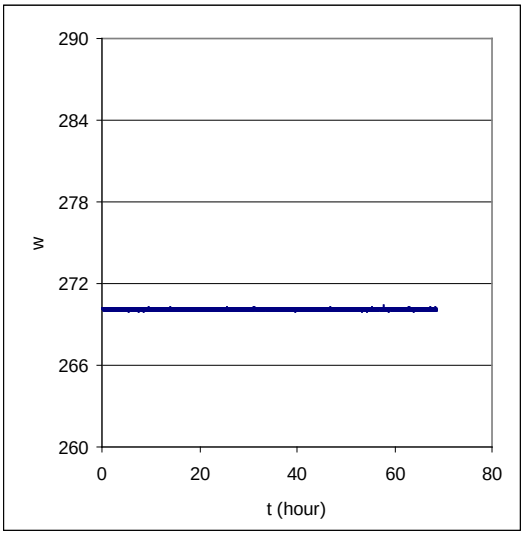

Fig.(5.f.30): Argument of perigee change due to Solar perturbation at hp=1200 Km and $i = 63.4^{o}$

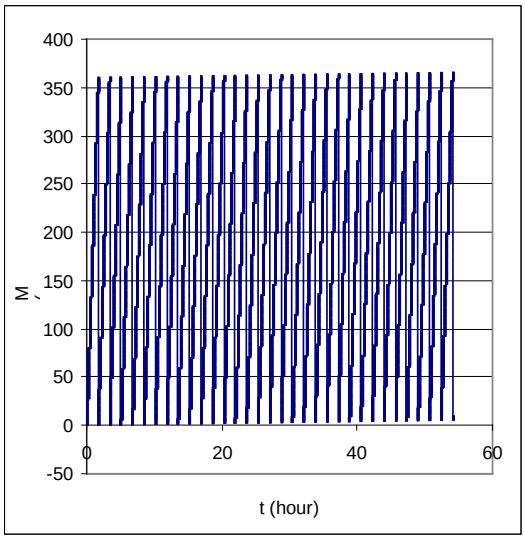

Fig.(5.f.31): Mean anomaly change due to Solar perturbation at hp=95 Km and $i = 8^{o}$

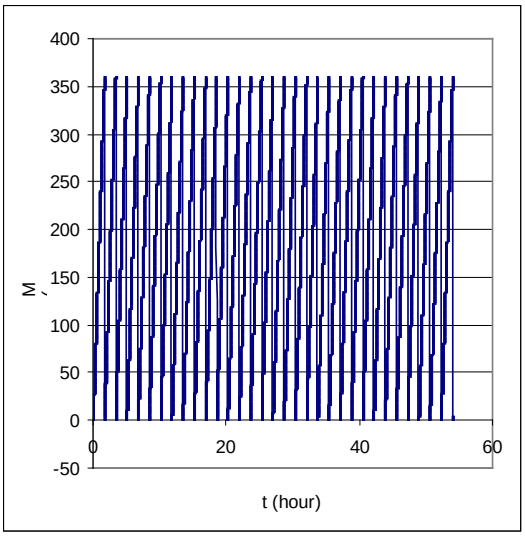

Fig.(5.f.32): Mean anomaly change due to Solar perturbation at hp=95 Km and $i = 63.4^{o}$

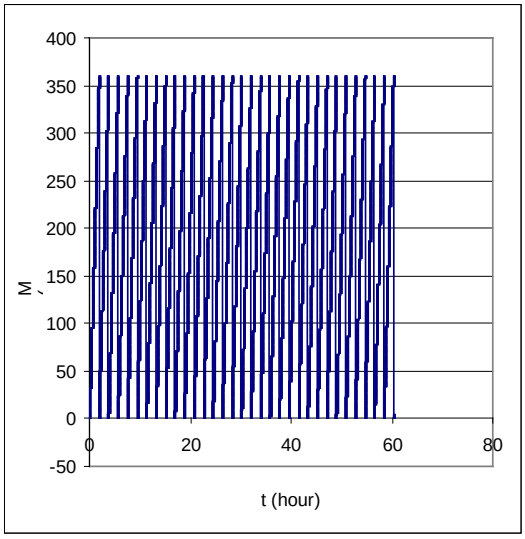

Fig.(5.f.33): Mean anomaly change due to Solar perturbation at hp=600 Km and $i = 8^{o}$

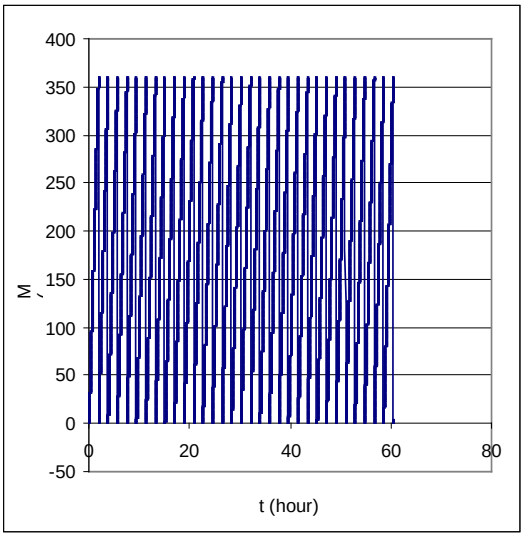

Fig.(5.f.34): Mean anomaly change due to Solar perturbation at hp=600 Km and $i = 63.4^{o}$

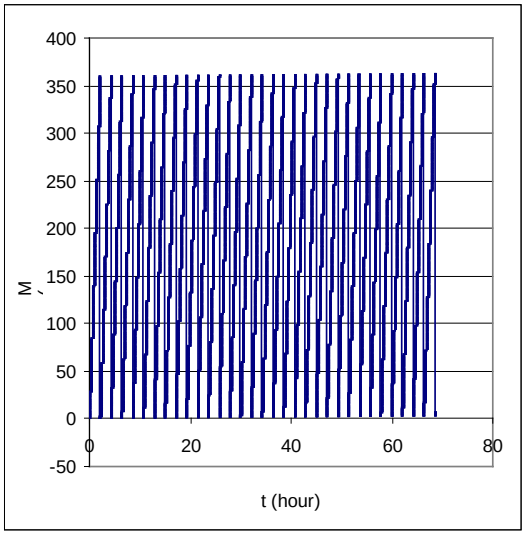

Fig.(5.f.35): Mean anomaly change due to Solar perturbation at hp=1200 Km and $i = 8^{o}$

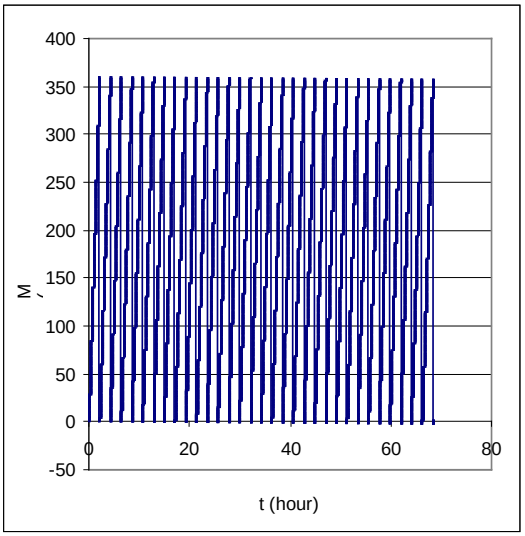

Fig.(5.f.36): Mean anomaly change due to Solar perturbation at hp=1200 Km and $i = 63.4^{o}$

g- Lunar attraction perturbation at hp=3000 Km

The changes due to the lunar attraction are very small in semi-major axis (a), eccentricity (e), inclination (i) and RAAN. It decreases with time by a larger amount at $i = 63.4^{o}$ than $i = 8^{o}$ (see figures from (5.g.1) to (5.g.8)). The difference between graphs (5.g.5) and (5.g.6) indicates that the lunar attraction has more effect when the satellite plane is shifted from the Moon plane which have $\left(i\ @m5^{o}\right)$. Also there is a small variation in argument of perigee (w), also small change in value of Mean anomaly (M) and it decreasing with time of satellite rotation.

h- Solar attraction perturbation at hp=3000 Km

The solar attraction effect shows little decrease in semi-major axis (a), eccentricity(e), inclination (i) and RAAN at $i = 8^{o}$ (see from figures (5.g.1) to (5.g.8), but it increasing in inclination (i) at $i = 63.4^{o}$ (see figure (5.h.6), and a small change in Mean anomaly see figures (5.h.11) and (5.h.12).

From figures (5.h) and figures (5.g) conclude the lunar attraction large effective than the solar attraction and both of them have more effect at high orbits. Also the same behavior with variation of the argument of perigee (w) and Mean anomaly (M) due to the effect of Solar attraction.

These behavior in Lunar and Solar because the force attraction pull and push the satellite toward them when altitude (hp) increasing reach from Sun and Moon and far from the gravity of the Earth.

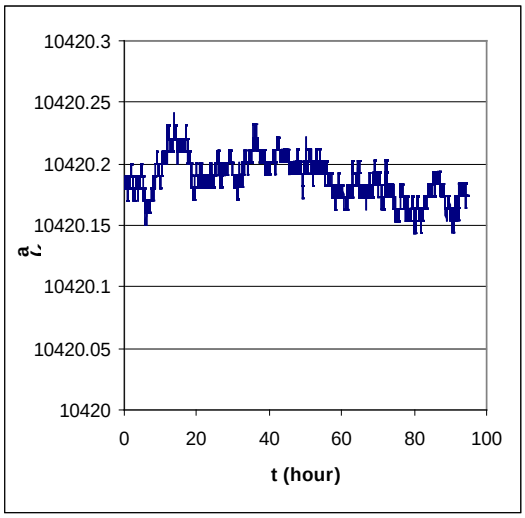

Fig.(5.g.1): Semi major axis change due to Lunar attraction at hp=3000 Km and $i = 8^{o}$

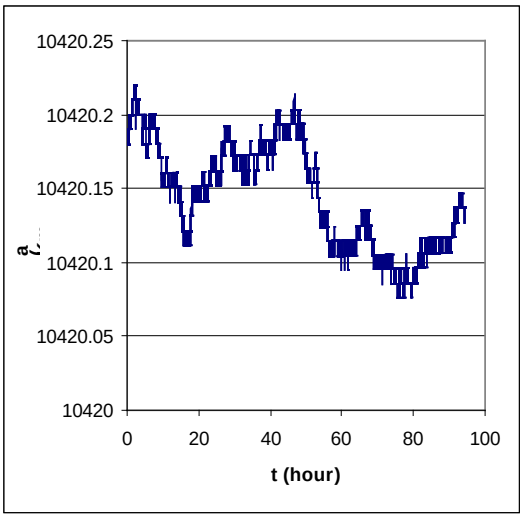

Fig.(5.g.2): Semi major axis change due to Lunar attraction at hp=3000 Km and $i = 63.4^{o}$

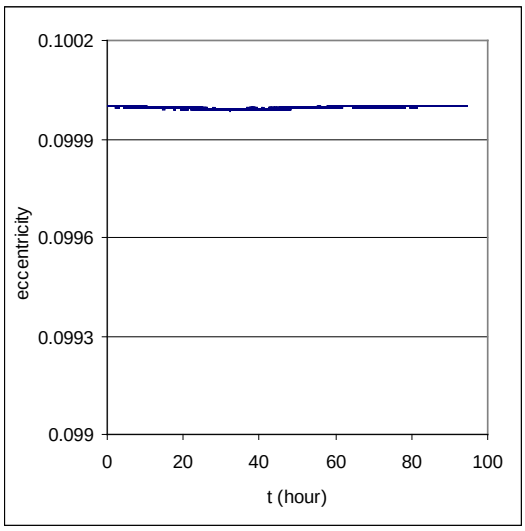

Fig.(5.g.3): eccentricity change due to Lunar attraction at hp=3000 Km and $i = 8^{o}$

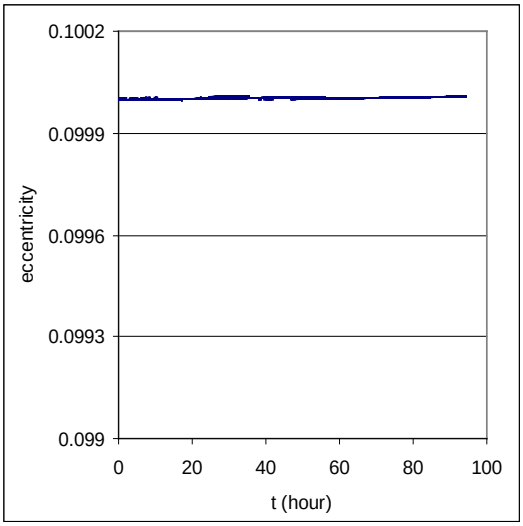

Fig.(5.g.4): eccentricity change due to Lunar attraction at hp=3000 Km and $i = 63.4^{o}$

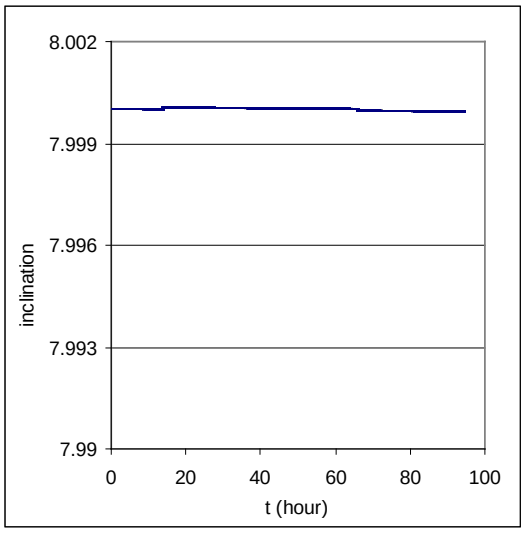

Fig.(5.g.5): inclination change due to Lunar attraction at hp=3000 Km and $i = 8^{o}$

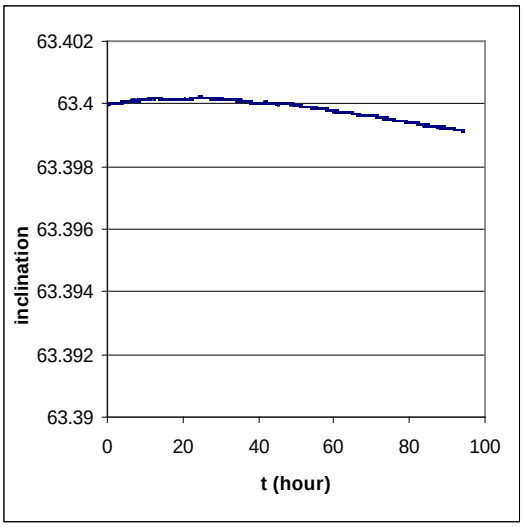

Fig.(5.g.6): inclination change due to Lunar attraction at hp=3000 Km and $i = 63.4^{o}$

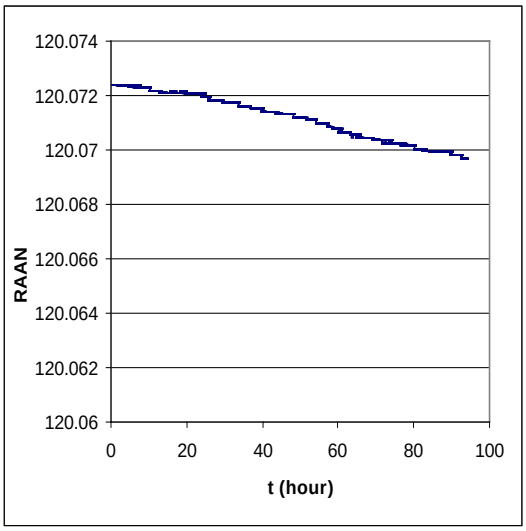

Fig.(5.g.7): Right ascension of ascending node change due to Lunar attraction at hp=3000 Km and $i = 8^{o}$

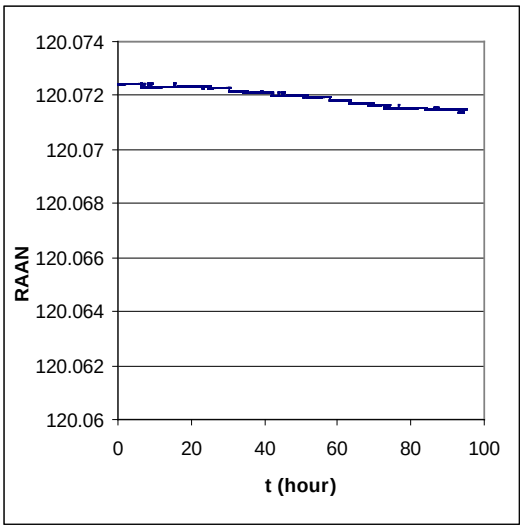

Fig.(5.g.8): Right ascnsion of ascending node change due to Lunar attraction at hp=3000 Km and $i = 63.4^{o}$

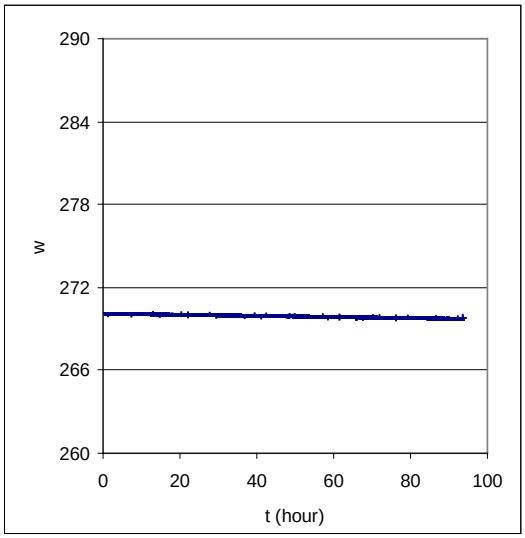

Fig.(5.g.9): Argument of perigee change due to Lunar attraction at hp=3000 Km and $i = 8^{o}$

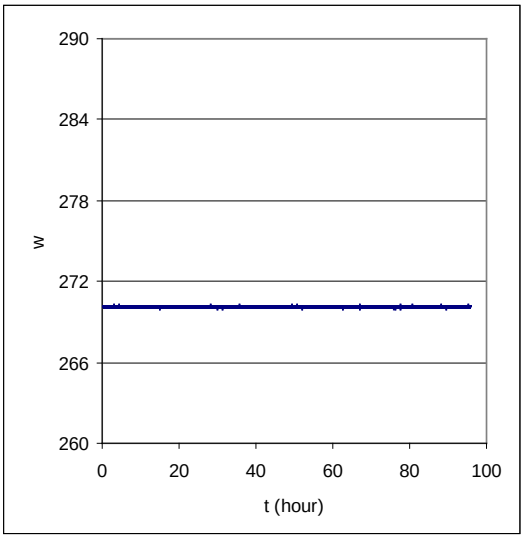

Fig.(5.g.10): Argument of perigee change due to Lunar attraction at hp=3000 Km and $i = 63.4^{o}$

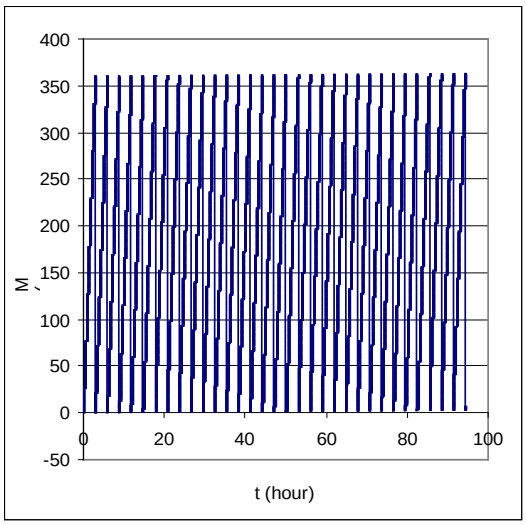

Fig.(5.g.11): Mean anomaly change due to Lunar attraction at hp=3000 Km and $i = 8^{o}$

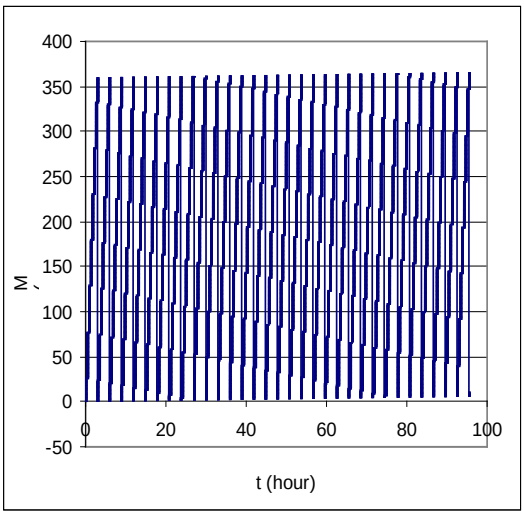

Fig.(5.g.12): Mean anomaly change due to Lunar attraction at hp=3000 Km and $i = 63.4^{o}$

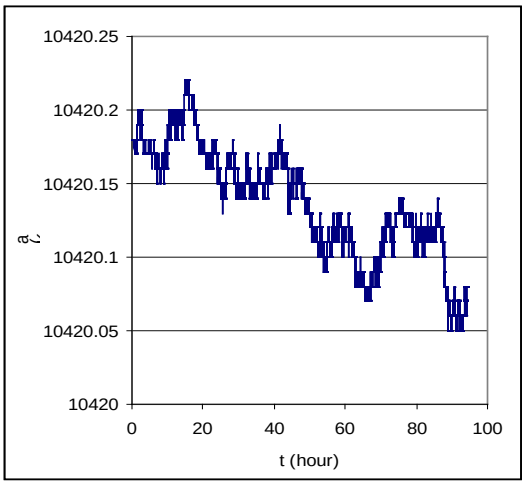

Fig.(5.h.1): Semi-major axis change due to Solar attraction at hp=3000 Km and $i = 8^{o}$

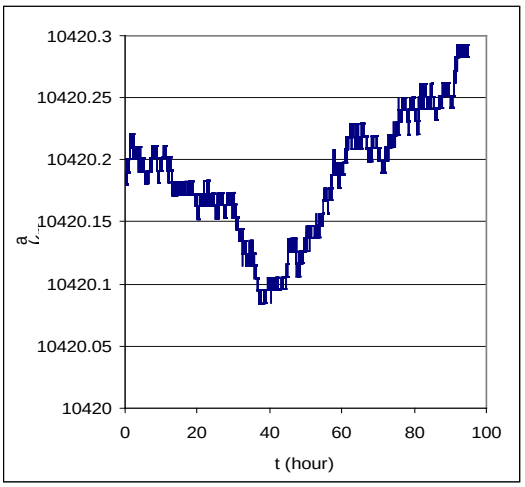

Fig.(5.h.2): Semi-major axis change due to Solar attraction at hp=3000 Km and $i = 63.4^{o}$

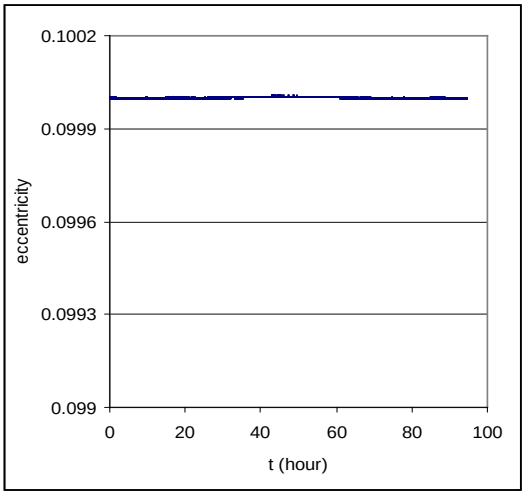

Fig.(5.h.3): Eccentricity change due to Solar attraction at hp=3000 Km and $i = 8^{o}$

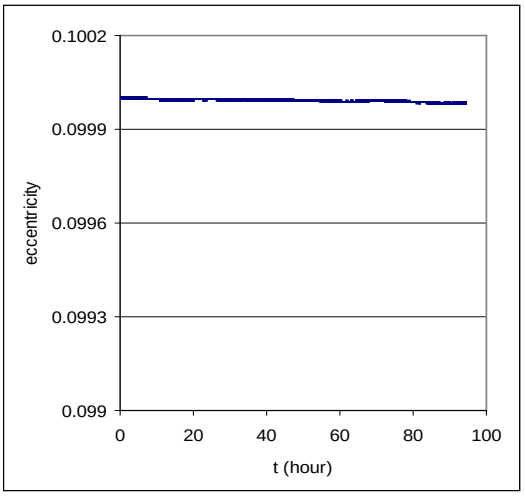

Fig.(5.h.4): Eccentricity change due to Solar attraction at hp=3000 Km and $i = 63.4^{o}$

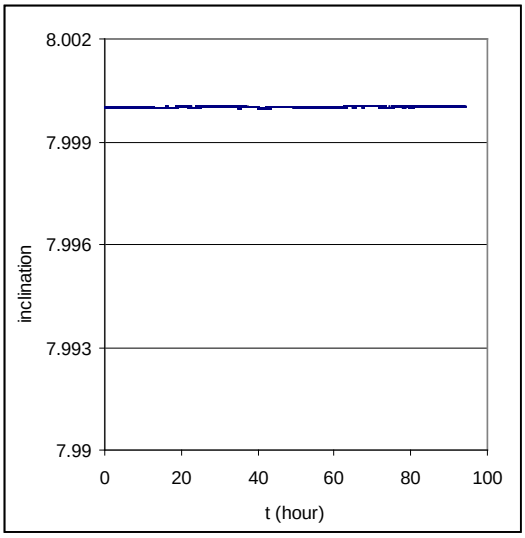

Fig.(5.h.5): Inclination change due to Solar attraction at hp=3000 Km and $i = 8^{o}$

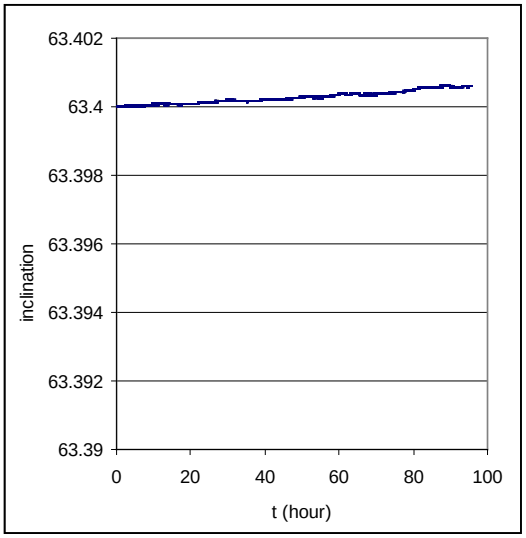

Fig.(5.h.6): Inclination change due to Solar attraction at hp=3000 Km and $i = 63.4^{o}$

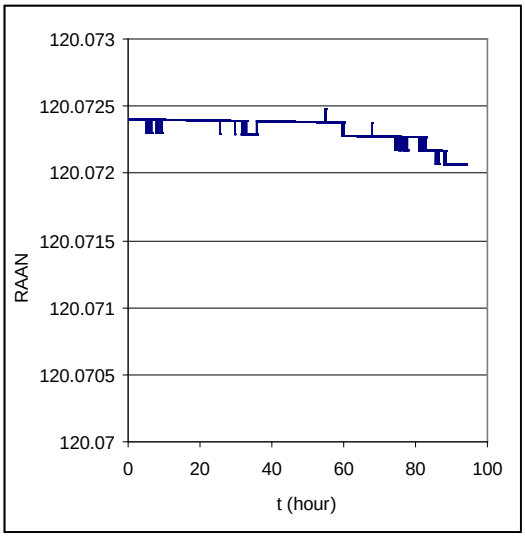

Fig.(5.h.7): Right ascension of ascending node change due to Solar attraction at hp=3000 Km and $i = 8^{o}$

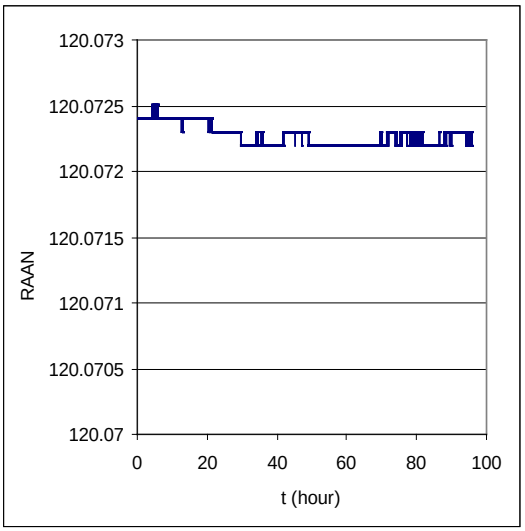

Fig.(5.h.8): Right ascension of ascending node change due to Solar attraction at hp=3000 Km and $i = 63.4^{o}$

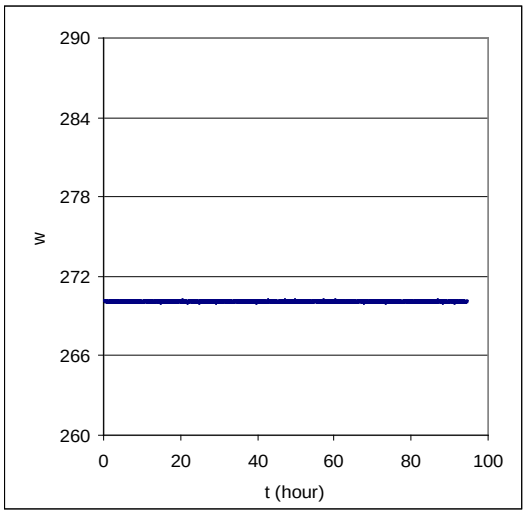

Fig.(5.h.9): Argument of perigee change due to Solar attraction at hp=3000 Km and $i = 8^{o}$

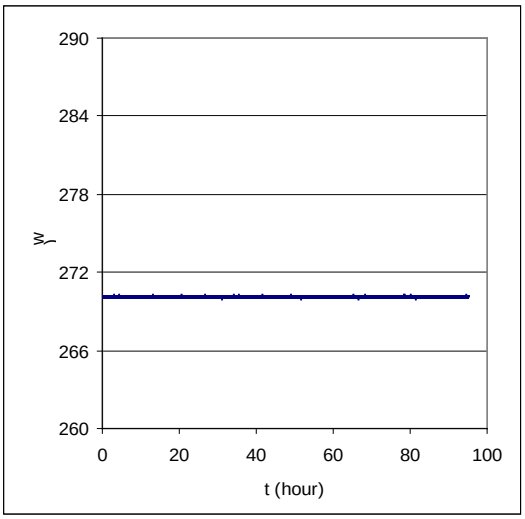

Fig.(5.g.10): Argument of perigee change due to Solar attraction at hp=3000 Km and $i = 63.4^{o}$

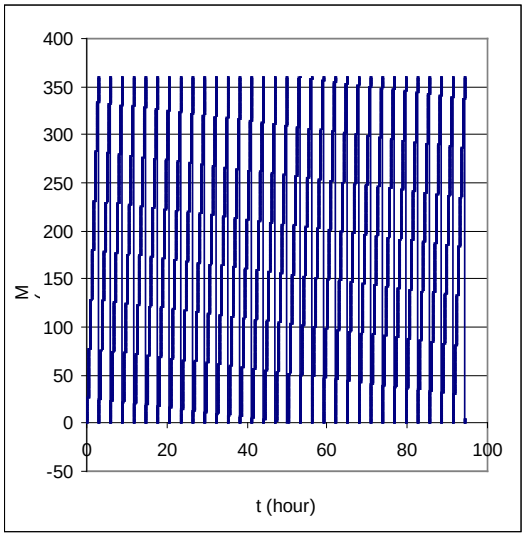

Fig.(5.h.11): Mean anomaly change due to Solar attraction at hp=3000 Km and $i = 8^{o}$

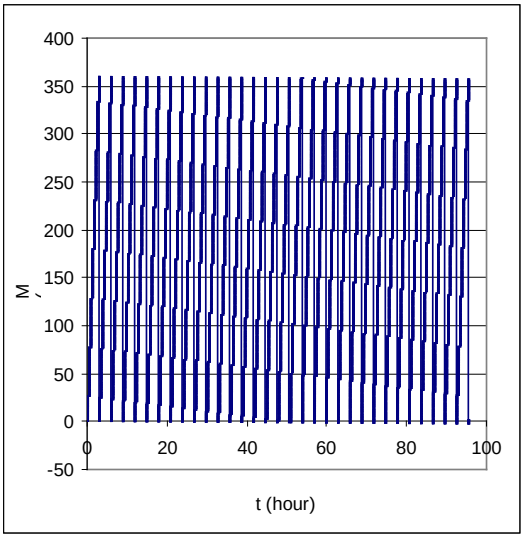

Fig.(5.h.12): Mean anomaly change due to Solar attraction at hp=3000 Km and $i = 63.4^{o}$

i- All perturbations result

When the effects of all perturbations (atmospheric drag, oblatness of Earth, solar radiation pressure and third-body attraction (such Lunar and Solar)) are included, it can be observed that the semi-major axis (a) decreases linearly and periodically with time at hp=95 Km with more vibrations at $i = 63.4^{o}$ (see figures (5.i.1) and (5.i.2)). Because the effect of the atmospheric drag is great for LEO, and semi-major axis (a) increases periodically with all periods at hp=600, 1200 Km (see figures from (5.i.3) to (5.i.6)), it decreases by 150 meters at hp=3000 Km (see figures (5.i.7) and (5.i.8)). Also the figures show that the perturbations are various because the variation of inclination at high altitude.

The eccentricity (e) for hp=95 Km decreases linearly and periodically with time (see figures (5.i.9) and (5.i.10)). For altitudes (hp=600, 1200 Km), the eccentricity (e) increases linearly and periodically with time, but it is periodic under 0.1 at $i = 8^{o}$, and above 0.1 at $i = 63.4^{o}$ (see figures from (5.i.11) to (5.i.14)), that it is because the effect of the atmospheric drag and SRP are more near the ecliptic plane $\left(i = \text{m}23.4^{o}\right)$. The eccentricity (e) shows a small decrease at hp=3000 Km (see figures (5.i.15) and (5.i.16)).

The inclination (i) for hp=95, 1200 Km decrease linearly and periodically with time, it becomes large at $i = 63.4^{o}$ than $i = 8^{o}$ (see figures (5.i.17), (5.i.18), (5.i.21) and (5.i.22)). The inclination (i) increase linearly and periodically with time, but it becomes large at $i = 8^{o}$ than $i = 63.4^{o}$ (see figures (5.i.19), and (5.i.20)), this is because the effect of the atmospheric drag and SRP. The inclination (i) shows a small increase at hp=3000 Km (see figures (5.i.23) and (5.i.24)).

For all altitude hp=95, 600, 1200, 3000 Km and inclination $i = 8^{o}, 63.4^{o}$ which are plotted in figures (5.i.25) - (5.i.36). RAAN observed decreases linearly with time and ΔW is smaller at $i = 63.4^{o}$ than $i = 8^{o}$. Where the $\Delta RAAN$ at $i = 63.4^{o}$ are between $(0.125^{o}, 0.333^{o})$, but $\Delta RAAN$ at $i = 8^{o}$ are between $(0.2727^{o}, 0.0737^{o})$.

At $i = 8^{o}$, the argument of perigee (w) increases linearly with time for all altitudes hp=95, 600, 1200, 3000 Km, but it decreases at $i = 63.4^{o}$, and hp=95 Km and periodic increasing at hp=600, 1200, 3000 Km (see figures (5.i.33) - (5.i.40)). But there is a small change in value of Mean anomaly (M), its change through one period between 0 and 360 degree (see figures (5.i.41) - (5.i.48)).

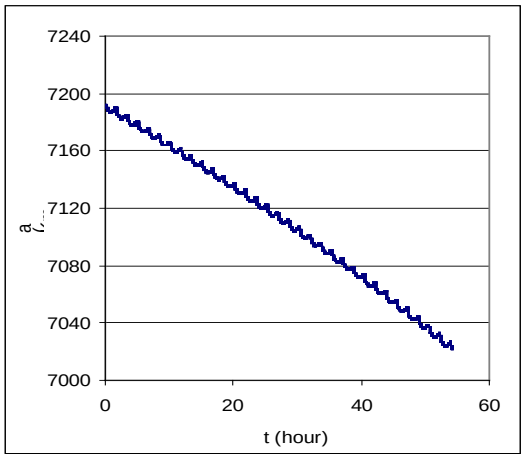

Fig.(5.i.1): Semi major axis change due to effect of all perturbations at hp=95 Km and $i = 8^{o}$

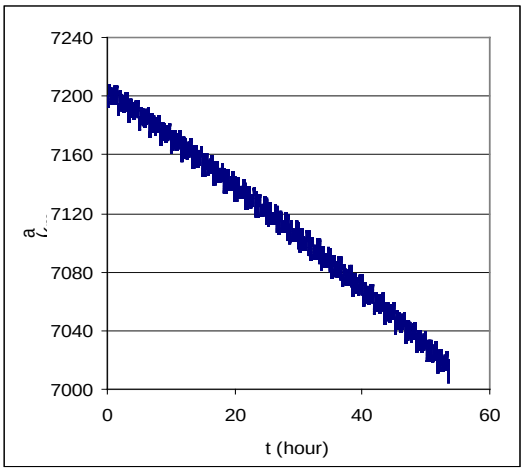

Fig.(5.i.2): Semi major axis change due to effect of all perturbations at hp=95 Km and $i = 63.4^{o}$

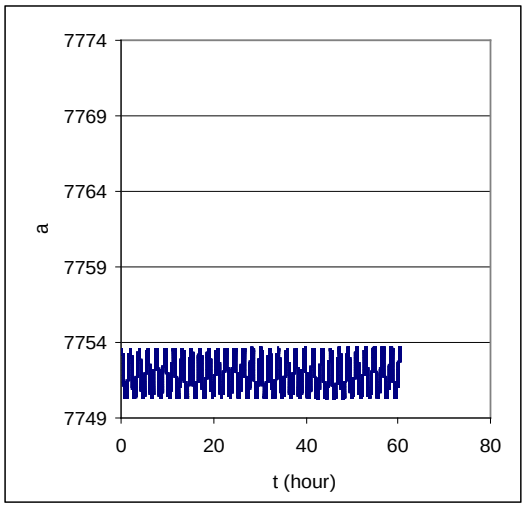

Fig.(5.i.3): Semi major axis change due to effect of all perturbations at hp=600 Km and $i = 8^{o}$

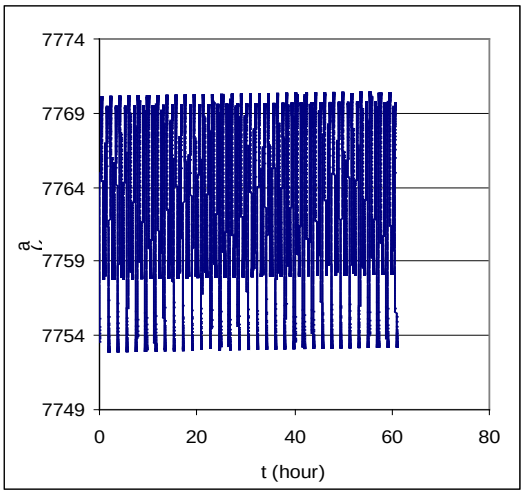

Fig.(5.i.4): Semi major axis change due to effect of all perturbations at hp=600 Km and $i = 63.4^{o}$

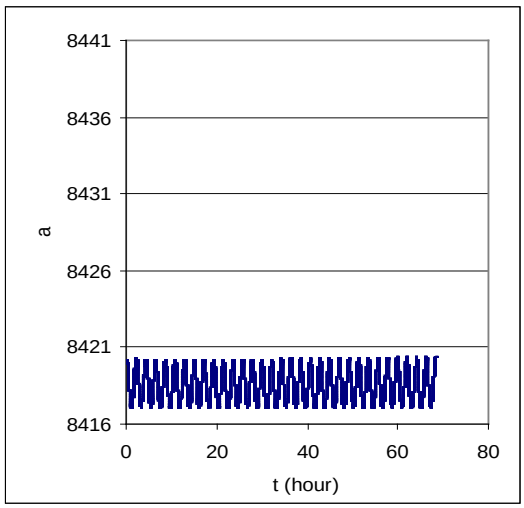

Fig.(5.i.5): Semi major axis change due to effect of all perturbations at hp=1200 Km and $i = 8^{o}$

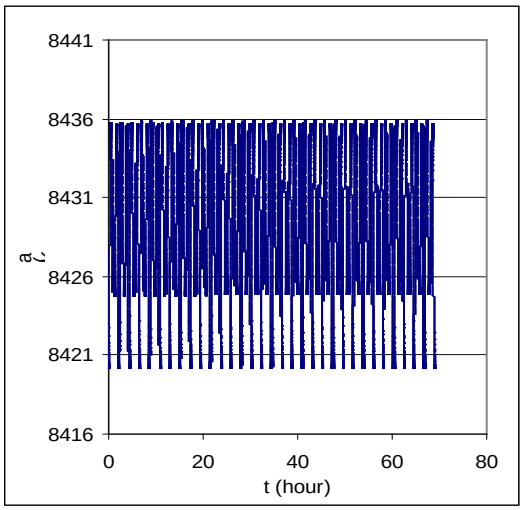

Fig.(5.i.6): Semi major axis change due to effect of all perturbations at hp=1200 Km and $i = 63.4^{o}$

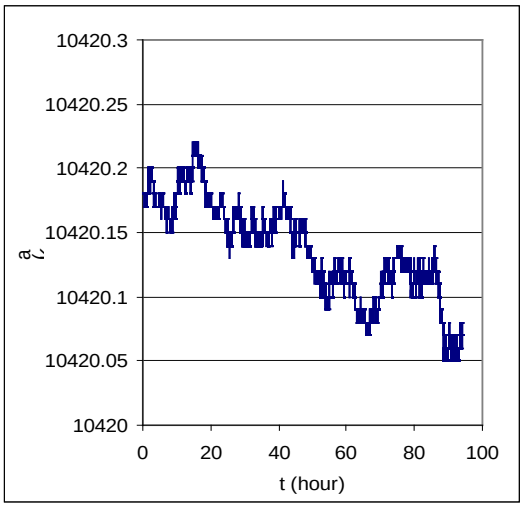

Fig.(5.i.7): Semi major axis change due to effect of all perturbations at hp=3000 Km and $i = 8^{o}$

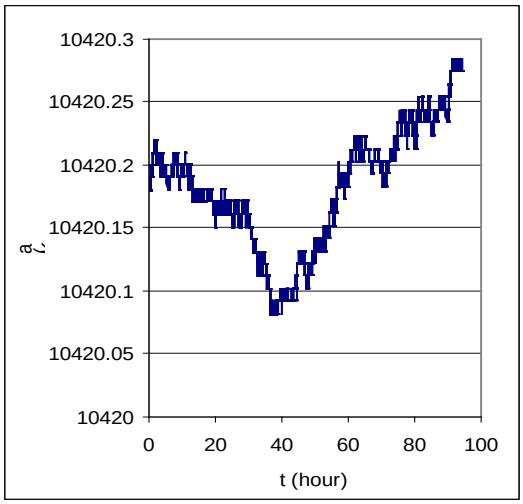

Fig.(5.i.8): Semi major axis change due to effect of all perturbations at hp=3000 Km and $i = 63.4^{o}$

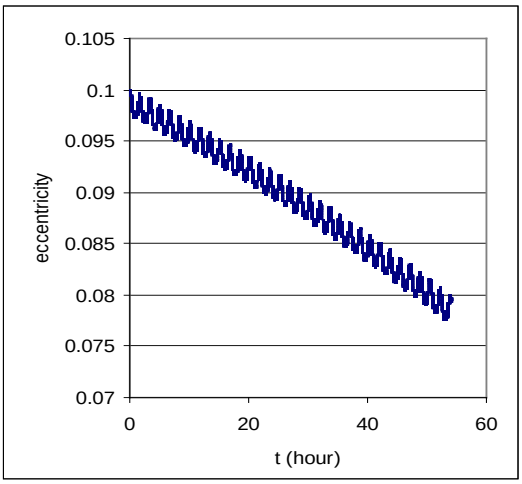

Fig.(5.i.9): eccentricity change due to effect of all perturbations at hp=95 Km and $i = 8^{o}$

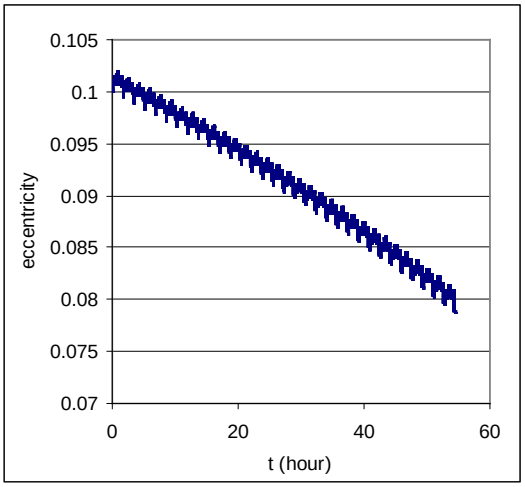

Fig.(5.i.10): eccentricity change due to effect of all perturbations at hp=95 Km and $i = 63.4^{o}$ **.**

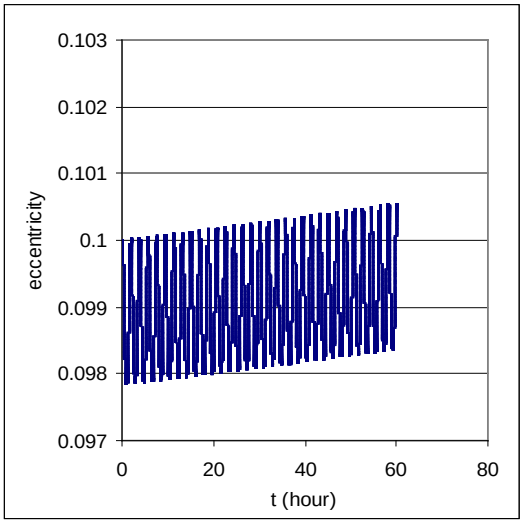

Fig.(5.i.11): eccentricity change due to effect of all perturbations at hp=600 Km and $i = 8^{o}$ **.**

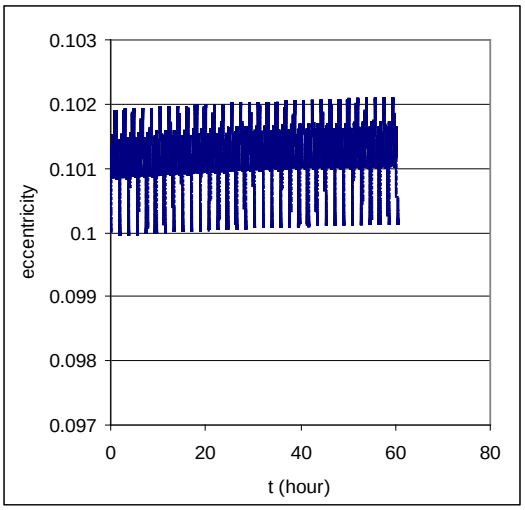

Fig.(5.i.12): eccentricity change due to effect of all perturbations at hp=600 Km and $i = 63.4^{o}$

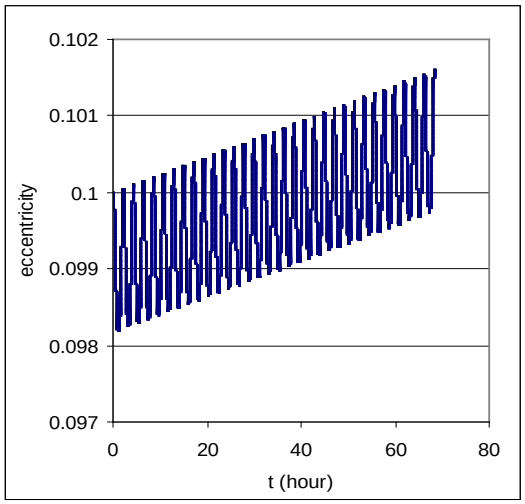

Fig.(5.i.13): eccentricity change due to effect of all perturbations at hp=1200 Km and $i = 8^{o}$

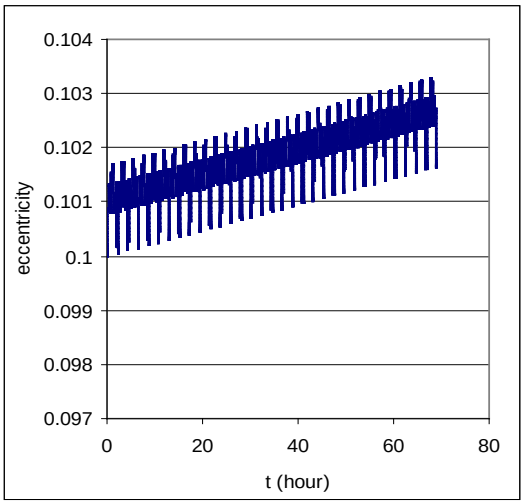

Fig.(5.i.14): eccentricity change due to effect of all perturbations at hp=1200 Km and $i = 63.4^{o}$

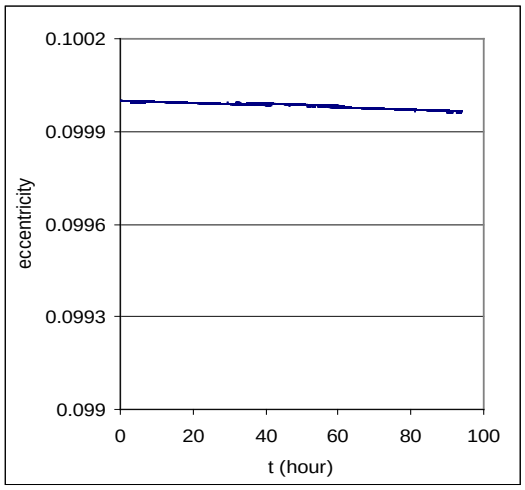

Fig.(5.i.15): eccentricity change due to effect of all perturbations at hp=3000 Km and $i = 8^{o}$

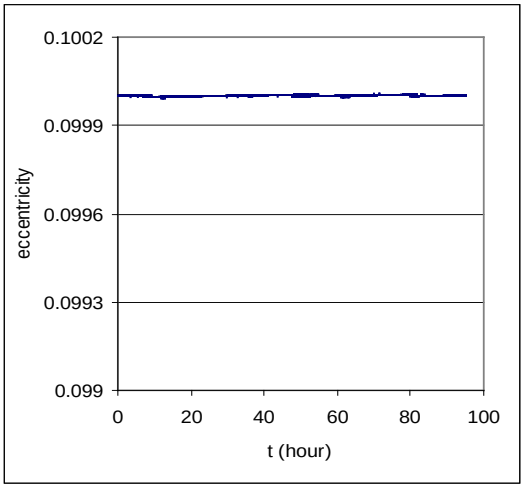

Fig.(5.i.16): eccentricity change due to effect of all perturbations at hp=3000 Km and $i = 63.4^{o}$

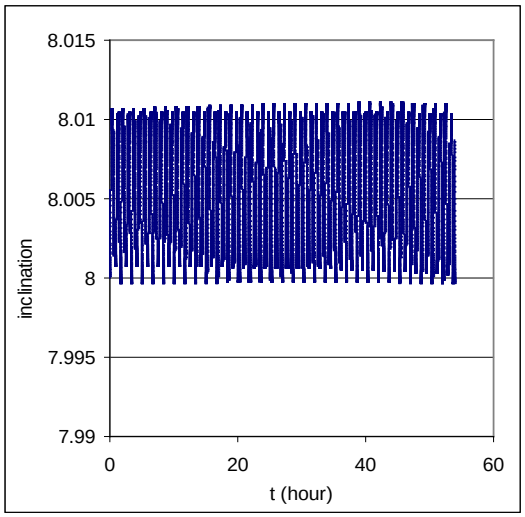

Fig.(5.i.17): inclination change due to effect of all perturbations at hp=95 Km and $i = 8^{o}$

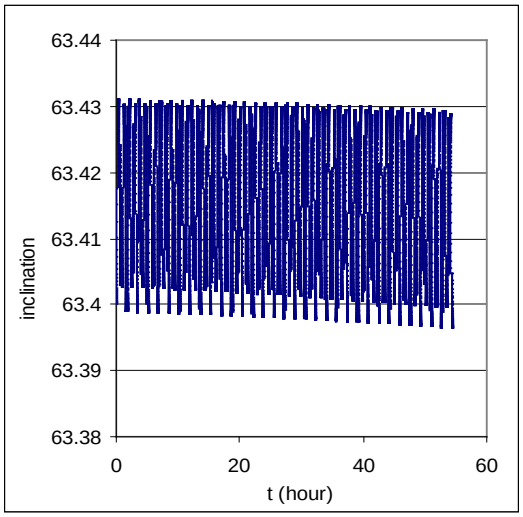

Fig.(5.i.18): inclination change due to effect of all perturbations at hp=95 Km and $i = 63.4^{o}$

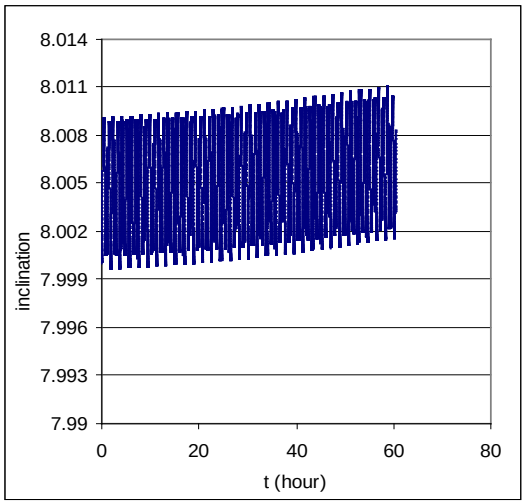

Fig.(5.i.19): inclination change due to effect of all perturbations at hp=600 Km and $i = 8^{o}$

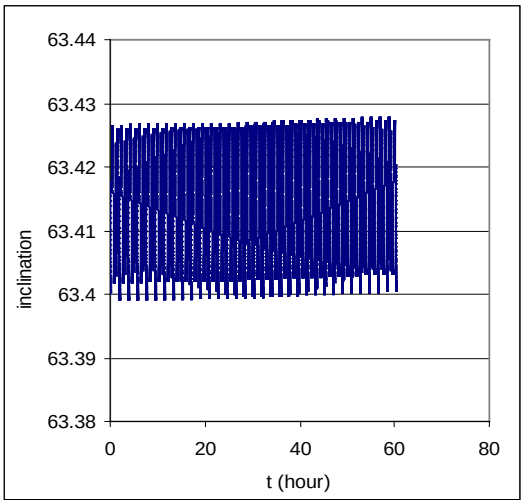

Fig.(5.i.20): inclination change due to effect of all perturbations at hp=600 Km and $i = 63.4^{o}$

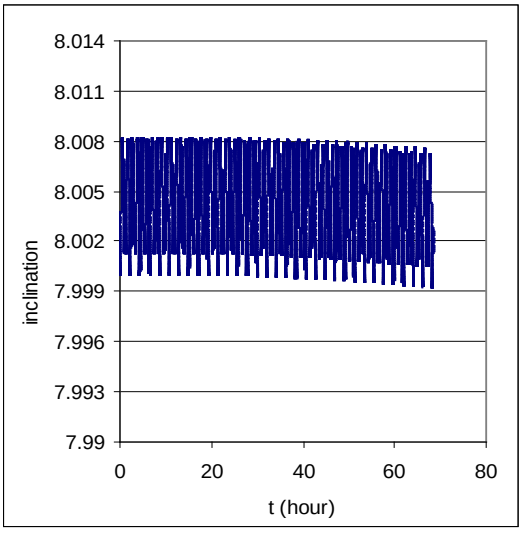

Fig.(5.i.21): inclination change due to effect of all perturbations at hp=1200 Km and $i = 8^{o}$

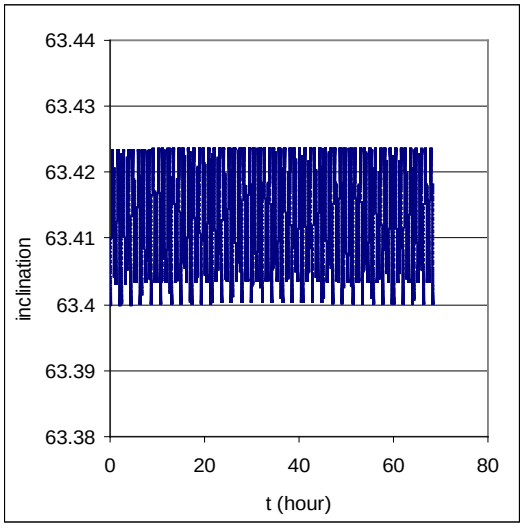

Fig.(5.i.22): inclination change due to effect of all perturbations at hp=1200 Km and $i = 63.4^{o}$

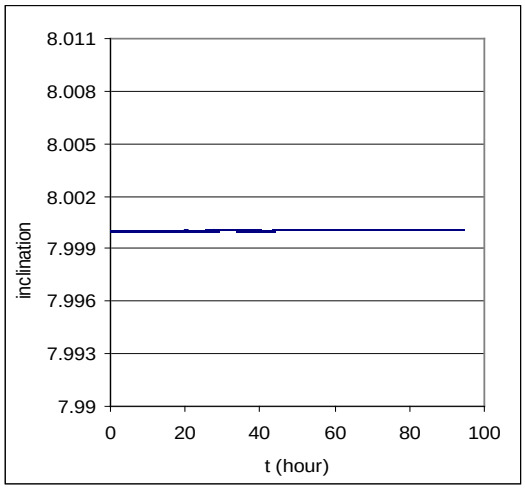

Fig.(5.i.23): inclination change due to effect of all perturbations at hp=3000 Km and $i = 8^{o}$

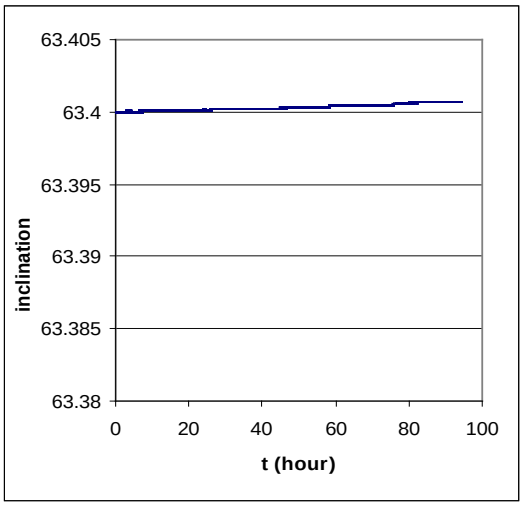

Fig.(5.i.24): inclination change due to effect of all perturbations at hp=3000 Km and $i = 63.4^{o}$

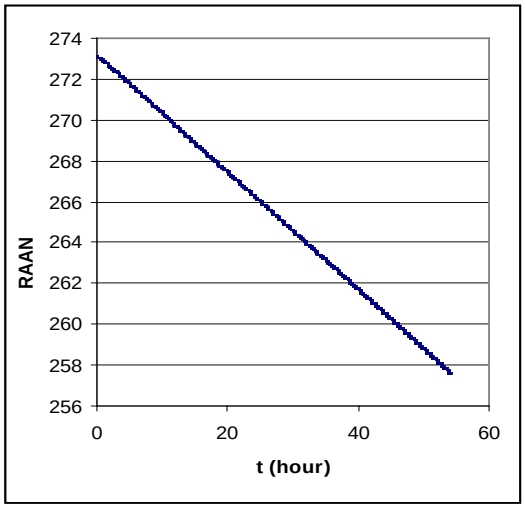

Fig.(5.i.25): Right ascension of ascending node change due to effect of all perturbations at hp=95 Km and $i = 8^{o}$

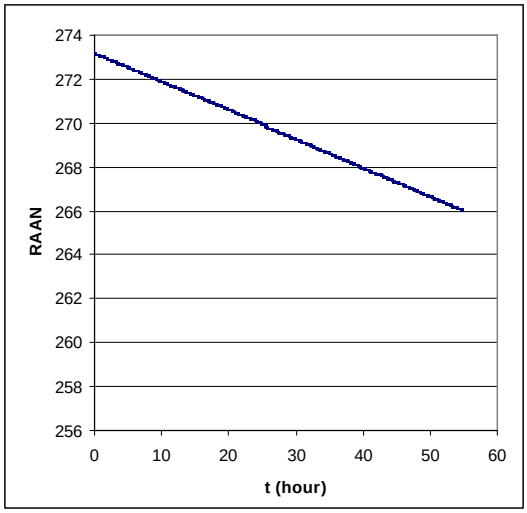

Fig.(5.i.26): Right ascension of ascending node change due to effect of all perturbations at hp=95 Km and $i = 63.4^{o}$

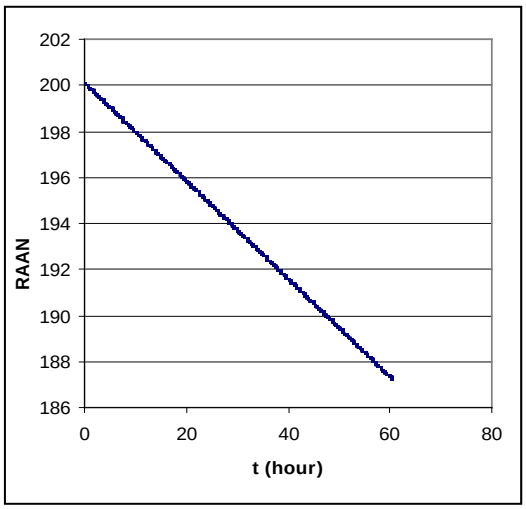

Fig.(5.i.27): Right ascension of ascending node change due to effect of all perturbations at hp=600 Km and $i = 8^{o}$

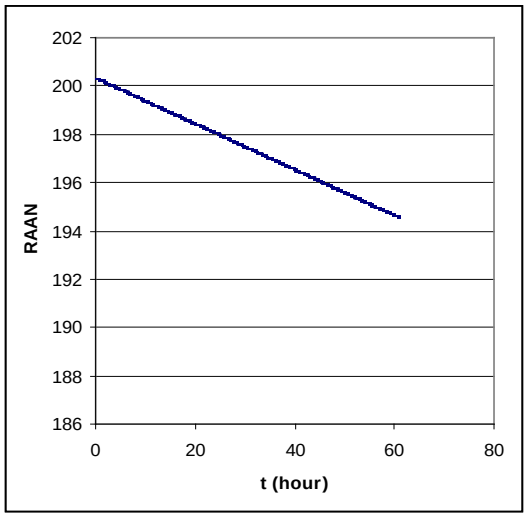

Fig.(5.i.28): Right ascension of ascending node change due to effect of all perturbations at hp=600 Km and $i = 63.4^{o}$

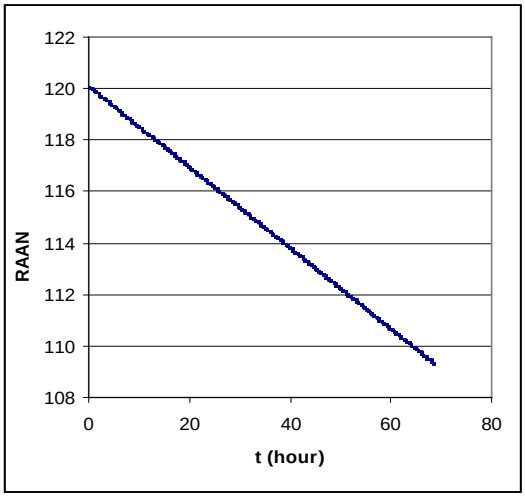

Fig.(5.i.29): Right ascension of ascending node change due to effect of all perturbations at hp=1200 Km and $i = 8^{o}$

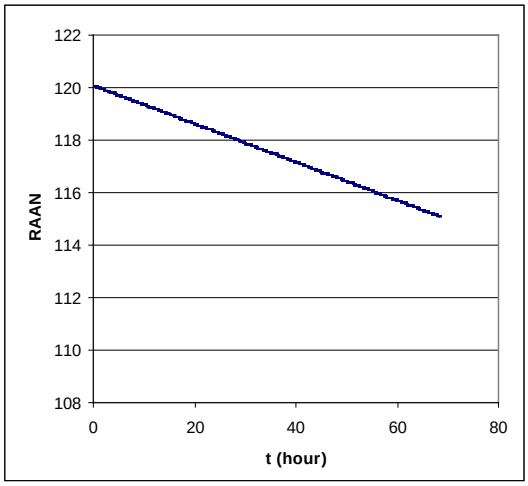

Fig.(5.i.30): Right ascension of ascending node change due to effect of all perturbations at hp=1200 Km and $i = 63.4^{o}$

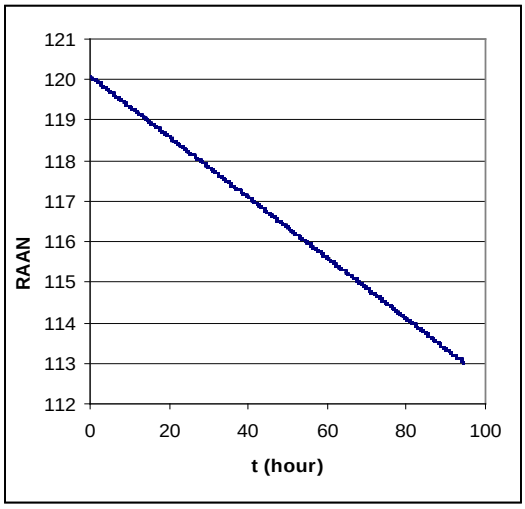

Fig.(5.i.31): Right ascension of ascending node change due to effect of all perturbations at hp=3000 Km and $i = 8^{o}$

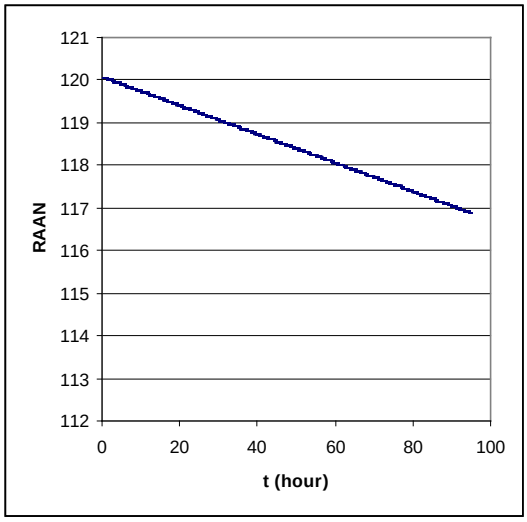

Fig.(5.i.32): Right ascension of ascending node change due to effect of all perturbations at hp=3000 Km and $i = 63.4^{o}$

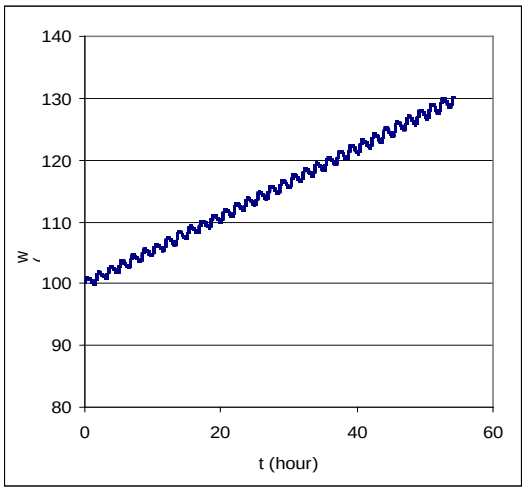

Fig.(5.i.33): Argument of perigee change due to effect of all perturbations at hp=95 Km and $i = 8^{o}$

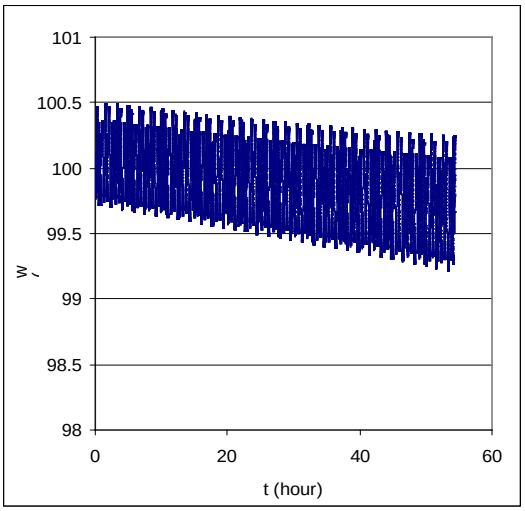

Fig.(5.i.34): Argument of perigee change due to effect of all perturbations at hp=95 Km and $i = 63.4^{o}$

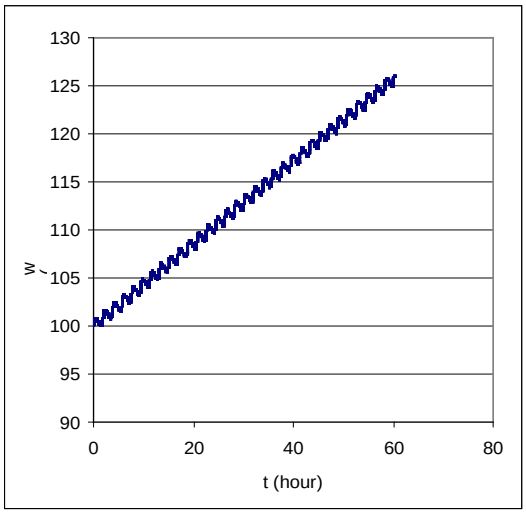

Fig.(5.i.35): Argument of perigee change due to effect of all perturbations at hp=600 Km and $i = 8^{o}$

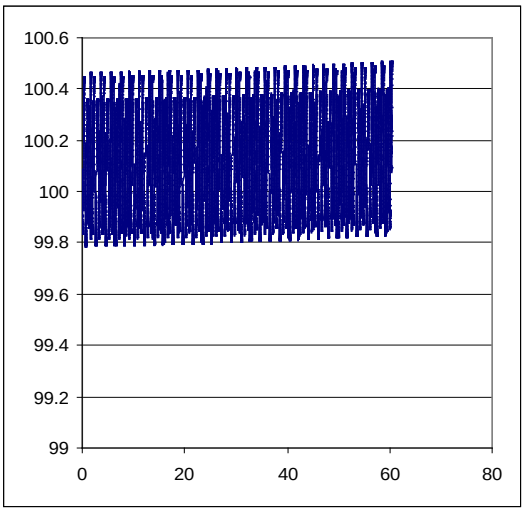

Fig.(5.i.36): Argument of perigee change due to effect of all perturbations at hp=600 Km and $i = 63.4^{o}$

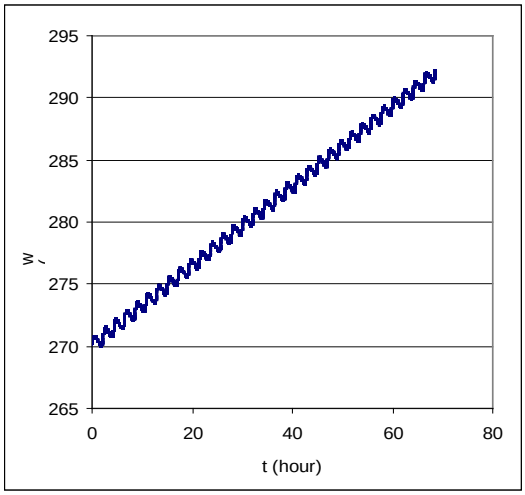

Fig.(5.i.37): Argument of perigee change due to effect of all perturbations at hp=1200 Km and $i = 8^{o}$

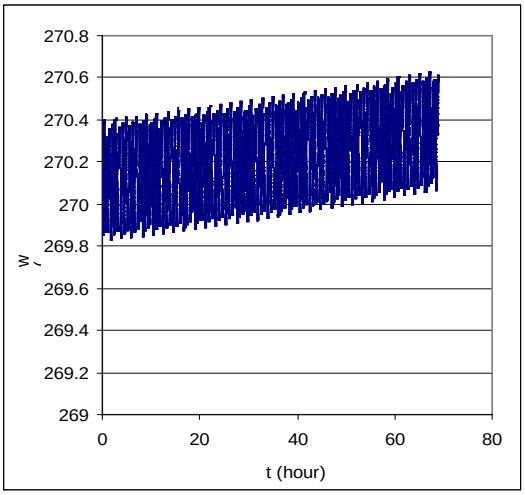

Fig.(5.i.38): Argument of perigee change due to effect of all perturbations at hp=1200 Km and $i = 63.4^{o}$

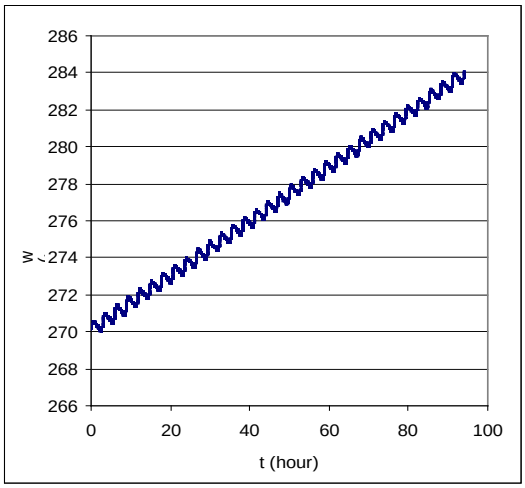

Fig.(5.i.39): Argument of perigee change due to effect of all perturbations at hp=3000 Km and $i = 8^{o}$

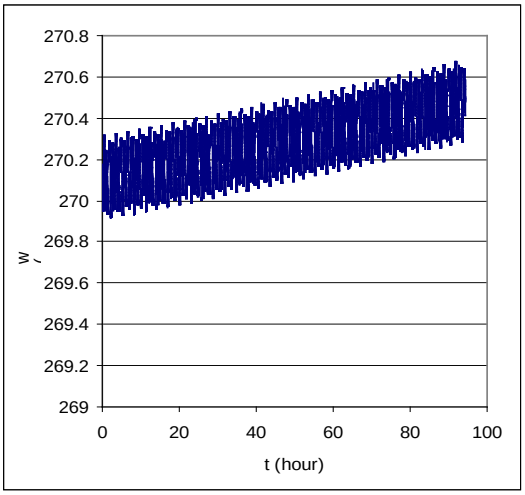

Fig.(5.i.40): Argument of perigee change due to effect of all perturbations at hp=3000 Km and $i = 63.4^{o}$

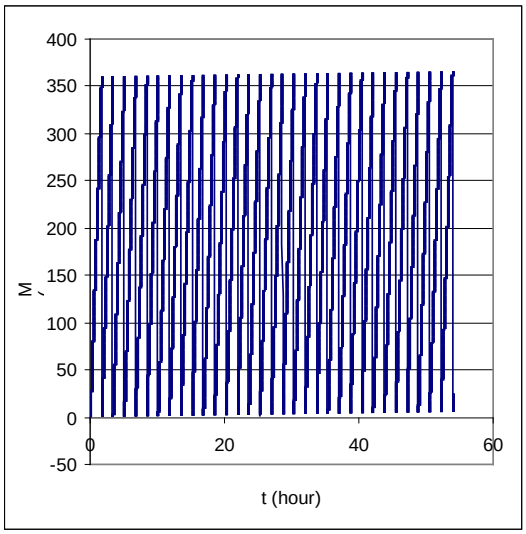

Fig.(5.i.41): Mean anomaly change due to effect of all perturbations at hp=95 Km and $i = 8^{o}$

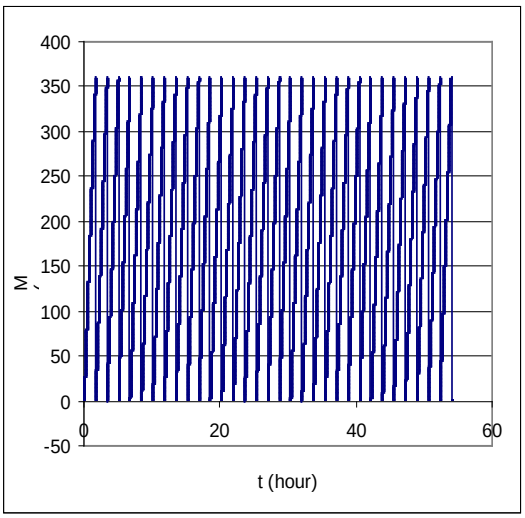

Fig.(5.i.42): Mean anomaly change due to effect of all perturbations at hp=95 Km and $i = 63.4^{o}$

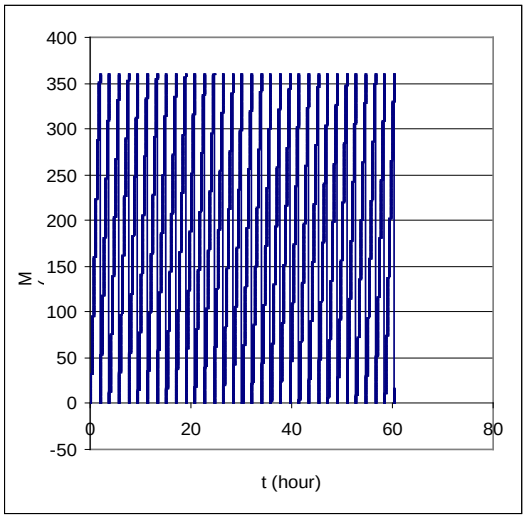

Fig.(5.i.43): Mean anomaly change due to effect of all perturbations at hp=600 Km and $i = 8^{o}$

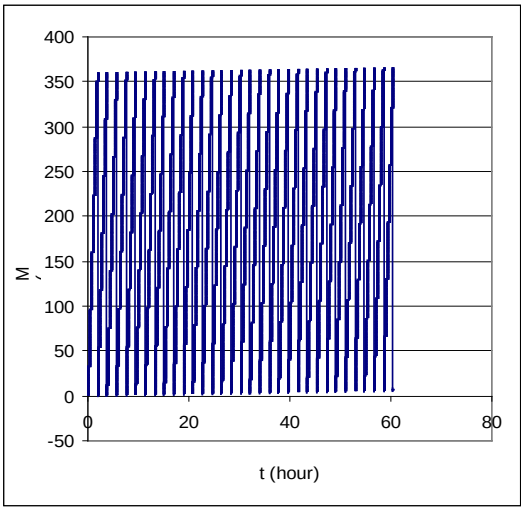

Fig.(5.i.44): Mean anomaly change due to effect of all perturbations at hp=600 Km and $i = 63.4^{o}$

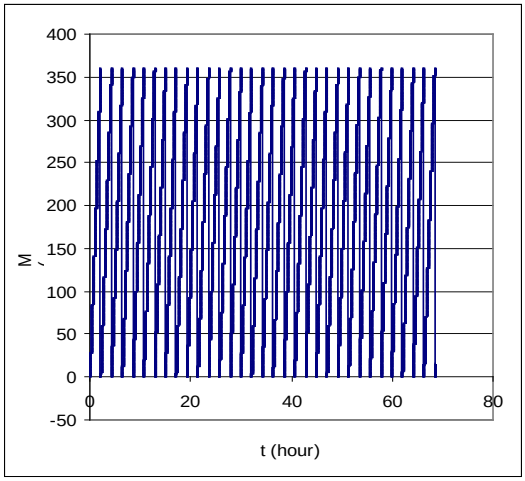

Fig.(5.i.45): Mean anomaly change due to effect of all perturbations at hp=1200 Km and $i = 8^{o}$

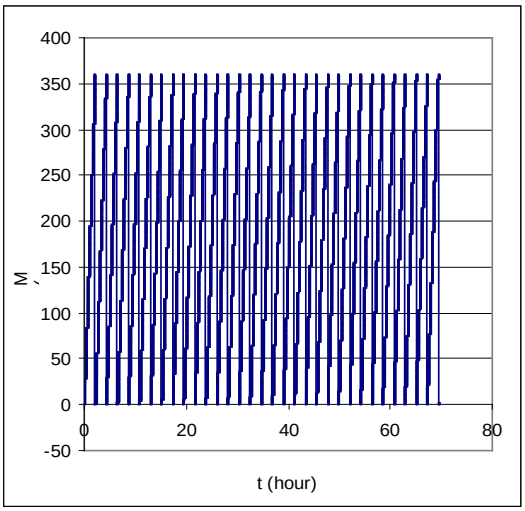

Fig.(5.i.46): Mean anomaly change due to effect of all perturbations at hp=1200 Km and $i = 63.4^{o}$

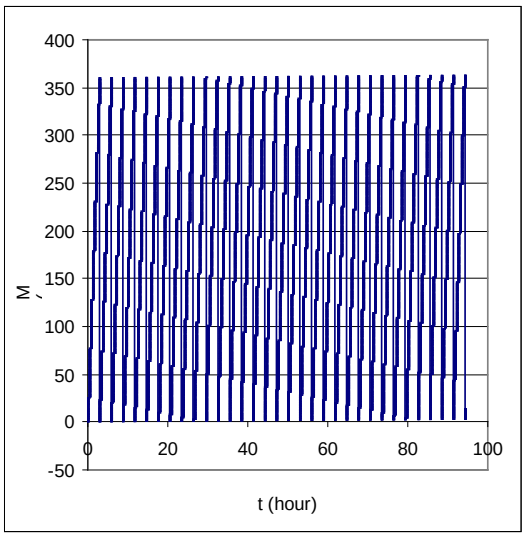

Fig.(5.i.47): Mean anomaly change due to effect of all perturbations at hp=3000 Km and $i = 8^{o}$

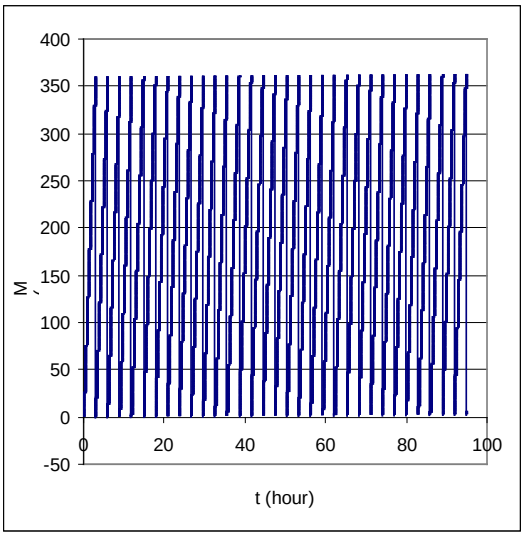

Fig.(5.i.48): Mean anomaly change due to effect of all perturbations at hp=3000 Km and $i = 63.4^{o}$

5.3 Discussion of the tables

Tables (5.1) to (5.12) show the variation in orbital elements through one period due to the effect of the perturbations for three inclinations and four altitudes.

Inspection table (5.1), at hp=95 and $i = 8^{o}$, notice that the most effective perturbations on the semi-major axis (a) and eccentricity is atmospheric drag perturbation and the next effective for the semi-major axis (a) are SRP, solar attraction, lunar attraction and oblatness of Earth (J2) sequentially. So as the next effective for the eccentricity (e) are SRP, oblatness of Earth (J2), lunar attraction and solar attraction sequentially. The most effective perturbation on the Argument of perigee (w), Mean anomaly (M), and Right ascension of ascending node (RAAN) is the oblatness of Earth (J2) perturbation and the next effective for the SRP, atmospheric drag, lunar attraction and solar attraction.

Inspection table (5.2), at hp=95 and $i = 63.4^{o}$, notice that the most effective perturbations on the semi-major axis (a) and eccentricity is atmospheric drag perturbation and the next effective for the semi-major axis (a) are oblatness of Earth (J2), SRP, solar attraction and lunar attraction sequentially, and for eccentricity the next effective are SRP, oblatness of Earth (J2), lunar attraction and solar attraction sequentially. The most effective perturbation on the inclination is the atmospheric drag perturbation and the next effective for the SRP, oblatness of Earth (J2), solar attraction and lunar attraction. The most effective perturbation on the Right ascension of ascending node is the oblatness of Earth (J2) perturbation and the next effective for the SRP, atmospheric drag, lunar attraction and solar attraction. There are effected to the SRP upon (w) and (M) greater than others orbital elements.

Inspection table (5.3), at hp=95 and $i = 85^{o}$, notice that the most effective perturbations on the semi-major axis (a) and eccentricity is atmospheric drag perturbation and the next effective for the semi-major axis (a) are oblatness of Earth (J2), lunar attraction, SRP, and solar attraction sequentially, and for eccentricity the next effective are SRP, oblatness of Earth (J2), lunar attraction and solar attraction sequentially. The most effective perturbation on the inclination and the Right ascension of ascending node (RAAN) is the atmospheric drag perturbation and the next effective for the SRP, oblatness of Earth (J2), solar attraction and lunar attraction. Also there are big effective to the Obltaness of Earth on (w).

Inspection table (5.4), at hp=600 and $i = 8^{o}$, notice that the most effective perturbations on the semi-major axis (a) is oblatness of Earth (J2) and the next effective are solar attraction, drag perturbation, SRP and lunar attraction sequentially. And the most effective perturbations on the eccentricity is the SRP. So as the next effective for the eccentricity (e) are oblatness of Earth (J2), lunar attraction, drag perturbation and solar attraction sequentially. The most effective perturbation on the Argument of perigee (w), inclination and Right ascension of ascending node is the oblatness of Earth (J2) perturbation and the next effective for the SRP, atmospheric drag, lunar attraction and solar attraction, but this effected be small compared with altitude hp=95 Km.

Inspection table (5.5), at hp=600 and $i = 63.4^{o}$, notice that the most effective perturbations on the semi-major axis (a) is oblatness of Earth (J2) perturbation and the next effective are solar attraction, atmospheric drag, lunar attraction and SRP sequentially, and the most effective perturbations on the eccentricity is SRP and the next effective are oblatness of Earth (J2), solar attraction, atmospheric drag and lunar attraction sequentially. The most effective perturbation on the inclination is the SRP perturbation, and the next effective are oblatness of Earth (J2), solar attraction, atmospheric drag and

lunar attraction sequentially. The most effective perturbation on the Argument of perigee (w), Right ascension of ascending node (RAAN) and Mean anomaly (M) are the oblatness of Earth (J2) perturbation and the next effective for the SRP, solar attraction, lunar attraction and atmospheric drag sequentially.

Inspection table (5.6), at hp=600 and $i = 85^{o}$, notice that the most effective perturbations on the semi-major axis (a) and eccentricity are oblatness of Earth (J2) perturbation and the next effective for the semi-major axis (a) are solar attraction, lunar attraction, atmospheric and drag SRP sequentially, and for eccentricity the next effective are SRP, atmospheric drag, solar attraction and lunar attraction sequentially. The most perturbation which acts on the inclination is the SRP perturbation, and the next effective for the lunar attraction, solar attraction, atmospheric drag and oblatness of Earth (J2), and the most effective perturbation on the Argument of perigee (w) and Right ascension of ascending node (RAAN) are oblatness of Earth (J2) perturbation, and the next effectiveness for the SRP, lunar attraction, solar attraction, and atmospheric drag sequentially.

Inspection table (5.7), at hp=1200 and $i = 8^{o}$, notice that the most effective perturbations on the semi-major axis (a) is atmospheric drag perturbation, and the next effective are SRP, solar attraction, oblatness of Earth (J2) and lunar attraction sequentially, and the most effective perturbations on the eccentricity is SRP and the next effective are oblatness of Earth (J2), solar attraction, lunar attraction and atmospheric drag sequentially. The most effective perturbation on the Argument of perigee (w), Right ascension of ascending node (RAAN) and inclination (i) are oblatness of Earth (J2) perturbation, and the next effective for the SRP, atmospheric drag, lunar attraction and solar attraction sequentially.

Inspection table (5.8), at hp=1200 and $i = 63.4^{o}$, notice that the most effective perturbations on the semi-major axis (a) is oblatness of Earth (J2) perturbation, and the next effective are SRP, lunar attraction, atmospheric drag and solar attraction sequentially, and the most effective perturbations on the eccentricity is SRP and the next effective are oblatness of Earth (J2), lunar attraction, solar attraction and atmospheric drag sequentially. The most effective perturbation on the inclination and the Right ascension of ascending node is oblatness of Earth (J2) perturbation, and the next effective for the SRP, lunar attraction, solar attraction and atmospheric drag sequentially. And the most effect on Argument of perigee (w) is SRP.

Inspection table (5.9), at hp=1200 and $i = 85^{o}$, notice that the most effective perturbations on the semi-major axis (a) and the eccentricity are SRP perturbation, and the next effective on the semi-major axis (a) are lunar attraction, solar attraction, oblatness of Earth (J2) and atmospheric drag sequentially, and the next effective on the eccentricity are oblatness of Earth (J2), solar attraction, lunar attraction and atmospheric drag sequentially. The most effective perturbation on the inclination is solar attraction perturbation, and the next effective for the lunar attraction, atmospheric drag, SRP and oblatness of Earth (J2) sequentially, the most effective perturbation on the Argument of perigee (w) and Right ascension of ascending node (RAAN) are oblatness of Earth (J2) and the next effective for the SRP, solar attraction, lunar attraction and atmospheric drag sequentially.

The state different in the high altitude hp=3000Km, see tables (5.10), (5.11) and (5.12), the variation in semi major axis to one rotation increase with increase inclination and for lunar and solar attractions perturbation. So as the behaviors for other orbital elements, just the solar attraction perturbation will observed as stronger form lunar attraction perturbation. The drag perturbation is little, and then its not given. Oblatness of Earth (J2) have the

little effect at hp=3000Km, and the attraction perturbation more turbulence through one period, because the satellite have high changing distance from the perturbed object (Moon or Sun).

The percentage effect of the total perturbation of the orbital element with altitude was written in the table (5.15).

When hp=95 Km, notice that the total perturbations for semi-major axis (a) and eccentricity (e) increase with increasing inclination, and it decrease for inclination (i) and RAAN.

At hp=600 Km, notice that the total perturbations for semi-major axis (a) increase at i=63.4 and decrease at $i = 85^{o}$ and vise versa for eccentricity (e), and it decrease, and RAAN increase with increasing inclination.

At hp=1200, notice that the total perturbations for semi-major axis (a) and eccentricity (e) increase at i=63.4 and decrease at $i = 85^{o}$, and the RAAN is decrease with increasing inclination.

The comparison of our results with other approximate results such Eshagh and Najafi [53], see table (5.13), and given a good agreement for most elements, which indicate the optimal perturbation model which we used is the best now.

The lifetime of the satellite at altitude hp=95Km is 132 hour and equal 84.173 periods. But the lifetime for hp=600, 1200, 3000 Km very high, because the perturbations effected by small values compared with altitude hp=95 Km, and the atmospheric drag is a strong perturbations from others.

Table (5.1): The mean variation of orbital elements through 33 periods with all perturbations at hp=95 Km, $i = 8^0$, e=0.1, the time of first period T=1.686914 h.

Per./Var.	$Da(Km)$	De	$Di(^0)$	$DW(^0)$	$Dw(^0)$	$DM(^0)$
Oblatness	1.2e-4	4e-6	2.235e-4	0.467318	0.6	2.88e-2
Drag	5.08376	6.38e-4	1.544e-5	1.52e-4	9e-4	2.8e-2
SRP	1.76e-3	3.878e-5	1.874e-5	1.58e-4	0.00142	6.82e-4
Lunar attraction	3.8e-4	2e-7	2e-7	2.8e-5	8.62e-4	2.404e-3
Solar attraction	1.52e-3	1.2e-7	2e-8	4e-6	7.22e-4	1.278e-3
Total perturbation	6.10354	7.38e-4	1.9786e-4	0.482952	0.6	7.78e-4

Table (5.2): The mean variation of orbital elements through 33 periods with all perturbations at hp=95 Km, $i = 63.4^0$, e=0.1, the time of first period T=1.686914 h.

Per./Var.	$Da(Km)$	De	$Di(^0)$	$DW(^0)$	$Dw(^0)$	$DM(^0)$
Oblatness	2.12e-3	4.6e-7	3e-6	0.210716	8.04e-4	1.028e-3
Drag	5.47332	6.88e-4	1.09e-4	1.68e-4	2e-5	9.12e-4
SRP	1.8e-3	3.566e-5	1.98e-5	1.68e-4	9.83e-3	1.104e-3
Lunar attraction	9.8e-4	1.6e-7	1.4e-6	1e-5	2.18e-4	2.9e-4
Solar attraction	1.34e-3	1e-7	2.8e-6	4e-6	3.36e-4	1.038e-3
Total perturbation	6.30376	7.62e-4	1.094e-4	0.217984	1.207e-2	8.26e-4

Table (5.3): The mean variation of orbital elements through 33 periods with all perturbations at hp=95 Km, $i = 85^0$, e=0.1, the time of first period T=1.686914 h.

Per./Var.	$Da(Km)$	De	$Di(^0)$	$DW(^0)$	$Dw(^0)$	$DM(^0)$
Oblatness	9.32e-3	3.4e-7	3e-6	4.038e-2	0.219	4.764e-3
Drag	5.77106	7.26e-4	1.252e-4	1.66e-4	2e-3	6.44e-3
SRP	7.4e-4	3.516e-5	6.8e-6	1.66e-4	1.487e-2	9.86e-4
Lunar attraction	1.44e-3	2e-8	1.4e-6	2e-6	2.428e-3	2.206e-3
Solar attraction	5e-4	2e-8	1e-6	0.0000	2.476e-3	3.534e-3
Total perturbation	6.6121	8e-4	1.204e-4	0.041864	0.237	1.402e-3

Table (5.4): The mean variation of orbital elements through 33 periods with all perturbations at hp=600 Km, $i = 8^0$, e=0.1, the time of first period T=1.888122 h.

Per./Var.	$Da(Km)$	De	$Di(^0)$	$DW(^0)$	$Dw(^0)$	$DM(^0)$
Oblatness	5.06e-3	2e-6	1.7434e-4	0.40087	0.5	1.102e-3
Drag	1.76e-3	8e-8	1.544e-5	6e-6	7.84e-4	1.8e-4
SRP	1.68e-3	1.318e-5	2.664e-5	1.026e-3	0.0241	1.394e-3
Lunar attraction	3e-4	2.4e-7	1.86e-6	2.4e-5	4.66e-4	2e-3
Solar attraction	2e-3	2e-8	3e-7	1.4e-5	6.74e-4	4.24e-4
Total perturbation	5.46e-3	1.828e-5	2.4412e-4	0.401888	0.53	4.94e-4

Table (5.5): The mean variation of orbital elements through 33 periods with all perturbations at hp=600 Km, $i = 63.4^{o}$, e=0.1, the time of first period T=1.888122 h.

Per./Var.	$Da(Km)$	De	$Di(^{o})$	$DW(^{o})$	$Dw(^{o})$	$DM(^{o})$
Oblatness	1.348e-2	2.12e-6	1.42e-5	0.179966	1.82e-3	1.424e-3
Drag	1.6e-3	4e-8	2e-6	2e-6	4.58e-4	1.6e-4
SRP	4.2e-4	5.7e-6	5.04e-5	3.08e-4	6.42e-4	6.88e-4
Lunar attraction	1e-3	4e-8	1.8e-6	8e-6	7.82e-4	2.76e-4
Solar attraction	3.04e-3	6e-8	2.2e-6	1e-5	4.88e-4	3.3e-4
Total perturbation	1.216e-2	9e-7	3.4e-5	0.18031	3.634e-3	3.054e-3

Table (5.6): The mean variation of orbital elements through 33 periods with all perturbations at hp=600 Km, $i = 85^{o}$, e=0.1, the time of first period T=1.888122 h.

Per./Var.	$Da(Km)$	De	$Di(^{o})$	$DW(^{o})$	$Dw(^{o})$	$DM(^{o})$
Oblatness	6.02e-3	2e-6	1.8e-6	0.034742	0.1863	3.08e-4
Drag	1.24e-3	4e-7	4.2e-6	2e-6	1.82e-4	5.24e-4
SRP	5e-4	2.44e-6	5.08e-5	2.62e-4	9.656e-3	4.68e-4
Lunar attraction	1.24e-3	4e-8	6e-6	2e-6	3.38e-4	1.932e-3
Solar attraction	2.44e-3	2.8e-7	5e-6	2e-6	1.68e-4	3.56e-4
Total perturbation	8.78e-3	4.78e-6	2.68e-5	0.035024	0.1963	3.152e-3

Table (5.7): The mean variation of orbital elements through 33 periods with all perturbations at hp=1200 Km, $i = 8^{o}$, e=0.1, the time of first period T=2.136801 h.

Per./Var.	$Da(Km)$	De	$Di(^{o})$	$DW(^{o})$	$Dw(^{o})$	$DM(^{o})$
Oblatness	1.82e-3	4.02e-6	1.4664e-4	0.340372	0.42	1.292e-3
Drag	4.3e-3	2e-8	6.4e-7	6.2e-5	1.122e-3	1.07e-3
SRP	2.76e-3	5.14e-5	1.3e-6	1.018e-3	6.142e-3	3.74e-4
Lunar attraction	1.38e-3	1.6e-7	2.2e-7	4.2e-5	9.74e-4	1.022e-3
Solar attraction	2e-3	2.2e-7	6e-8	6e-6	8.76e-4	3.17e-3
Total perturbation	4e-4	4.592e-5	1.1436e-4	0.339686	0.42	2.85e-3

Table (5.8): The mean variation of orbital elements through 33 periods with all perturbations at hp=1200 Km, $i = 63.4^{o}$, e=0.1, the time of first period T=2.136801 h.

Per./Var.	$Da(Km)$	De	$Di(^{o})$	$DW(^{o})$	$Dw(^{o})$	$DM(^{o})$
Oblatness	1.91e-2	2.8e-6	2.02e-5	0.15298	3.706e-3	2.787e-3
Drag	2.36e-3	2e-8	1.4e-6	4e-6	2.3e-4	5.153e-3
SRP	3.38e-3	5.166e-5	2.8e-6	1.5e-4	7.416e-3	4.32e-3
Lunar attraction	2.4e-3	1.4e-7	3.6e-6	2e-5	9.6e-5	5.88e-3
Solar attraction	2.6e-4	1.4e-7	7.8e-6	8e-6	1.84e-4	4.915e-3
Total perturbation	1.926e-2	5.5e-5	2.74e-5	0.152944	4.482e-3	4.35e-3

Table (5.9): The mean variation of orbital elements through 33 periods with all perturbations at hp=1200 Km, $i = 85^{o}$, e=0.1, the time of first period T=2.136801 h.

Per./Var.	$Da(Km)$	De	$Di(^{o})$	$DW(^{o})$	$Dw(^{o})$	$DM(^{o})$
Oblatness	8.4e-4	3.2e-7	8e-7	0.029538	0.1663	1.536e-3
Drag	4e-4	2e-8	1e-6	2e-6	3.4e-5	3.594e-3
SRP	2.52e-3	5.178e-5	8e-7	1e-4	0.01177	4.558e-3
Lunar attraction	2.4e-3	8e-8	4e-6	6e-6	4.4e-5	4.026e-3
Solar attraction	1.6e-3	1.2e-7	1.28e-5	8e-6	7e-5	5.77e-3
Total perturbation	1.82e-3	5.042e-5	1.18e-5	0.029456	0.1526	6.63e-3

Table (5.10): The mean variation of orbital elements through 33 periods with some perturbations at hp=3000 Km, $i = 8^{o}$, e=0.1, the time of first period T=2.941676 h.

Per./Var.	$Da(Km)$	De	$Di(^{o})$	$DW(^{o})$	$Dw(^{o})$	$DM(^{o})$
Lunar attraction	1.2e-3	1.2e-7	8.4e-7	6.8e-5	3.42e-4	3.316e-3
Solar attraction	2e-3	8e-8	2.8e-6	4e-6	3e-4	4.266e-3
Total perturbation	2e-3	8e-8	2.8e-6	0.220824	0.426	1.303e-3

Table (5.11): The mean variation of orbital elements through 33 periods with some perturbations at hp=3000 Km, $i = 63.4^{o}$, e=0.1, the time of first period T=2.941676 h.

Per./Var.	$Da(Km)$	De	$Di(^{o})$	$DW(^{o})$	$Dw(^{o})$	$DM(^{o})$
Lunar attraction	1.6e-3	1.2e-7	1.14e-5	3.2e-5	9.4e-4	3.984e-3
Solar attraction	2.2e-3	3.2e-7	2.08e-5	6e-6	6.64e-4	4.894e-3
Total perturbation	2.2e-3	3.2e-7	2.08e-5	0.099714	0.0114	7.133e-4

Table (5.12): The mean variation of orbital elements through 33 periods with some perturbations at hp=3000 Km, $i = 85^{o}$, e=0.1, the time of first period T=2.941676 h.

Per./Var.	$Da(Km)$	De	$Di(^{o})$	$DW(^{o})$	$Dw(^{o})$	$DM(^{o})$
Lunar attraction	2e-3	6e-8	6.4e-6	2e-6	1.14e-4	5.195e-3
Solar attraction	2.2e-3	2.4e-7	1.56e-5	4e-6	1.64e-4	5.11e-3
Total perturbation	2.2e-3	2.4e-7	1.56e-5	4e-6	0.088	3.25e-3

Table (5.13): The mean variation of orbital elements with all perturbations at hp=454 Km, $i = 87.3^{o}$, e=0.1, the time of first period T=2.667 h [53].

Per./Var.	$\Delta a(Km)$	Δe	$\Delta i(^{o})$	$\Delta W(^{o})$	$\Delta w(^{o})$	$\Delta M(^{o})$
Oblatness	2e-2	4e-4	3.8e-3	1.5	1.0	1.5
Drag	6e-3	1.4e-7	5e-7	7e-6	4.5e-3	2.5e-3
SRP	2e-3	1.2e-6	1.2e-5	6e-4	2.5e-3	1.2e-3
Lunar attraction	8e-4	2.5e-7	3e-5	1.1e-5	2.5e-3	2.5e-3
Solar attraction	8e-4	2.5e-7	3e-5	1.1e-5	2.5e-3	2.5e-3
Total perturbation	2.01e-2	4e-4	3.8e-3	1.5	10.003	15.002

Table (5.14): The percentage variation of orbital elements with altitudes, at e=0.10.

hp/Varation%	$\frac{\Delta a}{a}\%$	$\frac{\Delta e}{0.1}\%$	$\frac{\Delta i}{63.4^{o}}\%$	$\frac{\Delta W}{W}\%$
95	0.0882	0.767	2.2485e-4	0.0907
600	1.135e-4	0.00799	1.603e-4	0.10287
1200	8.503e-5	0.0505	8.074e-5	0.1450
3000	2.047e-5	0.0002133	2.061e-5	0.0890

6.1 Conclusions

The values of solar flux $F_{10.7}$ are very important in the calculation of atmospheric density, because it changes daily and leads to calculate High scale H, which depends on calculation of $F_{10.7}$, J_2 very large value against others $J_3, J_4, J_5, J_6, \ldots\ldots, J_n$.

Deduce from tables (5.1) to (5.12), the maximum values of the perturbations in orbital elements due to each one of the distributive accelerations. As one can see from the table, the semi-major axis (a) has periodic variations under almost all of the perturbing accelerations except the atmospheric drag. The inclination's behavior is secular for atmospheric drag, and for the rest of the acceleration it is periodic. The right ascension of the ascending node acts periodically for atmospheric drag, but it acts as secular for the rest of the acceleration. Argument of perigee has periodic variation due to atmospheric drag, and the rest for all accelerations. The eccentricity behaves periodically for Oblatness of Earth, 3-rd body attraction, solar radiation pressure and atmospheric drag. The Mean anomaly usually varies periodically but it is secular for some disturbing forces, see table (6.1).

Table (6.1): variation type of the orbital elements due to perturbations.

	Oblatness	3rd-body	Atm. Drag	SRP
a	P	P	P S	P
e	P	P	P S	P
i	P	P	P S	P
$RAAN$	P S	P S	P	P S
ω	P S	P S	P	P S
M	P S	P S	P	P S

P: Periodic variation

S: Secular variation

Also: coupling effects for P and S

From figures and tables presented, the following conclusions are made:

1. There is no change in accuracy between two numerical methods, but Runge-Kutta method is quicker and stable than Adames-Bashford method.
2. Atmospheric drag shows a secular effect on the semi-major axis (a), eccentricity (e), inclination (i) and RAAN. The effect is larger at altitude hp=95 Km than at altitudes hp=600, 1200 Km. Also it effects the shape of orbits (a, e).
3. Oblatness of Earth has a periodic effect on semi-major axis (a), eccentricity (e), inclination (i), and most large secular effect on RAAN, argument of perigee (w), and Mean anomaly. Very large effect at hp=95 Km, decreasing at hp=600, 1200 Km and increase when inclination (i) reach to equatorial circle.
4. Solar radiation pressure effect was periodic for semi-major axis (a), and not linear variation depending on (hp) and (i) more than other elements, and coupling effect (periodic and secular) for inclination (i), RAAN, argument of perigee (w), and Mean anomaly, but it's secular effect for eccentricity (e), which increasing values for most orbital elements.
5. There are finite changes in the orbital elements by the effect of Lunar and Solar attraction, it is large for RAAN and argument of perigee (w) for LEO (hp=95,600, 1200 Km), and it becomes very large at hp=3000Km. In general the solar and lunar attractions effects are neglected with polar orbit $\left(i = 85^0\right)$.
6. Lifetime of satellite increases with increasing inclination (i), it becomes maximum at i=90 degree when altitude at LEO.

6.2 Future works

1. Studying the perturbation effect for many values of (A/m), and more values of altitudes and for more periods.
2. Include the Earth shadow function (η), to find the Solar Radiation Pressure perturbation.
3. Studying the perturbations on the satellite at High Earth Orbit (HEO).
4. Study other perturbations which effect the satellite orbits, such Ocean Tide, Earth radiation pressure and General relativity.
5. Derivation of the equation which combine all perturbation to find satellite lifetime at high altitude.
6. Perturbations due to the eight planets on the artificial satellite.

References

[1] Anas, S. T. Al-Hity, (2002), "Perturbation effect on the Low satellites orbits", M. Sc. Thesis, Baghdad university.

[2] http://en.wikipedia.org/wiki/Satellite.

[3] King-Hele, D. G., (Oct. 28, 1958), "Perturbations of the orbit of a satellite near to the earth", Proceedings of the Royal Society of London. Series A, Mathematical and Physical Sciences, Vol. 248, No. 1252, pp. 55-62.

[4] Blitzer, L., (1959), "Lunar-Solar Perturbations of an Earth Satellite", American Journal of Physics, Vol. 27, No. 9, pp. 634-645.

[5] Kozai, Y., (1959), "On the Effects of the Sun and the Moon upon the Motion of a Close Earth Satellite", Smithsonian Astrophysical Observatory, Special Report 22, Cambridge, MA.

[6] Musen P., (1960), "The influence of the solar radiation pressure on the motion of an artificial satellite", J Geophys Res; 65:1391.

[7] Musen, P., Bailie, A., and Upton, E, (1961), "Development of the Lunar and Solar Perturbations in the Motion of an Artificial Satellite", NASA-TN, D494.

[8] Kozai, Y., (1961), Spec. Repr. Smithsonian Inst., Astrophys. Obs., 25.

[9] Kozai, Y., (1962), "Secular Perturbations of Asteroids with High Inclination and Eccentricity," The Astronomical Journal, Vol. 67, No. 9, pp. 591-598.

[10] Kaula, M. W., (1962), "Development of the Lunar and Solar Disturbing Functions for a Close Satellite," Astronautical Journal, Vol. 67, pp. 300.

[11] Frick, R. H. and Garber, T. B., (1962), "Perturbations of synchronous satellites", Rand Corp. Report NASA 399, 186 p.

[12] Cook, G. E, (1962), “Luni-Solar Perturbations of the Orbit of an Earth Satellite,” The Geophysical Journal, Vol. 6, No. 3, pp. 271-291.

[13] Kozai, Y. , (1963), “The effects of the Sun and Moon upon the motion of a close Earth satellite”, Smithsonian Inst. Astrophysical Observatory Vol. 6, 47 p.

[14] Kozai, Y., (1965), “Effects of the Tidal Deformation on the Motion of Satellites,” Publications of the Astronomical Society of Japan, Vol. 17, pp. 395-402.

[15] Giacaglia, G. E. O., (1973), “Lunar Perturbations of Artificial Satellites of the Earth,” Smithsonian Astrophysical Observatory, Special Report 352, Cambridge, MA.

[16] Kozai, Y., (1973), “A New Method to Compute Lunisolar Perturbations in Satellite Motions,” Smithsonian Astrophysical Observatory, Special Report 349, Cambridge, MA.

[17] Sehnal L. and Giacaglia T, Ed., (1975), “Satellite dynamics”, Berlin: New York: Springer-Verlag.

[18] King-Hele, D., (1964), “Theory of Satellite Orbits in an Atmosphere”, Butterworths, London.

[19] King-Hele, D., (1987), “Satellite Orbits in an Atmosphere: Theory and Applications”, Blackie and Son Ltd., London.

[20] King-Hele, D., (1969), “The upper atmosphere and its influence on satellite orbits”, Proceeding of COSPA-IAU-IAG/IUGG-IUTAM symposium, Prague, May 20-24.

[21] Danby, J. M. A., (1962), “Fundamentals of Celestial Mechanics”, Macmillan and Co. Ltd., New York.

[22] Escobal, P. R. , (1965), “Method of orbit determination”, Robert E. Krieger Publishing Co. Malabar, Florida.

[23] Bate, R. R., Mueller, D.D. and White, J.E., (1971), “Fundamentals of Astrodynamics”, Dover, New York.

[24] Battin, R. H., (1987), ”An Introduction to the Mathematics and Methods of Astrodynamics”, AIAA Education Series, ISBN 0-930403-25-8, New York.

[25] Roy, A. E., (1988), “Orbital Motion”, Third Edition, Adam Hilger, J. W., Arrow smith, Ltd., Bristol1, England.

[26] Chobotov, V. A., (1996), “Orbital Mechanics”, Second Edition, AIAA Educational Series, Washington DC, New York..

[27] Kaplan, M. H., (1976), “Modern Spacecraft Dynamics & Control”, John Wiley & Sons, New York.

[28] Wertz, J. R., (1978), “Spacecraft Attitude Determination and Control”, Astrophysics and Space Science Library,Vol. 73, D. Reidel Publishing Co., Boston.

[29] Larson, W. J. and Wertz, J. R., (1992), “Space Mission Analysis and Design”, (Second Edition), Microcosm Inc., California USA and Kluwer Academic Publishers, Dordrecht.

[30] I El'yasberg et al., (1967), “Determining the motion of space vehicles”, NASA, Washington DC.

[31] Morando, B., (1970), “Dynamics of satellites”, Proceeding of COSPA-IAU-IAG/IUGG-IUTAM symposium held in Prague on May 20-24 1969. Springer-Verlag, NEW York.

[32] Langton, N. H., (1969), “Space Research and Technology”, Volume (1), The Space Environment, University of London Press Ltd, London.

[33] Hough, M. E., (1981), “Lunisolar perturbations”, Celestial Mechanics and Dynamical Astronomy Vol.(25), No. 2, pp. 111-136.

[34] Anselmo L., Bertotti B., Farinella P., Milani A., Nobili A. M., (1983), “Orbital perturbations due to radiation pressure for a spacecraft of complex shape”. Celestial Mech; 29: 7.

[35] Schatten, Kenneth H., and S. Sofia, (1987), "Forecast of an Exponentially Large Even-numbered Solar Cycle". Geophysics Research Letters. Vol. 14: 632-635.

[36] Bhatnagar K. B. and Manjeet Kaur, (1990), "The in-Plane Motion of a Geosynchronous Satellite under the Gravitational Attraction of the Sun", the Moon and the Oblate Earth, J. Astrophys. Astr., V11, pp1–10.

[37] Broucke, R. A., (1992), "The Double Averaging of the Third Body Perturbations", Texas University, Austin, TX.

[38] Costa, I. V., (1998), "Estudo da Perturbação de Terceiro Corpo em Um Satélite Artificial da Terra", Master Thesis, National Institute for Space Research (INPE), São José dos Campos, SP., Brazil.

[39] Prado, A. F. B. A., and Costa, I. V., (1998), "Third-Body Perturbation in Spacecraft Trajectory", IAF Paper 98-A.4.05, 49th International Astronautical Congress, Melbourne, Australia.

[40] Delhaise, F. and Morbidelli, (1993), "A. Lunisolar effects of Geosynchronous orbits at the critical inclination", Celestial Mechanics and Dynamical Astronomy, Vol.57, pp155–173.

[41] Toshihiro Kubo-oka and Arata Sengoku, (1999), "Solar radiation pressure model for the relay satellite of SELENE", Earth Planets Space, Vol. 51, pp 979–986.

[42] Prado, A. F. B. A., (2002), "Third-Body Perturbation in Orbits Around Natural Satellites". Published in the Journal of Guidance, Control and Dynamics.

[43] Eanes, R. J., and Bettadpur, S., (1995), "The CSR 3.0 Global Ocean tide model diurnal and semi diurnal Ocean Tides from TOPEX/Poseidon Altimetry", Technical Report, University of Texas, United States of America.

[44] Seeber, G., (2003), "Satellite Geodesy", 2nd completely revised and extended edition, Walter de Gruyter. Berlin. New York.

[45] Hofmann, W., Lichtenegger, H., and Collins, J., (2001), “Global positioning system”, theory and practice, revised edition, Springer Wienna New York.

[46] Eshagh, M., and Najafi Alamdari M., (2003), “Precise orbit determination of a low Earth orbiting satellite”, MSc thesis, K. N. Toosi University of Technology, Tehran, Iran.

[47] Eshagh, M., (2003a), “Consideration of behaviour of orbital elements with respect to different degree and order of geopotential Models”, submitted to J. Earth Space Phys. Geophysics Institute, University of Tehran, Tehran, Iran.

[48] Leick, A., (1995), “GPS satellite surveying”, 2nd edn. Wiley interscience, New York Chichester Toronto Brisbane Singapore.

[49] Wolf, R., (2000), “Satellite orbit and ephemeris determination using inter satellite links”, Ph.D thesis, Department of Geodesy, University of Bundeswehr, Munchen, Germany.

[50] Su, H., (2000), “Orbit determination of IGSO, GEO and MEO satellites”, Ph.D thesis, Department of Geodesy, University of Bundeswehr, Munchen, Germany.

[51] Santos, M. C., (1994), “On real time orbit improvement for GPS satellites”, Ph.D thesis, Department of Geodesy and Geomatics Engineering, University of New Brunswick, Canada.

[52] Buffet, A., (1985), “Short arc orbit improvement of GPS satellite”, MSc thesis, University of Calgary, Department of Geodesy and Geomatics Engineering, Calgary, Canada.

[53] Eshagh, M. and Najafi, (2007), “Perturbations in orbital elements of a low earth orbiting satellite”, Journal of the Earth & Space Physics. Vol. 33, No. 1, P. 1-12.

[54] Solórzano, C. R. H., Prado, A. F. B. de Almeida, (2004), “Third-body perturbation using a single averaged model”, Instituto Nacional de

Pesquisas Espaciais – INPE, São José dos Campos, SP, Brazil, ISBN 85-17-00012-9.

[55] Bar-Sever Y. and Kuang D., (2005), “New Empirically Derived Solar Radiation Pressure Model for Global Positioning System Satellites During Eclipse Seasons”, IPN Progress Report 42-160 February 15.

[56] Prado, A. F. B. A., (2005), “Retrograde Orbits Perturbed by a Third-Body”, J. of the Braz. Soc. of Mech. Sci. & Eng. Copyright by ABCM October-December, Vol. XXVII, No. 4 / 371.

[57] Frank A. Marcos, Bruce R. Bowman and Robert E. Sheehan, (2006), “Accuracy of Earth’s Thermospheric Neutral Density Models”, AIAA - 6167.

[58] Narumi, Tomohiro and Hanada, Toshiya, (2007), “New Orbit Propagator to Be Used in Orbital Debris Evolutionary Models”, Memoirs of the Faculty of Engineering, Kyushu University, Vol.67, No.4, December.

[59] Domingos R. C., Vilhena deMoraes R., and Prado A. F. Bertachini De Almeida, (2008), “Third-Body Perturbation in the Case of Elliptic Orbits for the Disturbing Body”, Hindawi Publishing Corporation, Mathematical Problems in Engineering, Volume 2008, Article ID 763654, 14 pages doi:10.1155/763654.

[60] Vallado, David A. and Finkleman, David, (2008) “A Critical Assessment of Satellite Drag and Atmospheric Density Modeling”, American Institute of Aeronautics and Astronautics, Center for Space Standards and Innovation, Colorado Springs, Colorado, 80920.

[61] Abd El-Salam F. A., Abdel-Aziz Yehia A., El-Saftawy M., and Radwan M., (2008), “Analysis of Lunisolar Resonances in an Artificial Satellite Orbits”, Applied Mathematical Sciences, Vol. 2, no. 21, 1013 – 1021.

[62] Wright Jonathan W., (2008), “Minimizing secular J2 perturbation effects on satellite formations”, Second Lieutenant, USAF, department of the air force, Air university, Ohio, March.

[63] Nadia A. Saad, Kh. I. Khalil and Magdy Y. Amin, (2010), “Analytical Solution for the Combined Solar Radiation Pressure and Luni- Solar Effects on the Orbits of High Altitude Satellites”, The Open Astronomy Journal, 3, 113-122.

[64] Daniel N. J. du Toit, J. J. du Plessis and W. H. Steyn, (1998), “Using Atmospheric Drag for Constellation Control of Low Earth Orbit Micro-satellites”, University of Stellenbosch, 7600, Republic of South Africa.

[65] Costa, Ione Vicente da and Prado, Antonio Fernando Bertachini de Almeida, (2010), “Orbital evolution of a satellite perturbed by a third-body”, Instituto Nacional de Pesquisas Espaciais - São José dos Campos-SP-12227- Brazil.

[66] Bate, Roger R., Mueller, Donald D., and White, Jerry E., (1971), “ Fundamentals of Astrodynamics”, Dover Publicatinos, Inc., Mineola, N.Y.

[67] Fowles G. R., (1970), “Analatical Mechanics”, second edition, Holt, Rinehart and Winston, Lib. Of Congress, Catal. Cadr no.:79-116048.

[68] Schaub, H. and Junkins, J. L., (2003), “Analytical Mechanics of Space Systems”, AIAA Education Series, Reston, VA.

[69] Tattersfield D., (1976), “Orbits for Amateurs with computer”, Stanley Thornes(publishers) Ltd.

[70] Smith, G. R., (1979), “A Simple efficient starting value for the Iterative solution of Kepler’ s Equation”, Celestial Mechanics, 19, 163.

[71] Danby, J. M. A., Burkardt T. M., (1983), “The Solution of Kepler’s Equation I”, Celestial Mechanics, 31, 95-107.

[72] Taff , L. G., Brennan T. A., (1989), “Celestial Mechanics and Dynamical Astronomy", 46, 163-176.

[73] Upham, J., (1996), “An orbit propagator which models atmospheric drag J2 effect, and Lunar perturbations”, M. Sc. Thesis, University of Washington, Seattle, WA.

[74] Montenbruck, O. and Gill, E., (2000), “Satellite Orbits - Models, Methods, and Applications”, Springer-Verlag, Heidelberg.

[75] Wertz, J. R. and Larson, W. J., (1999), “Space Mission Analysis and Design”, (Second Edition), Kluwer Academic Publishers.

[76] Brown, Charles D., (2002), “Elements of spacecraft design”, AIAA, Education series.

[77] Riaz Ahmed, (2008), “Real time hardware in the loop simulation testbed of spacecraft formation flying”, Ph. D Thesis, university of Southampton.

[78] Lamia M. H. Smaisem, (2003), “The effect of perturbations on the Low satellite orbital elements”, Master Thesis, Baghdad university.

[79] Cook, G. E., (1966), “Drag coefficients of spherical satellites”, Ann. Geophysics, 22, 53.

[80] Abdul Jalil H. M., (2000), “The satellite orbits determination using visual observation”, M. Sc., Thesis, Department of Physics, College of Science, Babylon University.

[81] Scraton R. E, (1984), “Basic numerical method”, Spottiswoode Ballantyn, Colchester and London.

[82] Afonso, G., F. Barlier, C. Berger, F. Mignard, and J. J. Walch, (1985), “Reassessment of the Charge and Neutral Drag of LAGEOS and its Geophysical Implications”, *Jour. Geophys Res*., 90, 9381,.

[83] Bowman Bruce R., Barker William N., and Schick William G., (2000), “Orbit perturbation analysis of west ford Needles clusters”, American Institute of Aeronautics and Astronautics, AIAA-4236.

[84] Jacchia, L. G., (1971), “Revised Static Models of the Thermosphere and Exosphere with Empirical Temperature Profiles”, Smith. Astrophys. Obs. Spec. Rep., 332.

[85] Jacchia L. G., J. Slowey, and Uvon zohn, (1977), Journal of Geophysical Research, 82, 4, 684.

[86] Barlier, F., Berger, C., Falin, J. L., Kockarts, G., and Thuiller, G., (1977), “A Thermospheric Model Based on Satellite Drag Data”, Aeronomica Acta, Vol. 185.

[87] Bruinsma, S. L., and G. Thuillier, (2000), “A Revised DTM Atmospheric Density Model: Modeling Strategy and Results”, EGS XXV General Assembly, Session G7, Nice, France.

[88] Hedin, A. E., (1991), “Extension of the MSIS Thermosphere and Exosphere with Empirical Temperature Profiles”, J. Geophysics Res., 96, 1159-1172.

[89] Hedin, A. E., E. L. Fleming, A. H. Manson, F. J. Schmidlin, S. K. Avery, R. R. Clark, S. J. Franke, G. J. Fraser, T. Tsuda, F. Vidal, and R. A. Vincent, (1996), “Empirical Wind Model for the Upper, Middle and Lower Atmosphere”, J. Atmos. Terr. Phys., 58, 1421-1447.

[90] Kennewell, J., (1999), “Satellite orbital decay calculations”, IPS Radio and Space services, The Australian Space Weather Agency, Sydney.

[91] Rawa Oubaid Mizhir, (2002), “The effect of solar activity on the satellite orbits of low altitude”, M. Sc. Thesis, Babylon University.

[92] Svalgaard, L., (2009), “The Solar Radio Microwave Flux”, May.

[93] Agrawell, B. N., (1986), “Design of Geosynchronous Spacecraft”, Prentice- Hall, ISBN 0-13-200114-4 025.

[94] Meeus, J., (1991), “Astronomical Algorithms”, Willmann-Bell Inc. ISBN 0-943396-35-2.

[95] Abdul Rahman H. S., (1997), " Islamic Times with Respect to the physical motions of Sun and Moon and its application", Ph. D. Thesis, Universisty of Baghdad.

[96] McCarthy, D., (1996), "IERS Technical Note 21.", US Naval Observatory, Central Bureau of IERS-Observatoire, Paris 61, avenue de l'Observatoire, France.

[97] van der Ha J. C., Modi V.J., (1977), "Analytical evaluation of solar radiation induced perturbations of space structures", The Journal of the Astronautical Sciences, XXV No. 4, 283-306.

[98] Anderle, R. J., (1973), "Geodetic Analysis Through Numerical Integration", Proceedings of the International Symposium on the Use of Artificial Satellites for Geodesy and Geodynamics, Athens, Greece.

[99] Lundberg, J. B., (1985), "Computational Errors and their Control in the Determination of Satellite Orbits", Report *CSR-85-3*, The Center for Space Research, The University of Texas at Austin.

[100] Feulner, M. R., (1990), "The Numerical Integration of Near Earth Satellite Orbits Across SRP Boundaries Using the Method of Modified Back Differences", Thesis, Department of Aerospace Engineering and Engineering Mechanics, The University of Texas at Austin, August.

[101] Rim, H. J., and Schutz, B. E., (2001), "Precision orbit determination (POD)", Geoscience laser and altimeter satellite system, University of Texas, United States of America.

[102] Hardacre S., (1996), "Control Of Collocated Geostationary Satellites", Cranfield University, Ph.D. Thesis.

[103] Adnan, M. S. K., Razali R. and Said Md. A. Md., (2000), "A Study of perturbation effect on satellite orbit using Cowell' s method", University Science Malaysia 14300 Nibong Tebal Penang, Malaysia.

[104] Pocha, J. J., (1987), "Mission Design for Geostationary Satellites", Space Technology Library.

[105] Atkinson, (1983), “Numerical Analysis”.

[106] James L. Buchanan and Peter R. Turner, (1982), “Numerical methods and analysis”.

[107] Sharmpine, (1973), “Numerical Analysis”.

[108] Escobal, P. R., (1976), “Methods of orbit determination”, Robert E, Krieger, New York.

[109] Zee C., (1989), “Theory of Geostationary Satellites”, Kluwer Academic Publishers, ISBN 90-277-2636-1.

Appendix A: Derivation the equation of orbital motion

Let m_1 the mass of particle 1 and F_1 its force of attraction toward vector $\vec{r}$ to particle 2 that it's mass m_2 and F_2 its force of attraction toward inverse direction (shown in figure below)

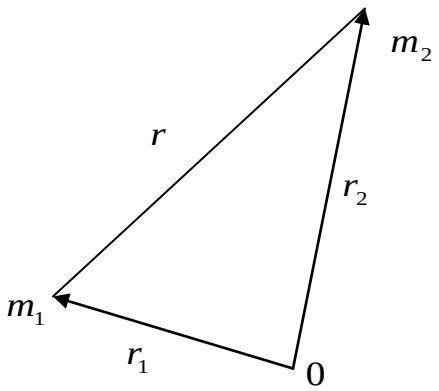

Figure (A.1): representation of two body problem [108].

From Newton's third law, which is given as:

$$F_1 = - F_2 \tag{A-1}$$

And from applying the gravitational law

$$F_1 = G\frac{m_1 m_2}{r_1^2}\frac{\hat{r}}{r} \tag{A-2}$$

$$F_2 = G\frac{m_1 m_2}{r_2^2}\frac{\hat{r}}{r} \tag{A-3}$$

Let the vectors (r_1, r_2) refers to dimension of particles (p_1, p_2) about the reference point (O), and from Newton's second law

$$F = m\frac{d^2 r}{dt^2} \tag{A-4}$$

From equation (A-2), (A-3), the equations of two particles that affected by the gravitational force can be written as follow:

$$m_1\frac{d^2 r_1}{dt^2} = G\frac{m_1 m_2}{r_1^2}\frac{\hat{r}}{r} \tag{A-5}$$

$$m_2 \frac{d^2 r_2}{dt^2} = - G \frac{m_1 m_2}{r_2^2} \frac{\hat{r}}{r} \tag{A-6}$$

By substitute the two equations (A-5) and (A-6) in equation (A.1)

$$m_1 \frac{d^2 r_1}{dt^2} + m_2 \frac{d^2 r_2}{dt^2} = 0 \tag{A-7}$$

And, from integration above equation twice, it get

$$MR = at + b \tag{A-8}$$

Where a, b represents constant vectors, and R represents the distance from origin of the point (O) to the center of mass of the particles m_1, m_2,

$$MR = m_1 r_1 + m_2 r_2 \tag{A-9}$$

$$M = m_1 + m_2 \tag{A10}$$

From these relations, it can be observed that the center of mass of system have constant velocity, and equations (A-5), (A-6) rewritten as follow

$$\frac{d^2 r_1}{dt^2} = G m_2 \frac{\hat{r}}{r^3} \tag{A-11}$$

$$\frac{d^2 r_2}{dt^2} = - G m_1 \frac{\hat{r}}{r^3} \tag{A-12}$$

By subtraction (A-12) from (A-11) obtain on

$$\frac{d^2}{dt^2}(r_1 - r_2) = G(m_1 + m_2)\frac{\hat{r}}{r^3} \tag{A-13}$$

Where

$$- r = (r_1 - r_2)$$

$$m = G(m_1 + m_2)$$

Therefore

$$\frac{d^2 r}{dt^2} + \frac{m\hat{r}}{r^3} = 0 \tag{A-14}$$

The above equation represents the equation of motion to the center of mass of system that contained from two gravitational particles [1, 78, 108].

Appendix B: Derivation the equation of radial distance of the satellite orbit

The fundamental equation of motion of a body in space rewritten from equation (A.14) as

$$\ddot{\vec{r}} = -\frac{m\vec{r}}{r^3}$$

Then by defining a unit vector pointing at the body, the equation above becomes

$$\ddot{\vec{r}} = -\frac{m}{r^2}\hat{u} \qquad \text{(B-1)}$$

Where

$$\hat{u} = \frac{\vec{r}}{r}$$

By taking the cross product of equation (B-1) with $\vec{h}$

$$\ddot{\vec{r}} \times \vec{h} = -\frac{m}{r^2}\hat{u} \times \vec{h} \qquad \text{(B-2)}$$

Where

$$\vec{h} = \vec{r} \times \dot{\vec{r}} \qquad \text{(B-3)}$$

Then

$$\ddot{\vec{r}} \times \vec{h} = -\frac{m}{r^2}\hat{u} \times \left(\vec{r} \times \dot{\vec{r}}\right) \qquad \text{(B-4)}$$

From the definition $A \times (B \times C) = (A \cdot C)B - (A \cdot B)C$, therefore

$$\ddot{\vec{r}} \times \vec{h} = -\frac{m}{r^2}\left[\left(\hat{u} \cdot \dot{\vec{r}}\right)\vec{r} - \left(\hat{u} \cdot \vec{r}\right)\dot{\vec{r}}\right] \qquad \text{(B-5)}$$

Hence, by definition $\hat{u} = \frac{\vec{r}}{r}$, which represent the unit vector

$$\dot{\vec{h}} = -\frac{m}{r^2}\left[\left(\frac{d}{dt}\left(\frac{\vec{r}}{r}\right)\right)\times\dot{\vec{r}}\right] - \left[\left(\frac{d}{dt}\left(\frac{\vec{r}}{r}\right)\right)\times\dot{\vec{r}}\right]$$

$$= \frac{m}{r^2}\left[\left(\vec{r}\dot{\vec{r}}\right) - \left(\dot{\vec{r}}\vec{r}\right)\right]$$

$$= m\frac{d}{dt}\left(\frac{\vec{r}}{r}\right) \qquad \text{(B-6)}$$

Also in term of $\hat{u}$

$$\dot{\vec{h}} = m\dot{\hat{u}} \qquad \text{(B-7)}$$

This can be integrated at once as

$$\dot{\vec{h}} = m[\hat{u} + e] \qquad \text{(B-8)}$$

Where e is a vector constant of integration. Upon dotting with $\vec{r}$ it is possible to write

$$\left(\dot{\vec{h}}\right)\times\vec{r} = m[\hat{u}\times\vec{r} + e\times\vec{r}] \qquad \text{(B-9)}$$

Let equation (B-3) be dotting with $\vec{h}$,

$$\left(\vec{r}\times\dot{\vec{r}}\right)\times\vec{h} = h^2 \qquad \text{(B-10)}$$

However, since

$$\left(\vec{r}\times\dot{\vec{r}}\right)\times\vec{h} \circ \left(\dot{\vec{r}}\times\vec{h}\right)\times\vec{r} \qquad \text{(B-11)}$$

It is evident that a direct comparison of equations (B-9) and (B-11) reveals that

$$h^2 = m[\hat{u}\times\vec{r} + e\times\vec{r}] \qquad \text{(B-12)}$$

But

$$\hat{u}\times\vec{r} = r$$

And

$$e\times\vec{r} = er\cos(\angle e, r) \qquad \text{(B-13)}$$

The angle between e and r called true anomaly and defined as (f).

By substitute equation (B-13) in equation (B-12), we obtain

$$h^2 = m[r + er\cos(f)]$$

$$\frac{h^2}{m} = r[1 + e\cos(f)] \qquad \text{(B-14)}$$

r can be written as below

$$r = \frac{h^2 / m}{1 + e\cos(f)} \qquad \text{(B-15)}$$

The equation above represents the equation of orbit to the conic section orbit in polar coordinates [1, 78, 108].

Appendix C: Potential function of the Oblatness of Earth perturbation

In order to have a clear picture of the gravity harmonics of the Earth and other planets, the concept of a gravity potential is introduced. Much as with the potential theory in fluid mechanics, the gravity field of a body with finite mass can be represented by a potential function. If the mass of a celestial body is assumed to be a point mass or uniformly distributed in a sphere, the potential function takes the following simple form

$$\Phi = \frac{m}{r} \qquad \text{.....(C.1)}$$

Function Φ indicates that the strength of the gravity potential at a point in space is directly proportional to the mass of the body $m = k^2 M$ and inversely proportional to the distance to the center of the body. From potential theory, the gravitational force or acceleration along a given direction is equal to the partial derivative or gradient in that direction. Thus, the equations of motion of a two-body orbit may be given as [25]:

$$\ddot{x} = \frac{\partial \Phi}{\partial x} \qquad \ddot{x} = -\frac{mx}{r^3} \qquad \text{.....(C.2)}$$

$$\ddot{y} = \frac{\partial \Phi}{\partial y} \qquad \ddot{y} = -\frac{my}{r^3} \qquad \text{.....(C.3)}$$

$$\ddot{z} = \frac{\partial \Phi}{\partial z} \qquad \ddot{z} = -\frac{mz}{r^3} \qquad \text{.....(C.4)}$$

Also, in polar coordinates

$$\ddot{r} - r\dot{\theta}^2 = \frac{\partial \Phi}{\partial r} \qquad \ddot{r} - r\dot{\theta}^2 = -\frac{m}{r^2} \qquad \text{.....(C.5)}$$

$$r\ddot{\theta} + 2\dot{r}\dot{\theta} = \frac{1}{r}\frac{\partial F}{\partial \theta} \qquad r\ddot{\theta} + 2\dot{r}\dot{\theta} = 0 \qquad \text{.....(C.6)}$$

In reality, the point-mass potential can not accurately represent the gravity field of Earth and other planets in the solar system because of the non-spherical shape of these bodies. Instead, the potential function should be derived from a spheroid that can closely represent the shape and mass distribution of the Earth or other planets.

The basis of the development of the potential of a spheroid is in the integral

$$F = k^2 \int \frac{dM}{s} \qquad \text{.....(C.7)}$$

Where dM is an element of the mass of the attracting body and s is the distance from this point mass element to the attracted particle, a satellite S whose mass is assumed to be negligible (because small with respect to mass of the Earth).

The external Geo-potential function at any point P specified by the spherical coordinates r, ϕ, λ defined in Fig. (C.1) can be expressed as

$$U(r,\lambda,\phi) = -\frac{m}{r}\left[1 - \sum_{n=2}^{\infty}\left(\frac{r_E}{r}\right)^n J_n P_n(\sin(\phi))\right.$$

$$\left. + \sum_{n=2}^{\infty}\sum_{m=1}^{n}\left(\frac{r_E}{r}\right)^n P_{nm}(\sin(\phi)) J_{nm}\cos(m(\lambda - \lambda_{nm}))\right] \text{.....(C.8)}$$

Through some lengthy mathematical integration over the entire body, equation (C.8) becomes, see reference [25].

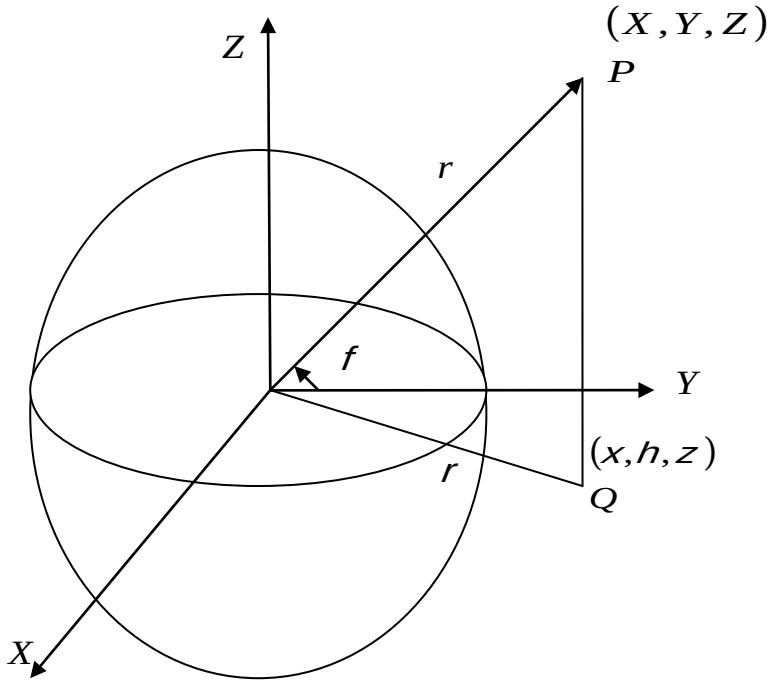

Fig. (C.1): Geo-potential function at a given point P in spherical coordinates [109].

$$U = \frac{m}{r} \sum_{n=0}^{\infty} \sum_{m}^{n} \left(\frac{r_E}{r}\right)^{n} P_{nm}(w)\left(C_{nm}\cos(m\lambda) + S_{nm}\sin(m\lambda)\right) \quad \text{.....(C.9)}$$

This infinite series is the potential function of a spheroid with coefficients C_{nm} and S_{nm} to be determined from observations, where

r = geocentric distance

r_E = equatorial radius of the Earth

$m = GM_E$ = Newtonian constant times mass of Earth

P_n = Legendre polynomial of degree n and order m=0

$P_{nm}(w)$ = associated Legendre polynomial of degree n and order m

$w = \sin(f)$, f = declination of satellite

l = longitude of the satellite in the body-fixed coordinates

l_{nm} = equilibrium longitude for J_{nm}

J_{nm} = harmonic coefficients

$J_n = J_{n0}$

The potential of a spheroid of revolution can be obtained from Equation (C.9), with the center of mass at the center of the coordinate system as

$$F = \frac{m}{r}\left[1 - \sum_{n=2}^{\infty}\left(\frac{r_E}{r}\right)^n J_n P_n(w)\right] \quad \text{.....(C.10)}$$

Where

$$J_n = -C_{n0} = -C_n \quad \text{.....(C.11)}$$

The mathematical definitions of C_{nm} and S_{nm} are

$$C_{nm} = \frac{2}{Mr_E^n}\frac{(n-m)!}{(n+m)!}\int r^n P_{nm}(w)\cos(ml)\,dM \quad \text{.....(C.12)}$$

$$S_{nm} = \frac{2}{Mr_E^n}\frac{(n-m)!}{(n+m)!}\int r^n P_{nm}(w)\sin(ml)\,dM \quad \text{.....(C.13)}$$

Where

$$r = \left(x^2 + h^2 + V^2\right) \quad \text{.....(C.14)}$$

M = mass of the spheroid

The preceding definitions indicate that the values of the harmonics depend on the shape and mass distribution of the central body.

For Earth, various sets of gravity harmonics have been determined in the past two decades. The most widely used set, which is probably the most accurate one, is the WGS 84 model. The values of the low-order harmonics (4 x 4) of that model are listed in table (C.1) for reference. It is important to know that the value of J_2 is about 400 times larger than the next-largest value J_3. That is why, for most satellite orbits, a reasonably good accuracy can be maintained by simply including the J_2 effect.

Table (C.1): Earth Spherical Harmonic Constants to Fourth Order Implementation of the Equations [109].

n	m	J_{nm}	$l_{nm}(^0)$
2	0	1082.6283×10^{-6}	
2	2	-1.8083×10^{-6}	-14.8949^0
3	0	-2.5418×10^{-6}	
3	1	-2.1791×10^{-6}	7.0669^0
3	2	-3.8480×10^{-7}	-17.0348^0
3	3	-2.2132×10^{-7}	21.3183^0
4	0	-1.6086×10^{-6}	
4	1	-6.7614×10^{-7}	220.7042^0
4	2	-1.6853×10^{-7}	31.3316^0
4	3	-5.9015×10^{-8}	-4.3093^0
4	4	-7.3147×10^{-9}	29.5502^0

Sometimes, it is more convenient to represent those harmonic coefficients in terms of J_{nm} and λ_{nm} instead of C_{nm} and S_{nm}. Where the relationships between J_{nm}/λ_{nm} and C_{nm}/S_{nm} are

$$J_{nm}^2 = C_{nm}^2 + S_{nm}^2 \quad \text{.....(C.15)}$$

$$\lambda_{nm} = \tan^{-1}\left(S_{nm}/C_{nm}\right)/m \quad \text{.....(C.16)}$$

Let us now review the mathematical expressions of those definitions of the Geo-potential harmonics in a slightly different representation. There are three types of harmonic:

1- **Zonal Harmonics** (m=0): For m=0, dependence of U on longitude vanishes, and the field is symmetric about the polar axis. For any $P_n(\sin\phi)$, there are n circles of latitude along which P_n is zero, and hence, (n+1) zones in which the function is alternately (+) and (-).

2- **Sectorial Harmonics** (n=m): The polynomial $P_{nm}(\sin\phi)$ is zero only at the poles $(\phi = \pm\pi/2)$. On the other hand, the terms $\begin{cases}\cos \\ \sin\end{cases} m\lambda$ are zero for 2n different values of λ; hence, the lines along which the function $\begin{cases}\cos \\ \sin\end{cases} m\lambda$, $P_{nm}(\sin\phi)$ vanish are meridians of longitude, which divide the sphere into 2n "orange-slice" sectors alternately (+) and (-).

3- **Tesseral Harmonics** ($n \neq m$): For $n \neq m$, the functions $\begin{cases}\cos \\ \sin\end{cases} m\lambda$

Appendix F: The flowchart of the Re-Correct of satellite orbital elements program and subprograms noticed as A, B, C, D, E, G.

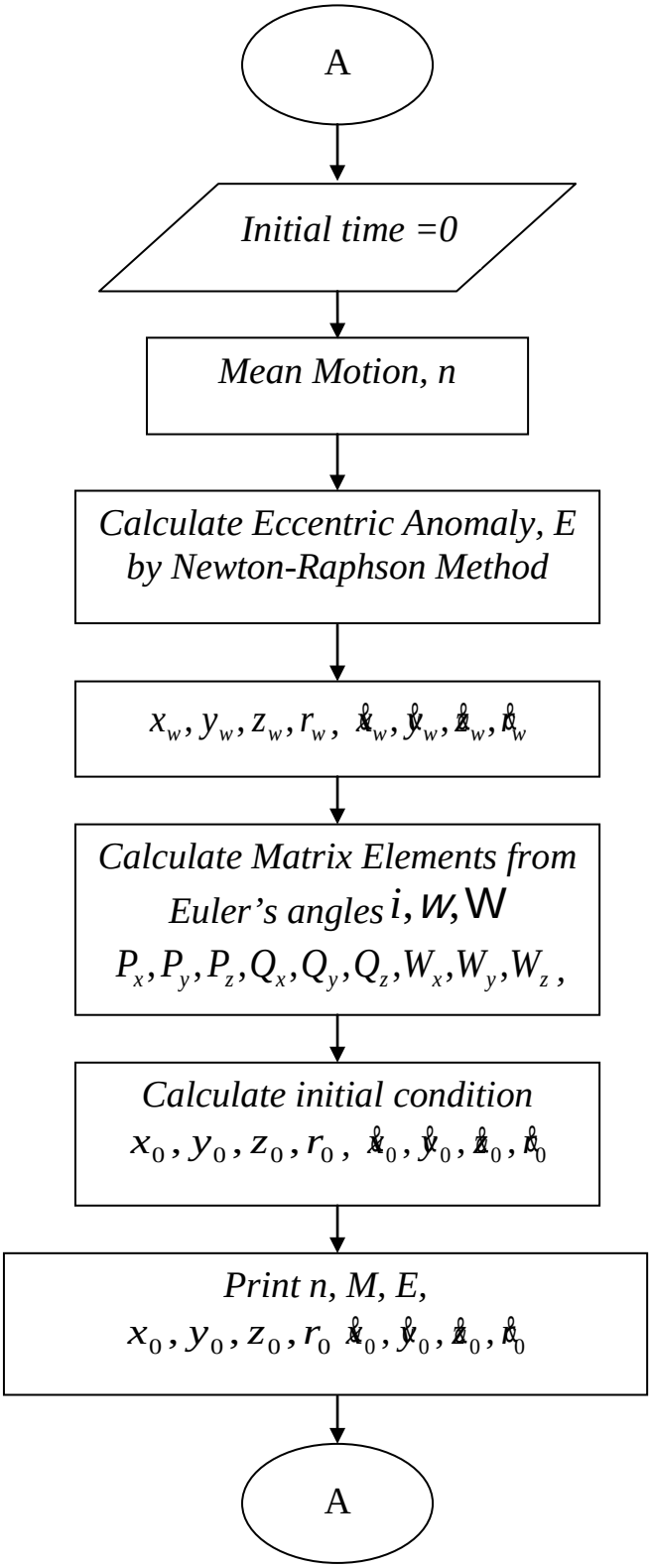

Figure (F1): Finding the initial condition which used to solving Runge-Kutta method.

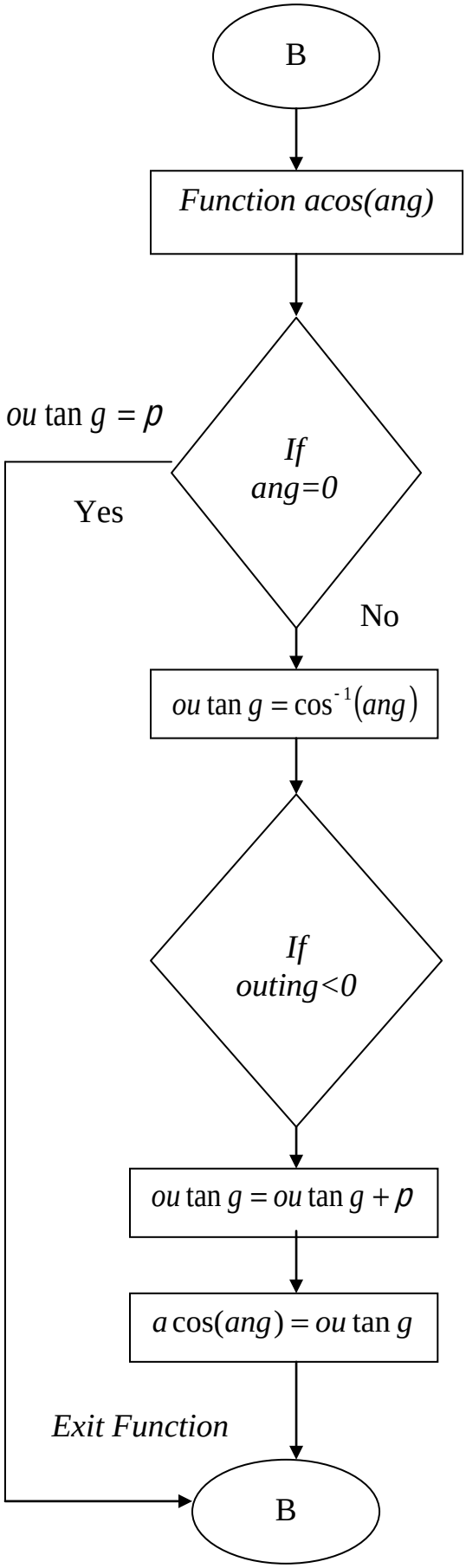

Figure (F2): Calculation angle values of f, E, w from cosine inverse function.

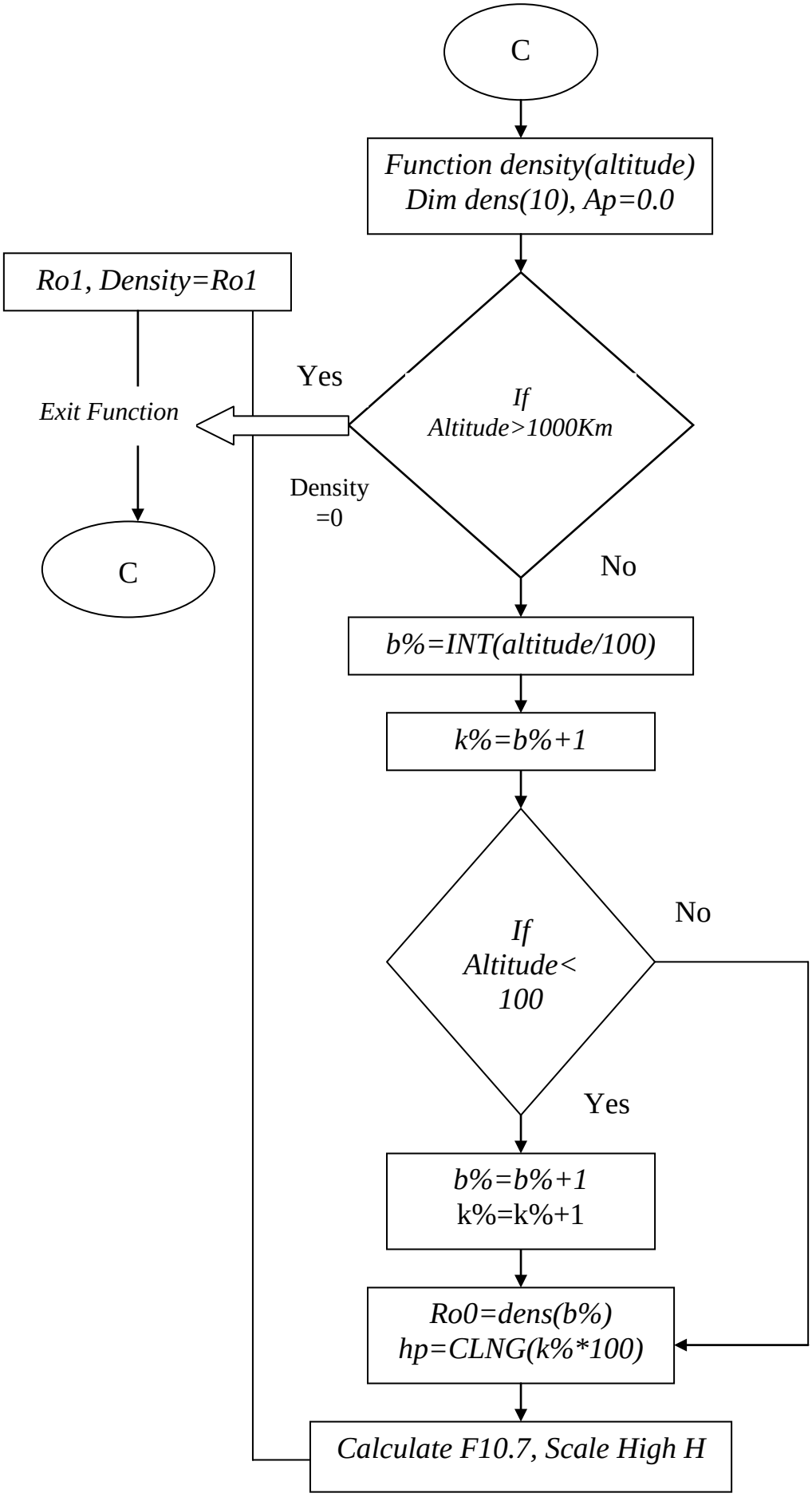
C
Function density(altitude)
Dim dens(10), Ap=0.0
Ro1, Density=Ro1
Yes
If
Altitude>1000Km
Exit Function
Density
=0
C
No
b%=INT(altitude/100)
k%=b%+1
If
Altitude<
100
No
Yes
b%=b%+1
k%=k%+1
Ro0=dens(b%)
hp=CLNG(k%*100)
Calculate F10.7, Scale High H

Figure (F3): Calculation the density of atmosphere (r) at each altitude.

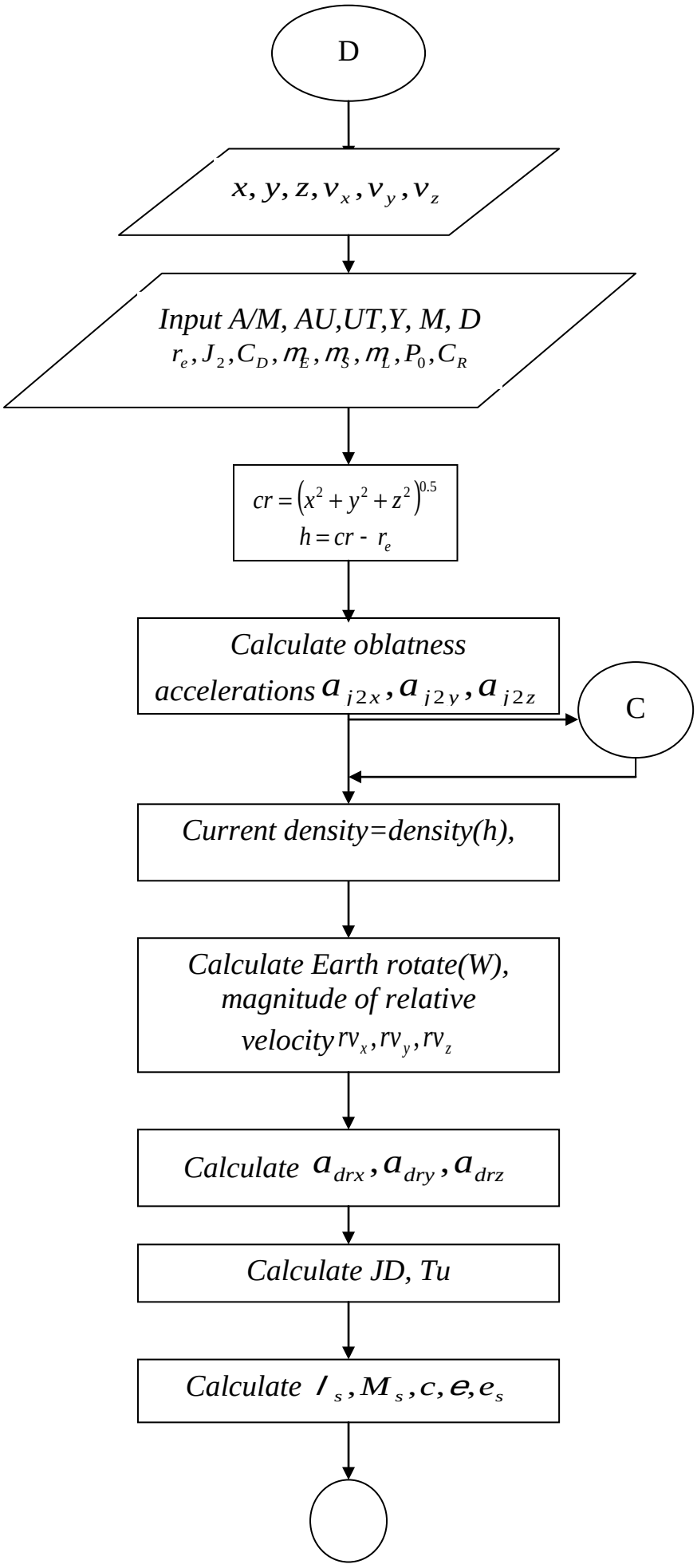

1

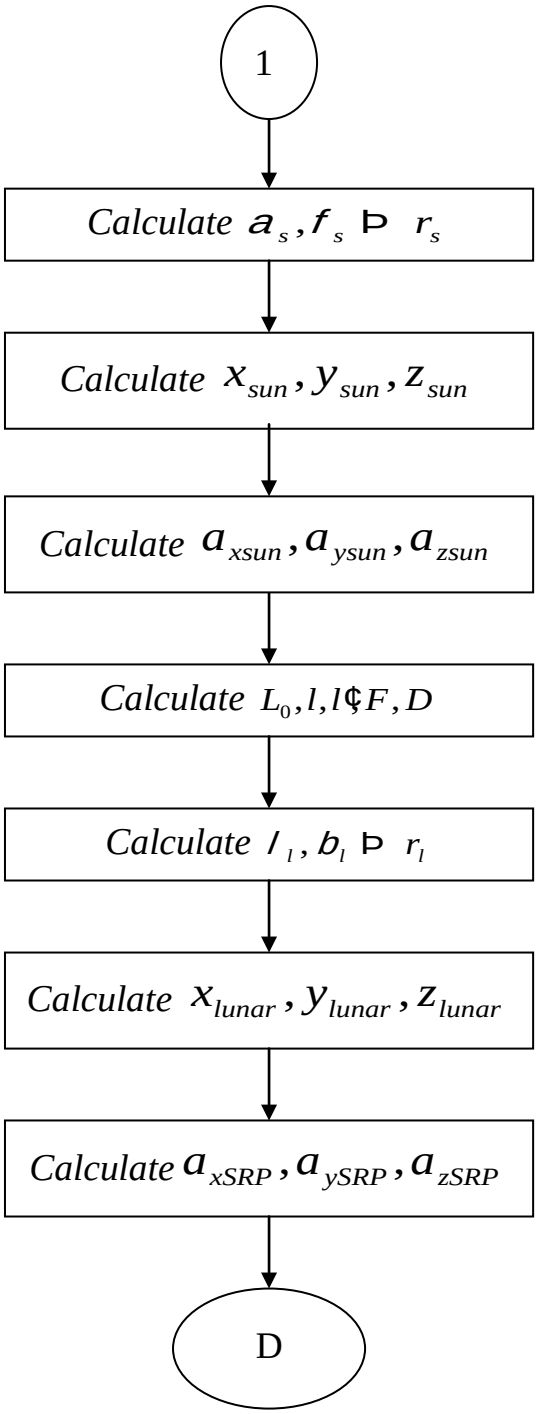
1
Calculate a_s, f_s Þ r_s
Calculate $x_{sun}, y_{sun}, z_{sun}$
Calculate $a_{xsun}, a_{ysun}, a_{zsun}$
Calculate $L_0, l, l¢, F, D$
Calculate l_l, b_l Þ r_l
Calculate $x_{lunar}, y_{lunar}, z_{lunar}$
Calculate $a_{xSRP}, a_{ySRP}, a_{zSRP}$
D

Figure (F4): Calculation the acceleration perturbation function for five perturbations effect on satellite orbit.

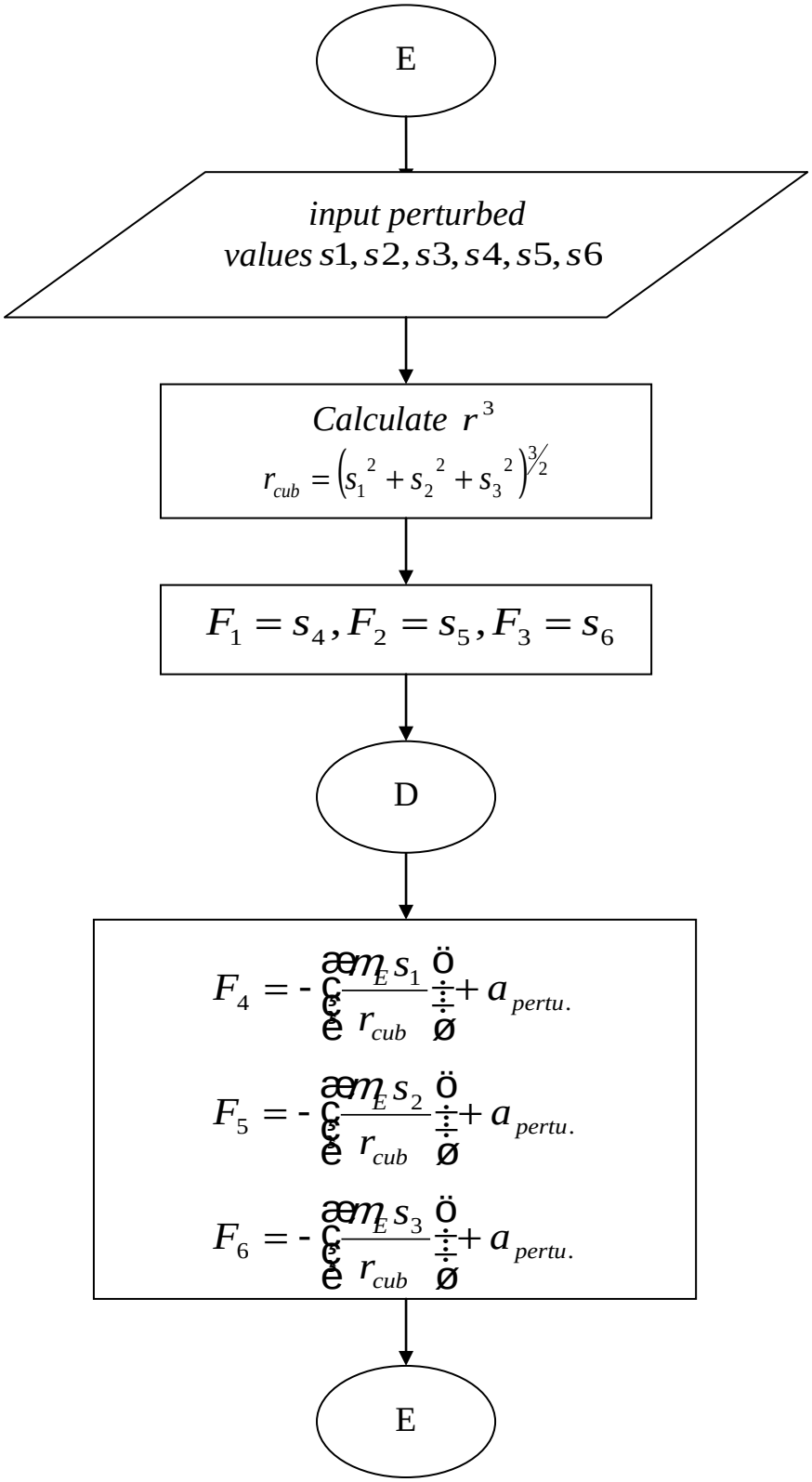

Figure (F5): Non-perturbation with perturbation acceleration function.

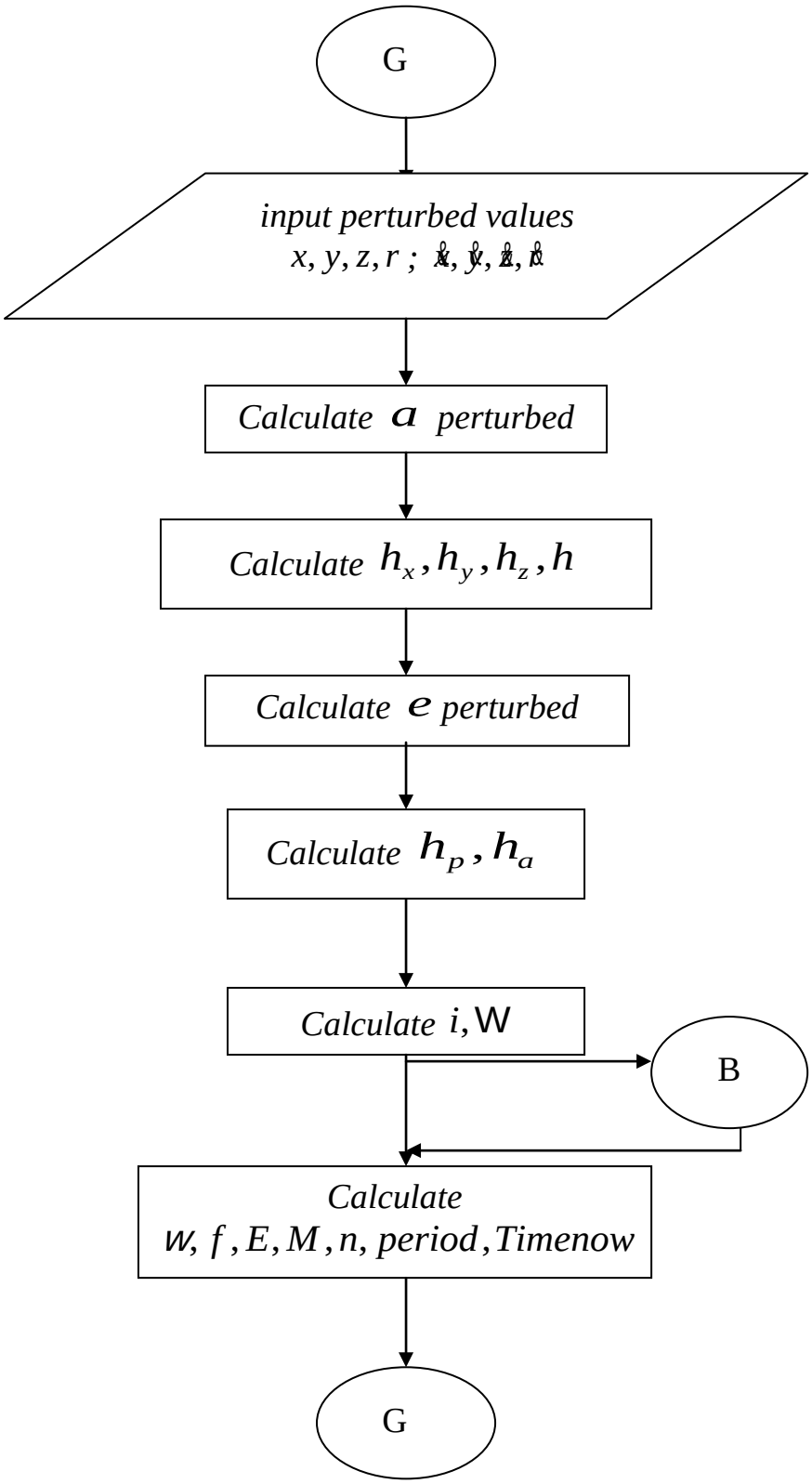

Figure (F6): Calculation an actual orbital elements of the satellite.

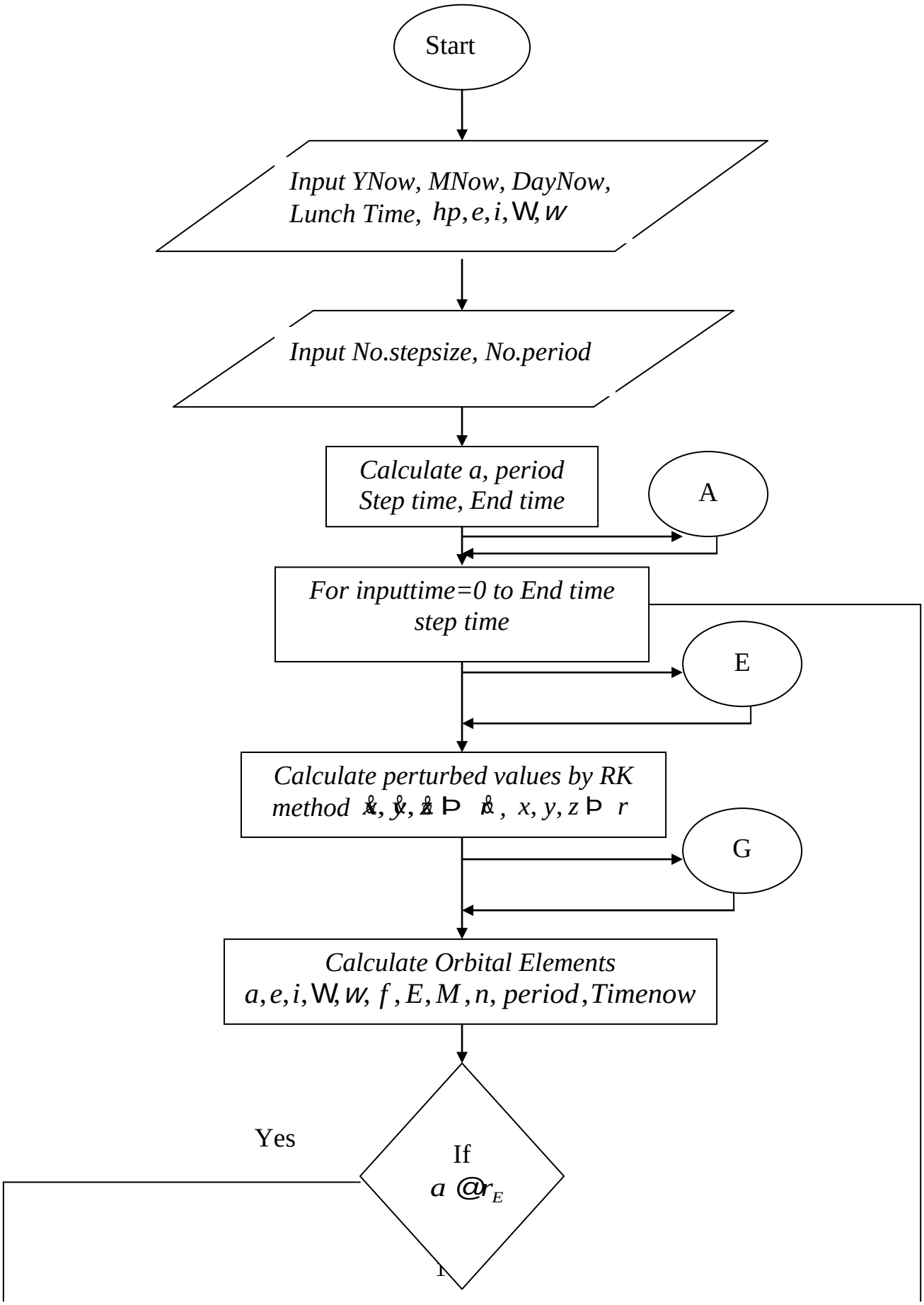

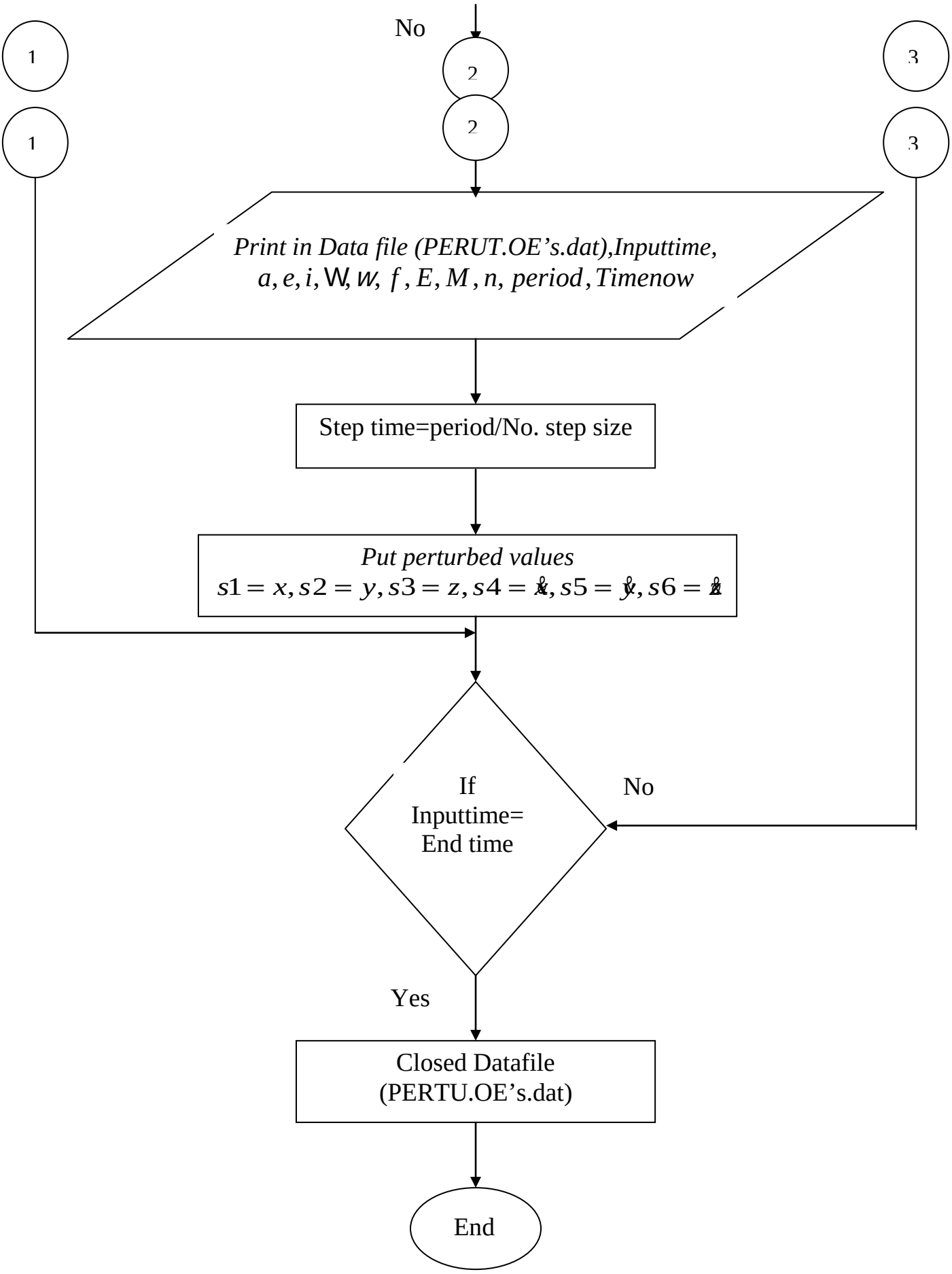
No
1
1
2
2
3
3
Print in Data file (PERUT.OE's.dat),Inputtime,
$a, e, i, W, w, f, E, M, n, period, Timenow$
Step time=period/No. step size
Put perturbed values
$s1 = x, s2 = y, s3 = z, s4 = \dot{x}, s5 = \dot{y}, s6 = \dot{z}$
If
Inputtime=
End time
No
Yes
Closed Datafile
(PERTU.OE's.dat)
End

Fig. (F7): The main program which solves perturbation acceleration functions by using Runge-Kutta 5-order method to calculate satellite orbital elements.

ملخص البحث

هناك عدة قوى تؤثر على مسارات الأقمار الصناعية حول الأرض لتعمل على حرف مسارها وبالتالي تغير عناصره المدارية. ولكونها صغيرة نسبة إلى القوة المركزية فهي اضطرابات جذبية وغير جذبية. من الممكن حل معادلة الحركة لكل الاضطرابات باستخدام طرق التكامل العددي.

تم في هذا البحث حساب مركبات الموقع والسرعة الحقيقة للقمر الصناعي في كل لحظة زمنية وبالتالي حساب العناصر المدارية الحقيقية المتأثرة بالأنواع الخمسة من الاضطرابات (عدم انتظام كروية الأرض، كبح الغلاف الجوي الأرضي، ضغط الإشعاع الشمسي، وتأثير جذب الشمس والقمر الأرضي). هذا يقود لمعرفة الاضطرابات المؤثرة للارتفاعات للمدارات الأرضية الواطئة والمتوسطة.

باستخدام لغة البيسك (QB) صمم برنامج متكامل لحل معادلة الحركة باستخدام طريقة رانج-كوتا وكذلك ادم- باشفورد ومعادلة الحركة عولجت بطريقة كول، وسمي البرنامج إعادة تصحيح العناصر المدارية للأقمار الصناعية، كذلك صممت الكثير من البرامج الفرعية لحساب كل الدوال المطلوبة.

تحل مجموع كل علاقات الاضطرابات لإيجاد الموضع والسرعة الحقيقية في كل لحظة زمنية من عمر القمر الصناعي وبالتالي حساب العناصر المدارية بوجود الاضطرابات ثم حساب التغيير الزمني في كل عنصر بوجود نوع واحد من الاضطرابات وبوجود كل الاضطرابات معا وللارتفاعات والميول التالية :

$$h_p = 95,600,1200,3000 Km \text{ and } i = 8^\circ, 63.4^\circ, 85^\circ$$

التغير لكل العناصر المدارية خلال ٣٣ دورة حسبت، كذلك تم حساب معامل الفيض الشمسي $(F_{10.7})$، ومقياس الارتفاع (H) والمسافة المدارية للشمس (r_s) والقمر (r_l) مع مركز الأرض، حيث تعتمد مع زمن إطلاق القمر الصناعي إضافتا إلى تغيرها مع الزمن ابتدأا من نقطة مرور القمر الصناعي بالحضيض. كذلك تم حساب عمر القمر الصناعي.

حساب مدارات الأقمار الاصطناعية تحت تأثير الاضطرابات

أطروحة مقدمة إلى كلية العلوم جامعة بغداد كجزء
من متطلبات الحصول على درجة الدكتوراه فلسفة في علوم
الفلك والفضاء

من قبل
وسام طالب ويس

بأشراف
أ. م. د. عبد الرحمن حسين صالح

ذو الحجة ١٤٣٢

تشرين الثاني ٢٠١١